Dissertations   Theses and Dissertations

12-1-2017

FOOTING FIXITY OF BRIDGE PIER WITH END-BEARING PILE FOUNDATION

Yunyi Jiang

Southern Illinois University Carbondale, yunyijiang@ymail.com

Follow this and additional works at: http://opensiuc.lib.siu.edu/dissertations

FOOTING FIXITY OF BRIDGE PIER WITH END-BEARING PILE FOUNDATION

by

Yunyi Jiang

M.S., Southern Illinois University Carbondale, 2013
B.S., Shenzhen University, 2011

A Dissertation
Submitted in Partial Fulfillment of the Requirements for the
Doctor of Philosophy Degree

Department of Engineering Science
in the Graduate School
Southern Illinois University Carbondale
December 2017

DISSERTATION APPROVAL

FOOTING FIXITY OF BRIDGE PIER WITH END-BEARING PILE FOUNDATION

By

Yunyi Jiang

A Dissertation Submitted in Partial

Fulfillment of the Requirements

for the Degree of

Doctor of Philosophy

in the field of Engineering Science

Approved by:

Dr. J. Kent Hsiao, Chair

Dr. Aslam Kassimali

Dr. Jale Tezcan

Dr. Prabir Kolay

Dr. Mingqing Xiao

Graduate School
Southern Illinois University Carbondale
November 2nd, 2017

AN ABSTRACT OF THE DISSERTATION OF

Yunyi Jiang, for the Doctor of Philosophy degree in Engineering Science, presented on November the 2nd, 2017, at Southern Illinois University Carbondale.

TITLE: FOOTING FIXITY OF BRIDGE PIER WITH END-BEARING PILE FOUNDATION

MAJOR PROFESSOR: Dr. J. Kent Hsiao

The degree of footing fixity G value of a column is a parameter which represents the rotation restraint at the base of a column. By using G values, the effective length factor K of the column can be calculated. The K value is used to check if the effect of slenderness needs to be considered for the column design. Moreover, the rotation of structural members is a major factor in determining the deflection of structures. The magnitude of structure deflection due to the rotation and elastic deformation are used to check if the second-order effect (P-delta effect) needs to be considered. When large axial loaded compression members, like bridge piers, are under lateral load impacts, the rotation at the base of the pier may cause a significant effect on the lateral deflection of the pier.

However, traditionally the computation of slenderness ratio and the structure deflection due to the lateral loads is carried out by considering that the pier footing is rigidly fixed on the ground. AASHTO recognized the significance of the footing fixity effect on bridge piers and recommended an approach to account those considerations and suggested some footing fixity G values for different footing conditions. The purpose of this study is to verify the accuracy of the G values recommended by AASHTO for the pier footing on multiple rows of end-bearing piles case. A comprehensive study using 20 models derived from the pier-pile design example presented by FHWA is developed for the finite element analysis using computer software. In order to investigate the difference of G values for different pile foundations, these models are generated using various pile lengths, soil contents, pile arrangements and pile head boundary

i

conditions. Also, the computations of the slenderness effect check, pier deflections and the G

values obtained from finite element models are provided for the comparisons with that

recommended by AASHTO.

ACKNOWLEDGMENTS

TABLE OF CONTENTS

LIST OF TABLES

LIST OF FIGURES

CHAPTER 1

INTRODUCTION

1.1 Background

Piers are commonly used to upright support heavy structures such as bridges, transmission towers, overhead railroads and so on as shown in Figure 1.1. In many pier design cases, the lateral loads would govern when they are in the areas which, for example, are seismic active, wind hazard affected or possible lateral impacted areas. Usually, pier design for lateral loads could be analyzed by ultimate load analysis with a factor of safety or an allowable deflection (Bhushan and Scheyhing, 2002). To determine the deflection of the pier, the rotation of the pier would play an essential role in determining the additional deflection besides the lateral deflection of pier due to lateral loads only.
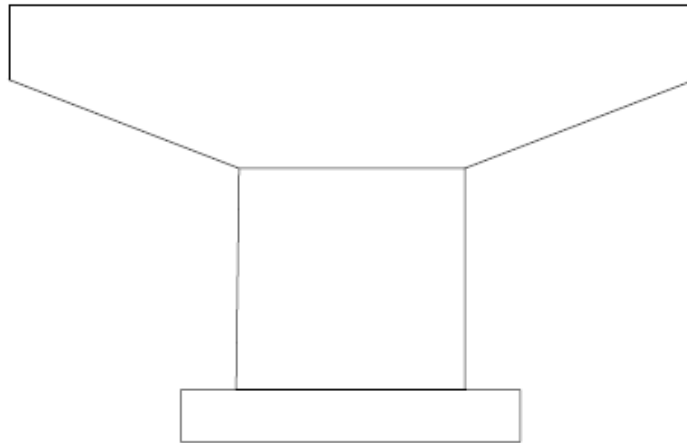
Figure 1.1 Typical hammerhead bridge pier

The degree of footing fixity G value is one of the parameters used to represent the rotation of structure members. As important as analyzing pier system by considering footing fixity, extra caution should apply to accurately determine the footing fixity due to its complicity conditions between pier foundation and ground. Traditionally, a pier is treated as a sway frame fixed on the ground when performing an analysis. However, depending on the various conditions at pier footings, the rotation of the pier could be significant and may lead to larger pier deflection comparing with the traditional approach (Hsiao and Jiang, 2014). Much research has been done recently regarding the complicity of different pier footing types. In 2010, Wu (Wu, 2010) used three models and concluded that if P-delta effect, structure- soil interaction and non-linear material behaviors for pier landed on soil cases were considered, much larger pier deflections could be obtained. Furthermore, the lateral response of pier footing on the different types of soils has been studied by Zeeshan (Zeeshan, 2016). He concluded that different pier footing fixities were obtained when the pier lands on the various types of soils, which will result in different pier lateral deflections. Nevertheless the determination of footing fixity is harder for pier footing on pile foundations due to more variables such as the length of piles, type of soils, different layers of soil, pile-soil interactions, pile arrangement and so on.

Pile foundations are majorly designed for vertically supporting heavy loads from superstructures, transmitting those loads into the bearing soil layers and preventing significant structure deformations. The capacity of pile foundations is depending on both material and geometry of piles, spacing between each pile, type of soil materials, method of installation, and direction of applied loadings. Normally, pile foundations have both axial and lateral behaviors. If no particular case is used, these two behaviors are treated separately (Mosher and Dawkins, 2000).
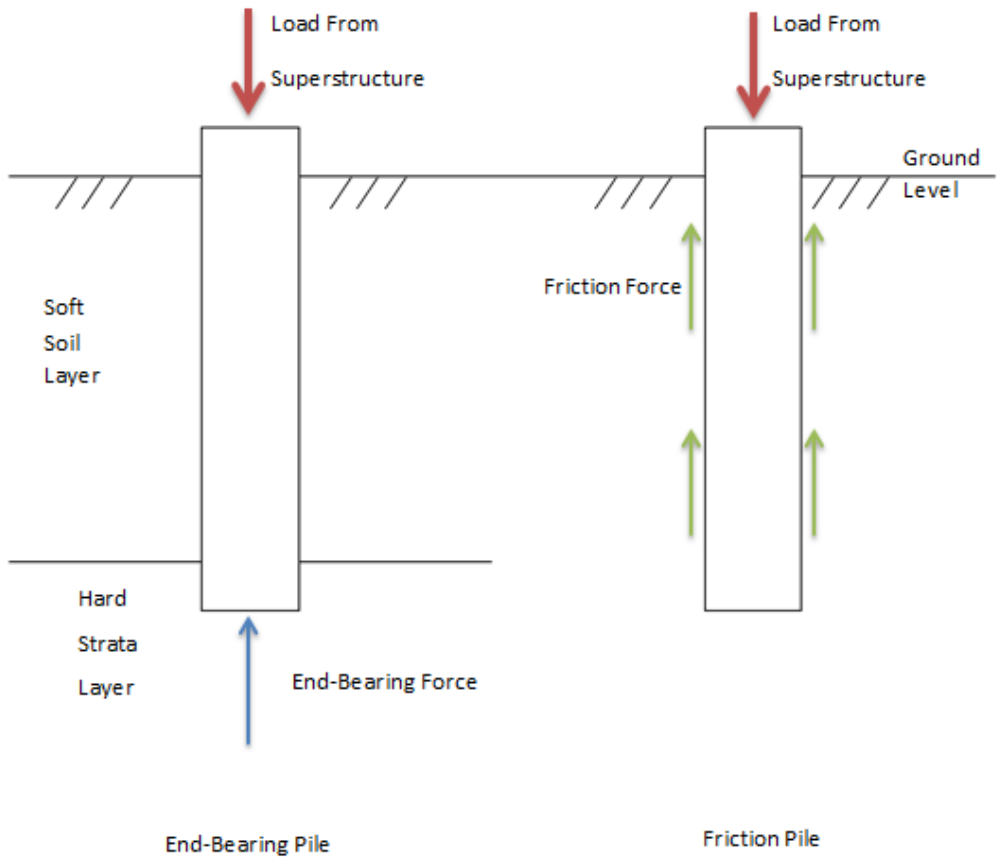
Figure 1.2 Pile load transfer mechanism (adapted from Valli, 2014)

Piles are classified as friction piles or end-bearing piles according to their load transfer mechanism shown in Figure 1.2. The axial behavior of piles can be easily observed from above figure. For friction piles, the vertical load from superstructure is taken care of by the skin friction of piles. For end-bearing piles, the vertical load will be majorly carried by the more stable layer at the bottom of the pile, which could be a stronger layer of soil or rock. The skin friction can be neglected.

As stated previously, lateral pile behavior is mostly treated independently. However, a high axial load can interact with lateral displacement to cause P-delta effect and lead to larger lateral deformation (Mosher and Dawkins, 2000). Different from axially loaded pile analysis, the laterally loaded pile analysis is more complicated due to the resistance for lateral loads are purely provided by soils. Lateral loaded single pile deformations vary from the geometry and boundary conditions as shown in Figure 1.3 derived from Salgado's work (Salgado, 2008). Laterally loaded pile group with lateral pile deflection, vertical pile rotation, and pile cap rotations is presented in Figure 1.4 also derived from Salgado's paper (Salgado, 2008).
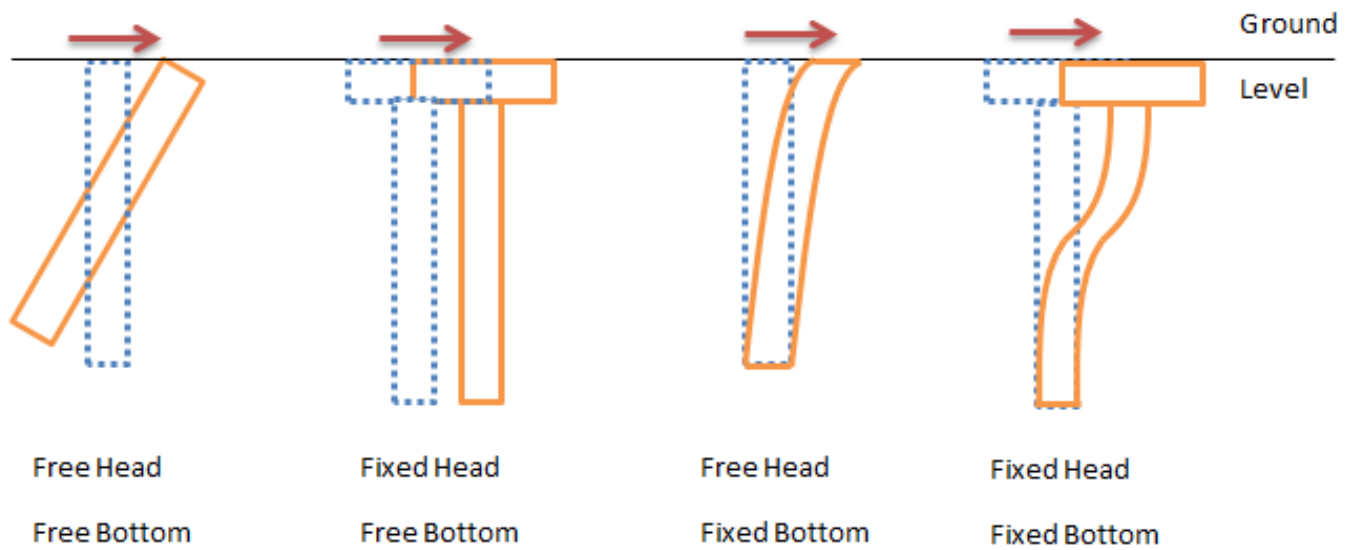
Figure 1.3 Single pile lateral loaded deformation (adapted from Salgado, 2008)
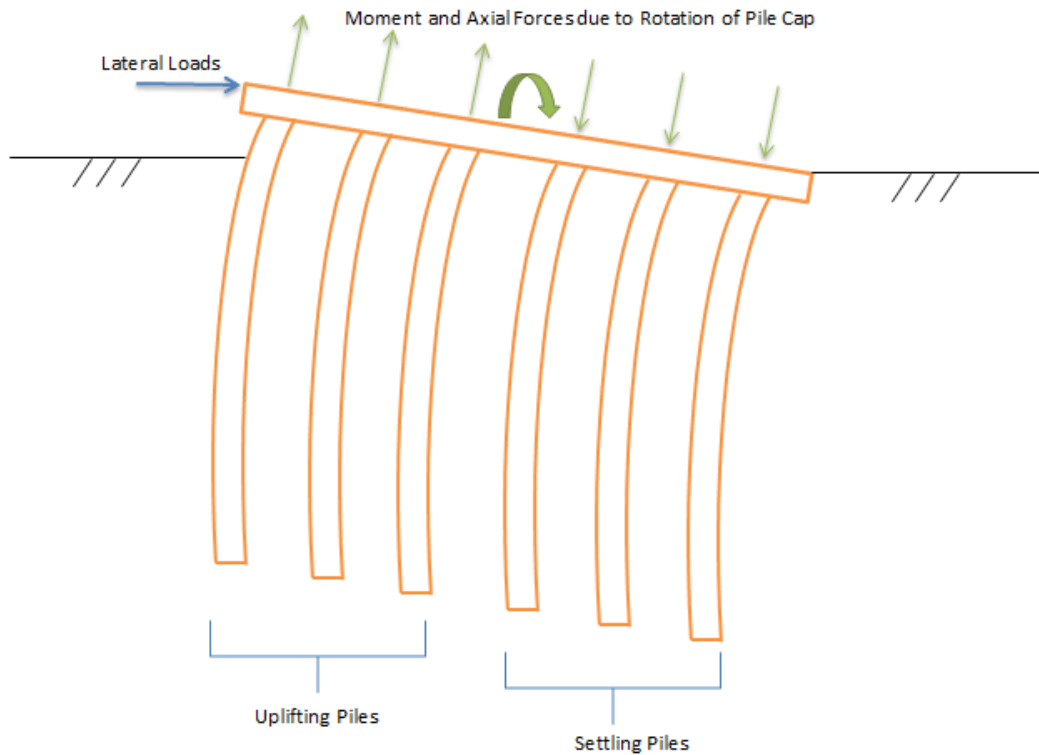
Figure 1.4 Pile group deformations under lateral load

(adapted from Salgado, 2008)

Much research has been done on analyzing lateral loaded piles. The most two popular methods are the m-method and p-y method. Simply explained, m-method assumes soil as linear springs and p-y method assumes soil as nonlinear springs (Qin et al., 2011) shown in Figure 1.5 derived from FHWA Report 2006. Therefore, the p-y method developed by Reese and his coworkers is more widely used in designing and analyzing laterally loaded piles because it can account nonlinearity and soil layering (Matlock et al., 1960; Reese, et al., 1974). In this method, P represents lateral loads, and y stands for the lateral deflection.
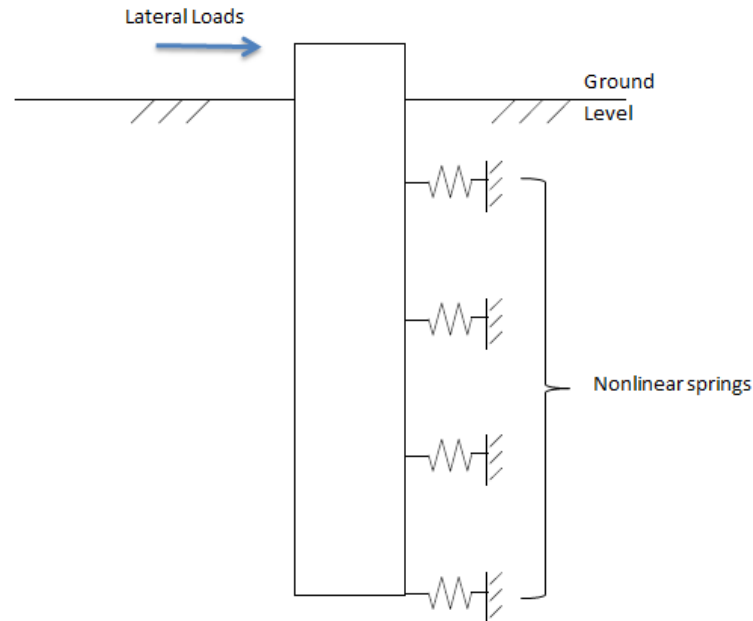
Figure 1.5 P-y method assumption illustration

Later, pile analysis software such as LPile and FB-MultiPier implemented the p-y method for pile designing. However, this approach has a certain limitation regarding the assumption of treating soil behavior as semi-empirical. To check the accuracy, 3D continuum-based finite element models have been studied to compare with the models generated in LPile and FB-Multpier. The continuum-based method treats the soil as an elastic or elastic-plastic continuum. The results from those two approaches have shown highly agreements (Zhang, et al., 2012).

On the contrary, structural design and analysis software adopted the m-method, considering soils and foundations as linear springs. Pier models with spring footings and supports have been created by using SAP 2000 to verify the m-method. It turns out the more springs applied on the models, the more close results will be obtained comparing with models from LPile and FB-MultiPier (Khodair and Abdel-Mohti, 2014).

For offshore superstructures and structures which are subjected to lateral loads, vertical pile group may not be sufficient to resist the large lateral forces. In this case, batter pile foundations can be used to resist the lateral loads. Given precise angles, batter piles can resist all of the lateral loads (Hsiao, 2012).

As stated above, footing fixity concerns are significant for structural engineers in designing laterally loaded superstructures.

1.2 Pier Lateral Deflection Analysis Approach, K Value, and G Value

There are two approaches to calculate the pier deflection now for structural engineers. The first approach is the traditional approach, as previously talked about in section 1.1, this is an approximate approach by assuming the base of pier is rigidly fixed on the ground. The second approach is a refined approach which considers the degree of fixity on the two ends of the piers. In determining pier deflections, two aspects should be checked: the slenderness ratio of the pier and the elastic deflection of the pier. Slenderness ratio is used to determine if the effect of slenderness should be considered, and the elastic deflection of the pier is used to decide if the p-delta effect should be considered. For a compression member, *KL* is the effective length defining the deflection portion of a member between zero curvature points (inflection points). The value K is the effective length factor which presents the ratio of an equivalent pin-ended compression member to the actual length end-restrained compression member (Caltran, 2000). The American Institute of Steel Construction (AISC,2011) Manual 14th edition Table C-A-7.1 has recommended effective length factor K values regarding various boundary conditions which are suggested by SSRC (Structural Stability Research Council).

Therefore, the traditional approach can be summarized as following steps (Hsiao and Jiang, 2014):

1. Get the effective length factor K from Table C-A-7.1(AISC,2011)

2. Check slenderness ratio, if

$$\frac{Kl_u}{r} \gg 22 \tag{1.1}$$

3. $\frac{Kl_u}{r} \gg 22$, consider slenderness effect on the pier

4. Compute the deflection at the top of the pier (consider base is rigidly fixed)

   Deflection due to the lateral load at top of the pier

$$\delta_1 = \frac{F_1 L_c^3}{3E_c I_c} \tag{1.2}$$

   Deflection due to the lateral load at height b of the pier

$$\delta_2 = \frac{F_2 b^2}{6E_c I_c}(3L_c - b) \tag{1.3}$$

$$\Delta_1 = \delta_1 + \delta_2 \tag{1.4}$$

5. If $\Delta_1 > \frac{l_u}{1500}$, moment magnification factor δ should apply, $\Delta = \delta\Delta_1$;

6. otherwise, $\delta = 1.0$, $\Delta = \Delta_1$

   Where l_u is the unbraced length of the pier

                  r is the radius of the gyration of the cross-section of a pier

             F_1, F_2 are the factored lateral load

                L_c is the height of a pier

                E_c is the modulus of the elasticity of the pier

                I_c is the moment of inertia of the pier

                Δ is the lateral deflection of the pier

Additionally, rotational restraint coefficient G is introduced in the refined approach, which is defined as following (AISC, 2011),

$$G_A = \frac{\sum(\frac{E_c I_c}{L_c})}{\sum(\frac{E_g I_g}{L_g})} \tag{1.5}$$

Where   c is denoting columns (pier) attached to end A

       g is denoting beams attached to end A

In this refined approach, the effective length factor K can be obtained by using the G values at the two ends of a member and the alignment charts provided by AISC Steel Manual Figure C-A-7.1 and Figure C-A-7.2 (AISC, 2011) for braced frame and moment frame respectively.

Alternatively, K value could be calculated by following French equation (Chen and Duan, 2014) using the G values at the two ends of a member:

For unbraced frames:

$$K = \sqrt{\frac{1.6 G_A G_B + 4.0(G_A + G_B) + 7.5}{G_A + G_B + 7.5}} \tag{1.6}$$

Most of the bridge piers are categorized as unbraced frames. Therefore, Equation (1.6) can be applied.

In lack of a more detailed calculation, AASHTO suggested using following G values to determine K factor:

For freely rotating column ends, G is theoretically equal to infinity; for column footing as a frictionless pin, G can be taken as 10; and for column end rigidly attached to a proper designed footing, G can be taken as 1.0.

For designing monolithic connections:

G = 1.5 footing anchored on rock

G = 3.0 footing not anchored on rock

G = 5.0 footing on soil

G = 1.0 footing on multiple rows of end bearing piles

Currently, structural engineers treat superstructure footings as rigidly fixed on the ground. They neglect the different conditions of the footings and approximately take G=1.0 for fixed boundary condition as recommended by AISC manual (AISC, 2011) and AASHTO manual (AASHTO, 2012). However, the deflection at the top of a pier computed using the approximate approach resulted in significant different from that using the G values recommended by AASHTO for different footing conditions (Hsiao and Jiang, 2014).

Since the footing fixity significantly affects the deflection of the pier, the primary purpose of this research is to verify the accuracy of rotational restraint coefficient G values recommended by AASHTO for the footing on multiple rows of end-bearing piles.

CHAPTER 2

METHODOLOGY

2.1 Verification of G Value

As introduced in the previous Chapter, rotational coefficient G of a structure member may significantly affect the determination of effective length factor K. In order to verify the accuracy of G values recommended by AASHTO, an equivalent tie beam system has been introduced by Hsiao and Jiang (Hsiao and Jiang, 2014) to determine the G value at the bottom of a cantilever single pier or a pier bent.

As shown in Figure 2.1, a typical hammer-head cantilever single pier can be transferred into a tie beam system shown in Figure 2.2, which is taken out from tie beam frame system shown in Figure 2.3, where the length L is calculated by reversely using Equation 1.5 and a given G value. The rotation of this tie beam system is represented by θ_A shown in Figure 2.4.
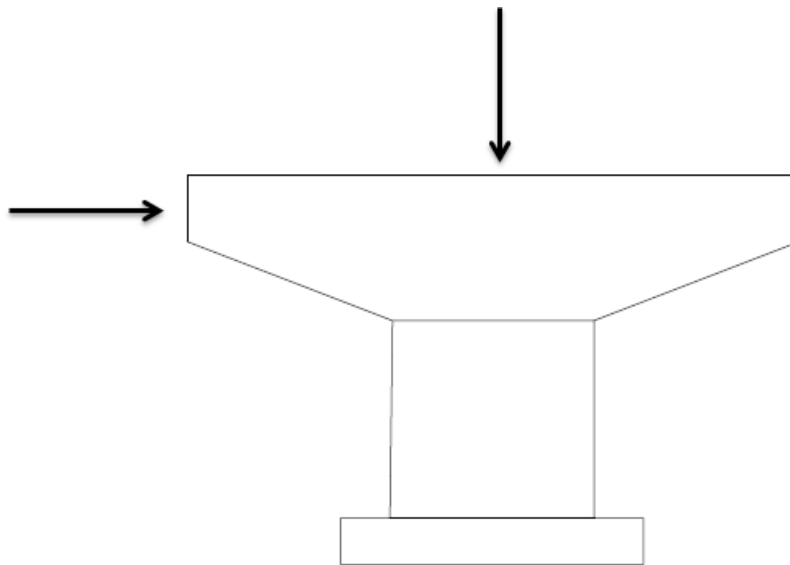
Figure 2.1 Typical cantilever single pier
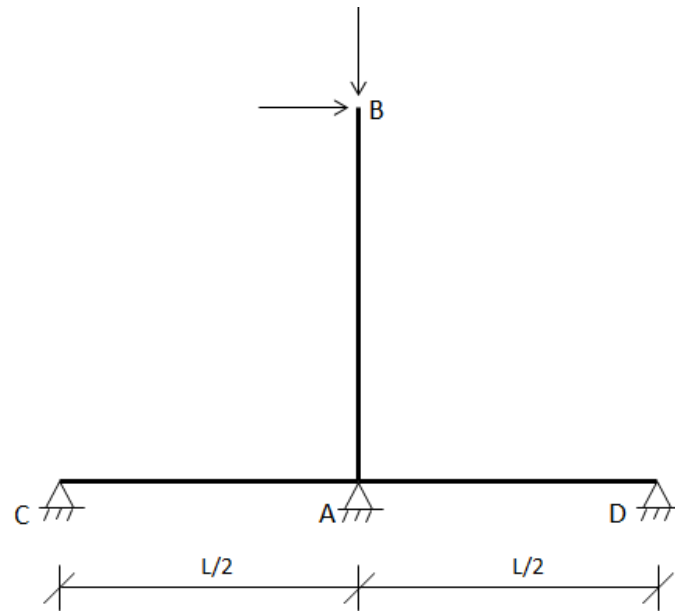
Figure 2.2 Equivalent tie beam system for a cantilever single pier (adapted from Hsiao and
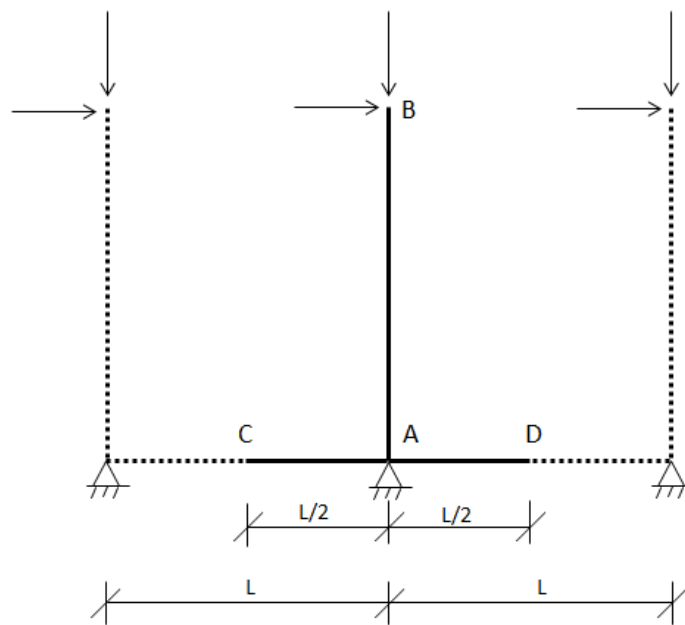
Jiang, 2014)

Figure 2.3 Equivalent tie beam frame system (adapted from Hsiao and Jiang, 2014)
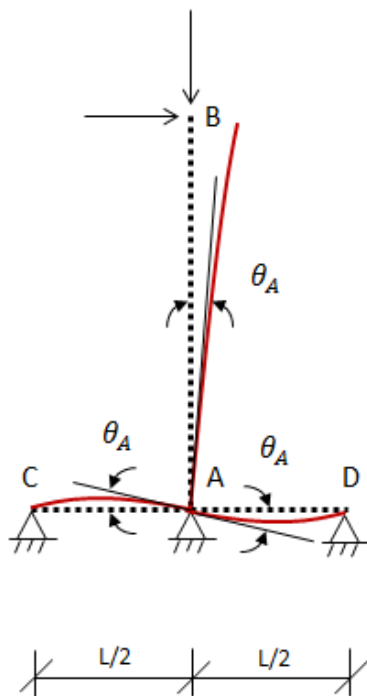
Figure 2.4 Rotation of the tie beam system (adapted from Hsiao and Jiang, 2014)

Therefore, with given G value, pier lateral deflection is determined by refined approach as following steps (Hsiao and Jiang, 2014):

(1) Obtain proper G values

(2) Determine L_{AD} by using Equation 1.5 with given G value (equivalent tie beam system is developed by this step)

(3) Calculate K value by Equation 1.6 (assuming $G = \infty$ at the free end)

(4) Check slenderness ratio, if

$$\frac{Kl_u}{r} \gg 22 \tag{1.1}$$

(5) $\frac{Kl_u}{r} > 22$ consider slenderness effect on pier

(6) Compute elastic deflection at the top of pier due to lateral load only

Deflection due to the load at top of the pier

$$\delta_1 = \frac{F_1 L_c^3}{3E_c I_c} \qquad (1.2)$$

Deflection due to the load at height b of the pier

$$\delta_2 = \frac{F_2 b^2}{6E_c I_c}(3L_c - b) \qquad (1.3)$$

$$\Delta_1 = \delta_1 + \delta_2 \qquad (1.4)$$

(7) Calculate θ_A (rotation at joint A shown in Figure 2.4),

$$\theta_A = \frac{M_{AD} L_{AD}}{3E_{AD} I_{AD}} \qquad (2.1)$$

(8) Compute lateral deflection of pier due to rotation

$$M_{AD} = M_{AC} = M_{AB}/2 \qquad (2.2)$$

$$M_{AB} = F \times L_{AB} \qquad (2.3)$$

$$\Delta_2 = L_{AB} \cdot \tan \theta_A \qquad (2.4)$$

$$\Delta_3 = \Delta_1 + \Delta_2 \qquad (2.5)$$

Where, M_{AD}, M_{AC}, and M_{AB} are moments at the end A of the members AD, AC, and AB, respectively

E_{AD} is the modulus of elasticity of member AD

I_{AD} is the moment of inertia of member AD

L_{AD} is the length of member AD

L_{AB} is the length of member AB, which is L_c

Δ_2 is the lateral deflection of pier due to rotation

Δ_3 is the total lateral deflection of pier

(9) If $\Delta_3 > \frac{l_u}{1500}$, moment magnification factor δ should apply, the final lateral deflection $\Delta = \delta\Delta_3$; otherwise, $\delta = 1.0$, and $\Delta = \Delta_3$

In finite element analysis, final deflection Δ' can be obtained. To determine the rotation angle θ_A' and rotational coefficient G' value at the bottom of a pier in real cases, use the Δ' from real cases and reversely apply the refined approach from step (9) to step (1).

2.2 Scope of Research

2.2.1 Group of Cases Studied

This paper is to investigate the accuracy of G =1.0 for bridge pier on end-bearing pile

foundations recommended by AASHTO. The capacity of pile foundation varies depending on

many factors, such as the material and geometry of piles, the spacing between each pile, the type

of surrounding soil materials, the method of installation and the direction of applied loadings,

etc. Therefore, the rotation at the base of the pier on different pile foundation systems due to the

same axial and lateral loads may also vary, resulting in various G values.

To conduct a comprehensive study, different types of pile groups are considered. There

are two categories of pile groups studied: straight piles group (Figure 2.5), and pile group with

batter piles (Figure 2.6). For both groups consider the pile pinned at the bottom of the pile cap

(pinned head pile) and pile fixed (embedded in) at the bottom of the pile cap conditions (fixed

head pile).
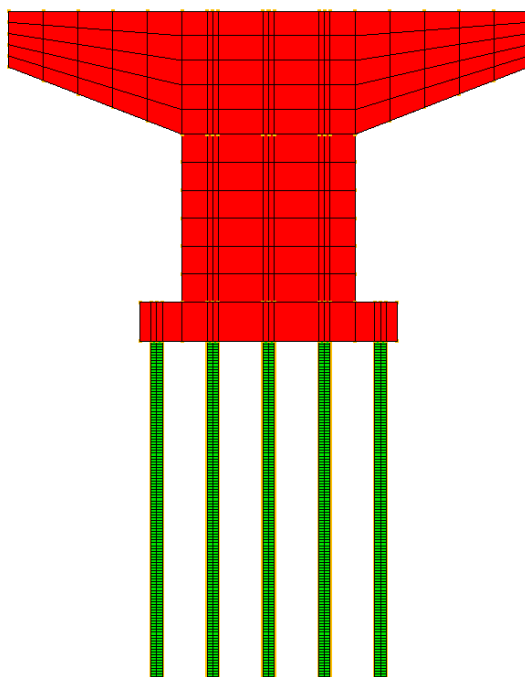
Figure 2.5 Straight pile groups
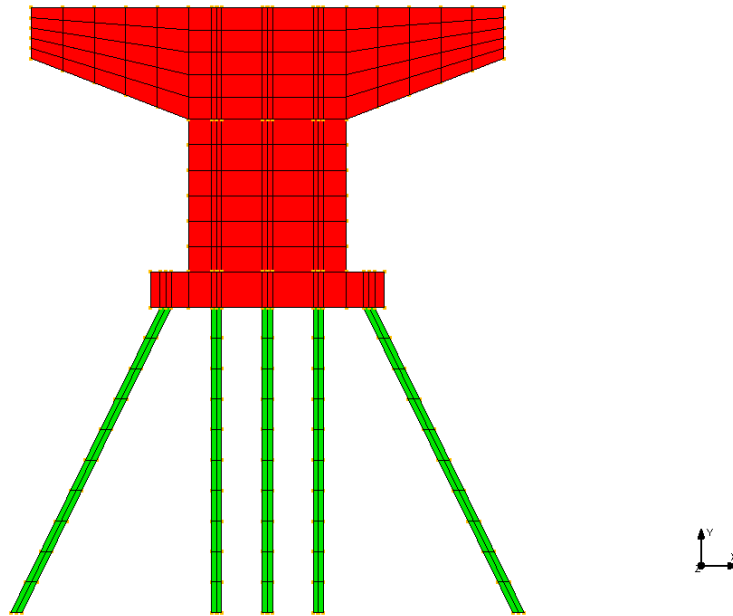
Figure 2.6 Pile groups with batter piles

Straight pile groups are only able to resist axial loads; the lateral loads are taken care of purely by soil resistance. This paper has studied structure system behaviors of straight pile cases under various soil types, multiple soil layers, and different pile lengths.

On the other hand, for structure system containing batter piles, the lateral loads can be taken fully by batter piles. Thus, this paper also studies for pile group with batter piles for offshore structures. In this case, there will be no soil environments to provide lateral support to piles. Due to the scope limit of this research, batter pile groups in different soil types will not be considered in this study.

In this study, three types of soil materials are used for straight pile foundations: sand, soft clay, and stiff clay. Pile foundations are studied in a single layer of various soil materials on a bearing layer of limestone independently (Figure 2.7-Figure 2.9) and in the multiple soil layer cases (Three layers) on limestone (Figure 2.10-Figure 2.11) using computer software LPile (LPile, 2004).
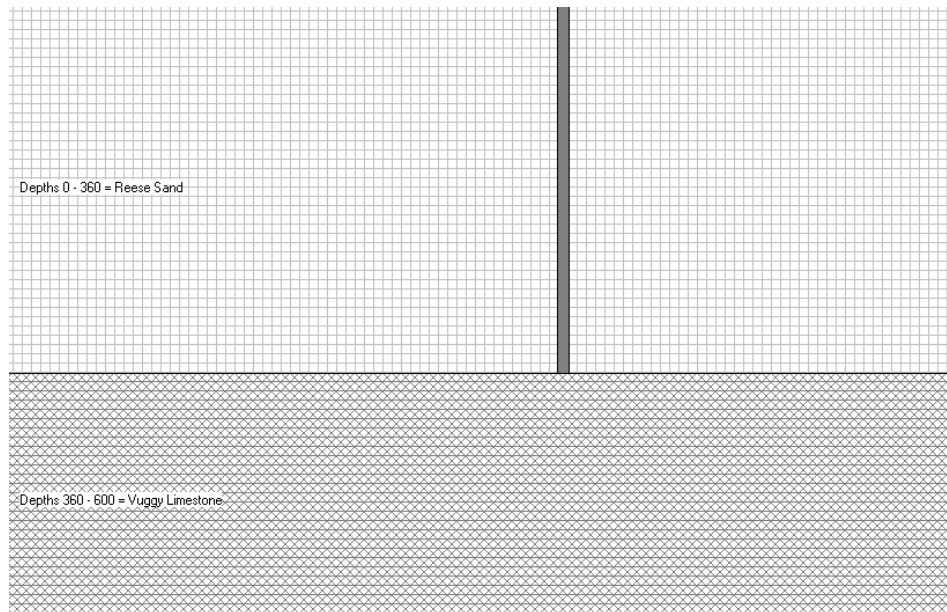
Figure 2.7 End-bearing straight pile in sand case
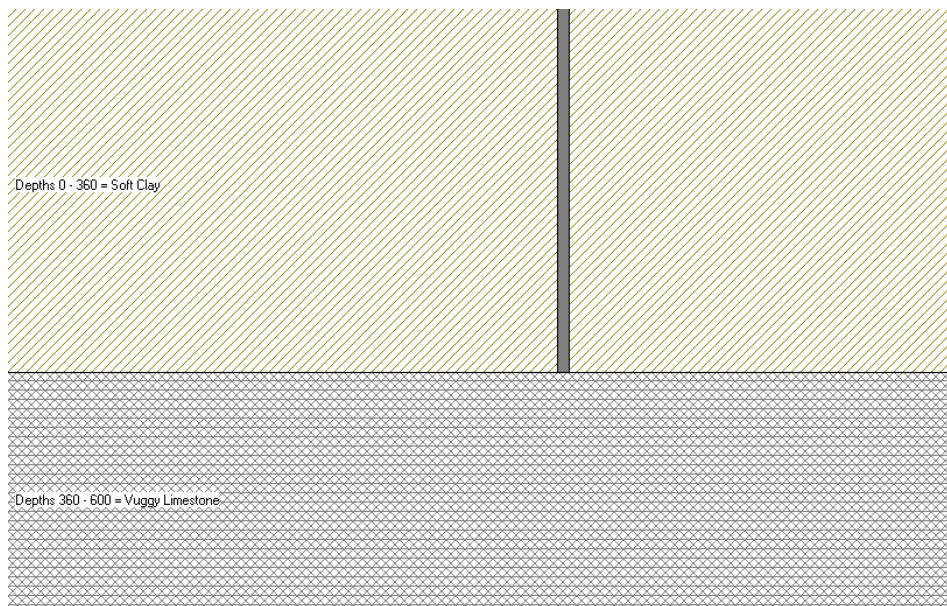
Figure 2.8 End-bearing straight pile in soft clay case

Depths 0 - 360 = Stiff Clay w/o free water

Depths 360 - 600 = Vuggy Limestone

Figure 2.9 End-bearing straight pile in stiff clay case

Depths 0 - 120 = Reese Sand

Depths 120 - 240 = Soft Clay

Depths 240 - 360 = Stiff Clay w/o free water

Depths 360 - 600 = Vuggy Limestone
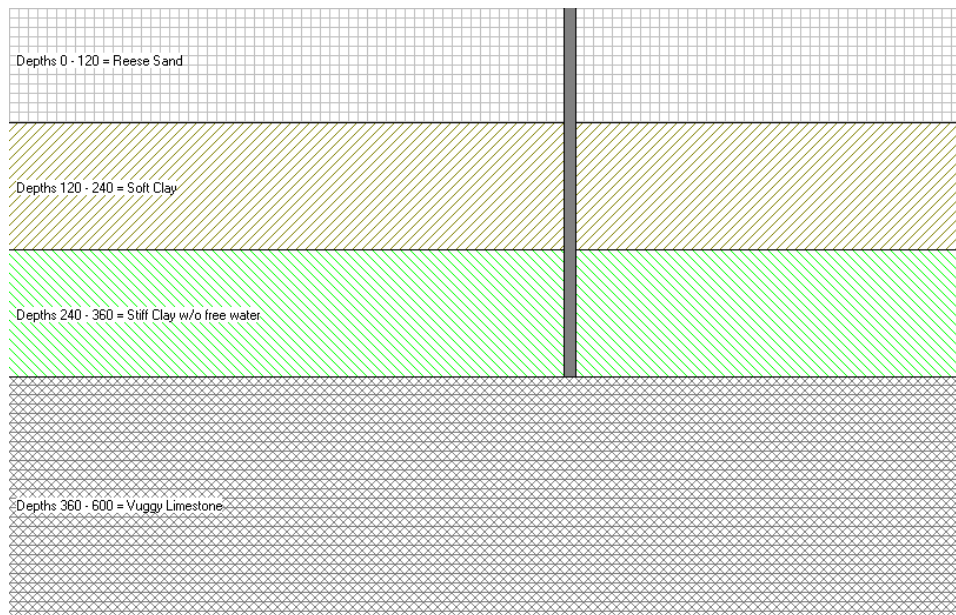
Figure 2.10 End-bearing straight pile in three layers of soil case

(sand, soft clay, stiff clay from top to bottom)

Depths 0 - 120 = Soft Clay

Depths 120 - 240 = Reese Sand

Depths 240 - 360 = Stiff Clay w/o free water

Depths 360 - 600 = Vuggy Limestone
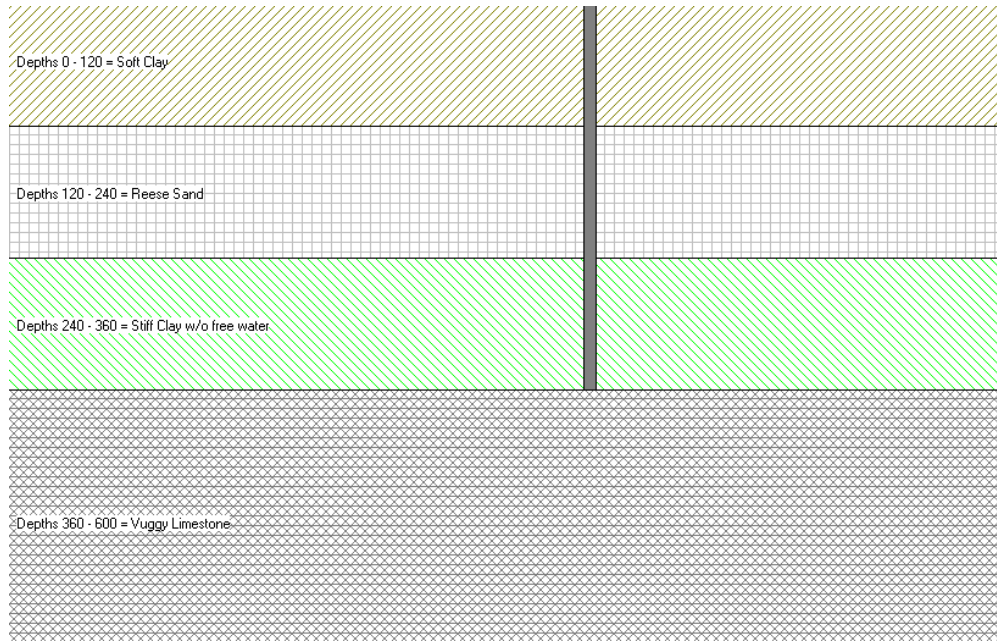
Figure 2.11 End-bearing straight pile in three layers of soil case

(soft clay, sand, stiff clay from top to bottom)

Different lengths of the pile may cause different superstructure deflections. In this study, the length of pile is considered to be 15 feet long according to Hamilton (Hamilton, 2014) and 30 feet long according to FHWA report (FHWA, 2006), which is categorized as short pile and long pile respectively according to Das (Das, 2007). These two different lengths are applied for both straight pile groups and pile groups with batter piles. Summarizing all the above, the cases studied in this research, and their model numbers are listed in following Table 2.1. All of the models are generated and analyzed in structural finite element analysis software NISA (NISA, 2003).

Table 2.1 *Cases studied and model numbers*

Cases Studied	Model Numbers
30 ft. Pinned head straight piles in sand	Model 1
30 ft. Pinned head straight piles in soft clay	Model 2
30 ft. Pinned head straight piles in stiff clay	Model 3
30 ft. Pinned head straight piles in (sand, soft clay, stiff clay)	Model 4
30 ft. Pinned head straight piles in (soft clay, sand, stiff clay)	Model 5
15 ft. Pinned head straight piles in sand	Model 6
15 ft. Pinned head straight piles in soft clay	Model 7
15 ft. Pinned head straight piles in stiff clay	Model 8
30 ft. Fixed head straight piles in sand	Model 9
30 ft. Fixed head straight piles in soft clay	Model 10
30 ft. Fixed head straight piles in stiff clay	Model 11
30 ft. Fixed head straight piles in (sand, soft clay, stiff clay)	Model 12
30 ft. Fixed head straight piles in (soft clay, sand, stiff clay)	Model 13
15 ft. Fixed head straight piles in sand	Model 14
15 ft. Fixed head straight piles in soft clay	Model 15
15 ft. Fixed head straight piles in stiff clay	Model 16
30 ft. Pinned head pile group with batter piles	Model 17
15 ft. Pinned head pile group with batter piles	Model 18
30 ft. Fixed head pile group with batter piles	Model 19
15 ft. Fixed head pile group with batter piles	Model 20

2.2.2 Study of Pile-Soil Interaction

As introduced in the previous chapter, for end-bearing piles, vertical loads are transferred through the pile axially onto the bearing layer (rock for example), frictions on pile skins can be neglected (Das, 2007), and the lateral resistance on pile will be provided by soils.

Also as stated earlier, for pile-soil interactions analysis, the p-y curve method is the most widely adopted approach which assumes the soil as nonlinear springs. P represents lateral force and y accounts for the pile lateral deflection.

However, the p-y curve method is not included in most structural design and analysis software. The software assumes soil environment as linear springs. Therefore, it is not appropriate to use structural analysis software to analyze pile-soil interaction.

In this study, LPile foundation design and analysis software is used to analyze the pile behavior in the soil environment, and to determine the soil resistance for laterally loaded piles. Taking Model 1 Pile Group as an example, a typical single end-bearing Model 1 pile with laterally loaded is generated and shown in Figure 2.12. The shear force in the pile and lateral deflection of the pile are shown in Figure 2.13 and Figure 2.14, respectively. More detailed data are shown in Table 2.2 and Table 2.3, respectively.
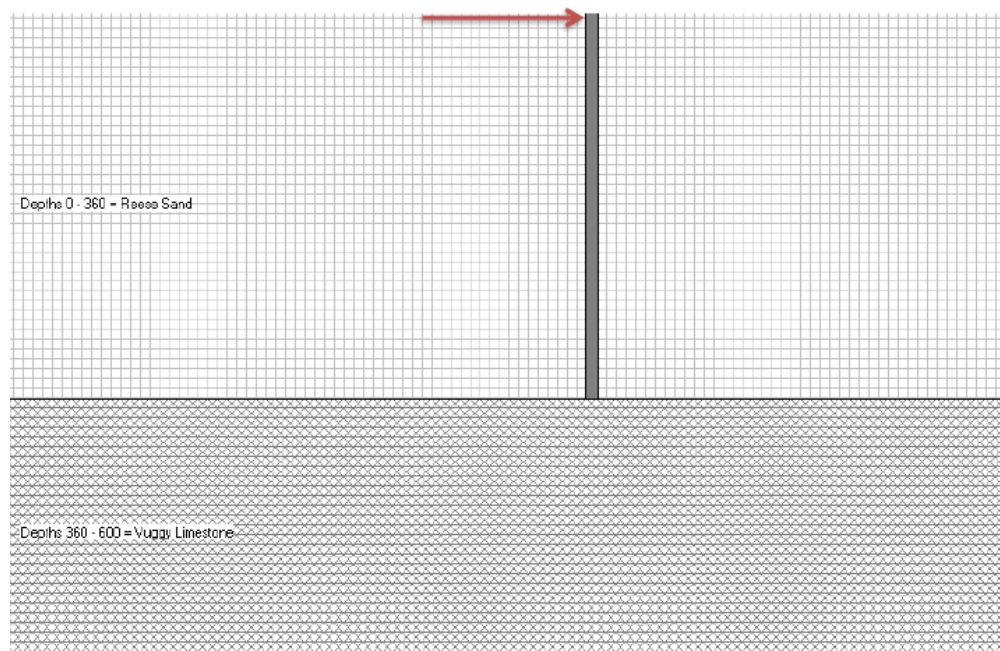
Figure 2.12 Single end-bearing Model 1 pile with laterally loaded
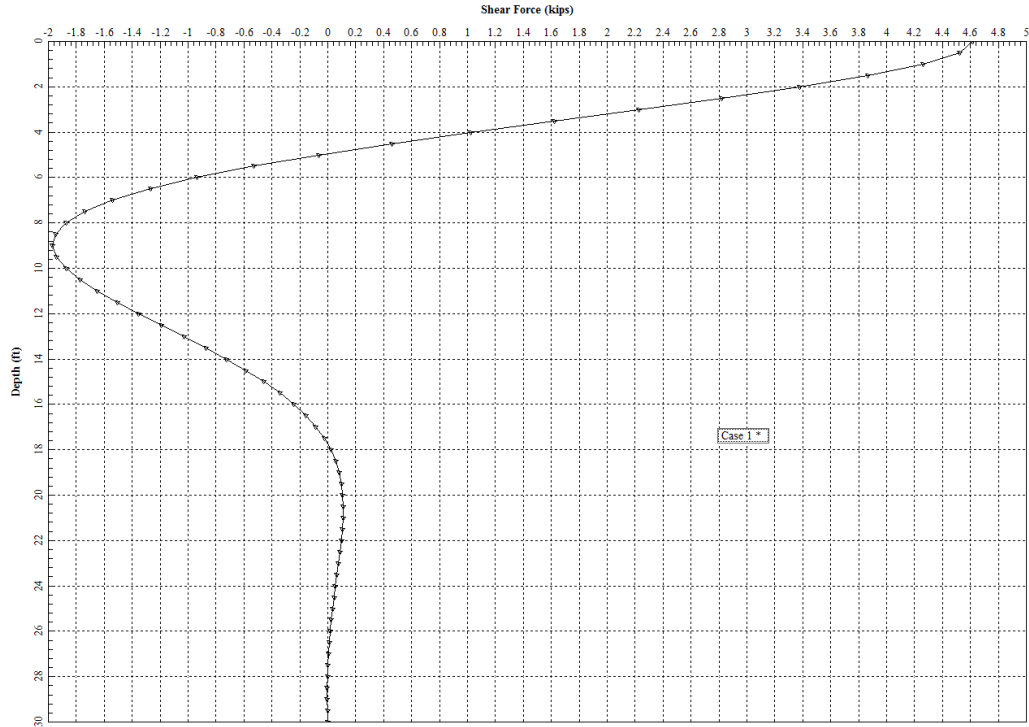
Figure 2.13 Model 1 pile shear forces along the pile length
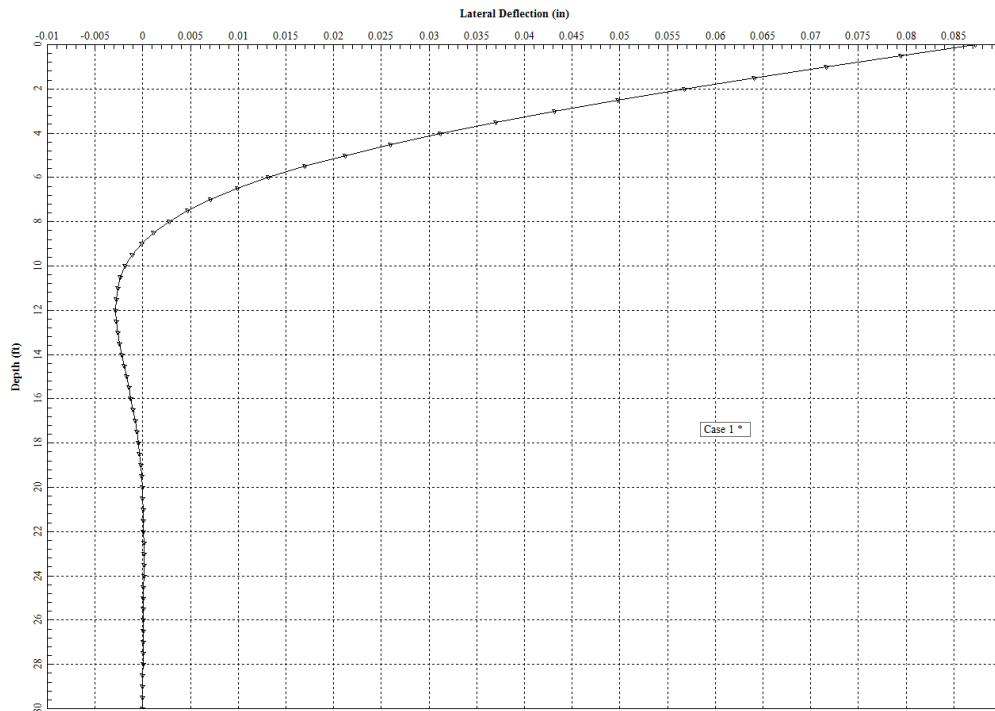
Figure 2.14 Model 1 pile lateral deflection along the pile length

Table 2.2 *Model 1 shear forces along the pile length*

Shear (kips)	Depth (ft.)	Shear (kips)	Depth (ft.)	Shear (kips)	Depth (ft.)
4.614	0	-1.7746571	10.5	0.1095355	21
4.52108962	0.5	-1.6498332	11	0.10448013	21.5
4.26046071	1	-1.5068428	11.5	0.09673526	22
3.8677177	1.5	-1.3522342	12	0.08717168	22.5
3.37690298	2	-1.1919035	12.5	0.07653232	23
2.81982244	2.5	-1.0310032	13	0.06543486	23.5
2.22548148	3	-0.8738904	13.5	0.05437864	24
1.61964816	3.5	-0.7241115	14	0.04375496	24.5
1.02455173	4	-0.5844182	14.5	0.03385967	25
0.45871665	4.5	-0.4568082	15	0.02490731	25.5
-0.0630742	5	-0.3425849	15.5	0.01704587	26
-0.5296983	5.5	-0.2424323	16	0.01037161	26.5
-0.9335098	6	-0.1564979	16.5	0.00494322	27
-1.2700713	6.5	-0.0844802	17	0.00079489	27.5
-1.5378192	7	-0.0257173	17.5	-0.0020522	28
-1.7376836	7.5	0.0207283	18	-0.0035805	28.5
-1.8726811	8	0.05598987	18.5	-0.0037687	29
-1.9474969	8.5	0.08132383	19	-0.0025878	29.5
-1.968074	9	0.09804635	19.5	0	30
-1.9412212	9.5	0.10747923	20		
-1.8742512	10	0.11090564	20.5		

Table 2.3 *Model 1 pile lateral deflection along the pile length*

Deflection(in.)	Depth (ft.)	Deflection(in.)	Depth (ft.)	Deflection(in.)	Depth (ft.)
0.08723379	0	-0.002320497	10.5	3.54E-05	21
0.079410578	0.5	-0.002634393	11	6.59E-05	21.5
0.071674589	1	-0.002793798	11.5	8.60E-05	22
0.064109536	1.5	-0.002828617	12	9.75E-05	22.5
0.056792789	2	-0.002765917	12.5	0.000102262	23
0.04979321	2.5	-0.002629757	13	0.000101722	23.5
0.043169613	3	-0.002441141	13.5	9.73E-05	24
0.036969797	3.5	-0.002218047	14	9.00E-05	24.5
0.031230105	4	-0.001975538	14.5	8.09E-05	25
0.025975432	4.5	-0.001725927	15	7.07E-05	25.5
0.021219618	5	-0.001478997	15.5	5.99E-05	26
0.016966166	5.5	-0.001242237	16	4.89E-05	26.5
0.01320919	6	-0.001021111	16.5	3.79E-05	27
0.009934548	6.5	-0.00081932	17	2.72E-05	27.5
0.007121087	7	-0.00063908	17.5	1.67E-05	28
0.00474194	7.5	-0.00048137	18	6.48E-06	28.5
0.002765833	8	-0.000346183	18.5	-3.59E-06	29
0.001158341	8.5	-0.000232742	19	-1.36E-05	29.5
-0.000116916	9	-0.000139707	19.5	-2.35E-05	30
-0.001097189	9.5	-6.53E-05	20		
-0.001819637	10	-7.68E-06	20.5		

Note that, the soil resistance is supposed to be in the opposite direction of shear forces.

Therefore, when applying soil resistance on the pile using structural analysis software NISA,

they are applied in the opposite direction of shear forces as shown in Table 2.4. To verify the

accuracy of this approach, test models are developed in NISA introduced in chapter 4, and the

results of pile deflection are compared between Lpile and NISA test models.

Table 2.4 *Model 1 pile soil resistance applied along the pile length*

Soil Resistance (kips)	Depth (ft.)	Soil Resistance (kips)	Depth (ft.)	Soil Resistance (kips)	Depth (ft.)
-0.09291038	0	0.12482388	10.5	-0.005055373	21
-0.26062891	0.5	0.14299037	11	-0.007744866	21.5
-0.39274301	1	0.15460866	11.5	-0.009563583	22
-0.49081472	1.5	0.16033065	12	-0.010639359	22.5
-0.55708054	2	0.16090028	12.5	-0.011097462	23
-0.59434096	2.5	0.15711287	13	-0.011056217	23.5
-0.60583332	3	0.149778894	13.5	-0.010623683	24
-0.59509643	3.5	0.139693229	14	-0.00989529	24.5
-0.565835081	4	0.127610041	14.5	-0.008952363	25
-0.521790824	4.5	0.114223271	15	-0.007861438	25.5
-0.466624086	5	0.100152593	15.5	-0.006674259	26
-0.403811576	5.5	0.085934452	16	-0.00542839	26.5
-0.336561493	6	0.07201765	16.5	-0.004148329	27
-0.26774786	6.5	0.058762896	17	-0.002847099	27.5
-0.19986445	7	0.046445646	17.5	-0.001528243	28
-0.13499745	7.5	0.035261566	18	-0.000188217	28.5
-0.07481578	8	0.02533396	18.5	0.001180825	29
-0.02057714	8.5	0.016722523	19	0.002587844	29.5
0.02685277	9	0.009432883	19.5	0	30
0.06697004	9.5	0.003426405	20		
0.09959412	10	-0.001370138	20.5		

CHAPTER 3

VERIFICATION OF COMPUTER SOFTWARE USING HAND CALCULATION APPROACH

3.1 Verification of LPile

There are two types of pile groups investigated: straight pile groups and pile groups with batter piles. For pile groups with batter piles, the pile foundation on river bed (offshore) situation is considered in this study. Therefore, the lateral loads are assumed to be resisted by batter piles' geometry arrangement, and there is no soil resistance provided. For straight pile groups, however, as introduced in previous chapter, the lateral loads are purely dependent on soil resistance. This research studied (1) the straight pile behaviors in three different soil materials: sand, soft clay and stiff clay; (2) two different pile lengths which are 15 ft. long and 30 ft. long; and (3) boundary conditions between pile and pile caps (fixed and pinned connections).

Model 1, the 30 ft. Long Pinned Head Straight Piles in Sand case, is taken as an illustrative example here to test the results obtained from the computer software LPile. The analysis results of Model 1 by LPile are compared with hand calculation approach results. Two parameters are compared: the lateral deflection of pile and the shear force on pile.

The test model used is a 30 feet long single straight pile embedded in sand as shown in Figure 2.12 last chapter. Below the sand layer, there is a limestone layer to provide end-bearing capacity to the pile. The pile head is pinned on the pile cap, which means the pile head can rotate freely. The lateral load applied on pile head is 4.614 kips.

According to Das (Das, 2007), pile deflection $x_z(z)$ at any depth z can be calculated by following equation:

$$x_z(z) = A_x \frac{Q_g T^3}{E_p I_p} + B_x \frac{M_g T^2}{E_p I_p} \qquad (3.1)$$

and shear force $V_z(z)$ on pile at any depth z:

$$V_z(z) = A_v Q_g + B_v \frac{M_g}{T} \qquad (3.2)$$

Where,

A_x, B_x, A_v, B_v are coefficients given by Das (Das, 2007)

Q_g is the lateral load;

M_g is the pile head rotation moment;

E_p is the modulus of elasticity in the pile material;

I_p is the moment of inertia of the pile section;

T is the characteristic length of the soil-pile system;

And,

$$T = \sqrt[5]{\frac{E_p I_p}{n_h}} \qquad (3.3)$$

In which, n_h is the constant of modulus of horizontal subgrade reaction of granular material. It is taken as 65 lb/in.^{3} for sand material (Das, 2007; LPile, 2004). The pile used in this study is HP12×53 steel pile. Therefore, E_p is 29000 kips/in.^{2} and I_p is 394 in.^{4} (AISC, 2011).

Thus,

$$T = \sqrt[5]{\frac{29000000 \text{ lb/in.}^2 \times 394 \text{ in.}^4}{65 \text{ lb/in.}^3}} = 44.56523 \text{ in.}$$

Test pile length $L = 30$ ft. $= 360$ in. $> 5T = 222.83$ in., consider test pile as long pile (When $L < 2T$, consider pile as short pile). Since test model is only loaded by horizontal force, and $A_x = 2.435$, $A_v = 1.0$ for depth $z = 0$ (Das, 2007), pile head deflection and pile head shear equals:

$$x_z(0) = 2.435 \times \frac{4614 \text{ lbs} \times (44.56523 \text{ in.})^3}{29000000 \text{ lb/in.}^2 \times 394 \text{ in.}^4} = 0.08703 \text{ in.}$$

$$V_z(0) = 1.0 \times 4614 \text{ lbs} = 4.614 \text{ kips}$$

Applying the same calculation approach, pile deflection and shear forces at other depths are easily obtained. The hand calculation results are shown in Table 3.1 and Table 3.2, respectively. Compared with LPile analysis results shown in Figure 2.13, Figure 2.14, Table 2.2 and Table 2.3, the difference between hand calculation approach and software analysis is within 0.2 %.

Table 3.1 *Test pile lateral deflection at different depth*

Depth z (ft.)	A_x	Deflection x_z(z) (in.)
0	2.435	0.08703
0.371376934	2.273	0.08124
0.742753868	2.112	0.075486
1.114130802	1.952	0.069767
1.485507736	1.796	0.064192
1.85688467	1.644	0.058759
2.228261605	1.496	0.053469
2.599638539	1.353	0.048358
2.971015473	1.216	0.043462
3.342392407	1.086	0.038815
3.713769341	0.962	0.034383
4.456523209	0.738	0.026377
5.199277077	0.544	0.019443
5.942030945	0.381	0.013617
6.684784814	0.247	0.008828
7.427538682	0.142	0.005075
11.14130802	-0.075	-0.00268
14.85507736	-0.05	-0.00179
18.5688467	-0.009	-0.00032

Table 3.2 *Shear forces on test pile at different depth*

Depth z (ft.)	A_v	Shear V_z(z) (in.)
0	1	4.614
0.371376934	0.989	4.118196
0.742753868	0.956	3.980784
1.114130802	0.906	3.772584
1.485507736	0.84	3.49776
1.85688467	0.764	3.181296
2.228261605	0.677	2.819028
2.599638539	0.585	2.43594
2.971015473	0.489	2.036196
3.342392407	0.392	1.632288
3.713769341	0.295	1.22838
4.456523209	0.109	0.453876
5.199277077	-0.056	-0.23318
5.942030945	-0.193	-0.80365
6.684784814	-0.298	-1.24087
7.427538682	-0.371	-1.54484
11.14130802	-0.349	-1.45324
14.85507736	-0.106	-0.44138
18.5688467	0.015	0.06246

3.2 Verification of NISA

3.2.1 Concrete Element Geometry Nonlinear Analysis Verification

NISA DISPLAY III/IV (NISA, 2003) finite element analysis software is used to perform

the analyses for all of the models in this study. To verify the results of the finite element analysis,

a simple cantilever column was developed. The percentage difference between the lateral

displacements generated by the finite element analysis and the hand calculation approach given

by the ASCE 7-10 manual (ASCE, 2010) is used as the verification measurement.

All of the models in this study use reinforced concrete with compressive strength of 4000

psi, and Poisson's ratio of 0.2 (Wang et al., 2007) for pier constructions. For normal weight,

normal density of concrete, the modulus of elasticity $E_c = 57000\sqrt{f_c'}$ is permitted to use by

ACI code (ACI, 2014).

A nonlinear static analysis which considers geometry nonlinearity is used to analysis

structure under P-delta effect. The height and width of the test model with a fixed base is shown

in Figure 3.1. The model is loaded with a random load of 2 kips time-step incremental lateral

load in 10 steps of 0.2 kips applied each step. At the same time, a random load of 20 kips as

constant vertical load is assigned to the top. The lateral displacements result of NISA for the

linear static analysis with solely lateral force loaded is 0.662 in.; while the lateral displacement

for the nonlinear static analysis for both lateral and vertical forces is 0.700 in. Figures 3.2 and 3.3
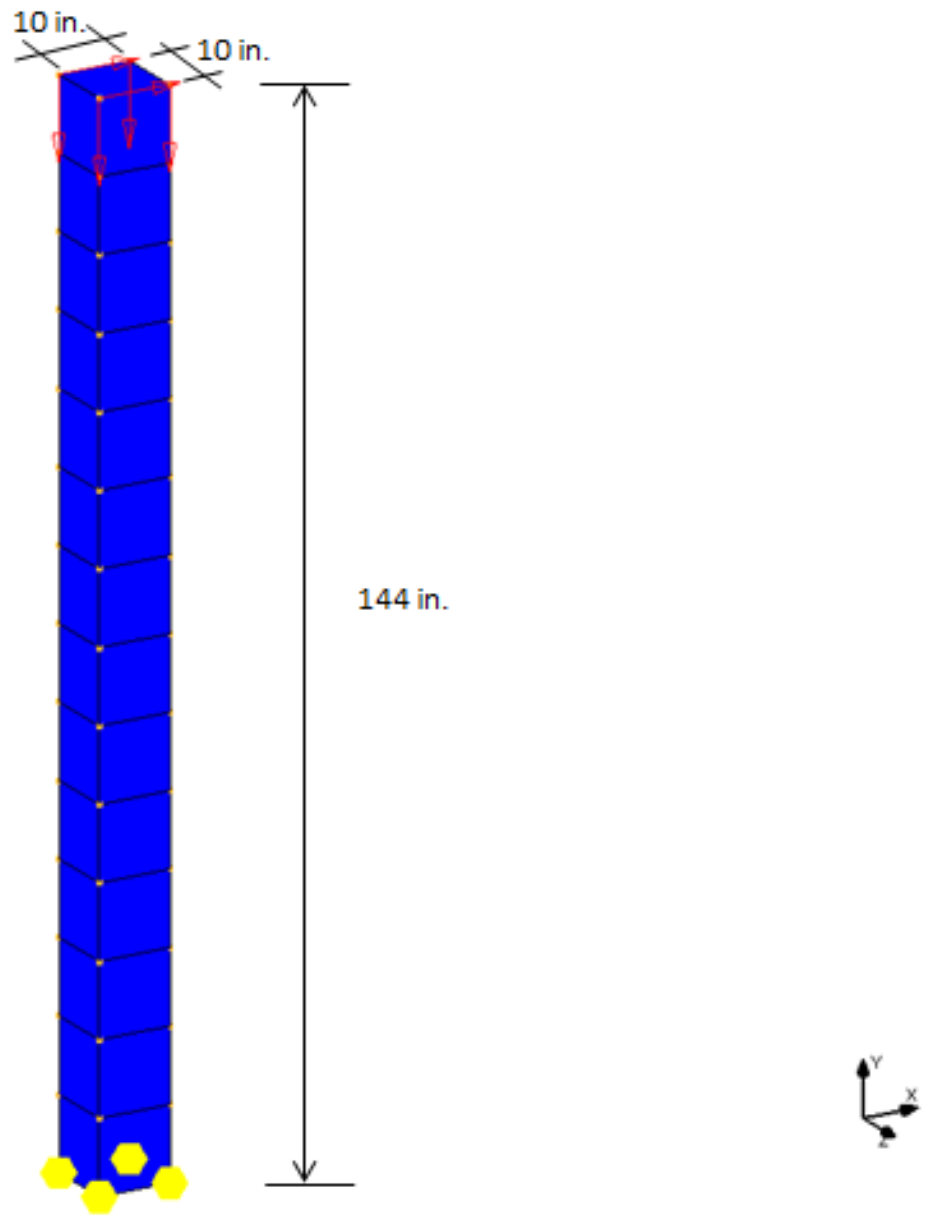
indicate the displacements.

Figure 3.1 Cantilever column test model
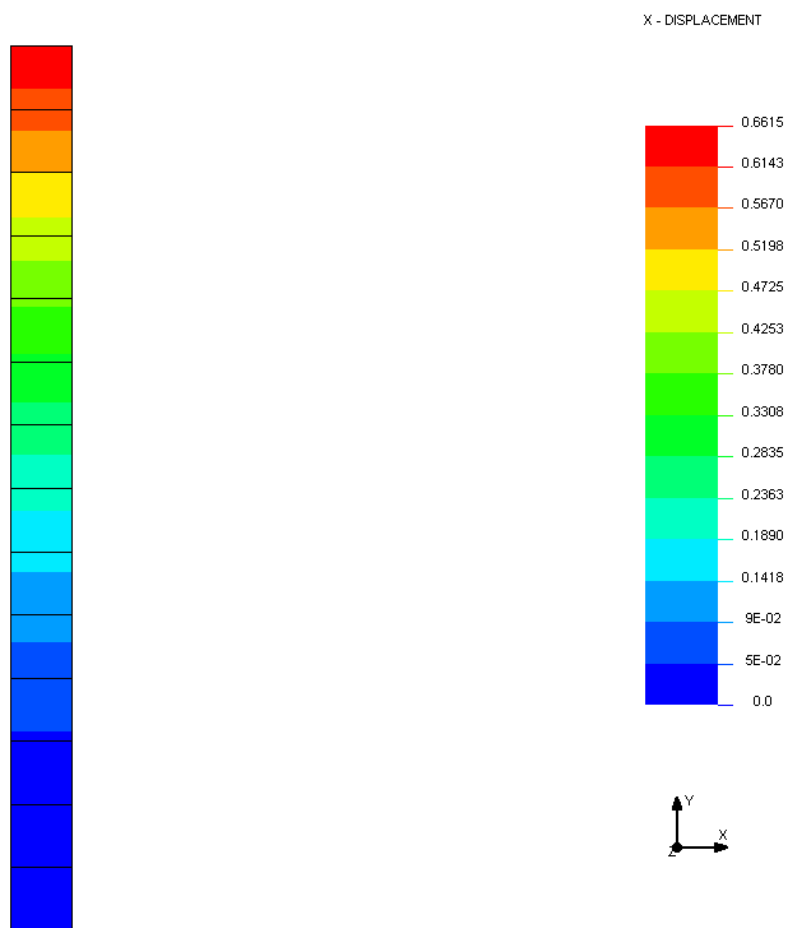
Figure 3.2 Lateral displacement of the concrete test model under lateral load only

X - DISPLACEMENT

0.7005
0.6505
0.6004
0.5504
0.5004
0.4503
0.4003
0.3502
0.3002
0.2502
0.2001
0.1501
0.1001
5E-02
0.0

Y
X
Z

TIME 0.10000E+02

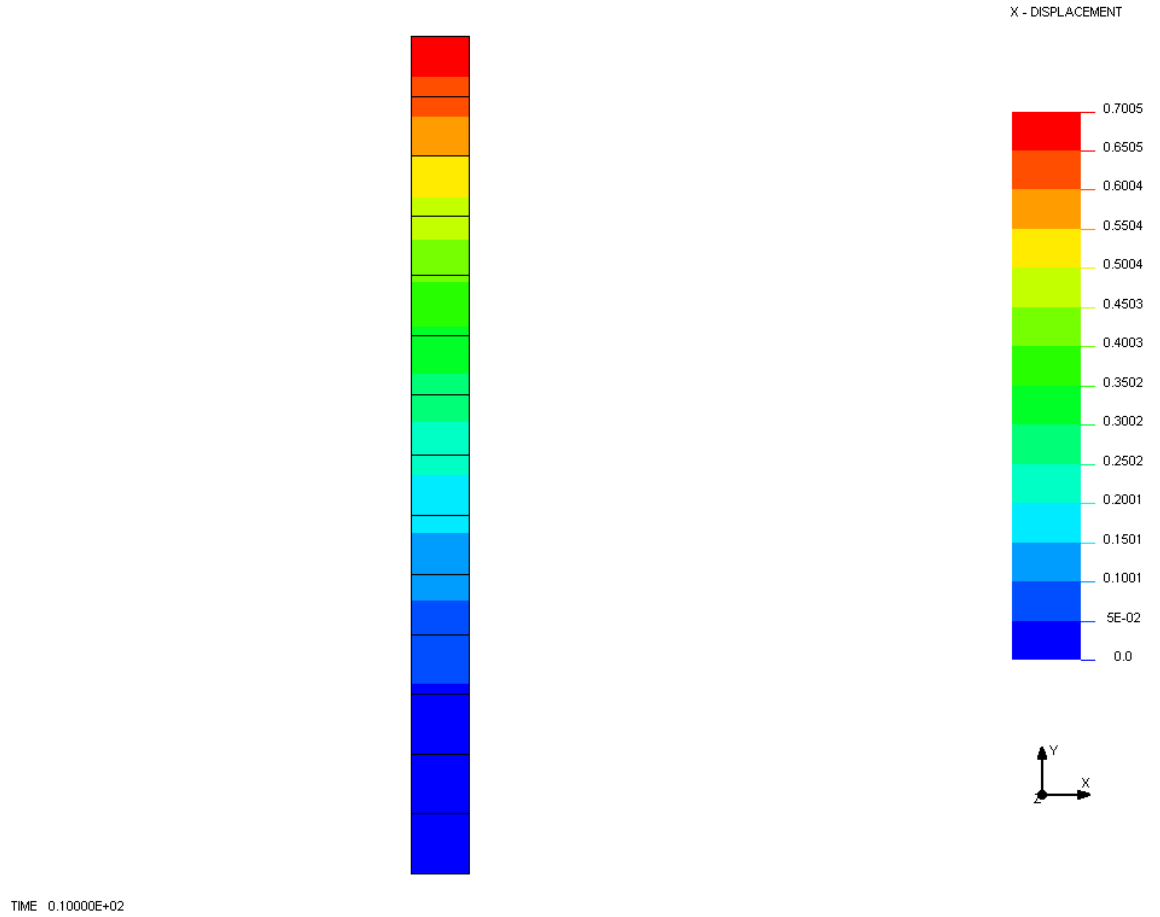*Figure 3.3* Lateral displacement of the concrete test model under lateral load and vertical

load

For hand calculation approach, similar to Equation 1.2, the elastic lateral displacement of the test model due to lateral force only is calculated by following equation provided by ASCE (ASCE, 2010):

$$\delta_{xe} = \frac{HL^3}{3E_cI_c} = \frac{2 \text{ kips} \times (144 \text{ in.})^3}{3 \times 3605 \text{ ksi} \times 833.33 \text{ in.}^4} = 0.663 \text{ in.}$$

Where,

H is the lateral force;

L is the length of the structure element;

E_c is the modulus of elasticity for concrete; and

I_c Is the moment of inertia of concrete section

The elastic displacement is multiplied by the amplification factor $1.0/(1.0 - \theta)$ to account the P-delta effect. The θ value can be calculated as:

$$\theta = \frac{P_x\delta_{xe}}{V_xh_{sx}} = \frac{20 \text{ kips} \times 0.663 \text{ in.}}{2 \text{ kips} \times 144 \text{ in.}} = 0.0460$$

Where,

P_x is the total vertical design load at and above Level x;

V_x is the lateral force acting between Levels x and x-1 (which equals the sum of the lateral forces at and above Level x); and

h_{sx} is the story height below Level x.

Therefore, the total elastic story drift due to P-delta effect is:

$$\Delta = \left[\frac{1}{1-\theta}\right] \times \delta_{xe} = \left[\frac{1}{1-0.0460}\right] \times 0.663 \text{ in.} = 0.695 \text{ in.}$$

Table 3.3 *Comparison of hand calculation and NISA results for the concrete element*

	Lateral Displacement with Lateral Load Only (in.)	Lateral Displacement With Lateral Load and Vertical Load (P-delta Effect) (in.)
Hand Calculation	0.663	0.695
NISA Results	0.662	0.700
Percentage Difference	0.2%	0.8%

The accuracy of the finite element elastic static analysis (lateral load only) and the procedure using time-step applied to control incremental lateral load for nonlinear static analysis (lateral load plus vertical load) of concrete elements have been verified from above results.

3.2.2 Steel Element Geometry Nonlinear Analysis Verification

A572 G50 Steel is used for all of the pile members in this study, with a Poisson's ratio of 0.3, and a Modulus of Elasticity of 29000 ksi.

A Cantilever column test model with same dimensions and loading conditions is used for steel material's nonlinear analysis verification as shown in Figure 3.1. The lateral displacements result for the linear static analysis with solely lateral force loaded is 0.0819 in.; while the lateral displacement for the nonlinear static analysis for both lateral and vertical forces is 0.0825 in. Figures 3.4 and 3.5 indicate the displacements.
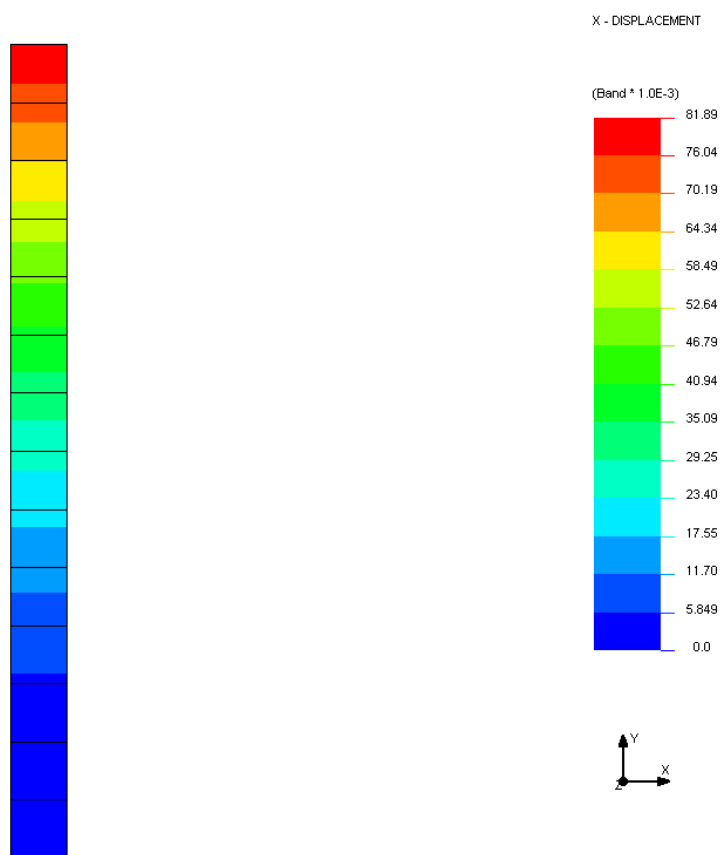
Figure 3.4 Lateral displacement of the steel test model under lateral load only

X - DISPLACEMENT

(Band * 1.0E-3)

82.45

76.56

70.67

64.78

58.89

53.00

47.12

41.23

35.34

29.45

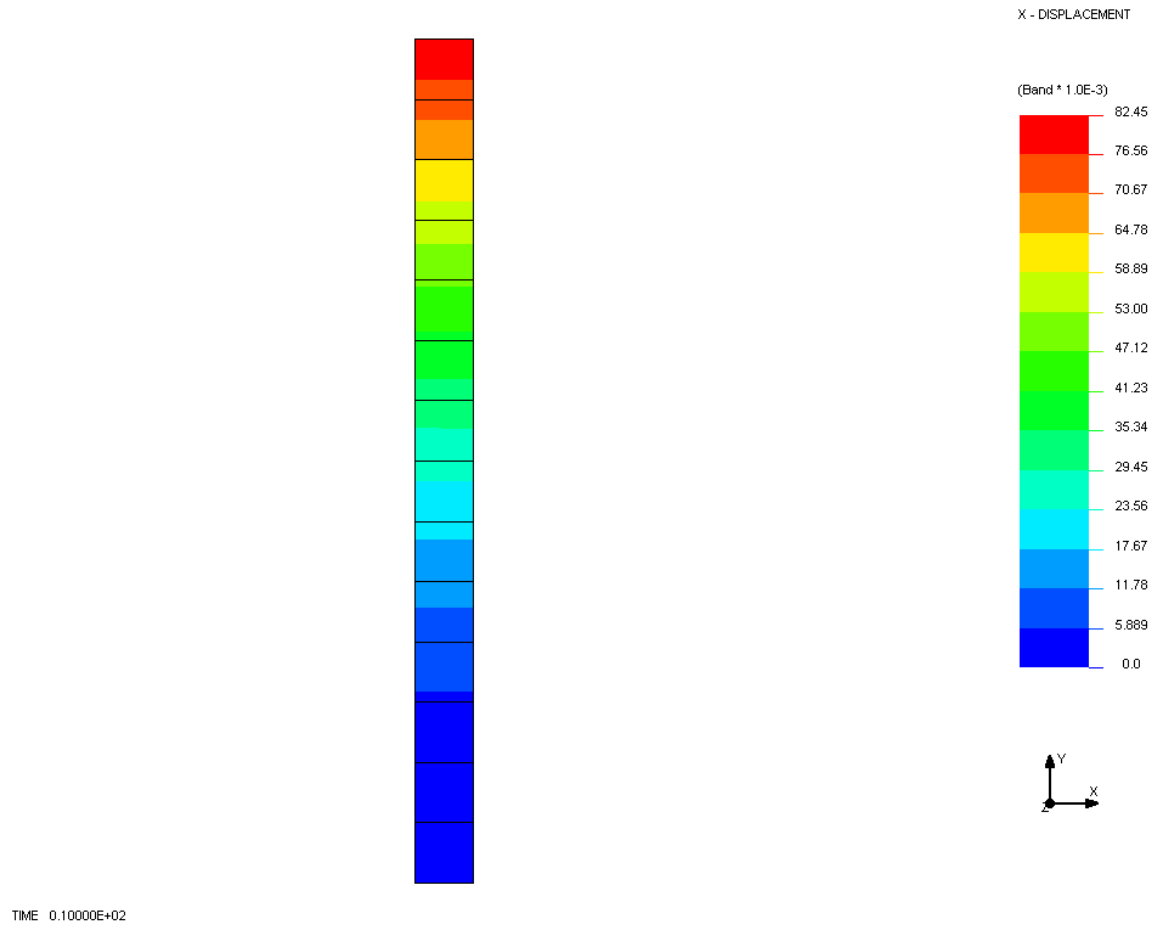23.56

17.67

11.78

5.889

0.0

TIME 0.10000E+02

Figure 3.5 Lateral displacement of the steel test model under lateral load and vertical

load

For the hand calculation approach, the elastic lateral displacement of test model due to lateral force only is calculated:

$$\delta_{xe} = \frac{HL^3}{3E_s I_s} = \frac{2 \text{ kips} \times (144 \text{ in.})^3}{3 \times 29000 \text{ ksi} \times 833.33 \text{ in.}^4} = 0.0824 \text{ in.}$$

Thus,

$$\theta = \frac{P_x \delta_{xe}}{V_x h_{sx}} = \frac{20 \text{ kips} \times 0.082372 \text{ in.}}{2 \text{ kips} \times 144 \text{ in.}} = 0.00572$$

The total elastic story drift due to P-delta effect is:

$$\Delta = \left[\frac{1}{1-\theta}\right] \times \delta_{xe} = \left[\frac{1}{1-0.00572}\right] \times 0.0824 \text{ in.} = 0.0828 \text{ in.}$$

Table 3.4 *Comparison of hand calculation and NISA results for steel*

	Lateral Displacement with Lateral Load Applied Only (in.)	Lateral Displacement With Lateral Load and Vertical Load (P-delta Effect) (in.)
Hand Calculation	0.0824	0.0828
NISA Results	0.0819	0.0825
Percentage Difference	0.6%	0.4%

The accuracy of the finite element elastic static analysis (lateral load only) and the procedure using time-step applied to control incremental lateral load for nonlinear static analysis (lateral load plus vertical load) of steel elements have been verified from above results.

CHAPTER 4

FINITE ELEMENT MODELS AND ANALYSIS

4.1 Geometry and Material of Models

In this study, a total of 20 models of bridge pier with various pile foundations are constructed. The model used is derived from FHWA LRFD Steel Girder Superstructure Bridge Design Example (FHWA, 2017). The typical model is a concrete pier with HP 12×53 pile groups. The layout of piles is shown in Figure 4.1, and the dimensions of the pier are shown in Figure 4.2. The minimum center to center spacing between piles has been checked, see details in Appendix A.1.
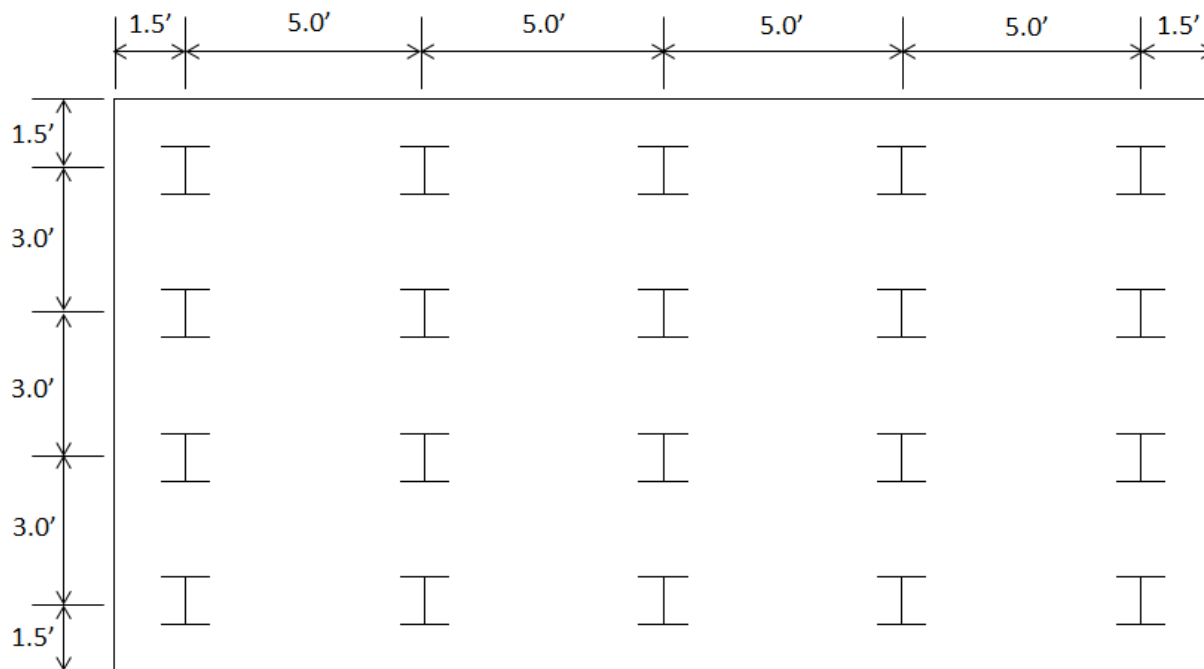
Figure 4.1 Pier pile layouts (adapted from FHWA 2017)
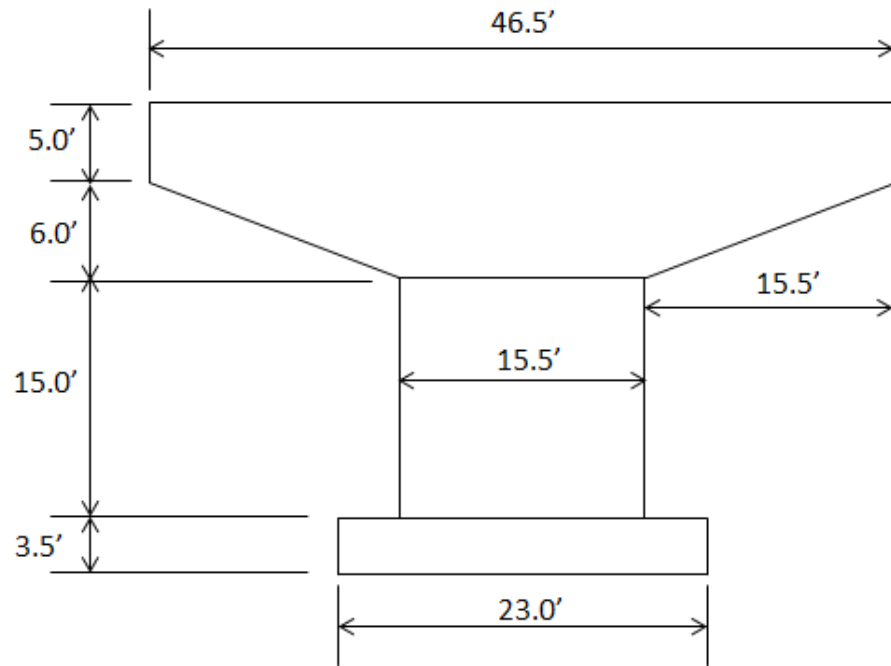
(a)
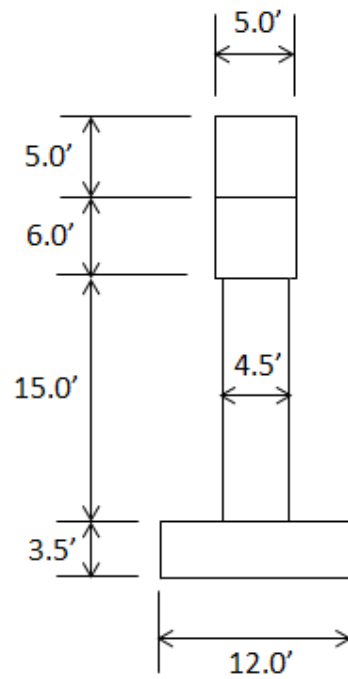
(b)

Figure 4.2 Typical pier dimensions (adapted from FHWA 2017)

Typical cases with 30 ft. long piles are shown in Figure 4.3. Typical cases with 15 ft. long piles are shown in Figure 4.4. The models contain two different materials. The pier and pile cap use $f_c' = 4000$ psi concrete, and the piles use A572 G50 steel.
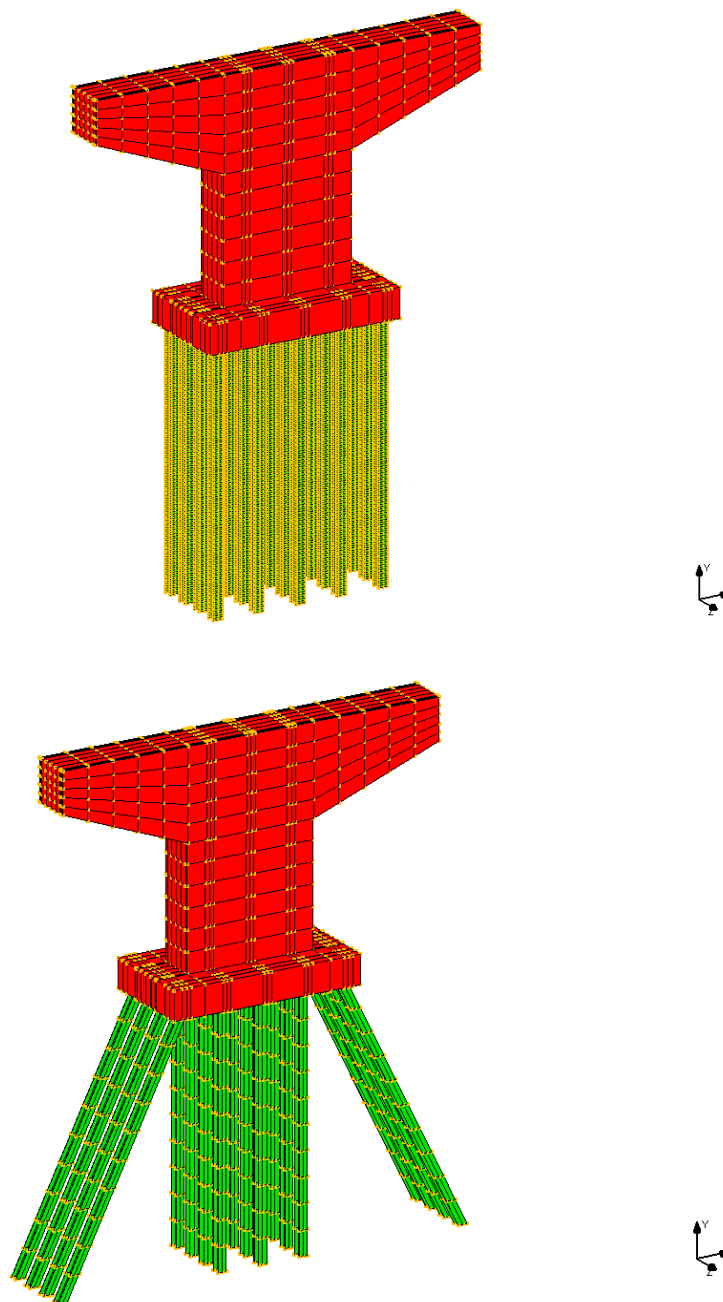

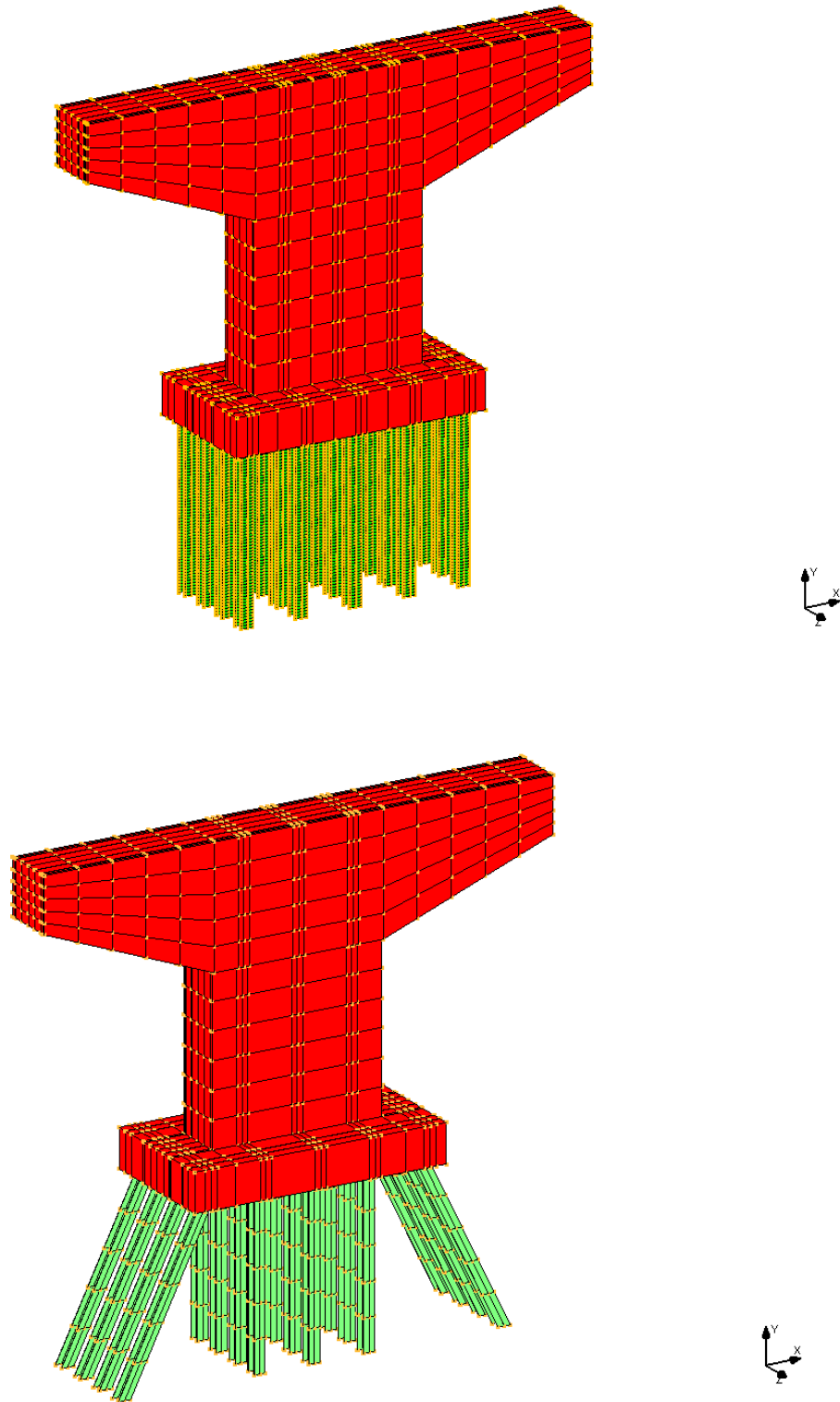*Figure 4.3* Typical cases with 30 ft. long piles

Figure 4.4 Typical cases with 15 ft. long piles

4.2 Loading and Boundary Conditions

According to the FHWA design example (FHWA, 2017), all of the models in this study are loaded with a factored vertical load of 3583 kips calculated from the combination of dead loads, live loads and other load effects, which are uniformly distributed on the top surface of pier. A factored wind load (controlling lateral load) of 92.28 kips is also applied, in which 85.93 kips of factored wind load is applied at the top of bridge pier; the remaining 6.35 kips of factored wind load is applied at the mid-height of pier shown in Figure 4.5.

For straight pile groups, lateral loads are distributed equally on to 20 piles (figure 4.2). For each pile, there are $92.28 \text{ kips}/20 \text{ piles} = 4.614 \text{ kips}$ lateral loads to resist. Thus, 4.614 kips lateral loads are applied on the head of single pile in LPile software to compute the soil resistance. For pile group with batter piles, the lateral load are majorly resisted by batter piles, in order to make sure there are no residual lateral loads left for straight piles to resist, the batter angle is given as 1: 2 as shown in Figure 4.6 (Hsiao, 2012). Batter pile angle checking details is shown in Appendix A.2.

There are two categories of models classified by boundary conditions. The first category is pile with pined head and pined bottom, which means the pile is free to rotate on both ends. Another category is piles with fixed head and pinned bottom (similar to pile head embedded into pile cap case), which means the pile is rotationally restrained on the head and free to rotate on the bottom.
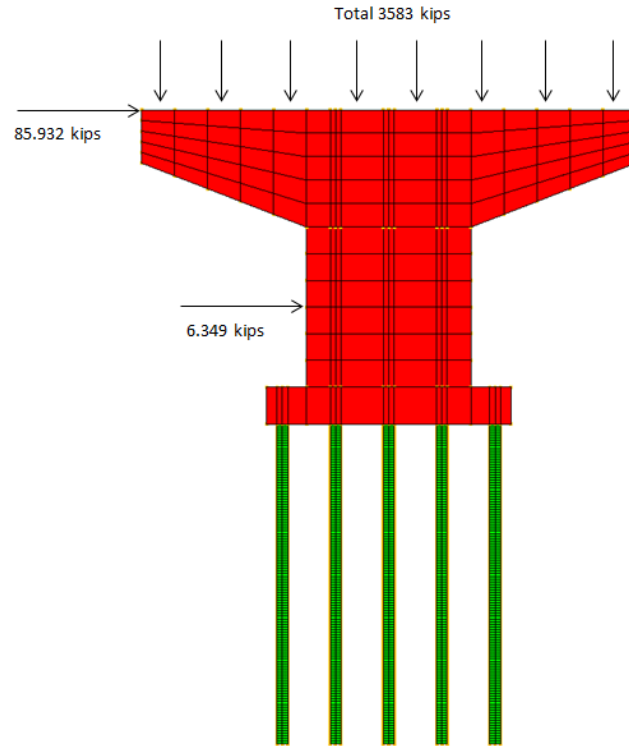
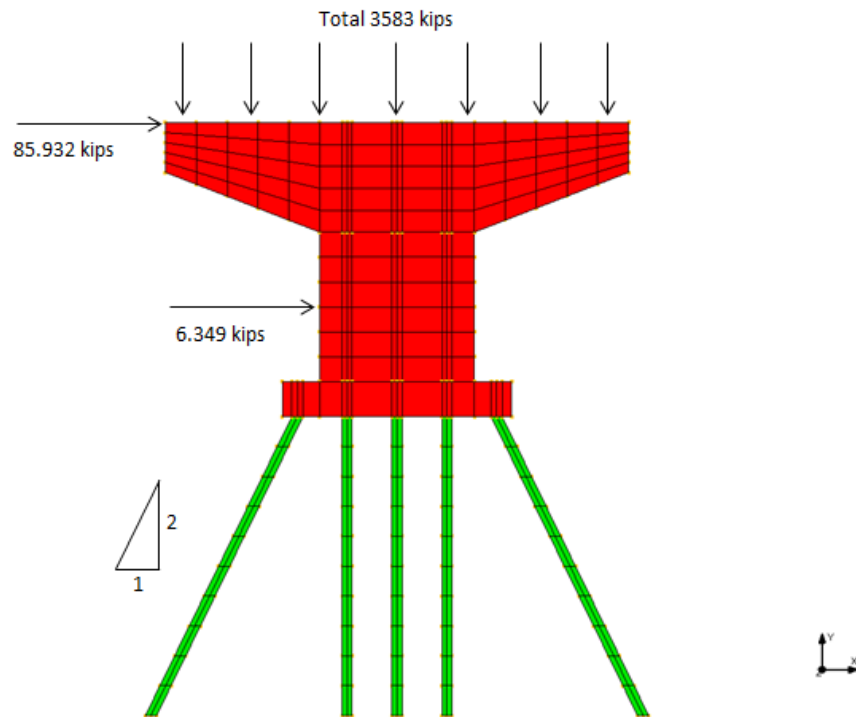*Figure 4.5* Typical loading condition on straight pile group

Figure 4.6 Typical loading condition on pile group with batter piles

**4.3 Soil Properties and Application of Soil Resistance**

As shown in Figure 2.7-Figure 2.11, totally three different types of soil and five kinds of soil layer combinations are studied in this paper. For three individual layer soil cases, each layer of soil has the same length as pile length with a layer of limestone at the bottom to provide the piles end-bearing capacity. For the two cases of three layer soil combinations, due to the scope of study and feasibility, they are only applied on 30 ft. long pile group cases, and each layer of soil is 10 ft. long also with a layer of limestone at the bottom. The end-bearing capacity for each case is sufficient verified. The detailed example is shown in Appendix A.3.

According to LPile Reference Manual (LPile, 2004) and FB-MultiPier Soil Parameter Table (FB-MultiPier , 2013), this paper used an effective unit weight of 110 psf, a friction angle of 40 degree, and a p-y modulus of 65 lbs/in^3 for sand material analysis. Soft Clay material analysis used an effective unit weight of 76 psf, an undrained cohesion C of 2.605 lbs/in^2, and a strain factor E_{50} of 0.02. Stiff clay material analysis used an effective unit weight of 106 psf, an undrained cohesion C of 10.42 lbs/in^2, and a strain factor E_{50} of 0.005. Together with limestone material which used an effective unit weight of 153 psf, and uniaxial compression strength of 15000 lbs/in^2 for analysis of determining soil resistance in LPile software. All of the soil and rock properties are shown in Table 4.1.

Table 4.1 *Soil and rock properties*

Material Type	Effective unit weight (psf)	Friction angle (degree)	Undrained cohesion C (lbs/in^2)	Strain Factor E_{50}	Uniaxial compression strength (lbs/in^2)	Subgrade Reaction Modulus ((lbs/in^3)
Sand	110	40	/	/	/	65
Soft Clay	76	/	2.605	0.02	/	/
Stiff Clay	106	/	10.42	0.005	/	/
Limestone	153	/	/	/	15000	/

After obtained the soil resistance from Lpile, a test model for straight pile groups in NISA is launched before starting the real finite element analysis for each case. Taking Model 1 as example, the soil resistance has obtained shown in Table 2.4. Thus, the test model is developed by applying soil resistance on pile groups and lateral load only on each pile head. Then pile deflection is compared between NISA and LPile to verify if NISA accounts soil resistance correctly. Figure 4.7 shows test model 1 with soil resistance applied on each pile and 4.614 kips lateral load applied on each pile head. Figure 4.8 shows the von-mises stress of analysis for test model 1, which indicated the concrete materials has a max stress smaller than its max compressive stress 4 kips, and the steel materials has a max stress smaller than its yielding stress 50.09 kips. It means the results of this model are valid. In results, Figure 4.9 shows the lateral deflection at pile head of this test model is 0.0877 in., which is about 0.6% off from LPile results shown in Table 2.3. The accuracy is verified. Therefore, typical finite element analysis models with time-step incremental lateral loads and constant vertical loads of straight pile groups and pile groups with batter piles are developed and shown in Figure 4.10 and Figure 4.11.The LPile analysis results and test model results of other cases are shown in Appendix B.
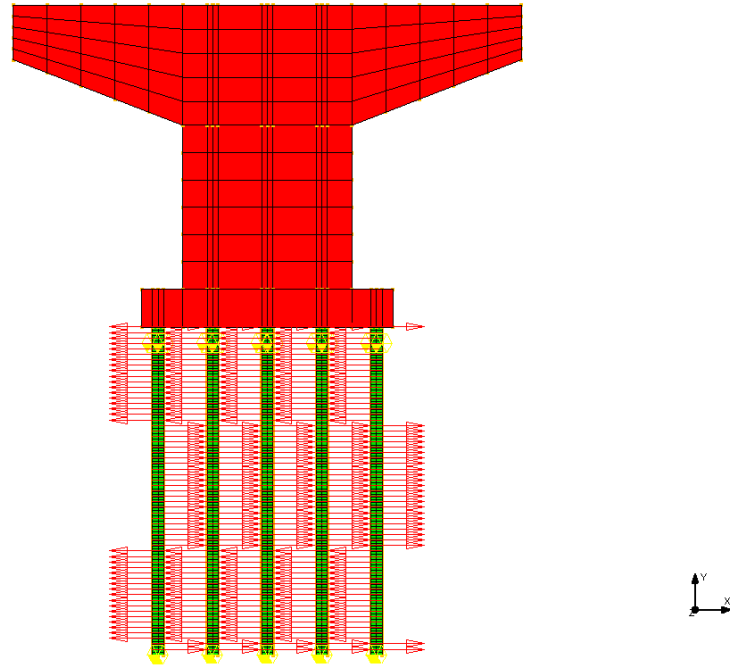
(a)
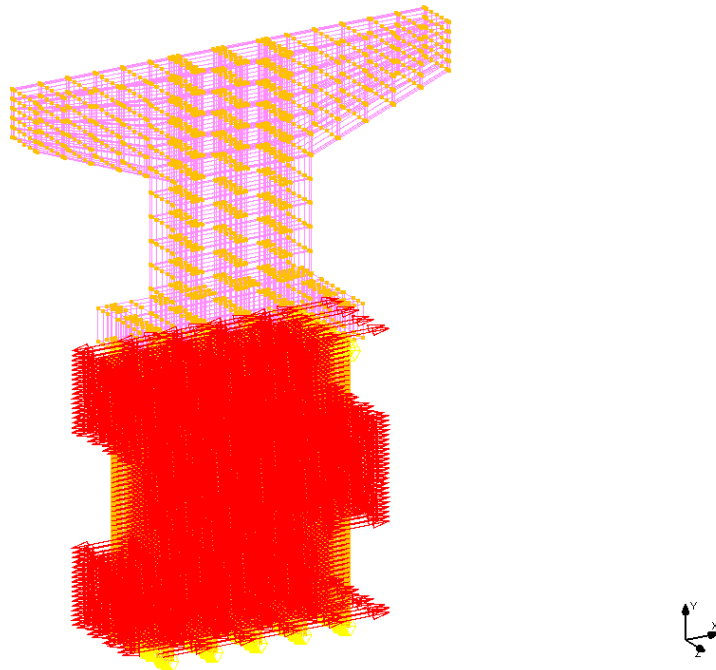
(b)

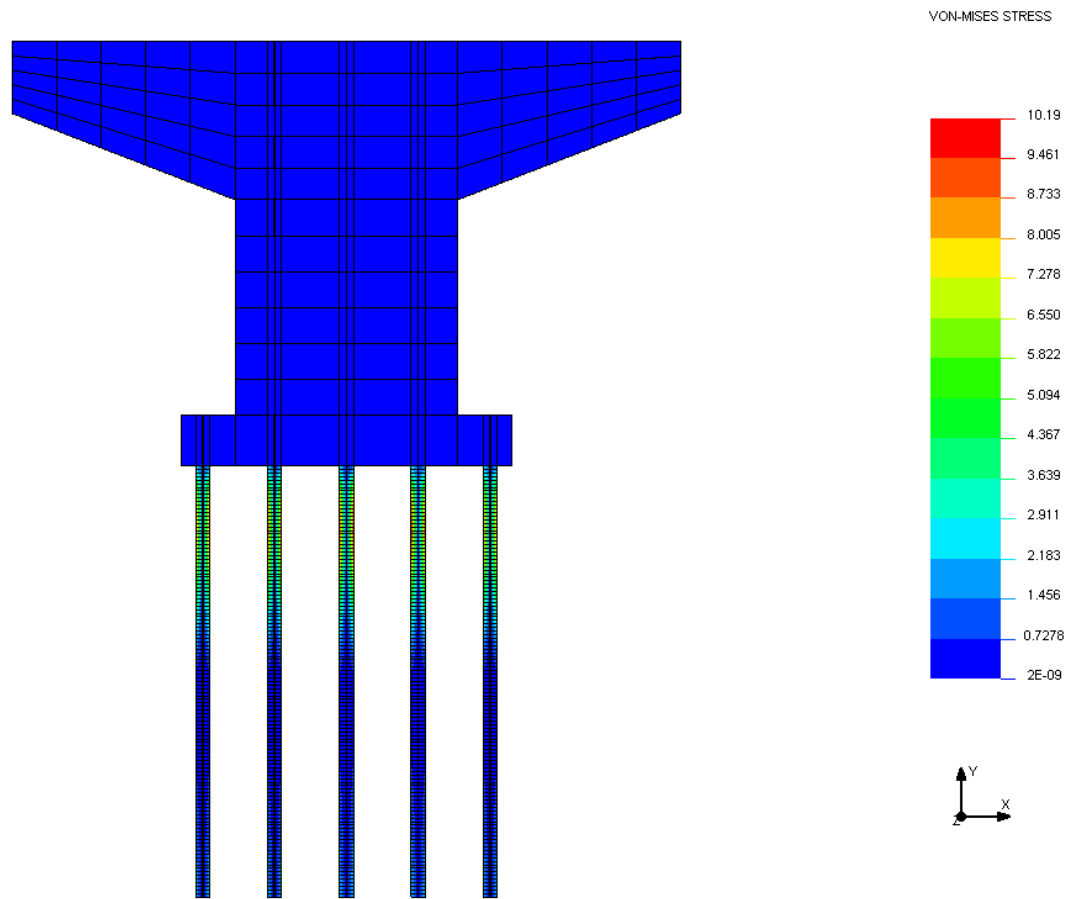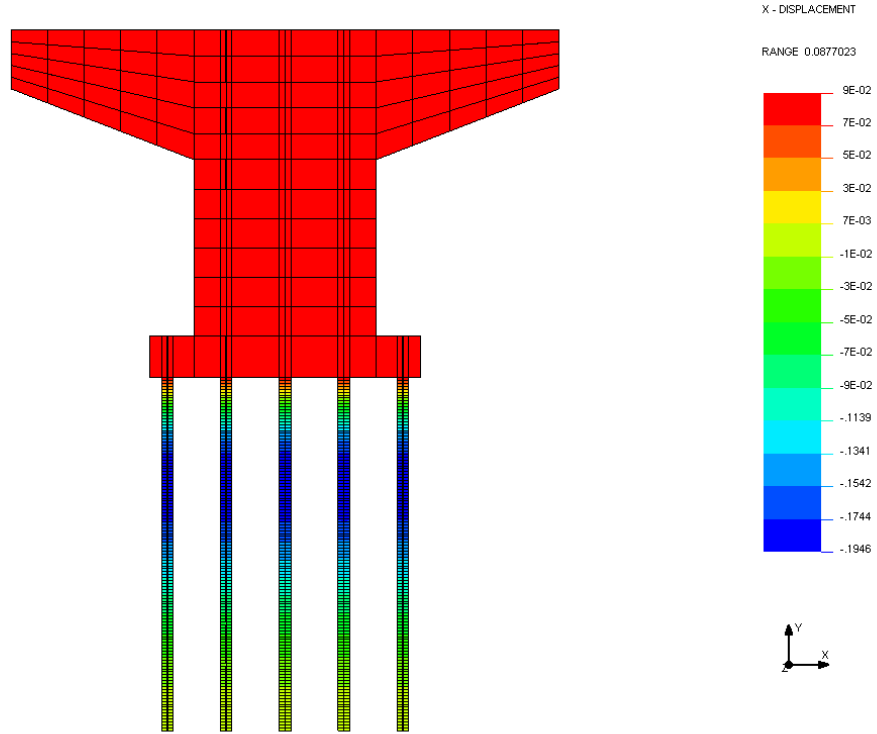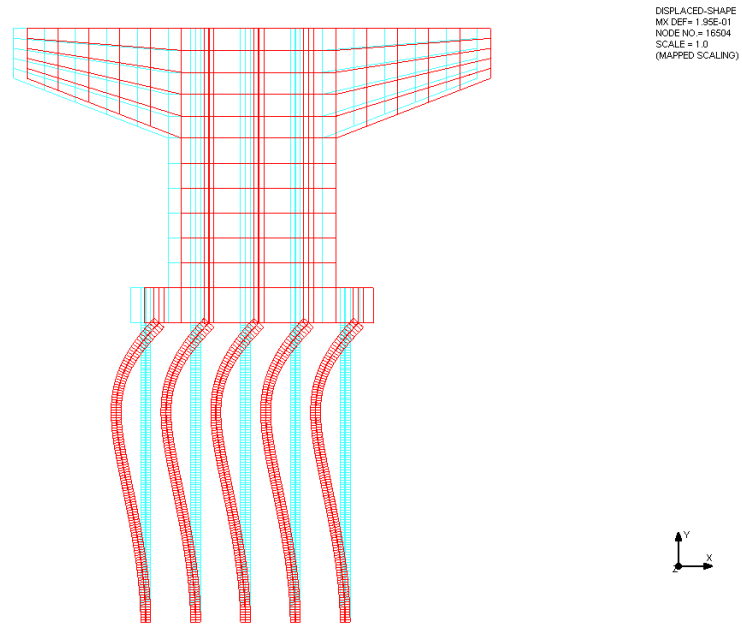*Figure 4.7* Test model (Model 1) with lateral load and soil resistance on piles in NISA
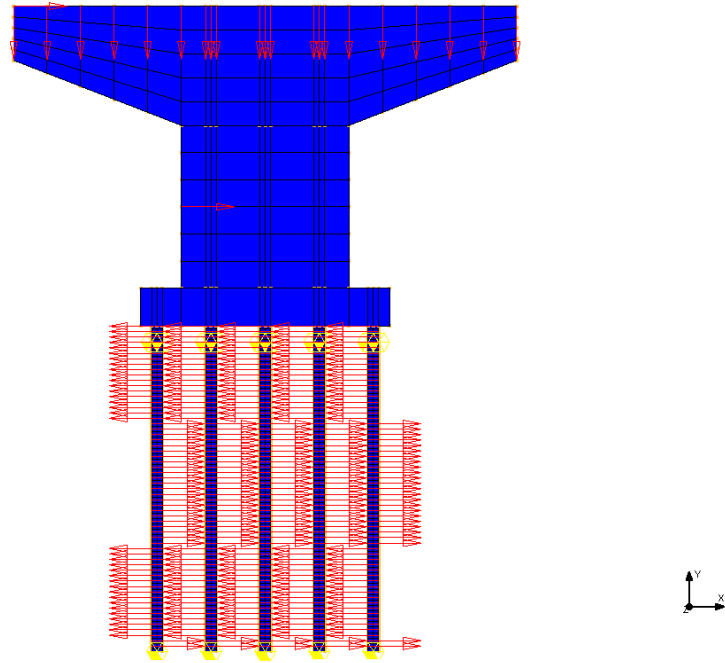
Figure 4.8 Test model (Model 1) von-mises stress
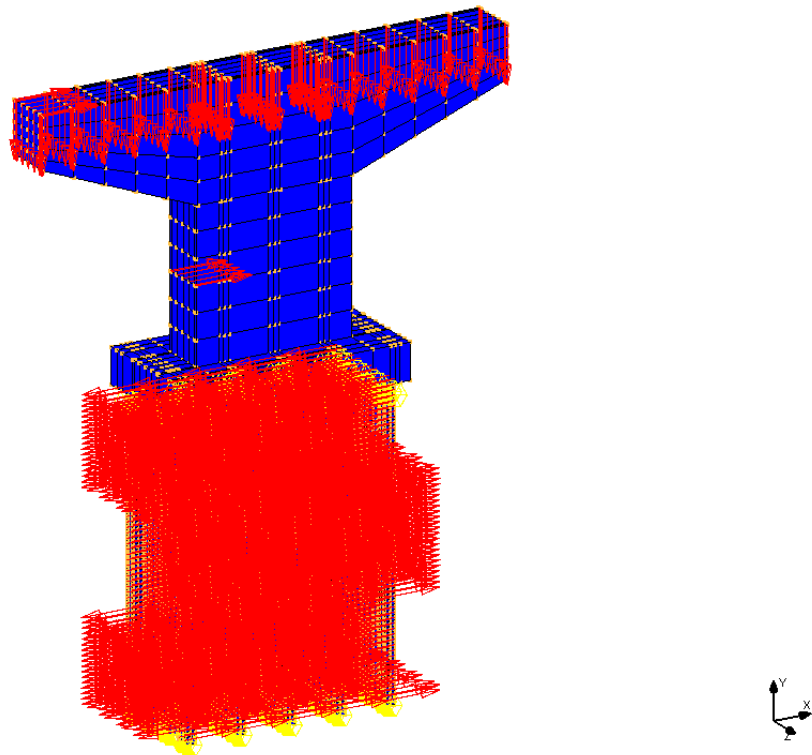
(a)

(b)

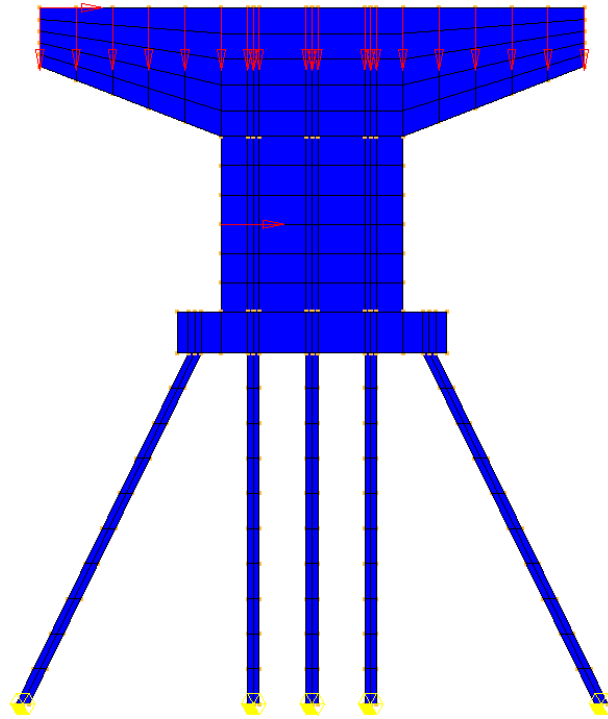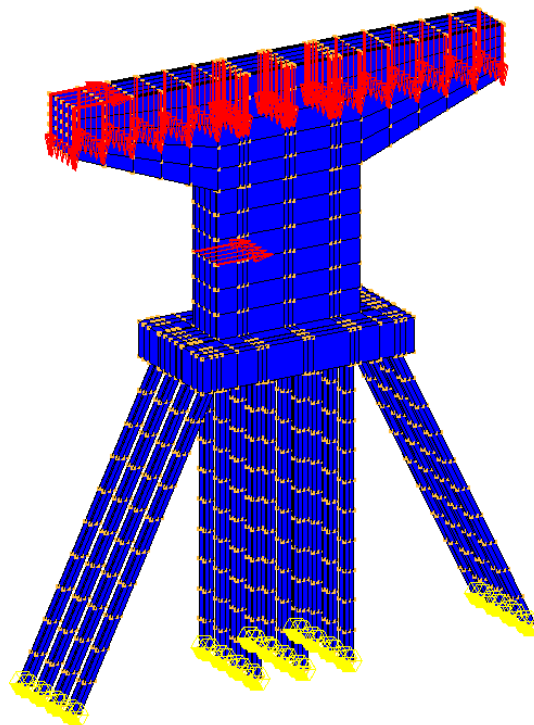*Figure 4.9* Test model (Model 1) lateral deflection

(a)

(b)

Figure 4.10 Typical finite elements analysis model for straight pile groups

(a)

(b)

Figure 4.11 Typical finite elements analysis model for pile groups with batter piles

CHAPTER 5

RESULTS

This chapter is using Model 1 as an illustrative example, while the result figures of other models are shown in Appendix C.

It is necessary to make sure that the models work properly throughout the process of the finite element analysis. As introduced in the chapter 4, von-mises stress is checked to ensure the models were working with the normal working state. Von-mises stress is related to the max compressive stress of concrete and yielding stress for steel, which are 4 kips and 50.09 kips in this study, respectively. Therefore, model 1's von-mises stress is within the allowable range as shown in Figure 5.1.

Lateral displacements of models are compared between NISA results, and refined calculation approach explained in methodology chapter. The G values computed from the deflections of real case models are compared with G=1.0 recommended by AASHTO for bridge pier footing on multiple rows of end-bearing piles case. The lateral deflection of Model 1 is shown in Figure 5.2. The relative lateral displacement obtained is $0.14881 \text{ in.} - 0.07441 \text{ in.} = 0.0744 \text{ in.}$.

According to the refined calculation approach (Hsiao and Jiang, 2014)., the relative lateral displacement is the summation of elastic displacement of pier due to lateral loads only and the displacement of pier due to the rotation for pier structure. However, for pile groups with batter piles, the relative lateral displacement equals the lateral displacement due to rotation subtract the elastic displacement due to lateral load only regarding pier's different directions of rotation.
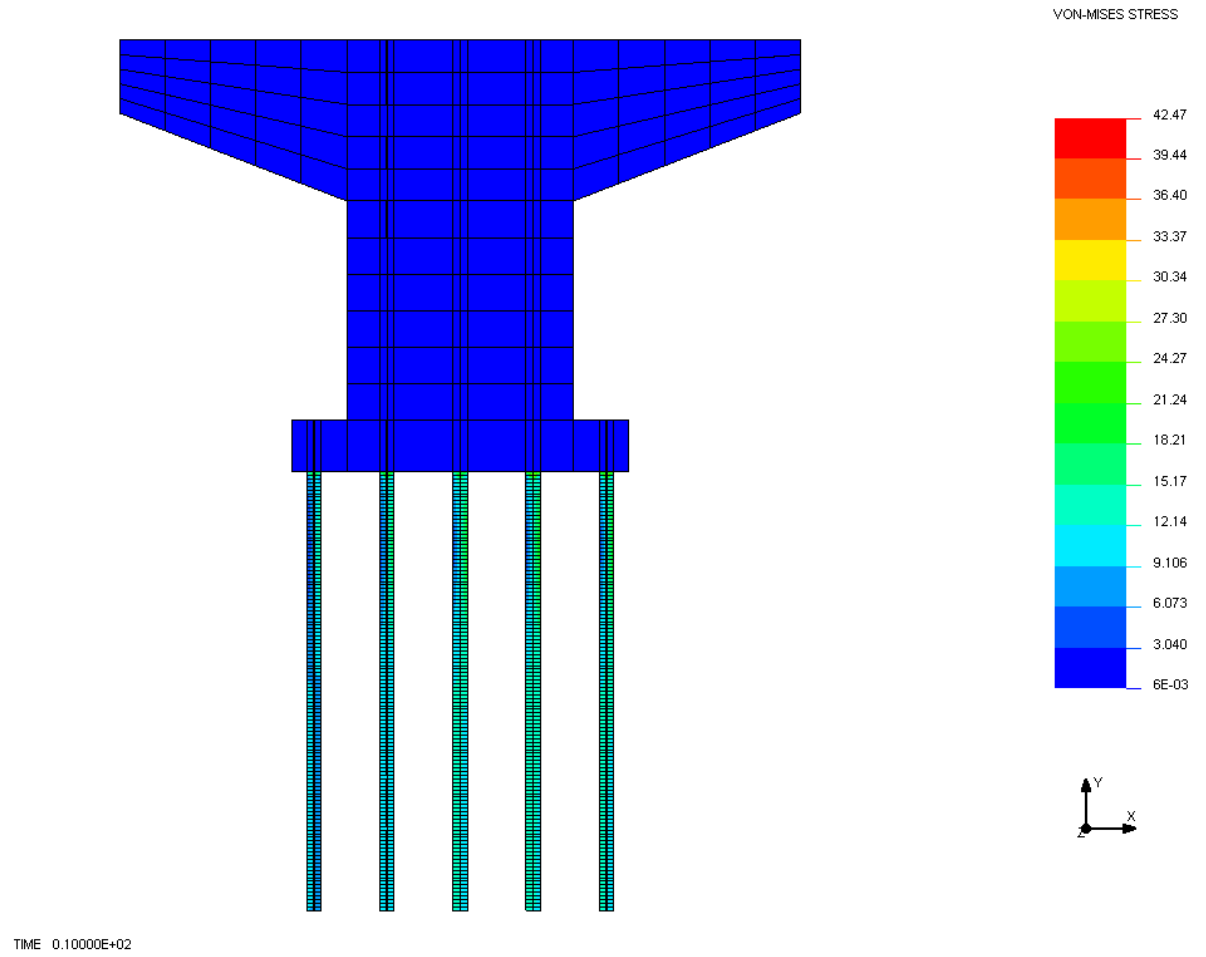
VON-MISES STRESS

	42.47
	39.44
	36.40
	33.37
	30.34
	27.30
	24.27
	21.24
	18.21
	15.17
	12.14
	9.106
	6.073
	3.040
	6E-03

TIME   0.10000E+02

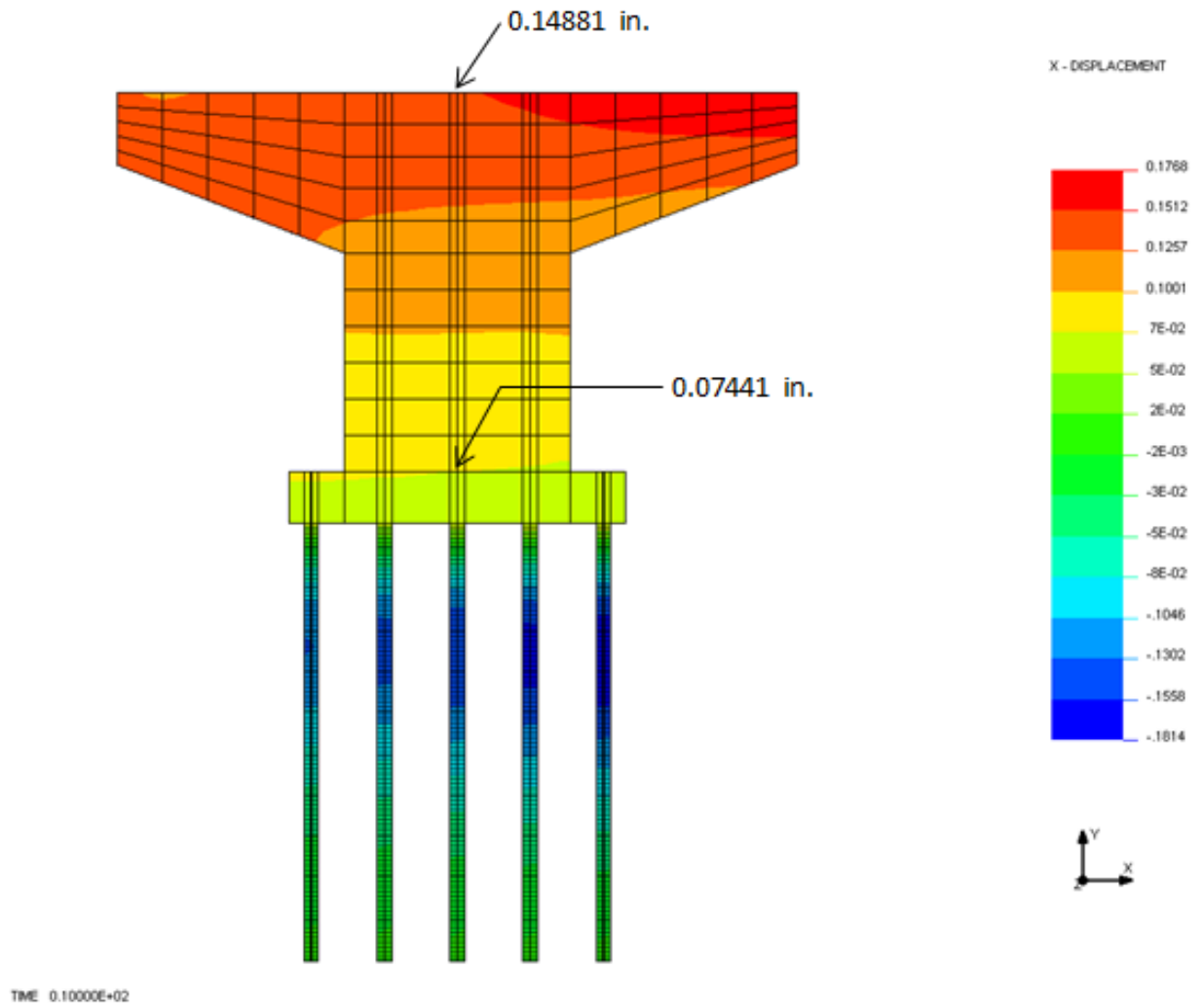*Figure 5.1* Von-mises stress of Model 1 under finite element analysis

Figure 5.2 Lateral displacement of Model 1 under finite element analysis

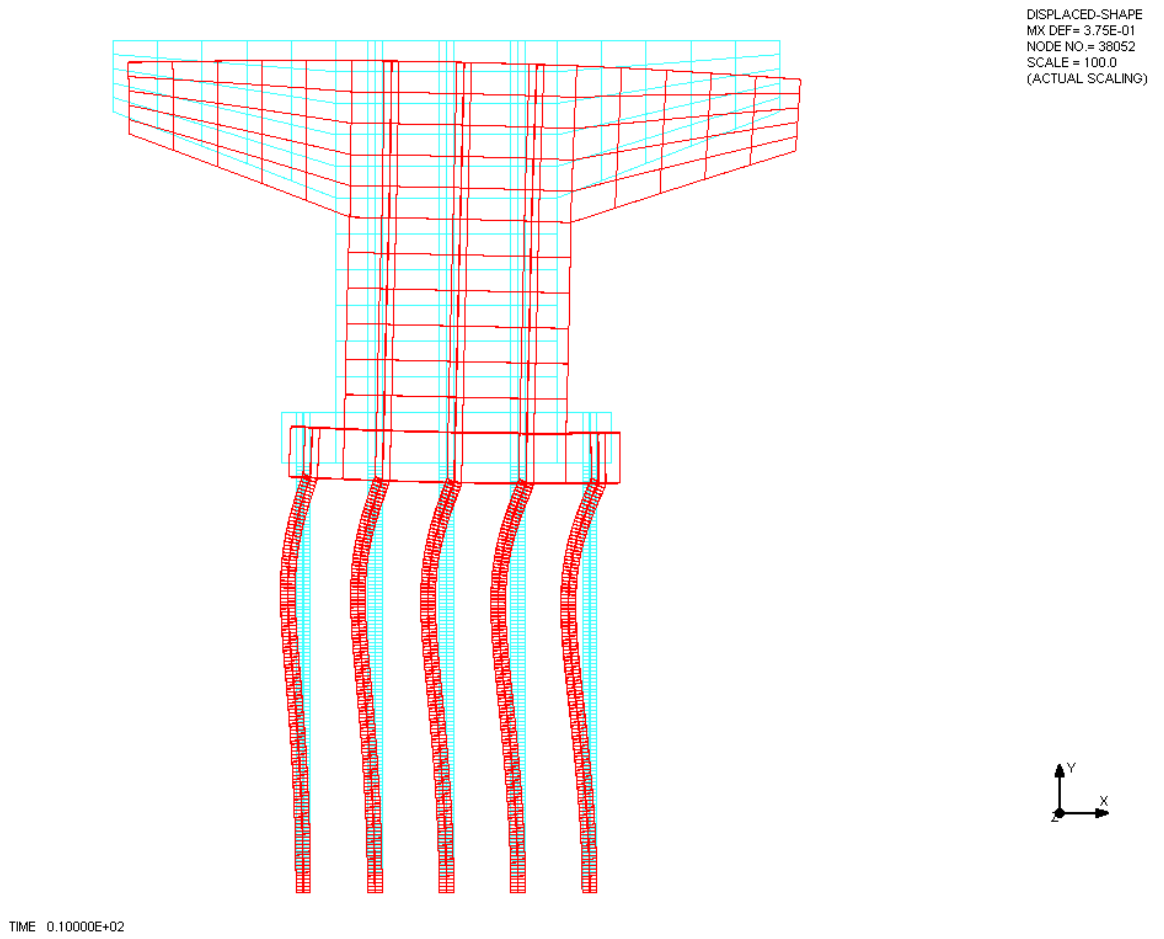*Figure 5.3* Deflection of Model 1 under finite element analysis (in scale of 100)

The entire hand calculation approach for lateral displacement and G value of Model 1 is shown as below (Hsiao and Jiang, 2014):

As known:

Factored Axial load $A_x = 3583$ kips

Factored Wind load $V = 92.28$ kips

Pier Length $L_c = 15 + 6 + 5 = 26$ ft.

The pier model is translated into equivalent tie beam system shown in Figure 5.4.
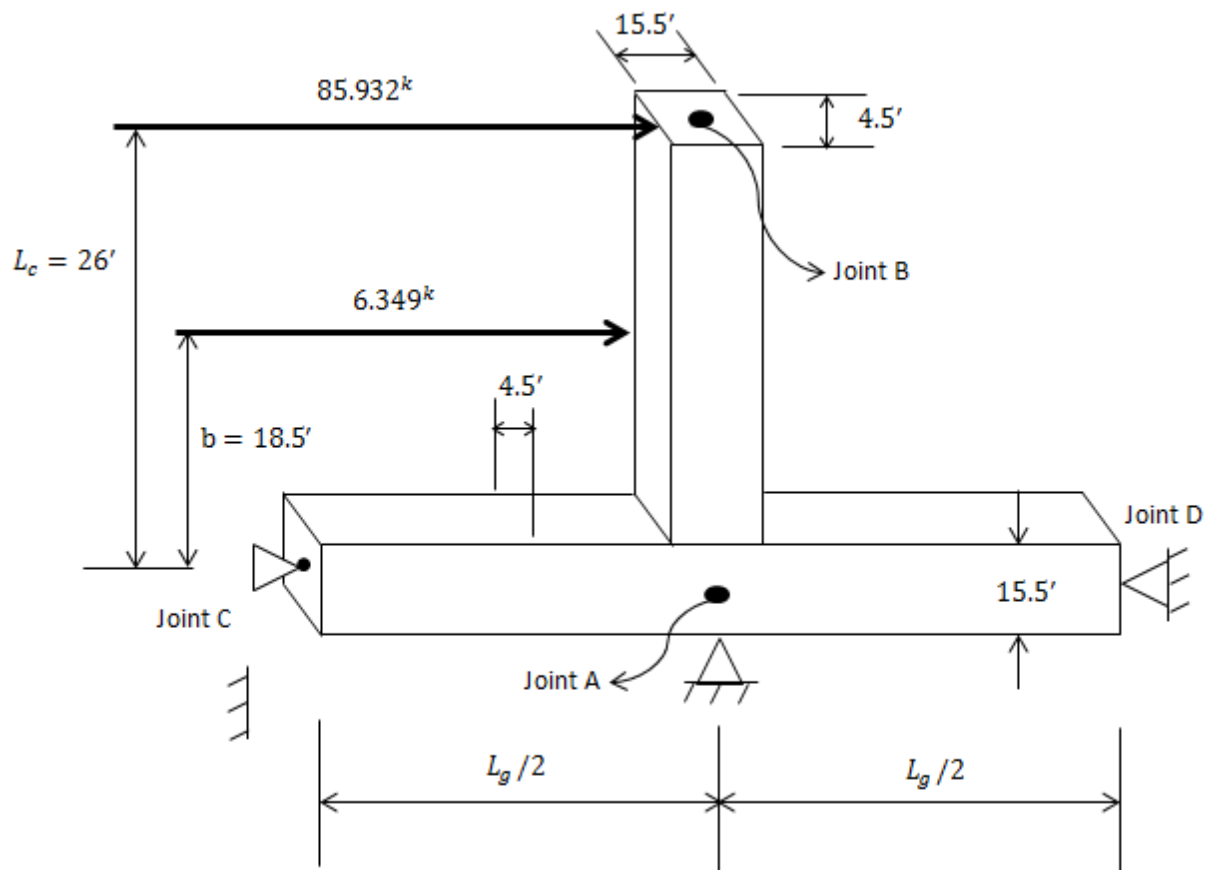
Figure 5.4 Equivalent tie beam system for pier with lateral loads only (adapted Hsiao and Jiang, 2014)

In this case, the moment of inertia of the column and beams is same as

$$I_c = I_g = \frac{4.5 \text{ ft.} \times (15.5 \text{ ft.})^3}{12} = 1396.45 \text{ ft}^4$$

.

The elastic modulus of column and beams ($f_c' = 4000$ psi concrete) is same as

$$E_c = E_g = 57000\sqrt{f_c'} = 57000 \times \sqrt{4000} \text{ psi} = 3605 \text{ ksi}$$

Therefore, the elastic lateral displacement due to lateral loads only is calculated using

Equation 1.2, Equation 1.3 and Equation 1.4 as following:

$$\delta_1 = \frac{F_1 L_c{}^3}{3E_c I_c} = \frac{85.932^k \times (26 \times 12)^3 \text{ in.}^3}{3 \times 3605 \text{ ksi} \times 1396.45 \times 12^4 \text{ in.}^4} = 0.00833 \text{ in.}$$

$$\delta_2 = \frac{F_2 b^2}{6E_c I_c}(3L_c - b) = \frac{6.349^k \times (18.5 \times 12)^2}{6 \times 3605 \text{ ksi} \times 1396.45 \times 12^4 \text{ in.}^4} \times (3 \times 26 - 18.5) \times 12 \text{ in.}$$

$$= 0.000357 \text{ in.}$$

$$\Delta_1 = \delta_1 + \delta_2 = 0.00869 \text{ in.}$$

As shown in Figure 2.3, the original beam length on both sides of joint A is $L = L_g$;

using $G_A = 1.0$ for the footing on multiple rows of end-bearing piles by AASHTO, referring to

Equation 1.5 and Figure 5.4:

$$G_A = \frac{\sum \frac{E_c I_c}{L_c}}{\sum \frac{E_g I_g}{L_g}} = 1 = \frac{\frac{E_c \times 1396.45 \text{ ft}^4}{L_c}}{2 \times \frac{E_g \times 1396.45 \text{ ft}^4}{L_g}}$$

Then,

$$L_g = 2L_c = 26' \times 2 \times 12 = 624 \text{ in.}$$

Moment caused by lateral loads is calculated using Equation 2.3 and referring to Figure

5.4 as

$$M_{AB} = 85.932^k \times 26' \times 12 + 6.349^k \times 18.5' \times 12 = 28220.262 \text{ kips} - \text{in.}$$

Using Equation 2.2 to get,

$$M_{AD} = M_{AC} = \frac{M_{AB}}{2} = 14110.131 \text{ kips} - \text{in.}$$

and since,

$$L_{AD} = \frac{L_g}{2} = \frac{624 \text{ in.}}{2} = 312 \text{ in.}$$

The rotation at the joint A of the tie beam is calculated using Equation 2.1,

$$\theta_A = \frac{M_{AD}L_{AD}}{3E_{AD}I_{AD}} = \frac{14110.131 \text{ kips} - \text{in.} \times 312 \text{ in.}}{3 \times 3605 \text{ ksi} \times 1396.45 \times 12^4 \text{ in.}^4} = 1.41 \times 10^{-5} \text{ rad}$$

Therefore, the lateral displacement of pier due to rotation is calculated using Equation

2.4,

$$\Delta_2 = L_c \times \tan \theta_A = 312 \text{ in.} \times \tan(1.41 \times 10^{-5} \text{ rad}) = 0.00439 \text{ in.}$$

And the total lateral displacement of pier is calculated using Equation 2.5

$$\Delta_3 = \Delta_1 + \Delta_2 = 0.00869 \text{ in.} + 0.00439 \text{ in.} = 0.0131 \text{ in.}$$

Since $\Delta_3 = 0.0131$ in. $< l_u/1500 = L_c/1500 = 312$ in./$1500 = 0.208$ in., for hand calculation approach, there is no need to multiply Δ_3 with the magnification factor to consider P-delta Effect. Therefore, the final lateral deflection of pier $\Delta = \Delta_3 = 0.0131$ in..

However, the relative lateral displacement obtained from NISA finite element analysis $\Delta' = \Delta'_3 = 0.0744$ in. is way larger than the hand calculation result.

Furthermore, the G value for Model 1 is obtained by reversely applying the finite element result of lateral displacement into the refined approach shown as following:

The real lateral displacement due to rotation

Using Equation 2.5:

$$\Delta'_2 = \Delta'_3 - \Delta_1 = 0.0744 \text{ in.} - 0.00869 \text{in.} = 0.0657 \text{ in.}$$

Using Equation 2.4:

$$\tan \theta'_A = \frac{\Delta'_2}{L_c} = \frac{0.0657 \text{ in.}}{312 \text{ in.}} = 0.000211$$

Using Equation 2.1:

$$\theta'_A = \frac{M_{AD} L'_{AD}}{3 E_{AD} I_{AD}} = \tan^{-1}(0.000211) = 0.000211 \text{ rad}$$

Thus, the equivalent length of AD member for Model 1 is

$$L'_{AD} = \frac{3E_{AD}I_{AD}\theta'_A}{M_{AD}} = \frac{3 \times 0.000211 \times 3605 \text{ ksi} \times 1396.45 \times 12^4 \text{ in.}^4}{14110.131 \text{ kips} - \text{in.}} = 4674.33 \text{ in.}$$

And the G value for Model 1 is calculated using Equation 1.3,

$$G'_A = \frac{\sum \frac{E_c I_c}{L_c}}{\sum \frac{E_g I_g}{L_g}} = \frac{\frac{E_c \times 1396.45 \text{ ft.}^4}{312 \text{ in.}}}{2 \times \frac{E_c \times 1396.45 \text{ ft.}^4}{2 \times 4674.33 \text{ in.}}} = 14.98$$

, which is much larger than $G_A = 1.0$ recommended by AASHTO.

By applying the same approach, G values for all other models are summarized in following Table 5.1.

Table 5.1 *NISA finite element analysis results and G values for studied cases*

Cases Studied	Model Numbers	FEM Results Δ'_3 (in.)	Pier Rotation (rad)	G
30 ft. Pinned head straight piles in sand	Model 1	0.0657	0.000211	14.98
30 ft. Pinned head straight piles in soft clay	Model 2	0.0659	0.000211	15.03
30 ft. Pinned head straight piles in stiff clay	Model 3	0.0655	0.000210	14.93
30 ft. Pinned head straight piles in (sand, soft clay, stiff clay)	Model 4	0.0657	0.000211	14.98
30 ft. Pinned head straight piles in (soft clay, sand, stiff clay)	Model 5	0.0659	0.000211	15.03
15 ft. Pinned head straight piles in sand	Model 6	0.0423	0.000136	9.64
15 ft. Pinned head straight piles in soft clay	Model 7	0.0425	0.000136	9.69
15 ft. Pinned head straight piles in stiff clay	Model 8	0.0419	0.000134	9.56
30 ft. Fixed head straight piles in sand	Model 9	0.06826	0.000219	15.56
30 ft. Fixed head straight piles in soft clay	Model 10	0.06964	0.000223	15.88
30 ft. Fixed head straight piles in stiff clay	Model 11	0.06807	0.000218	15.52
30 ft. Fixed head straight piles in (sand, soft clay, stiff clay)	Model 12	0.06822	0.000219	15.55
30 ft. Fixed head straight piles in (soft clay, sand, stiff clay)	Model 13	0.06963	0.000223	15.88
15 ft. Fixed head straight piles in sand	Model 14	0.0376	0.000121	8.57
15 ft. Fixed head straight piles in soft clay	Model 15	0.0385	0.000123	8.77
15 ft. Fixed head straight piles in stiff clay	Model 16	0.0374	0.000120	8.52
30 ft. Pinned head pile group with batter piles	Model 17	0.0878	0.000281	20.01
15 ft. Pinned head pile group with batter piles	Model 18	0.0439	0.000141	10.01
30 ft. Fixed head pile group with batter piles	Model 19	0.0836	0.000268	19.07
15 ft. Fixed head pile group with batter piles	Model 20	0.0418	0.000134	9.54

CHAPTER 6

DISCUSSION AND CONCLUSION

6.1 Results Discussion

As previously mentioned, this research investigates the degree of footing fixity G values for bridge pier on different types of end-bearing pile foundations. Twenty (20) different cases are studied, and a comprehensive study of the pier-pile interactions was conducted. In chapter 5, a detailed calculation example was illustrated, and the result summation was shown, in which a total of six aspects are compared. The following discussion statements are made:

(1) First of all, as shown in Figure 6.1, under the comparison of the G values, all of 20 cases' G values obtained are larger than the recommendation, G=1.0, by AASHTO, regardless the variation of pile length, soil conditions, pile arrangements or boundary conditions.

(2) This study considered 30 ft. long pile groups and 15 ft. long pile groups to account long pile foundation case and short pile foundation case. By comparing the G values of different pile length cases shown in Figure 6.2, one statement can be made that the G value is pile length sensitive. With the same other condition controls, for example, the same boundary conditions, the G values of the 15 ft. long pile group cases are all smaller than that of the 30 ft. long pile group cases. For most of the cases, G values of the 15 ft. long pile group cases are approximately around half of the G values for the 30 ft. long pile group cases.

(3) There were three different soil materials discussed in this study: sand, soft clay and stiff clay. As shown in Figure 6.3, after comparing straight pile groups in various single-layer soil materials, it is clear that with the same other conditions, the G values are almost the same. In other words, regardless of various soil materials, for piles in single layer soil condition, there is no significant effect of soil materials on G values.

(4) For soil conditions with multiple layers, G values comparisons are shown in Figure 6.4. In which, G value of the three soil layers with sand as the top layer case is extremely close to that of the single sand layer case. Meanwhile, G value of three soil layers with the soft clay as top layer case is also very close to that of the single soft clay layer case. It is certain that G is insensitive with different soil layers, and the top layer of soil always controls.

(5) Comparisons of real G values for pinned head piles and fixed head piles are shown in Figure 6.5. For both straight pile groups and the pile groups with batter pile cases, the G values obtained from those two different boundary conditions failed to show a great difference, which indicates the pile head boundary conditions are not a controlling factor for G values.

(6) Finally, comparisons are made between different pile arrangements. For the batter pile cases investigated in this study, lateral loads are fully resisted by batter piles. From the G results are shown in Figure 6.6, it is clear that even though batter pile groups are better than straight pile groups on lateral loads resistance, they are worse with regard to rotational resistance. The G values of batter pile groups are larger than that of the straight pile groups with the same other conditions, and the difference between each other increases as pile length increases.
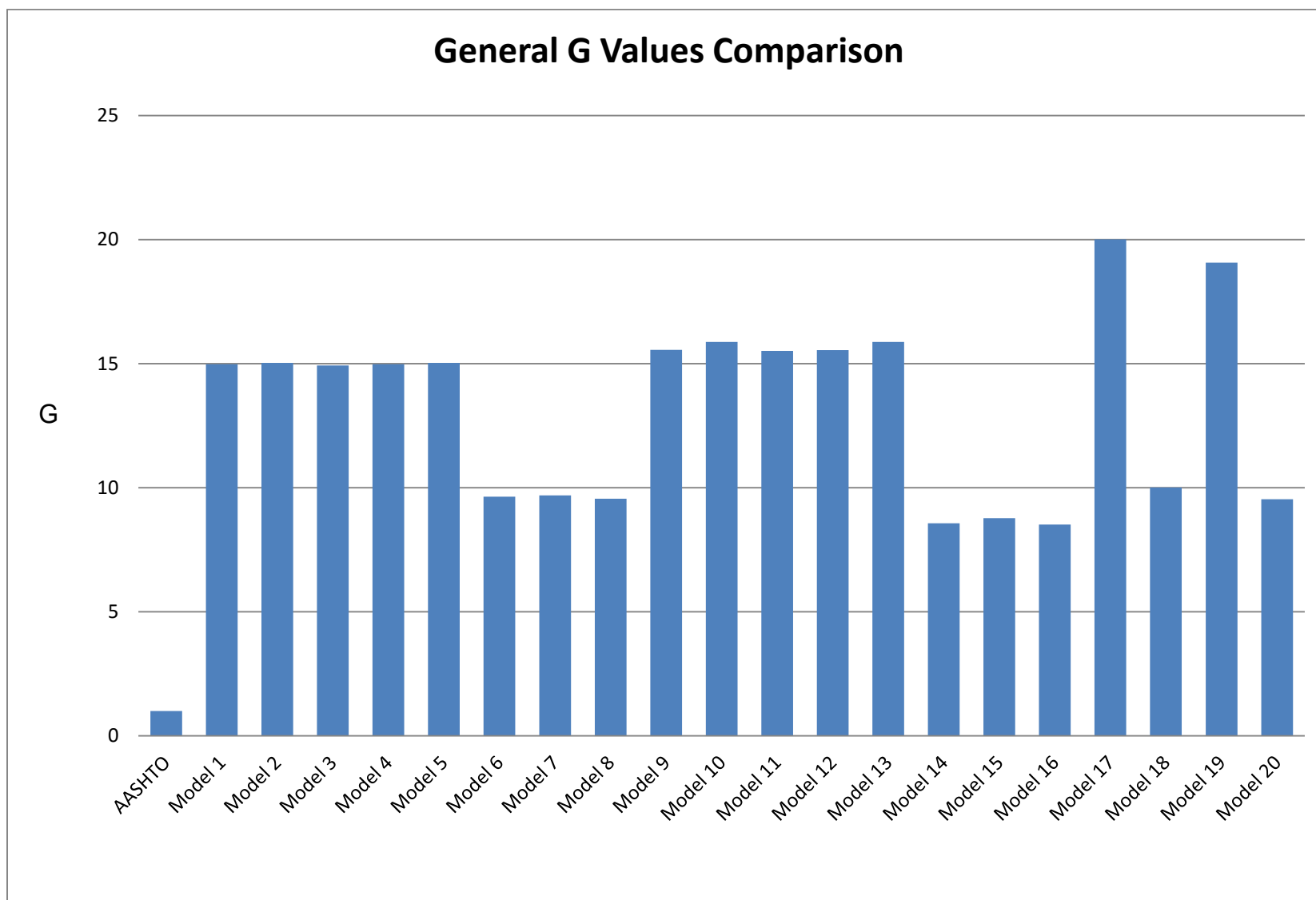
Figure 6.1 Comparisons of G values

Comparisons of G values by Pile Length

	PHSS	PHSSO	PHSST	FHSS	FHSSO	FHSST	PHB	FHB
■ 30 ft. Long Pile Groups	14.98	15.03	14.93	15.56	15.88	15.52	20.01	19.07
■ 15 ft. Long Pile Groups	9.64	9.69	9.56	8.57	8.77	8.52	10.01	9.54
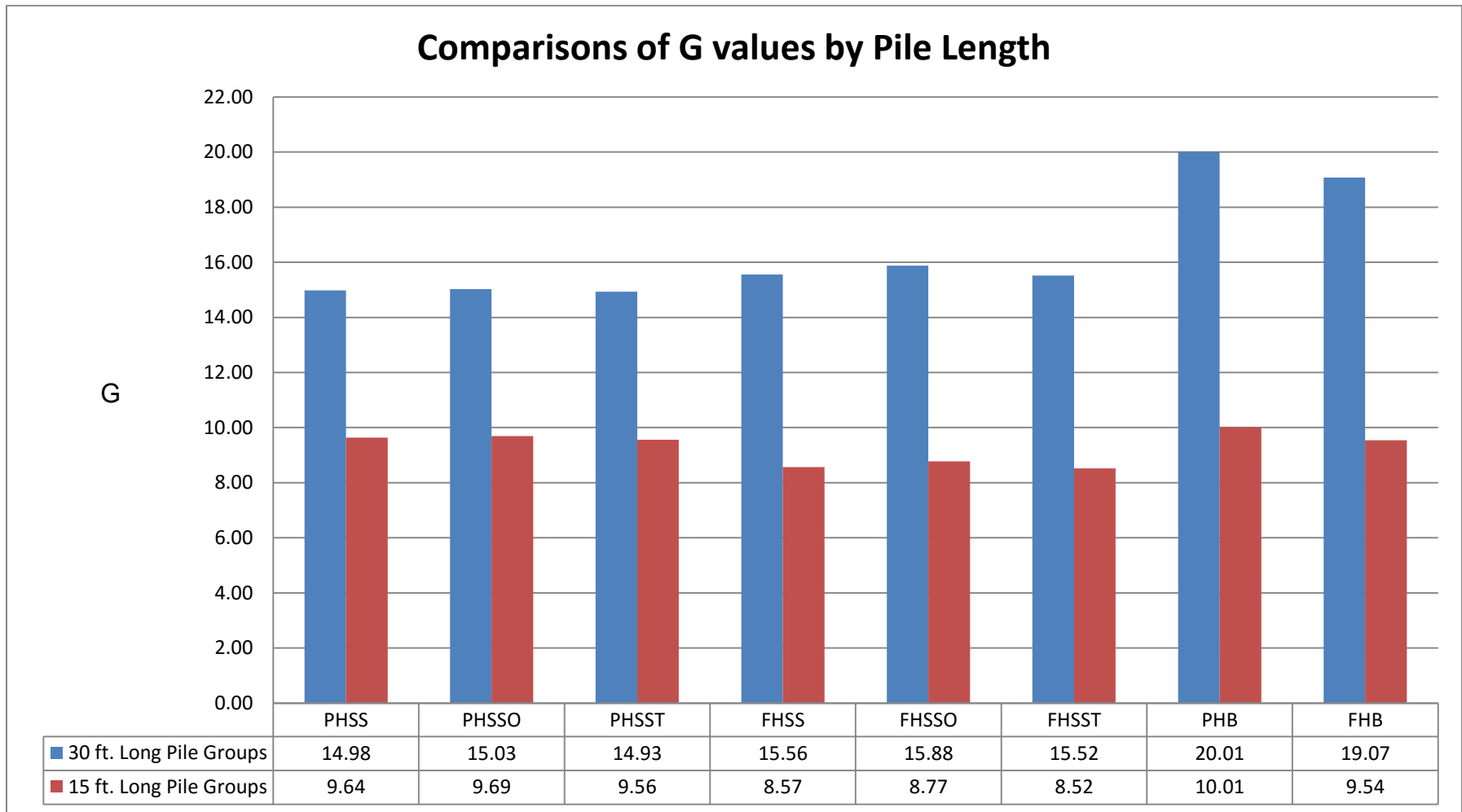
Figure 6.2 Comparisons of G values by pile length

Notes: PHSS= Pinned Head Straight Pile in Sand   FHSSO=Fixed Head Straight Pile in Soft Clay
     PHSSO=Pinned Head Straight Pile in Soft Clay   FHSST=Fixed Head Straight Pile in Stiff Clay
     PHSST=Pinned Head Straight Pile in Stiff Clay   PHB=Pinned Head Piles with Batter Pile
     FHSS= Fixed Head Straight Pile in Sand   FHB=Fixed Head Piles with Batter Pile
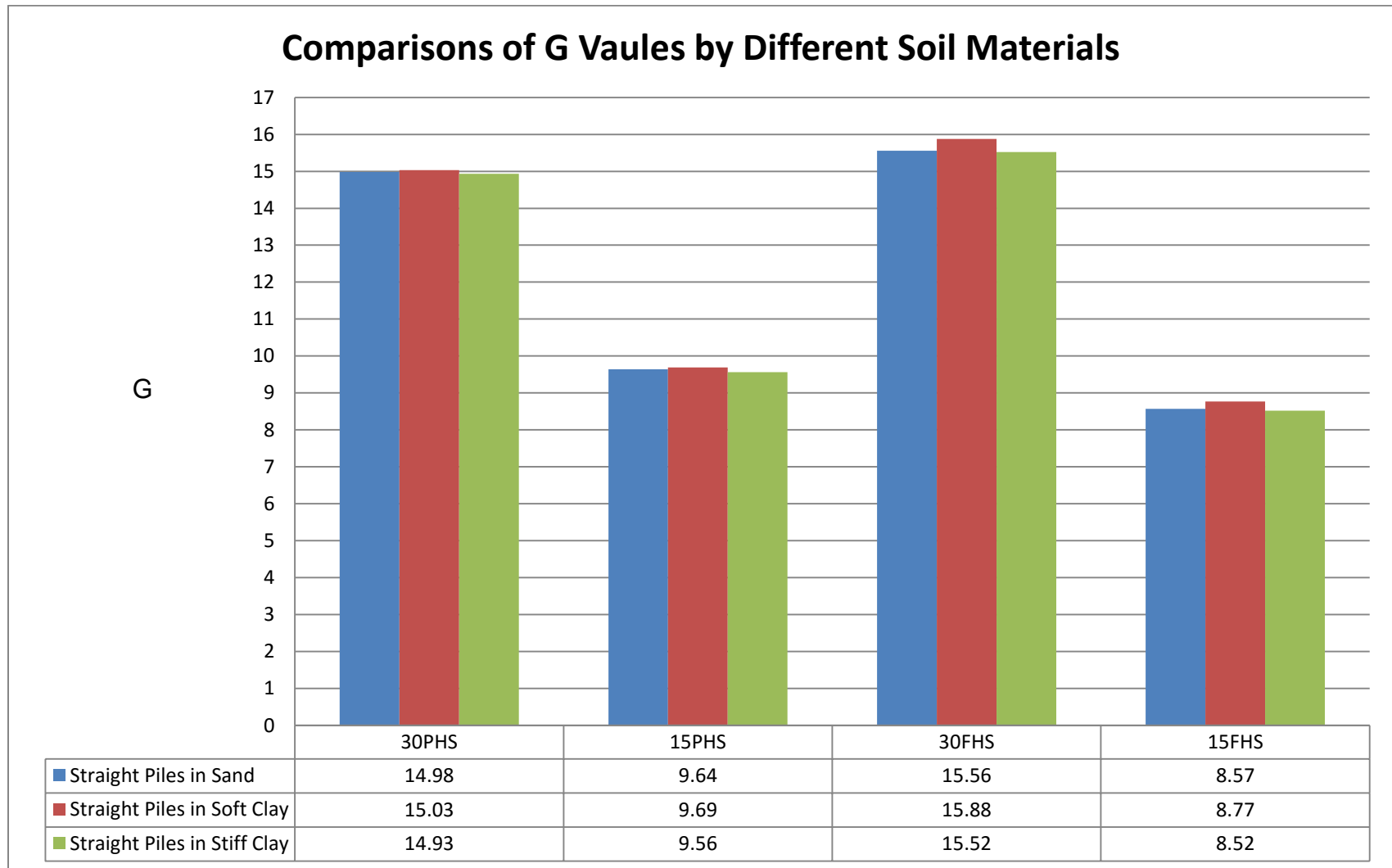
Figure 6.3 Comparisons of G values by different soil materials

Notes: 30PHS= 30 ft. Pinned Head Straight Piles   30FHS=30ft. Fixed Head Straight Piles

     15PHS= 15ft. Pinned Head Straight Piles   15FHS= 15 ft. Fixed Head Straight Piles

Comparisons of G values by Soil Layers

G	30PHS	30FHS
Single Sand Layer	14.98	15.56
Three Layers (Sand, Soft Clay, Stiff Clay)	14.98	15.55
Single Soft Clay Layer	15.03	15.88
Three Layers (Soft Clay, Sand, Stiff Clay)	15.03	15.88
Single Stiff Clay Layer	14.93	15.52
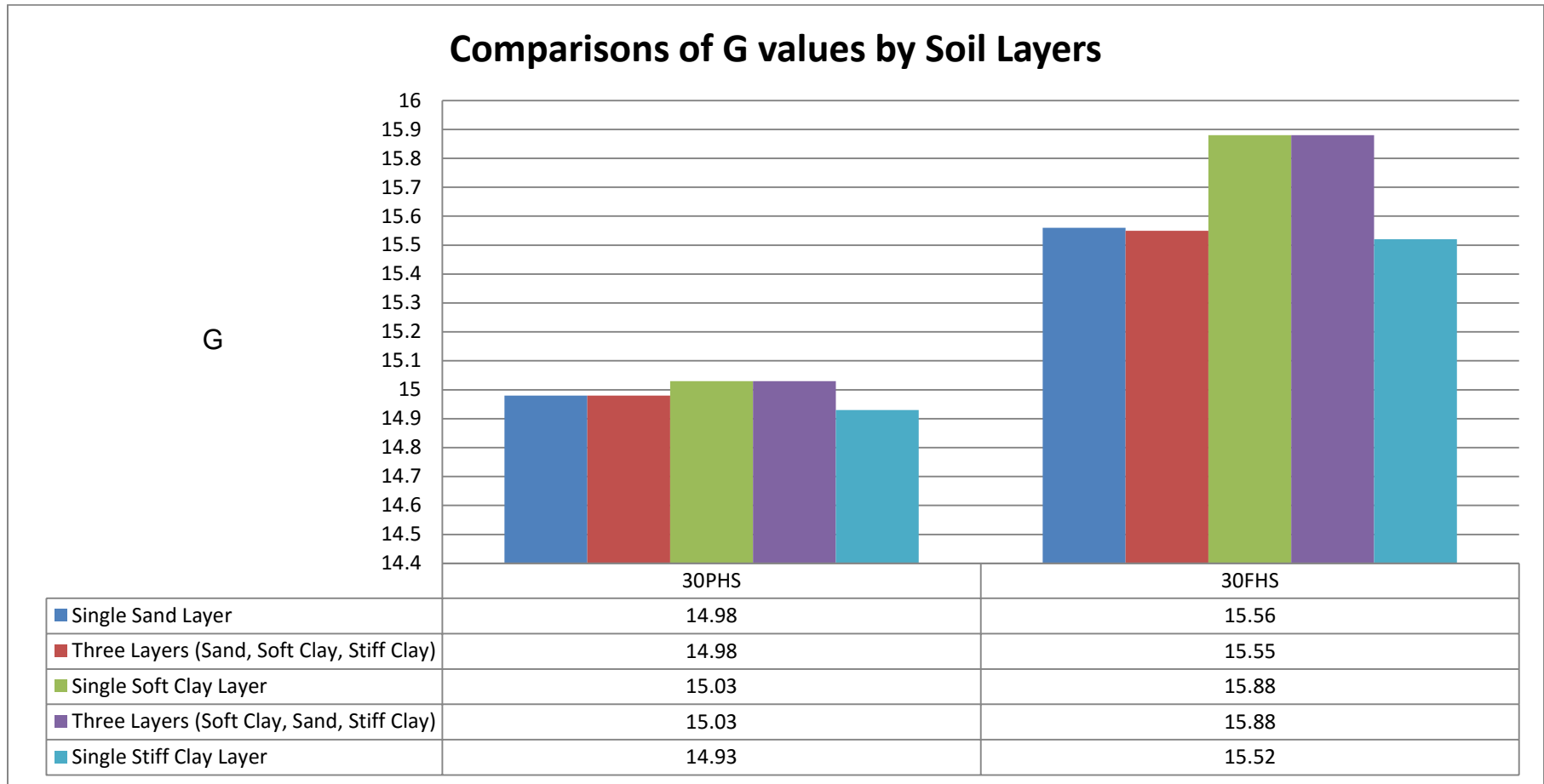
Figure 6.4 Comparisons of G values by soil layers

Notes: 30PHS= 30 ft. Pinned Head Straight Piles   30FHS= 30 ft. Fixed Head Straight Piles

Comparisons of G Values by Pile Head Boundary Conditions

	30SS	30SSO	30SST	30SSOT	30SOST	15SS	15SSO	15SST	30PB	15PB
Pinned Head	14.98	15.03	14.93	14.98	15.03	9.64	9.69	9.56	20.01	10.01
Fixed Head	15.56	15.88	15.52	15.55	15.88	8.57	8.77	8.52	19.07	9.54
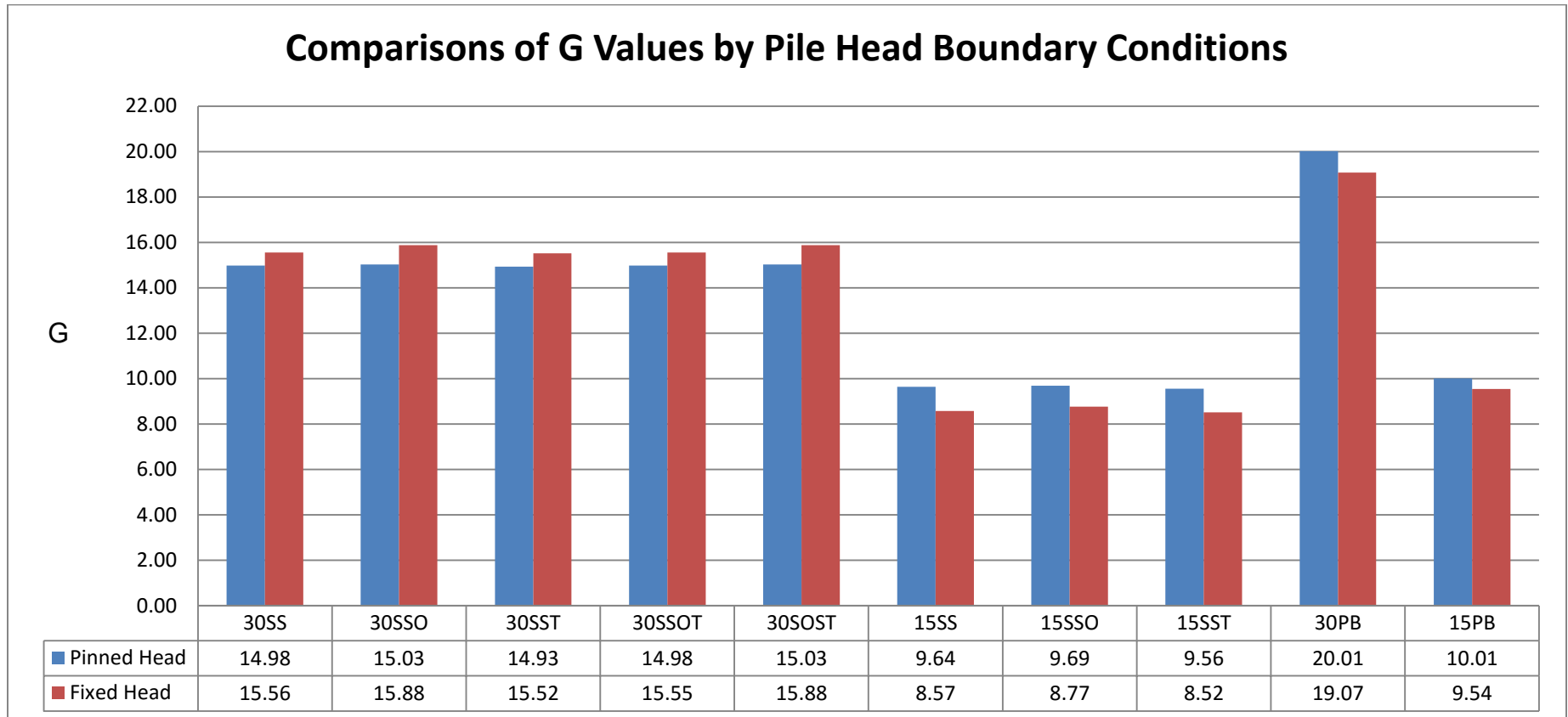
Figure 6.5 Comparisons of G values by pile head boundary conditions

Notes: 30SS= 30 ft. Straight Piles in Sand   15SS= 15 ft. Straight Piles in Sand

     30SSO= 30 ft. Straight Piles in Soft Clay   15SSO= 15 ft. Straight Piles in Soft Clay

     30SST= 30 ft. Straight Piles in Stiff Clay   15SST= 15 ft. Straight Piles in Stiff Clay

     30SSOT= 30 ft. Straight Piles in (Sand, Soft Clay, Stiff Clay)   30PB= 30ft. Piles with Batter Piles

     30SOST= 30 ft. Straight Piles in (Soft Clay, Sand, Stiff Clay)   15PB= 15 ft. Piles with Batter Piles

Comparisons of G Values by Different Pile Arrangments

	30PHS	15PHS	30FHS	15FHS
■ Straight Piles in Sand	14.98	9.64	15.56	8.57
■ Straight Piles in Soft Clay	15.03	9.69	15.88	8.77
■ Straight Piles in Stiff Clay	14.93	9.56	15.52	8.52
■ Batter Pile Group	20.01	10.01	19.07	9.54
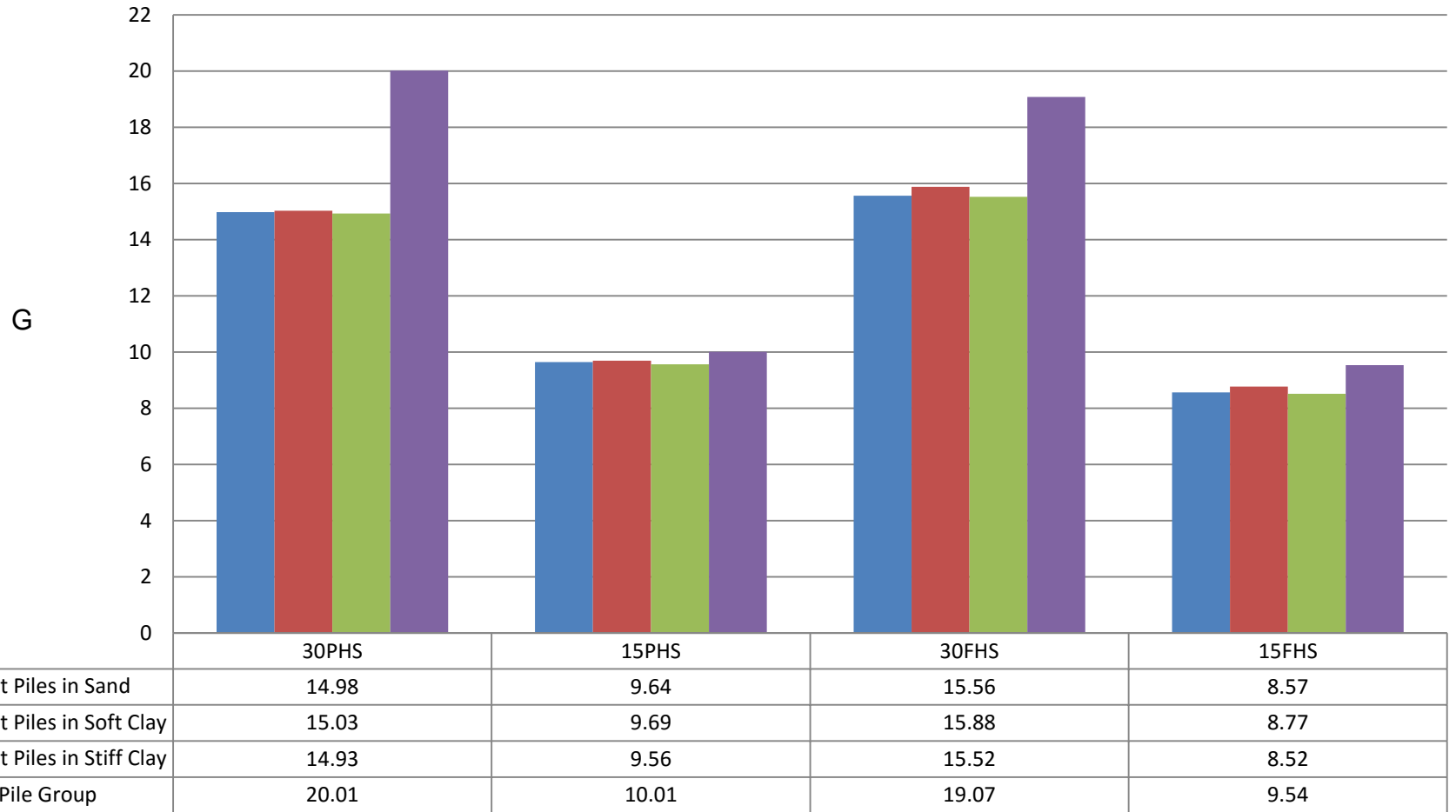
Figure 6.6 Comparisons of G values by different pile arrangements

Notes: 30PHS= 30 ft. Pinned Head Straight Piles   30FHS=30ft. Fixed Head Straight Piles
15PHS= 15ft. Pinned Head Straight Piles   15FHS= 15 ft. Fixed Head Straight Piles

6.2 Conclusion

Lateral deflection is an essential criterion to check when a structure may be hugely impacted by lateral loads, especially for heavy vertical loads supporting structures such as bridge piers. Footing fixity has been studied and is known to play a significant role in correctly determining structure lateral displacement. Meanwhile, AASHTO has suggested several footing fixity values to simplify the computation approach. However, before this study, the accuracy of footing fixity G=1.0 for footing on multiple rows of end-bearing piles was recommended by AASHTO as a too approximate value due to the complex conditions of pile foundations.

In this study, in order to verify if G=1.0 suggested by AASHTO is accurate enough for the various type of pile foundations, 20 models of bridge pier-pile foundations with various pile length, soil materials, pile arrangements and boundary conditions are developed using finite element analysis software to study the pier-pile interaction behaviors. Furthermore, footing fixity G values are procured for those 20 models. By comparing the finite element results and AASHTO hand calculation approach results, following conclusions are drawn:

(1) The G=1.0 footing fixity value recommended by AASHTO for the pier on multiple rows of end-bearing piles is highly underestimated. All of the G values from those 20 models are much larger than suggested (G=1.0). This study indicates that the pier footing rotates under lateral loads are an essential factor which affects the lateral deflection of the pier.

(2) After comparing the G values for pile foundations with different pile lengths, it is noticed that the G value is pile length sensitive. The difference between G values is approximately proportional to the length of the pile.

(3) The G values of straight pile groups in three different materials of single layer soils (sand, soft clay, and stiff clay) failed to show a significant difference when all the other conditions (pile length, boundary conditions, pile arrangement, etc.) are same. This study indicates that the soil materials are not a major controlling factor to affect pier rotations.

(4) It is unexpected to recognize that G value is not mainly affected by multiple soil layers also. According to the results obtained, the pier rotations and G values are controlled by the very top layer of soils. The G values for piles in multiple layer soils are almost the same as the G values of piles in single layer soil cases when the top layer soil material of the multiple layers case is the same as the single layer soil material.

(5) Pile head boundary conditions are not showing a significant influence on G value determination. For both straight pile group cases and pile groups with batter piles cases, the results of G values for both boundary conditions are very close.

(6) The comparisons of G values for straight pile groups and pile groups with batter piles are obtained. Even though batter pile cases are well known for their better lateral load resisting abilities, they have larger pile cap rotations than those of straight pile group cases, the longer the piles, the larger the rotations. To determine if the soils provide any assistance in reducing the rotations, further research is required.

In the results of this study, by studying the effect of footing fixity of bridge pier on end-bearing pile foundations, one major conclusion has been made, that is, G=1.0 recommended by AASHTO is only an approximate value. The G values vary depending on pile length, soil types, pile arrangements, boundary conditions and many other uncertain factors.

REFERENCE

AASHTO LRFD Bridge Design Specifications (2012), customary U.S. units. Washington, DC: American Association of State Highway and Transportation Officials.

American Concrete Institute (2014), Building code requirements for structural concrete (ACI 318-14):an ACI standard : commentary on building code requirements for structural concrete (ACI 318R-14), an ACI report

American Institute of Steel Construction (AISC) (2011). Steel Construction Manual, 14th Ed, Chicago, IL.

American Society of Civil Engineers (ASCE). (2010). *Minimum Design loads for Buildings and Other Structures, ASCE/SEI 7-10*, ASCE publications, Reston, Virginia.

Bhushan, K., & Scheyhing, C. (2002). "Lateral load tests on drilled piers in San Diego area residual and formational soils." In *Proceedings 27th annual conference on deep foundations, San Diego, CA*.

California Department of Transportation (2008),Bridge Design Specifications, Appendix C, <http://www.dot.ca.gov/hq/esc/techpubs/manual/bridgemanuals/bridge-design-specifications/page/appendix.pdf>, Nov. 7th, 2008

Chen, W. & Duan, L.(2014), *Fundamentals*, Bridge Engineering Handbook, Second Edition, Taylor & Francis Group, Boca Raton, FL.

Das, B. M. (2007). Principles of Foundation Engineering. (6th edition). Toronto, Ontario:

    Thomson Canada Limited.

Federal Highway Administration (2017), "LRFD Steel Girder Superstructure Design Example:

    Pier Design Example Design Step 8" , Bridges & Structures, U.S. Department of

    Transportation <https://www.fhwa.dot.gov/bridge/lrfd/us_ds8.cfm>, June 27th, 2017

Federal Highway Administration (2017), "LRFD Steel Girder Superstructure Design Example:

    Pile Foundation Design Example Design Step P" , Bridges & Structures, U.S.

    Department of Transportation < https://www.fhwa.dot.gov/bridge/lrfd/us_dsp.cfm >,

    June 27th, 2017

Federal Highway Administration (2006), "Design and Construction of Driven Pile Foundations

    Reference Manual – Volume I ", FHWA NHI-05-042，U.S. Department of

    Transportation, <http://apps.itd.idaho.gov/apps/manuals/Materials/Materials%

    20References/FHWA-NHI-05-042-Volume%20I.pdf>, April, 2006

Federal Highway Administration (2006), "Chapter 8: Analysis of the Lateral Load Tests at the

    Route 351 Bridge", Federal Highway Administration Research and Technology, U.S.

    Department of Transportation,

    <https://www.fhwa.dot.gov/publications/research/infrastructure/structures/04043/

    08.cfm>, March, 2006

FB-MultiPier Soil Parameter Table (2013), Bridge Software Institute, Department of Civil & Coastal Engineering, University of Florida, December 2013. <https://bsi.ce.ufl.edu/downloads/files/MultiPier_Soil_Table.pdf>

Hamilton, M. (2014). "Pile-Soil Interaction in Unsaturated Soil Conditions". *University of New Hampshire.*

Hsiao, J. K., & Jiang, Y. (2014) "Footing Fixity Effect on Pier Deflection". *International Journal of Bridge Engineering (IJBE)*, *2*(2).

Hsiao, J. K. (2012). "Statical analysis of pile groups containing batter piles". *Electronic Journal of Structural Engineering*, *12*(1), 74-81.

Hsiao, J. K. (2001). "Strength and ductility of the enlarged beam section connection: A new fully-restrained steel moment connection". University of Utah.

Khodair, Y., & Abdel-Mohti, A. (2014). "Numerical Analysis of Pile–Soil Interaction under Axial and Lateral Loads". *International Journal of Concrete Structures and Materials*, *8*(3), 239-249.

LPile Plus Version 5 [Computer Software]. (2004). ENSOFT INC., Austin, TX.

Matlock, H., & Reese, L. C. (1960). "Generalized solutions for laterally loaded piles". *Journal of the Soil Mechanics and foundations Division*, *86*(5), 63-94.

Mosher, R. L., & Dawkins, W. P. (2000). *Theoretical manual for pile foundations* (No. ERDC/ITL-TR-00-5). ENGINEER RESEARCH AND DEVELOPMENT CENTER VICKSBURG MS INFORMATION TECHNOLOGY LAB.

NISA/DISPLAY IV Ver.12.0 [Computer Software]. (2003). Engineering Mechanics Research Corporation, Troy, MI.

Qiu, W., Hu, M., & Zhou, Y. (2011, July). "Influence of structure-soil interaction on seismic responses of bridge". In *Multimedia Technology (ICMT), 2011 International Conference on* (pp. 1576-1579). IEEE.

Reese, L. C., Cox, W. R., & Koop, F. D. (1974). "Analysis of laterally loaded piles in sand". *Offshore Technology in Civil Engineering Hall of Fame Papers from the Early Years*, 95-105.

Salgado, R. (2008). The engineering of foundations. The McGraw-Hill Companies, Inc.

Valli, (2014). "Types of Pile Foundations", Civil Training for Young Engineers, <http://civiltraining.in/types-of-pile-foundation/>, March 20th, 2014.

Wang, C.K, Salmon, C.G. and Pincheira, J.A. (2007). Reinforced Concrete Design, 7th Edition, University of Wisconsin- Madison, John Wiley and Sons.

Wu, T. L. (2010). "The P-DELTA and Soil-Structure Interaction Effect ON Bridge Piers." Civil and Environmental Engineering, Southern Illinois University at Carbondale.

Zhang, Y., Abu-Farsakh, M., & Voyiadjis, G. (2012). "Finite Element Analysis of a Full-Scale

    Lateral Load Test on Batter Pile Group Foundation". In *Proceedings of the*

    Transportation Research Board 91st Annual Meeting (pp. 22-26).

Zeeshan, S. (2016). "Verification of Bridge Foundation Fixity for Three Different Types of

    Soil". Civil and Environmental Engineering, Southern Illinois University at Carbondale.

APPENDICES

APPENDIX A

SUPPLEMENT OF CALCULATION PROCEDURES

A.1 Checking For Minimum Center To Center Spacing between Piles

Minimum Center to Center Spacing (Das, 2007)

$$S_m = D + 300 \text{ mm}$$

Where, D is the dimension of pile cross-section on loading direction.

$D = 12.045''$ (For HP12×53 Piles)

Minimum center to center spacing of this study $S = 3'$ (from Figure 4.2)

Therefore,

$$S_m = D + 300 \text{ mm} = 12.045'' + 11.811'' = 23.865'' < 3' = 36''$$

The Minimum center to center spacing is sufficient.

A.2 Batter Pile Angles Determination
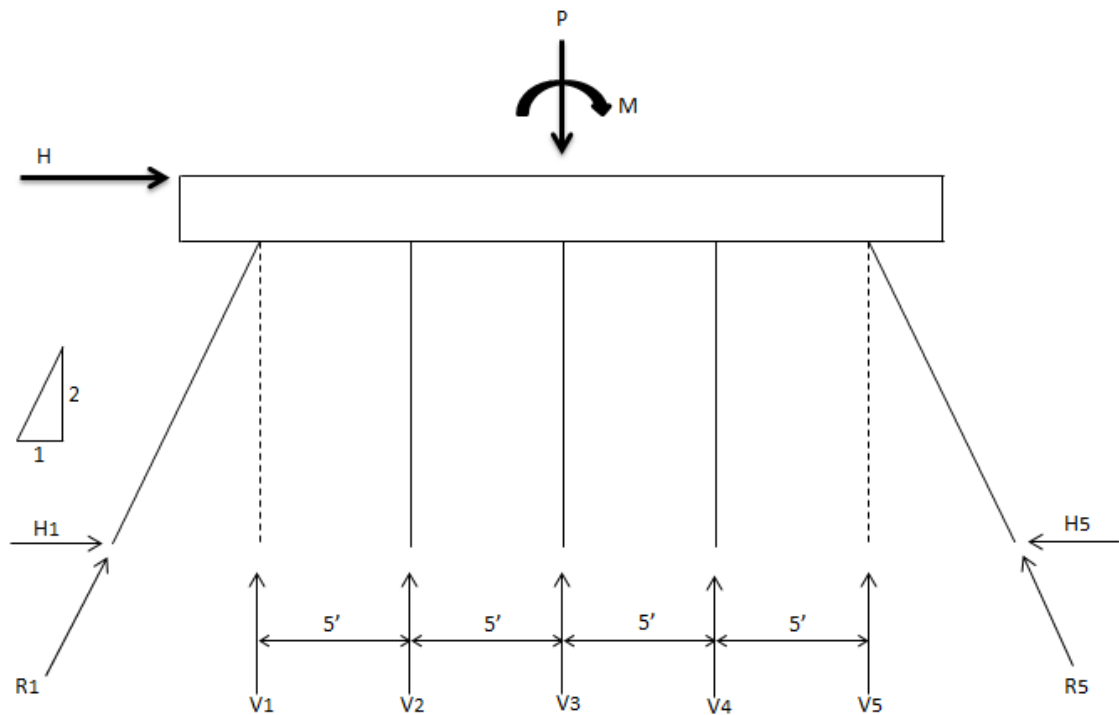
Figure A.1 Batter pile case loadings and reaction forces

Vertical Results of Pile groups (Hsiao, 2012)

$$V_i = \frac{P}{n} \pm \frac{M_t}{\sum x_i^2} x_i$$

Where, V_i is the axial force of vertical pile or the vertical component of the axial

force in a batter pile;

P is the vertical load;

n is the total pile numbers

M_t is the overturning moment

x_i is the distance of a pile to the neutral axis of a pile group

Known factored vertical load $P = 3583^k$, $M_t = M_{AB} = 2351.69\text{k} - \text{ft.}$, n = 20,

(FHWA, 2017)

, and $H = 92.28^k$ from FHWA Design Example.

$$\sum x_i^2 = x_1^2 \times 4 + x_2^2 \times 4 + x_4^2 \times 4 + x_5^2 \times 4 = 5^2 \times 8 + 10^2 \times 8 = 1000 \text{ ft.}^2$$

Therefore,

$$V_1 = 155.63^k$$

$$V_2 = 167.39^k$$

$$V_3 = 179.15^k$$

$$V_4 = 190.91^k$$

$$V_5 = 202.67^k$$

V_5 is the largest axial force, and it controls.

By given batter piles a batter angle as 1:2 shown in Figure A.1, the lateral force are fully resisted by batter piles, there is no residual horizontal resistance in the other straight piles (Hsiao, 2012).

Checking:

$$V_1 = 155.63^k$$

$$V_5 = 202.67^k$$

Thus，

$$H_1 = 155.63^k \times \frac{1}{2} = 77.82^k$$

$$H_5 = 202.67^k \times \frac{1}{2} = 101.34^k$$

Therefore, the residual lateral load

$$H' = \frac{H}{4} + H_1 - H_5 = \frac{92.28^k}{4} + 77.82^k - 101.34^k = -0.45^k \approx 0^k$$

Using 1:2 batter piles is sufficient for this study.

A.3 Checking Design Strength of Pile Bearing Capacity P_c

Using Model 1 30ft. long straight pile in the sand as an illustrative example

The required axial force to carry $P_r = V_5 = 202.67^k$

Checking if the design pile bearing capacity $P_c \geq P$ (Das,2007)

(1) Allowable structural capacity for steel pile

$$Q_{all} = A_s f_s$$

Where, A_s is the cross-section area of steel $= 15.5$ in.^{2} for HP 12×53 piles

f_s is the allowable stress of steel (≈ 0.33 to $0.5 f_y$)

Pick $f_s = 0.42 f_y$, and $f_y = 50$ ksi for A572 G50 Steel

$$\therefore Q_{all} = 15.5 \text{ in.}^2 \times 0.42 \times 50 \text{ ksi} = 325.5^k$$

(2) Point Bearing Capacity of Piles Resting on Rock

$$Q_{all} = \frac{q_p A_p}{FS}$$

Where, A_p is the area of cross-section of pile

$$(A_p = 12.045 \times 11.78 = 141.8901 \text{in.}^2)$$

FS is the safety factor (FS $\gg$ 3, pick FS $= 4$)

, and

$$q_p = q_{u(design)}(N_\varphi + 1)$$

Where, N_φ is a parameter equals $tan^2(45° + \varphi'/2)$

q_u is the unconfined compression strength of rock

φ' is the drained angle of friction of rock

Used Limestone in this research, $\varphi' = 30° - 40°$ for limestone

Pick $\varphi' = 30°$ for conservative consideration,

$$\therefore N_\varphi = tan^2(45° + 30°/2) = 3$$

$q_{u(lab)} = 15000 - 30000 \frac{\text{lbs}}{\text{in.}^2}$ for limestone (Das, 2007)

Pick $q_{u(lab)} = 15000 \frac{\text{lbs}}{\text{in.}^2}$ for conservative consideration,

$$q_{u(design)} = \frac{q_{u(lab)}}{5} = \frac{15 \text{ kips/in.}^2}{5} = 3 \text{ kips/in.}^2$$

$$\therefore q_p = 3\frac{\text{kips}}{\text{in.}^2} \times (3 + 1) = 12\text{ksi}$$

$$\therefore Q_{all} = \frac{12\text{ksi} \times 141.8901\text{in.}^2}{4} = 425.67^k > 325.5^k \ (from \ (1))$$

And the smaller Q_{all} controls,

Therefore, the design strength of pile $P_c = Q_{all} = 325.5^k > 202.67^k \; required$

Checking Bending with Axial Loading (AISC,2011; Das, 2007):

$$\frac{P_r}{P_c} = \frac{202.67^k}{325.5^k} = 0.623 > 0.2$$

Check if

$$\frac{P_r}{P_c} + \frac{8}{9}\left(\frac{M_{rx}}{M_{cx}} + \frac{M_{ry}}{M_{cy}}\right) \ll 1.0$$

For 30ft. long piles in the sand:

Check max allowed lateral load $Q_{u(g)}$, and max moment M_{max} due to max lateral load.

$E_p = 29000$ ksi and $I_p = 394$ in.^{4} for HP 12×53 piles

$n_h = 0.065$ kips/in.^{3} for sand property

$$\therefore \text{T} = \sqrt[5]{\frac{E_p I_p}{n_h}} = \sqrt[5]{\frac{29000 \times 394}{0.065}} = 44.565 \text{ in.}$$

$$\therefore \frac{L}{T} = \frac{360}{44.565} = 8.08 > 5$$

Thus, 30 ft. long pile is classified as long piles.

For long piles in sand,

Relative stiffness of pile

$$K_r = \frac{E_p I_p}{E_s L^4} < 0.01$$

In which, E_s is the average horizontal soil modulus of elasticity = 7.25 to 11.6 ksi

according to USCS for sand, pick $E_s = 9.425$ ksi

$$\therefore K_r = \frac{29000 \times 394}{9.425 \times 360^4} = 7.218 \times 10^{-5} < 0.01$$

Since the smaller value controls,

$$\therefore K_r = 7.218 \times 10^{-5}$$

$$\frac{L_e}{L} = 1.65 K_r^{0.12} \ll 1$$

Where, L_e is the effective length,

$$\therefore \frac{L_e}{L} = 1.65(7.218 \times 10^{-5})^{0.12} = 0.5254 < 1$$

The smaller value controls,

Thus, $L_e = 0.5254 \times 360 = 189.145$ in.

And the ultimate lateral load resistance

$$Q_{u(g)} = 0.12\gamma DL_e^2 K_{br} \ll 0.4 P_l DL_e$$

Where,

γ is the unit weight of sand= 0.0636574 lbs/in.^{3}

K_{br} is the resultant net soil pressure coefficient and $K_{br} = 21$ for

      $\varphi' = 40°$ sand (Das, 2007)

P_l is the limit pressure obtained from pressuremeter tests

      And $P_l = 0.4 P_a N_q \tan\varphi'$ or $P_l = 0.6 P_a N_q \tan\varphi'$, $N_q = 64.2$

P_a is the atmospheric pressure= 2000 lbs/ft.^{2}

Pick $P_l = 0.4 P_a N_q \tan\varphi'$ for conservative consideration, and then

$$P_l = 0.4 \times 2000 \times 64.2 \times \tan40° = 299.279 \text{ lbs/in.}^2$$

$$\therefore Q_{u(g)} = 0.12 \times 0.0636574 \times 12.054 \times 189.145^2 \times 21 = 69.127 \text{ kips}$$

And $Q_{u(g)} = 0.4 \times 299.279 \times 12.054 \times 189.145 = 272.73$ kips

The smaller $Q_{u(g)} = 69.127$ $kips$ controls.

Therefore, the max allowed lateral resistance

$$Q_{u(g)} = 69.127^k > \frac{92.28^k}{20} = 4.614^k/\text{pile}$$

And the max moment due to lateral loads,

$$M_{max} = 0.3K_r^{0.2}Q_gL \ll 0.3Q_gL$$

$$\therefore M_{max} = 0.3 \times (7.218 \times 10^{-5})^{0.2} \times 69.127 \times 360 = 1108.537 \text{ kips} - \text{in.}$$

And $M_{max} = 0.3 \times 69.127 \times 360 = 7465.716 \text{ kips} - \text{in.}$

The smaller $M_{max} = 1108.537 \ kips - in.$ controls, and $M_{cx} = M_{max}$

First order analysis results of 30 ft. pinned head single pile in the sand with axial load and lateral load are obtained from LPile,

$$M_{rx} = M_{max} = -193.46 \text{ kips} - \text{in.}$$

And $M_{ry} = 0$

Therefore,

$$\frac{P_r}{P_c} + \frac{8}{9}\left(\frac{M_{rx}}{M_{cx}} + \frac{M_{ry}}{M_{cy}}\right) = \frac{202.67^k}{325.5^k} + \frac{8}{9} \times \frac{193.46 \text{ kips} - \text{in.}}{1108.537 \text{ kips} - \text{in.}} = 0.778 < 1.0$$

The pile is proved sufficient to carry both axial and lateral loads in this study.

APPPENDIX B

LPILE ANALYSIS RESULTS AND NISA TEST MODEL RESULTS

FOR STRAIGHT PILE GROUPS
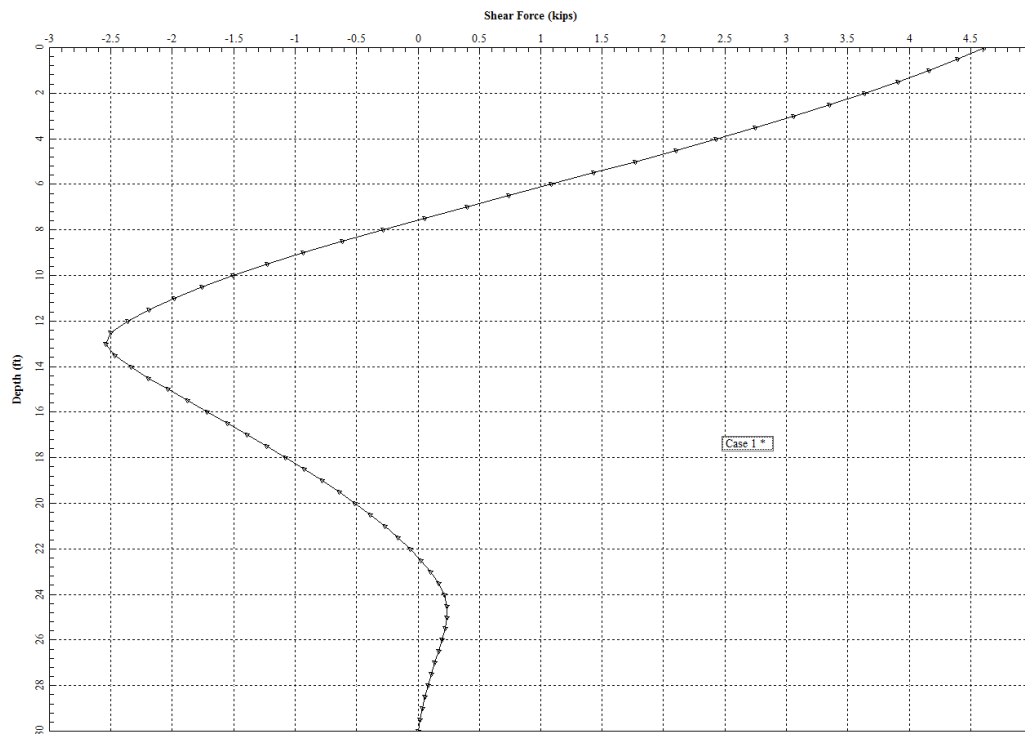
Figure B.1 Model 2 shear force along the pile depth (LPile)
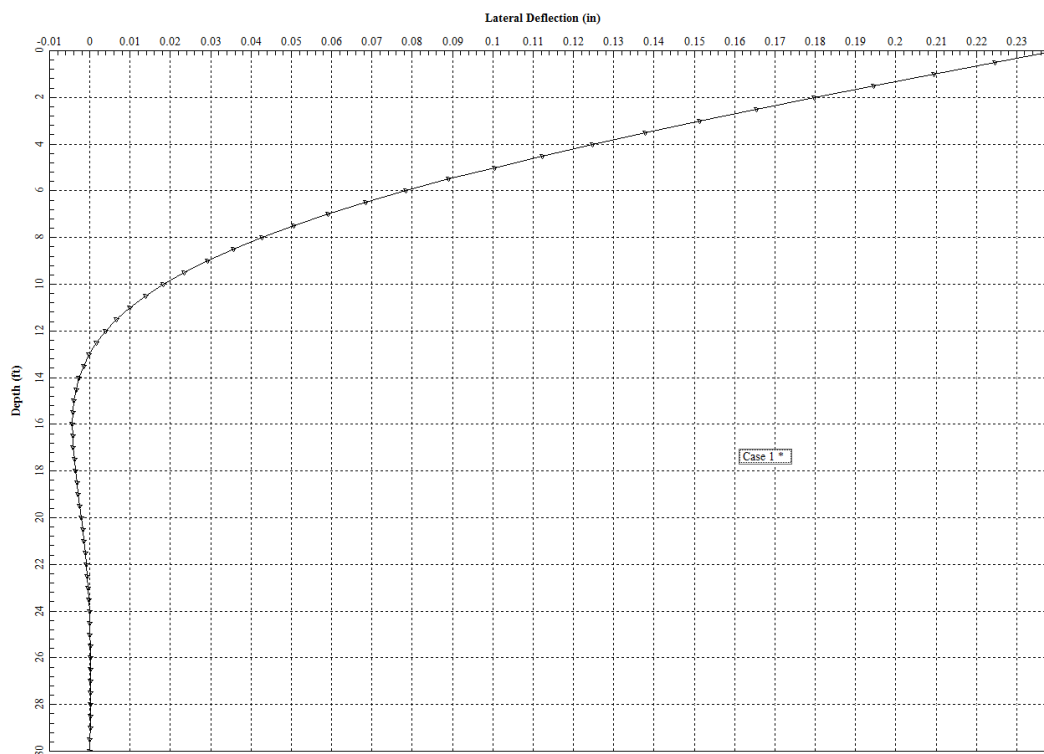
Figure B.2 Model 2 lateral deflection along the pile depth (LPile)
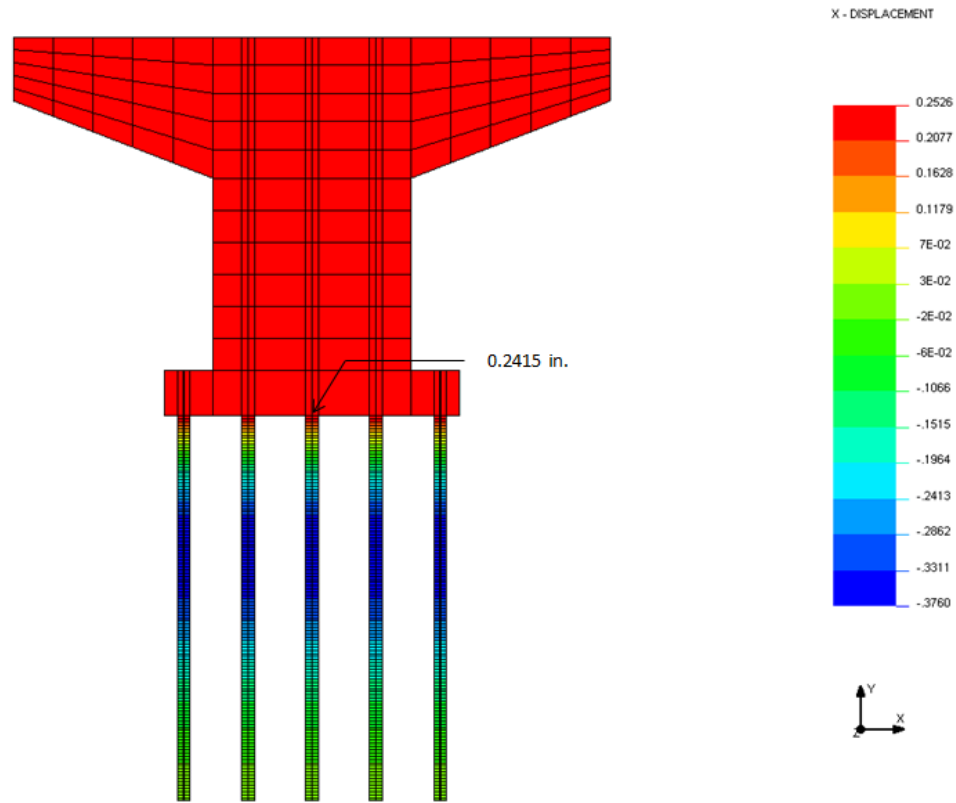
Figure B.3 NISA finite element result for Test Model 2
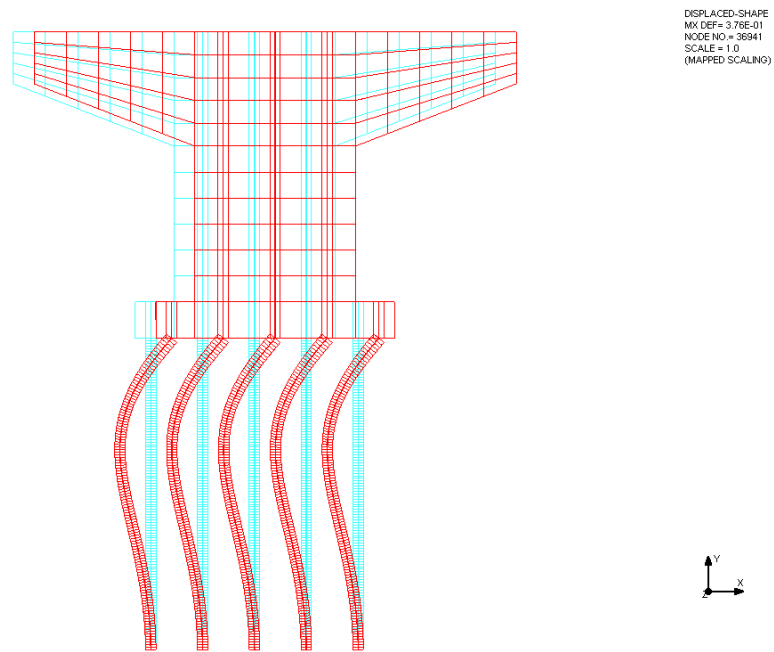
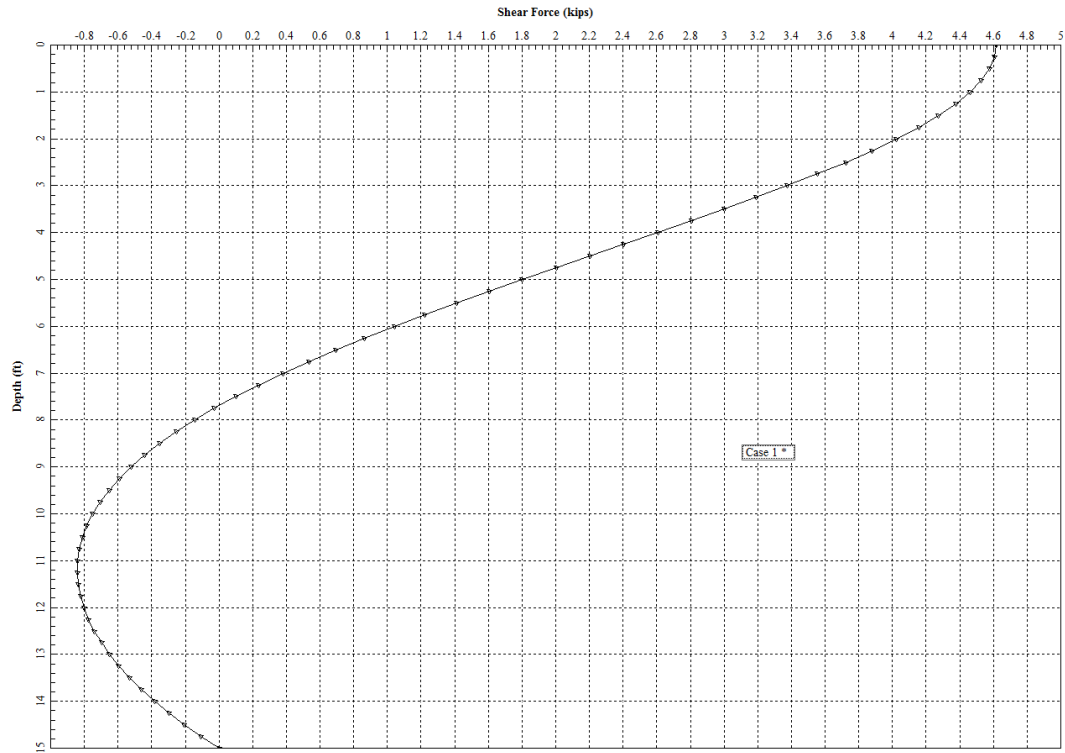*Figure B.4* Lateral deflection for Test Model 2 (in scale of 1)
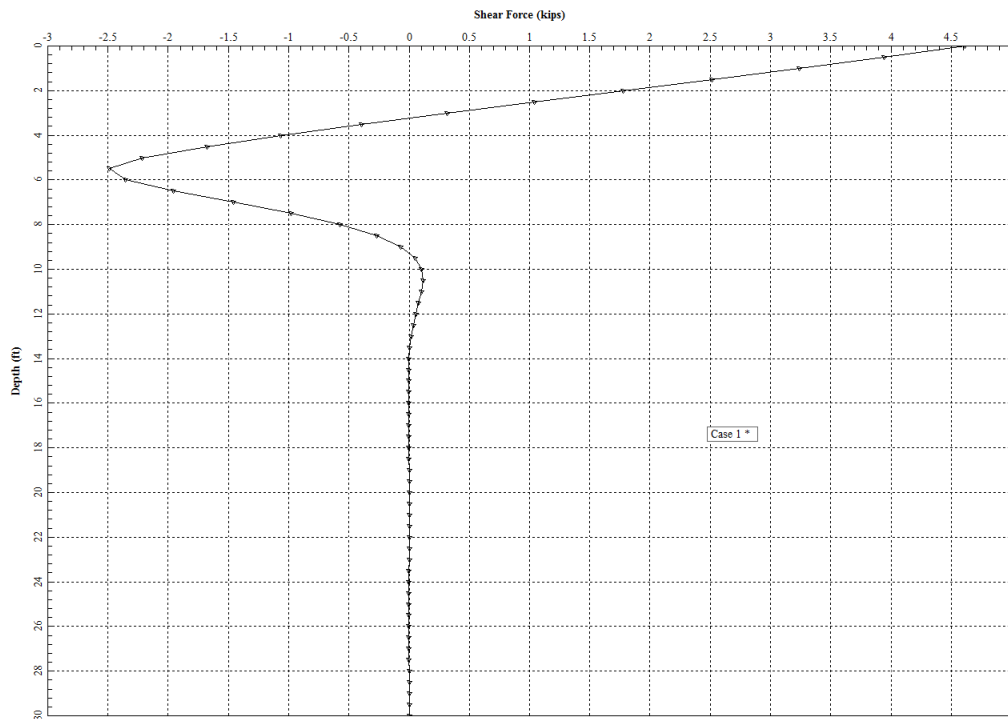
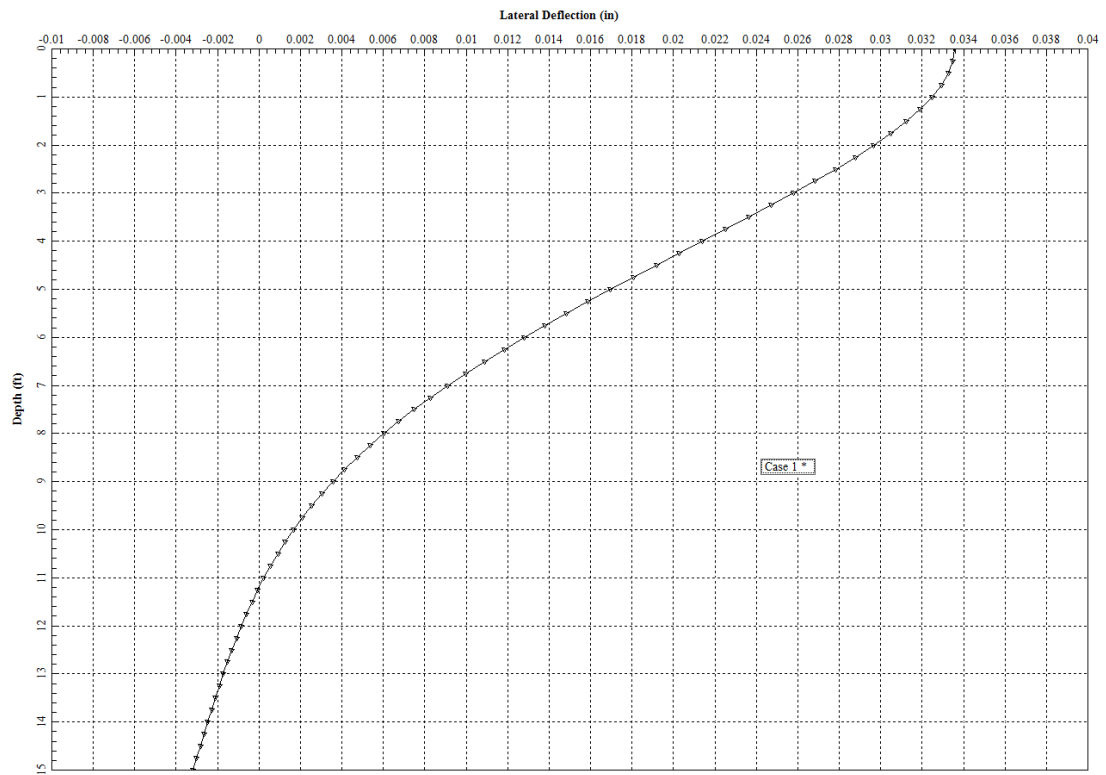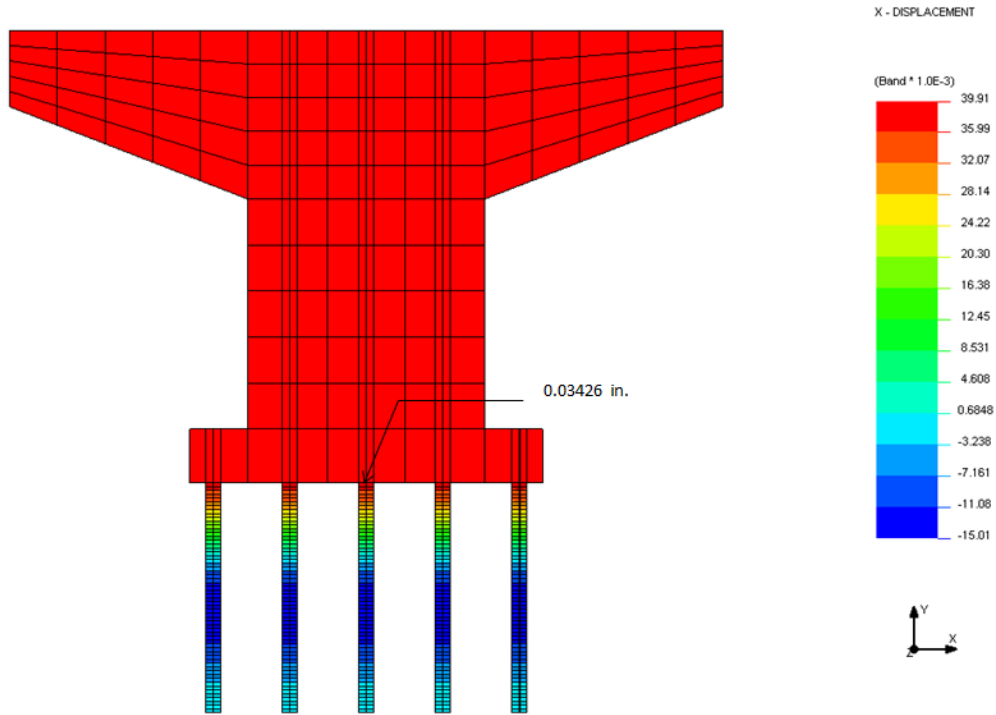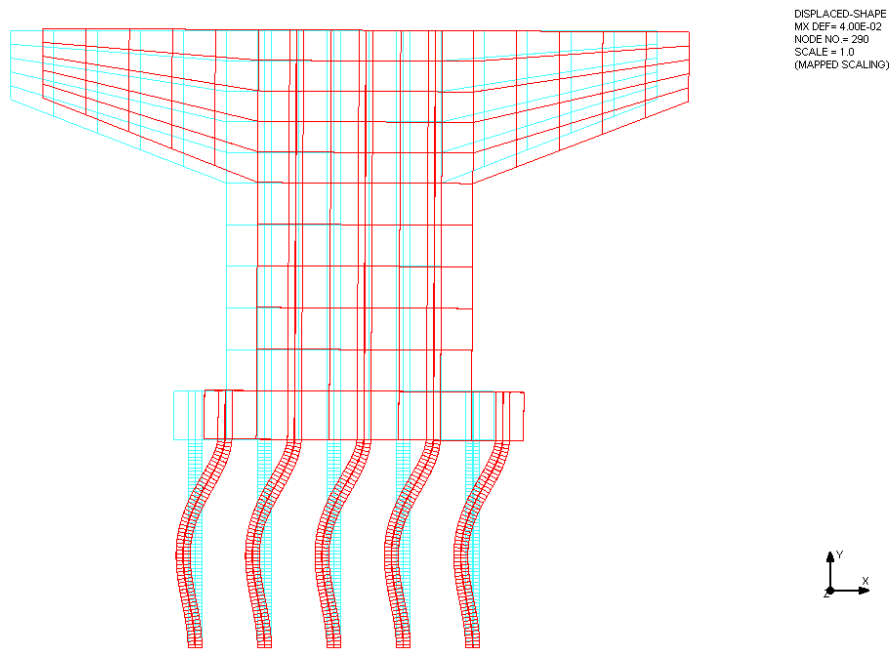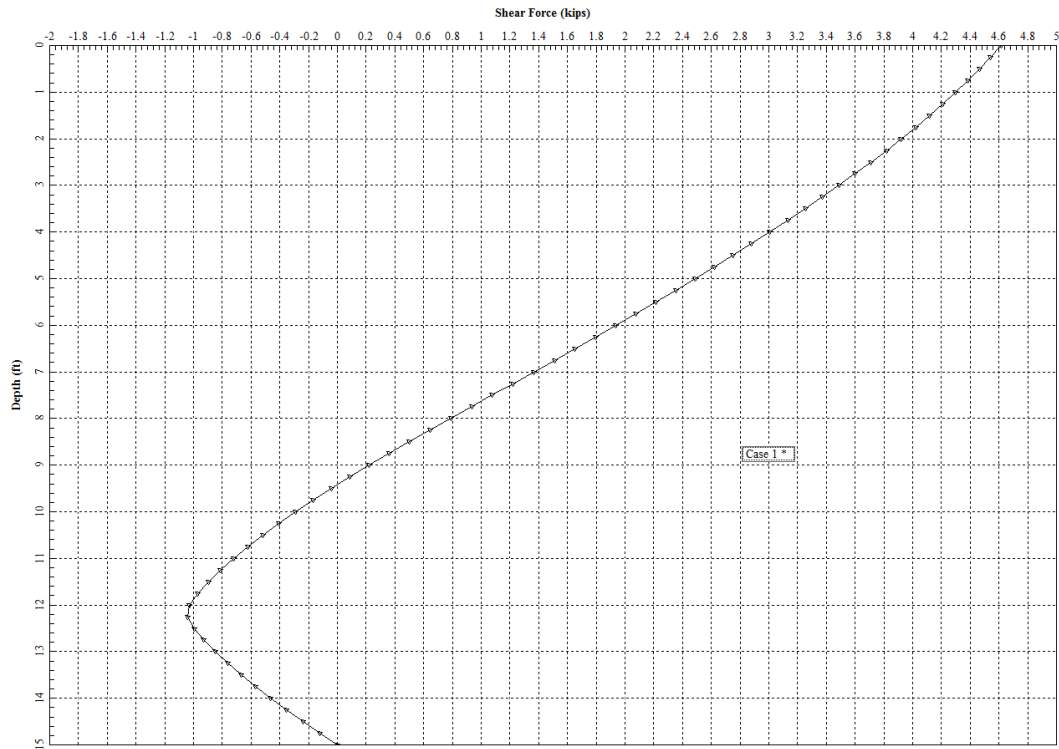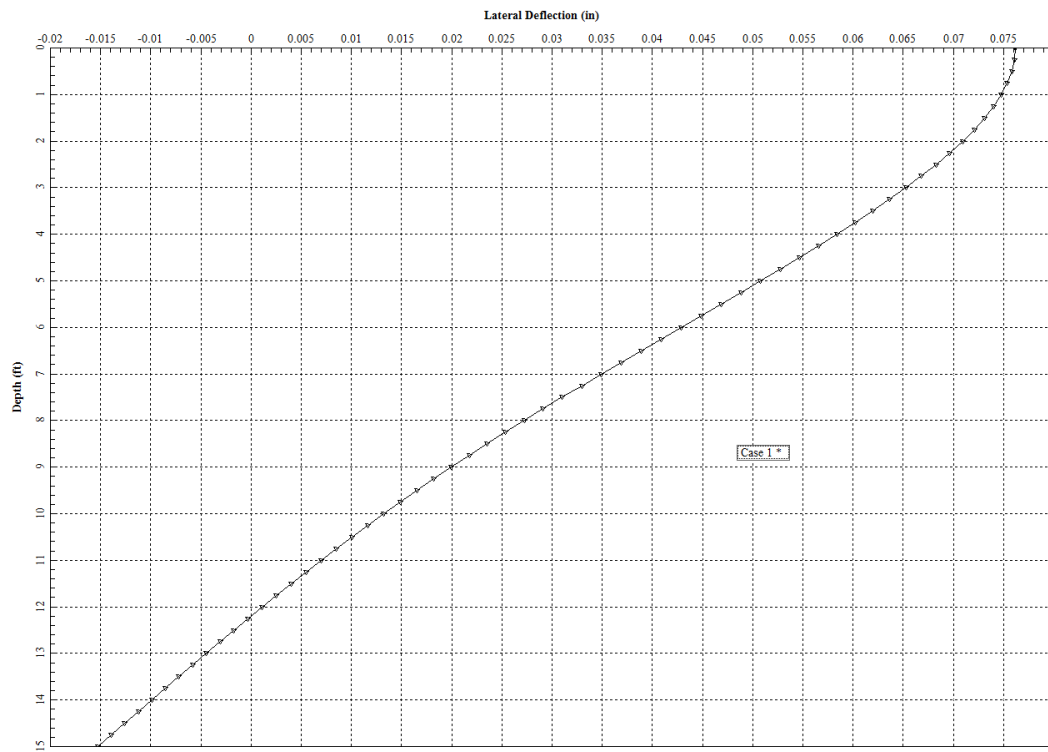*Figure B.5* Model 3 shear force along the pile depth (LPile)
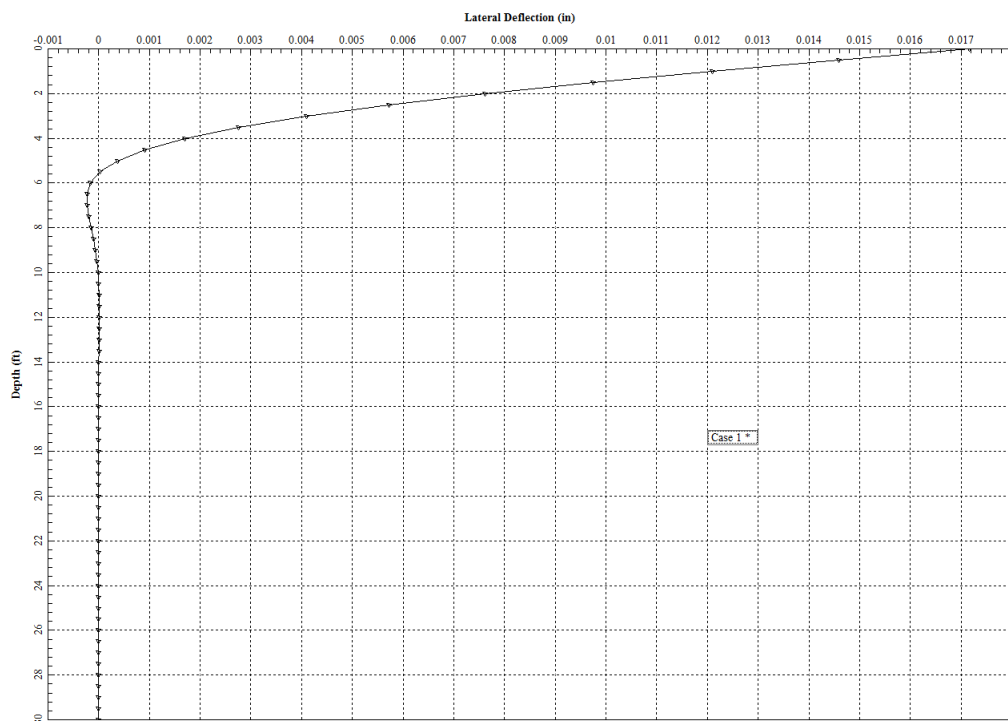
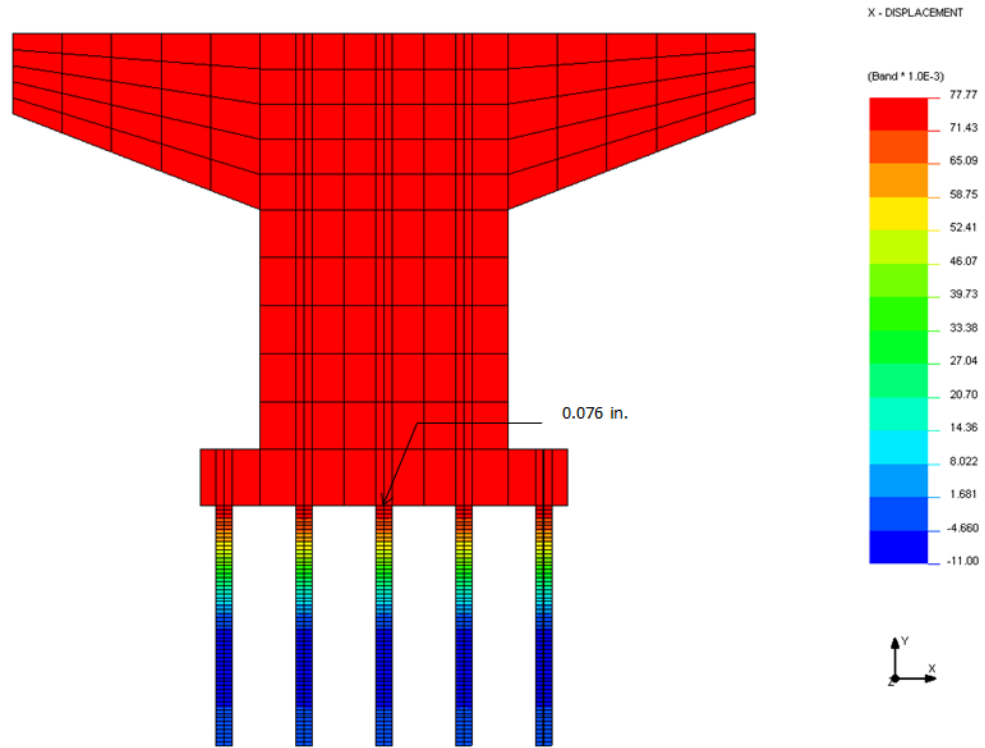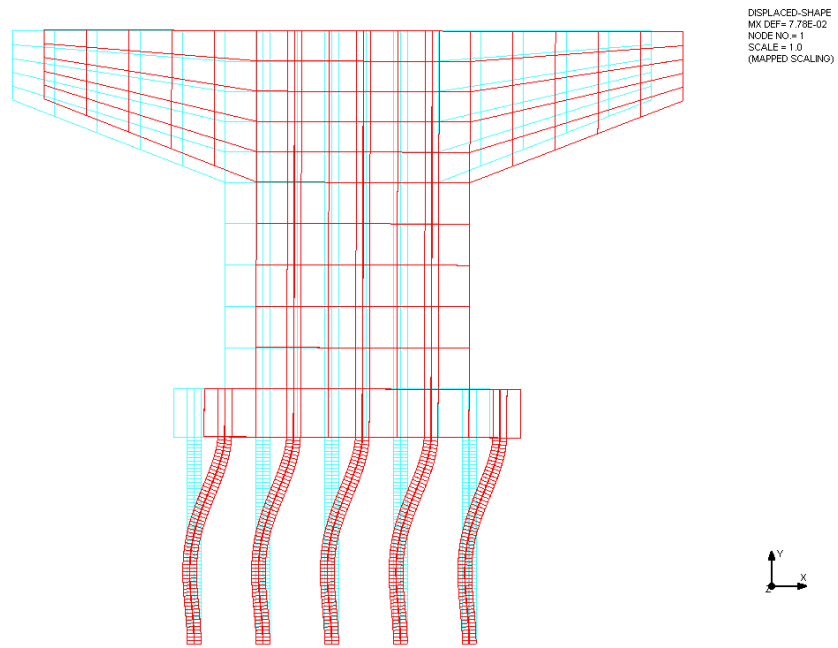*Figure B.6* Model 3 lateral deflection along the pile depth (LPile)
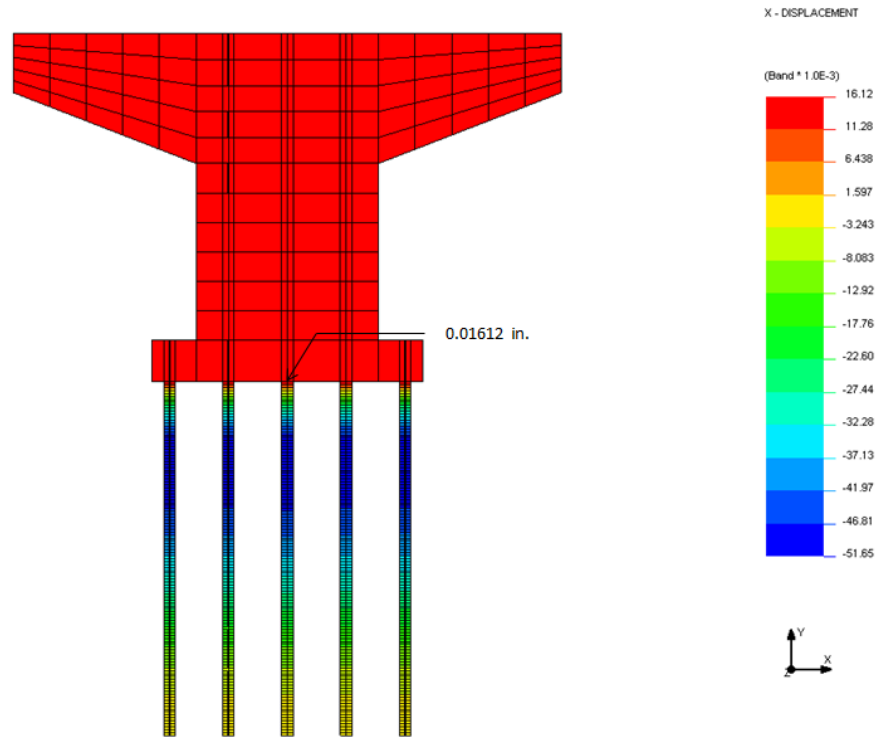
Figure B.7 NISA finite element result for Test Model 3
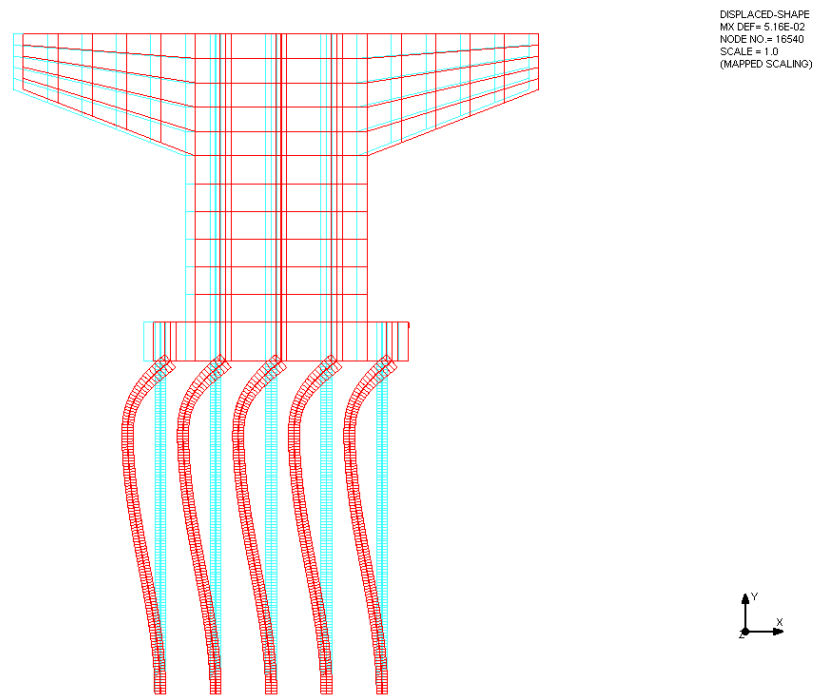
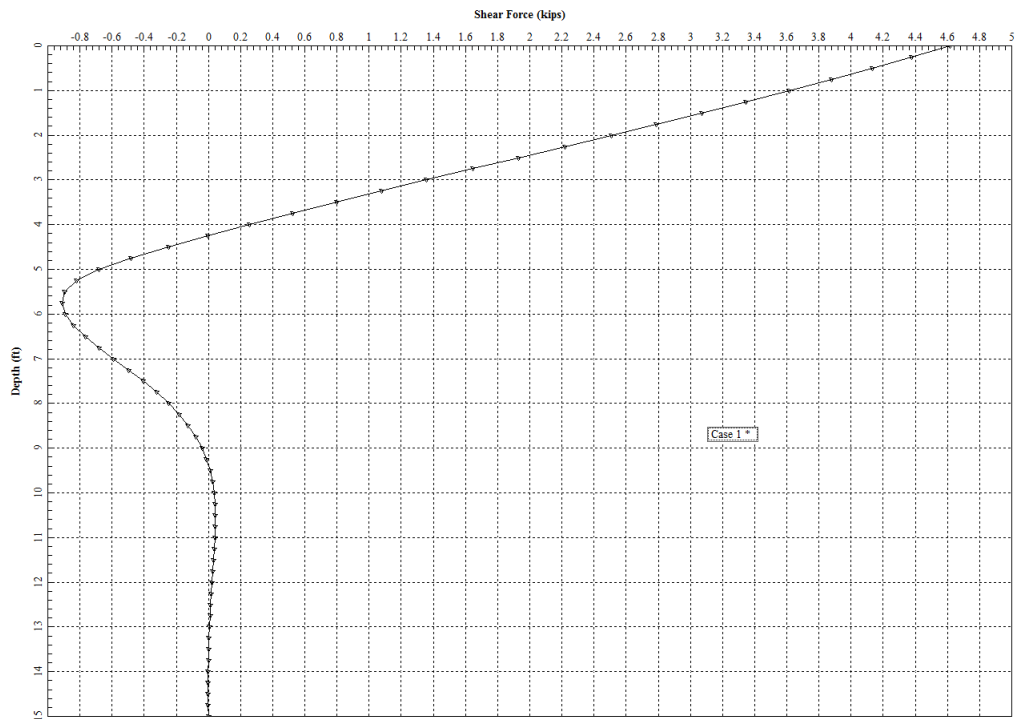*Figure B.8* Lateral deflection for Test Model 3 (in scale of 1)
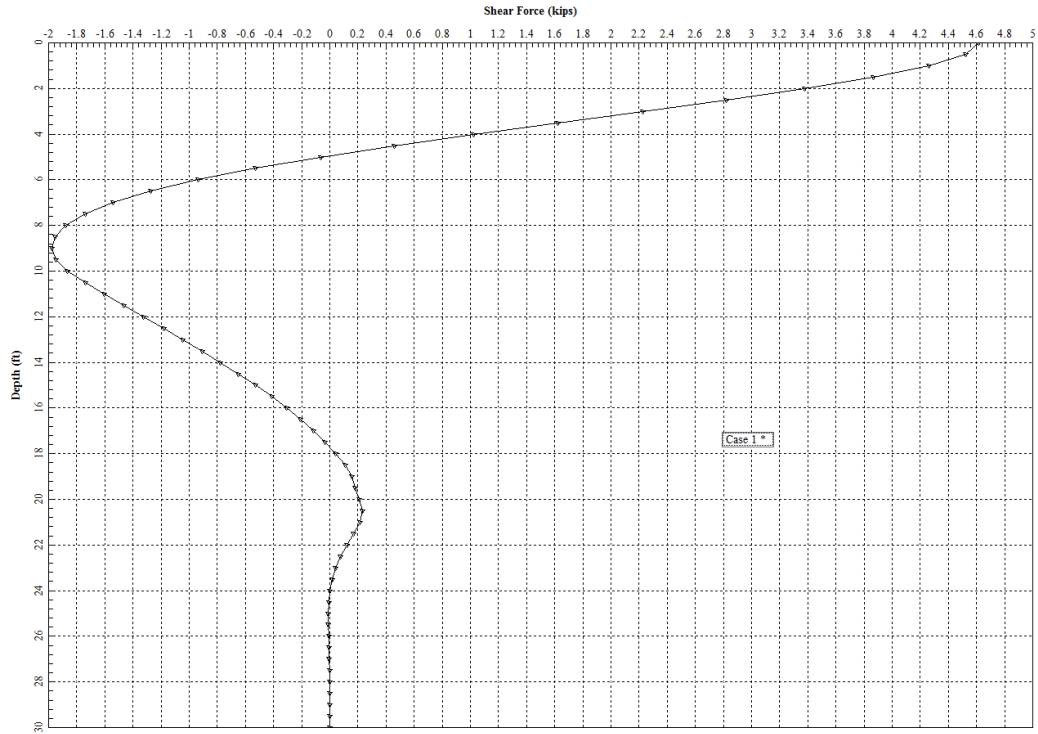
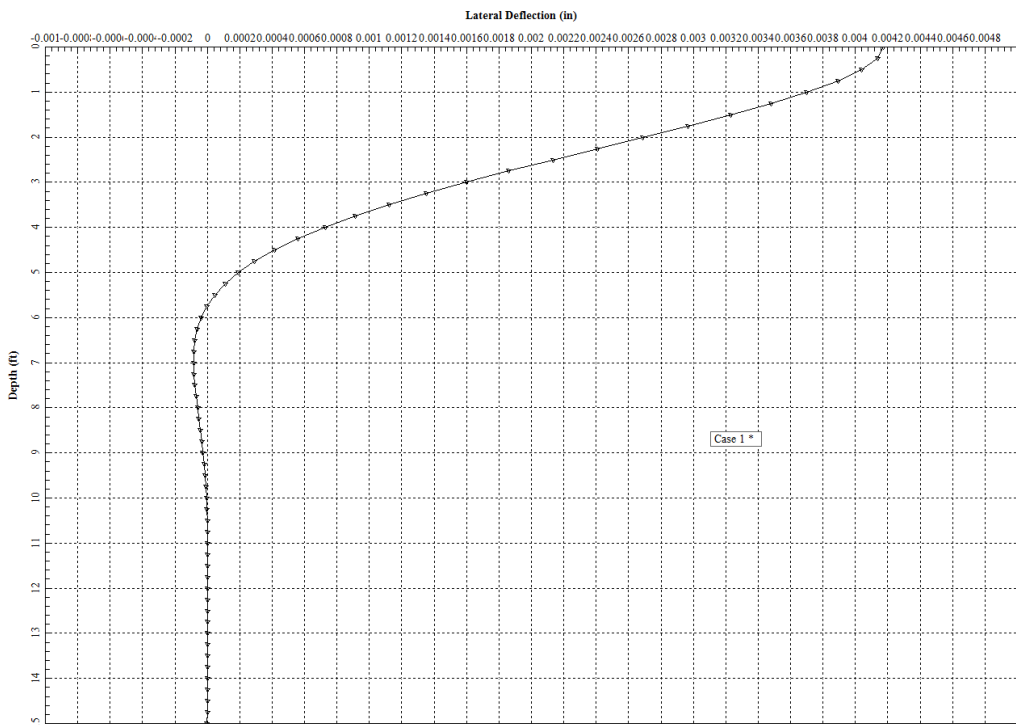*Figure B.9* Model 4 shear force along the pile depth (LPile)
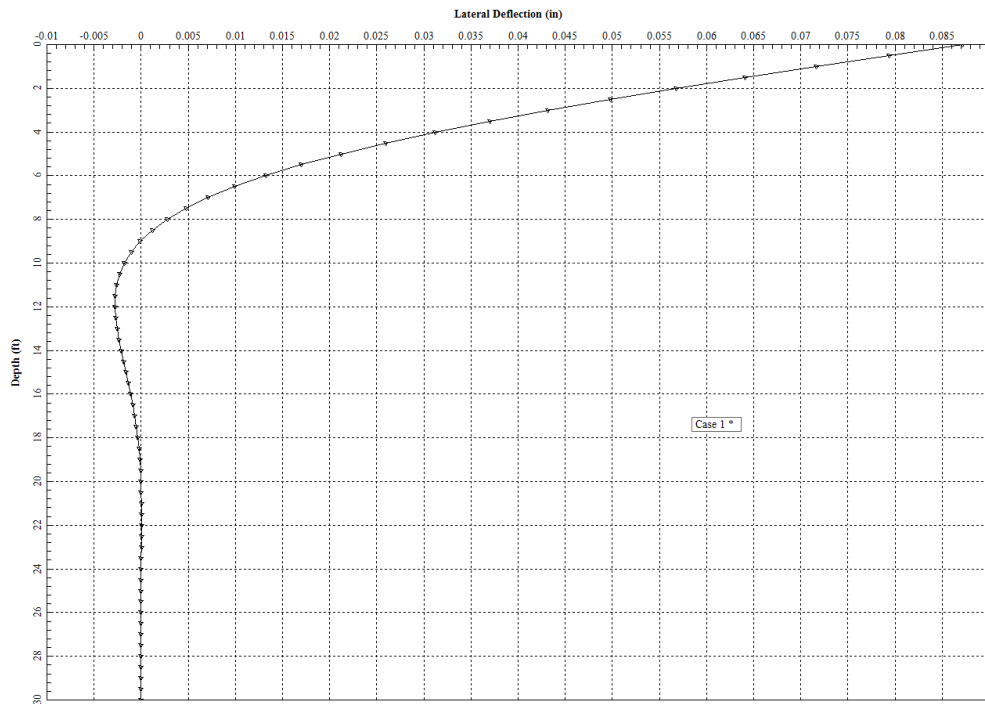
Figure B.10 Model 4 lateral deflection along the pile depth (LPile)
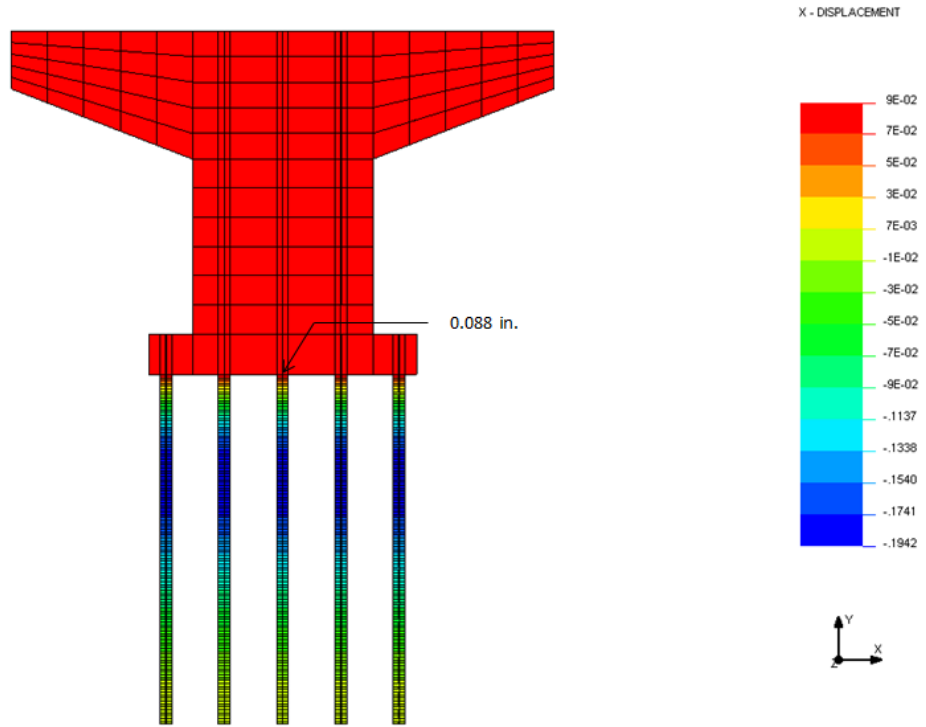
Figure B.11 NISA finite element result for Test Model 4
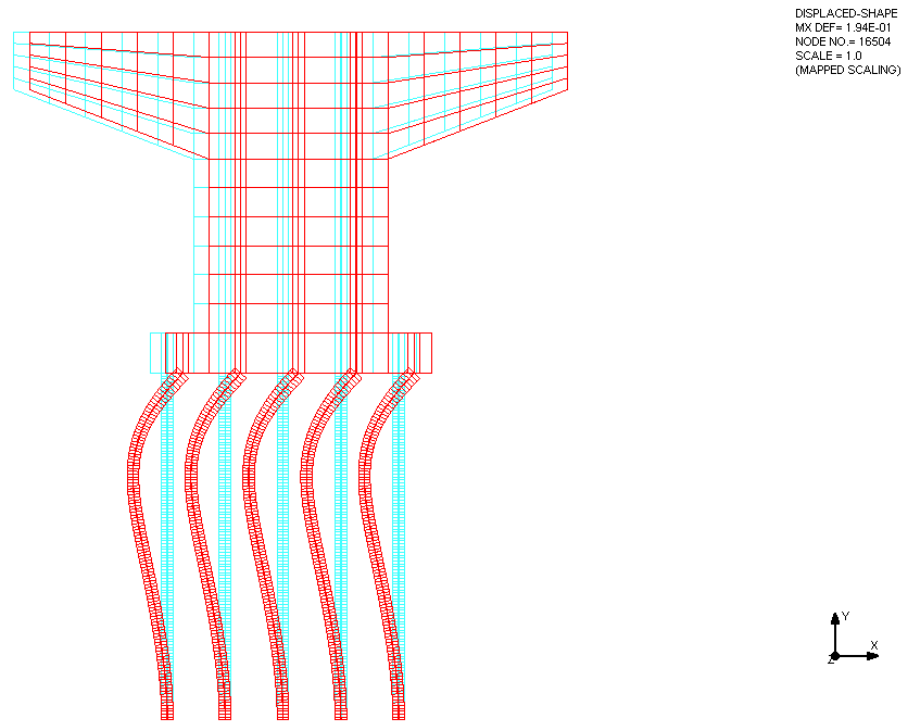
Figure B.12 Lateral deflection for Test Model 4 (in scale of 1)
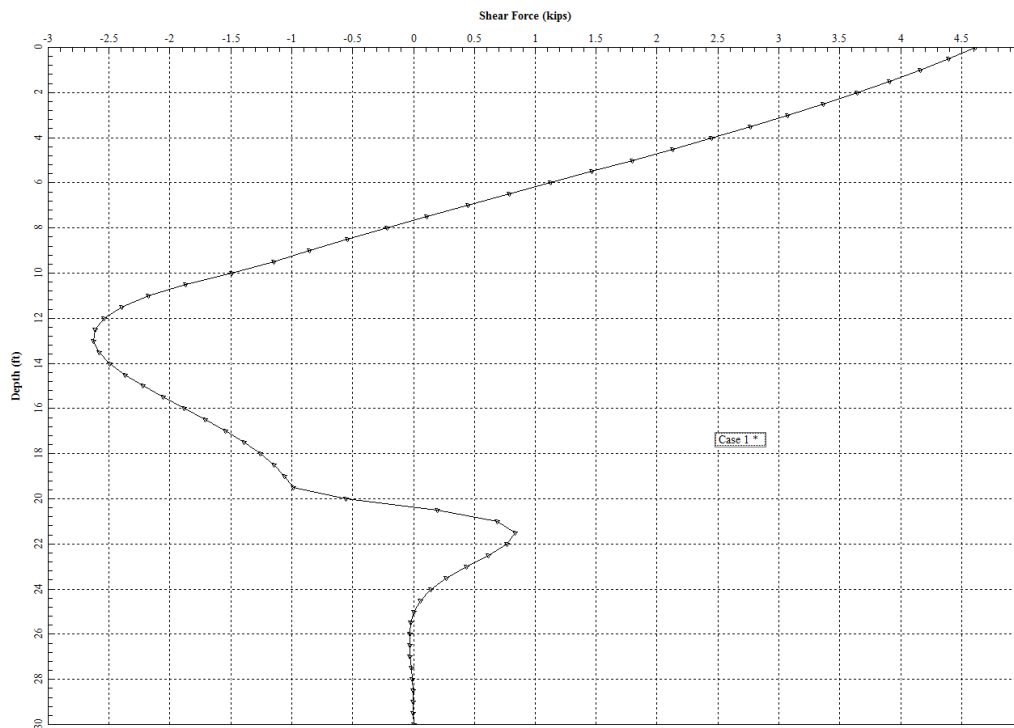
Figure B.13 Model 5 shear force along the pile depth (LPile)
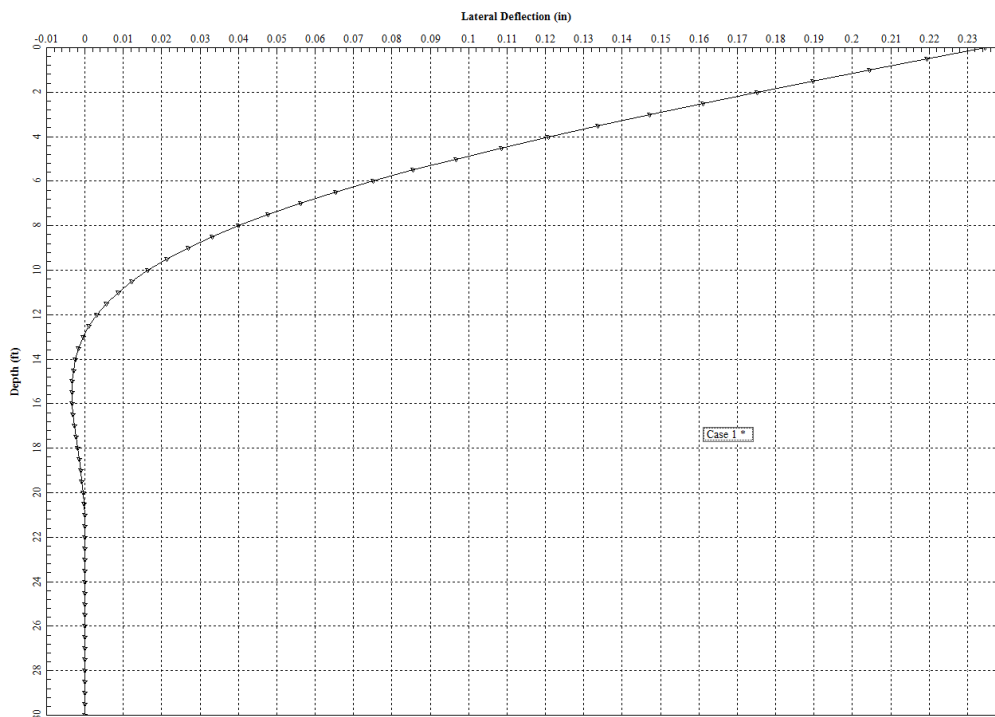
*Figure B.14* Model 5 lateral deflection along the pile depth (LPile)
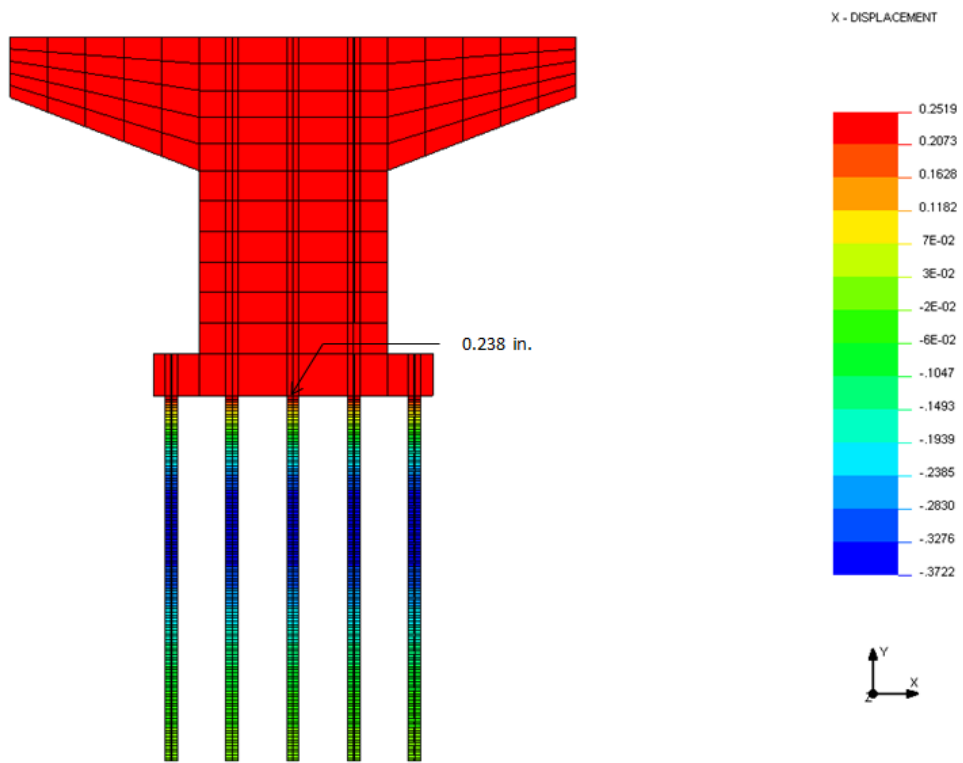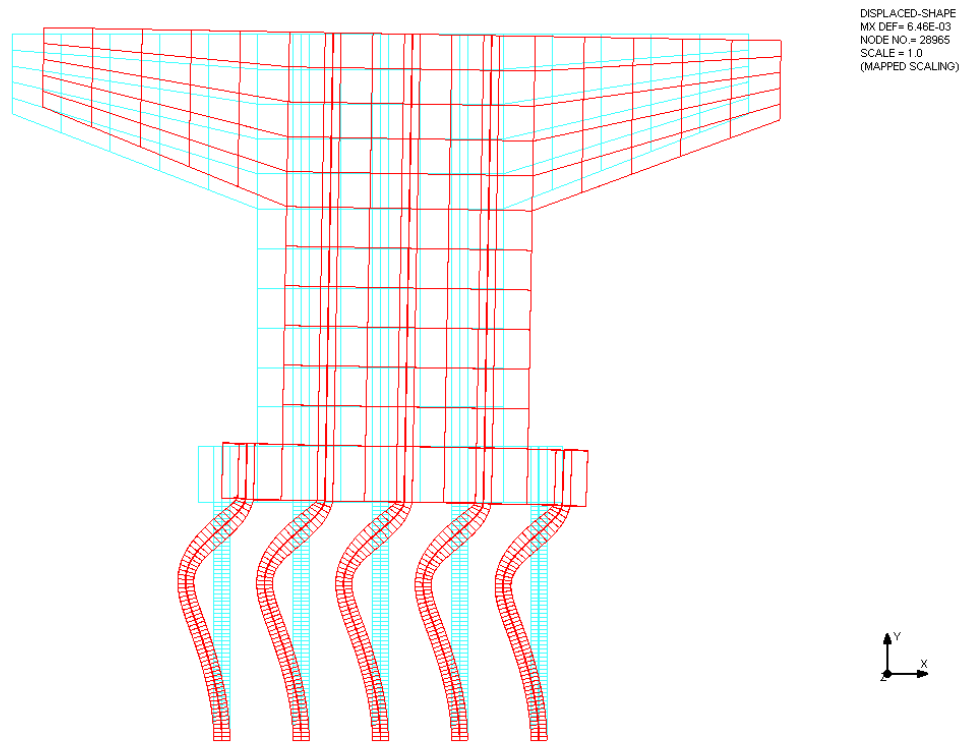
Figure B.15 NISA finite element result for Test Model 5
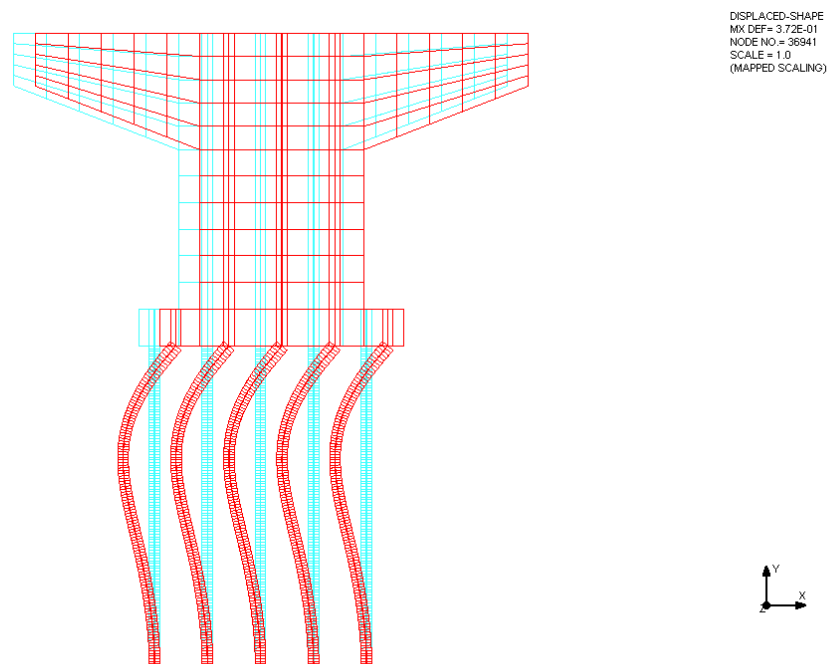
Figure B.16 Lateral deflection for Test Model 5 (in scale of 1)
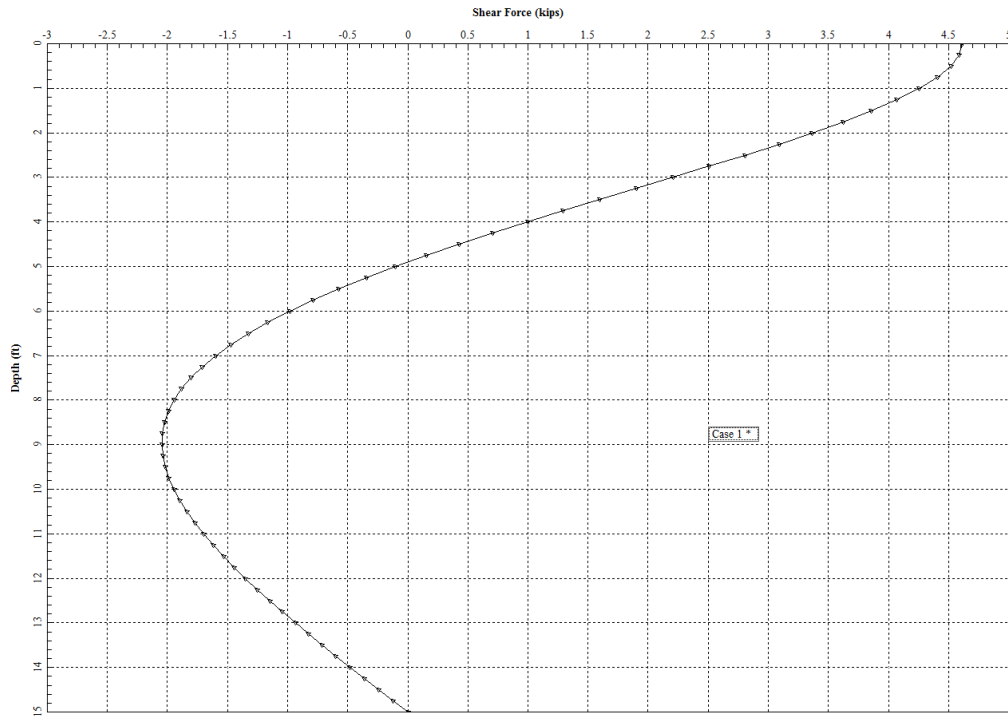
Figure B.17 Model 6 shear force along the pile depth (LPile)
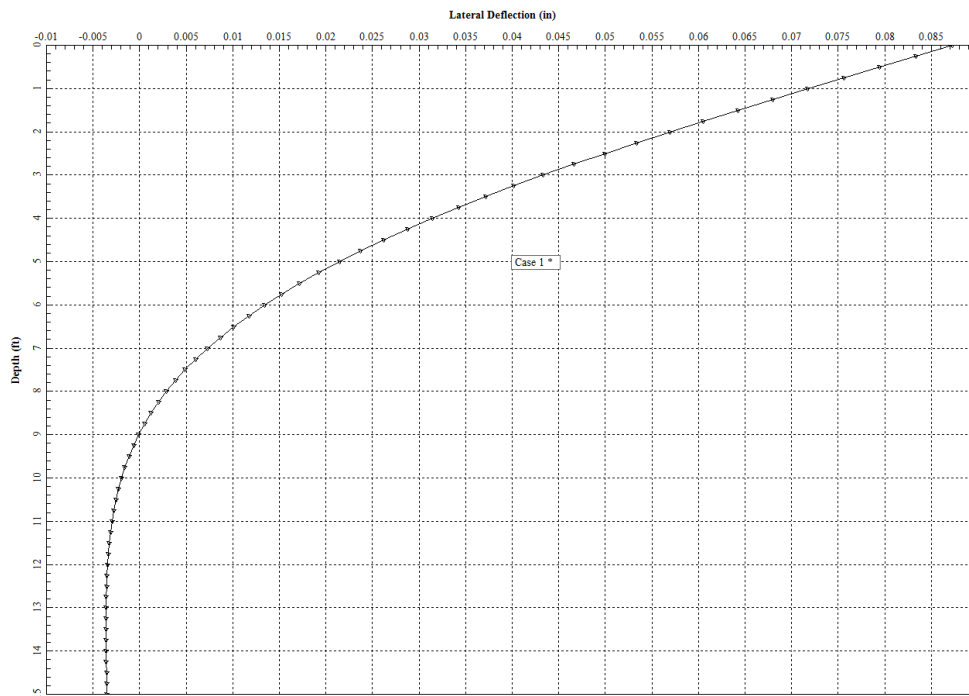
Figure B.18 Model 6 lateral deflection along the pile depth (LPile)
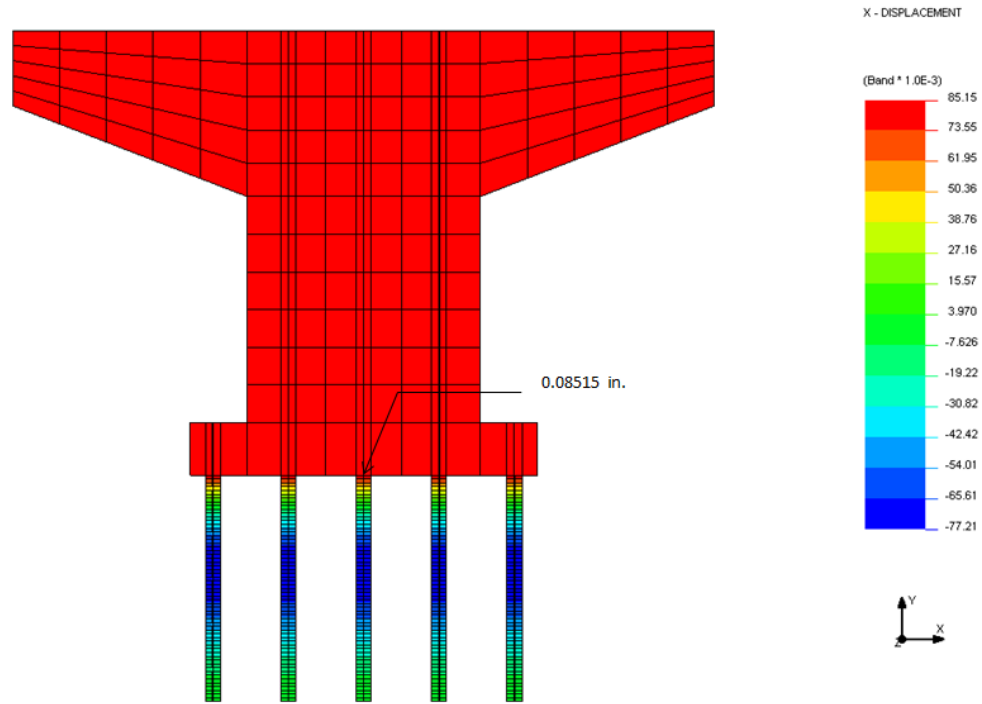
Figure B.19 NISA finite element result for Test Model 6
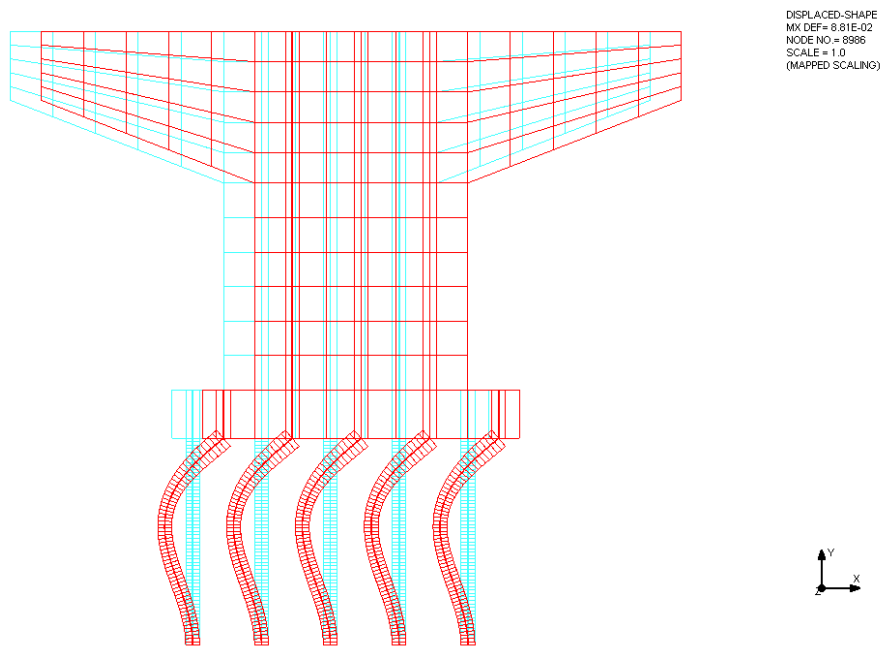
Figure B.20 Lateral deflection for Test Model 6 (in scale of 1)
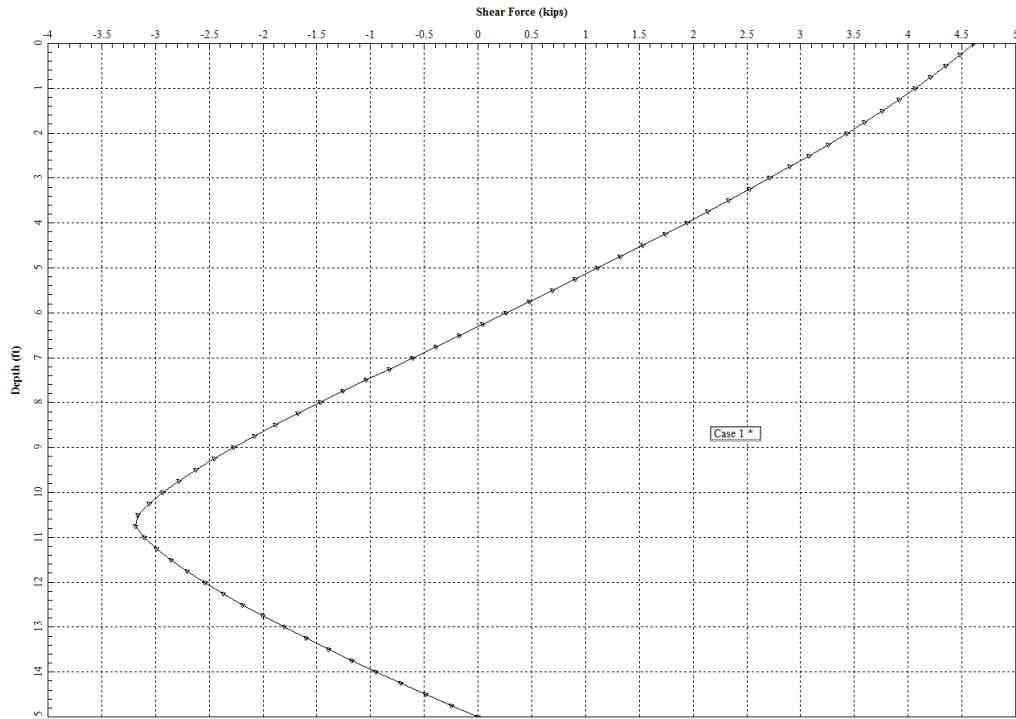
Figure B.21 Model 7 shear force along the pile depth (LPile)
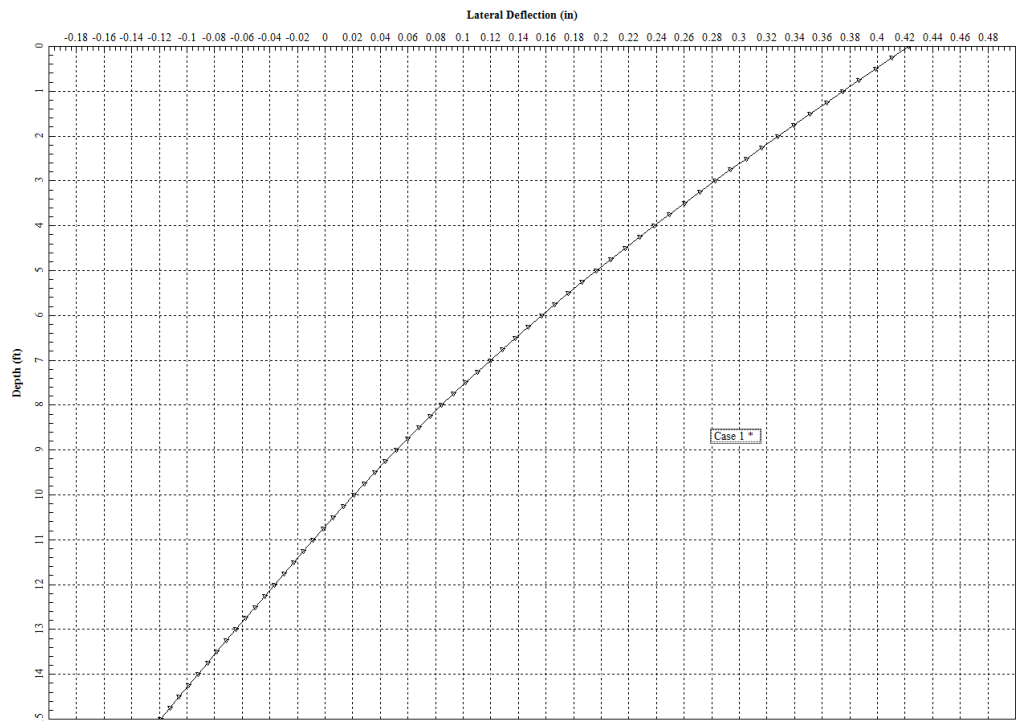
Figure B.22 Model 7 lateral deflection along the pile depth (LPile)

X - DISPLACEMENT

0.425 in.

0.4330
0.3969
0.3608
0.3248
0.2887
0.2526
0.2165
0.1804
0.1443
0.1083
7E-02
4E-02
9E-06
-4E-02
-7E-02
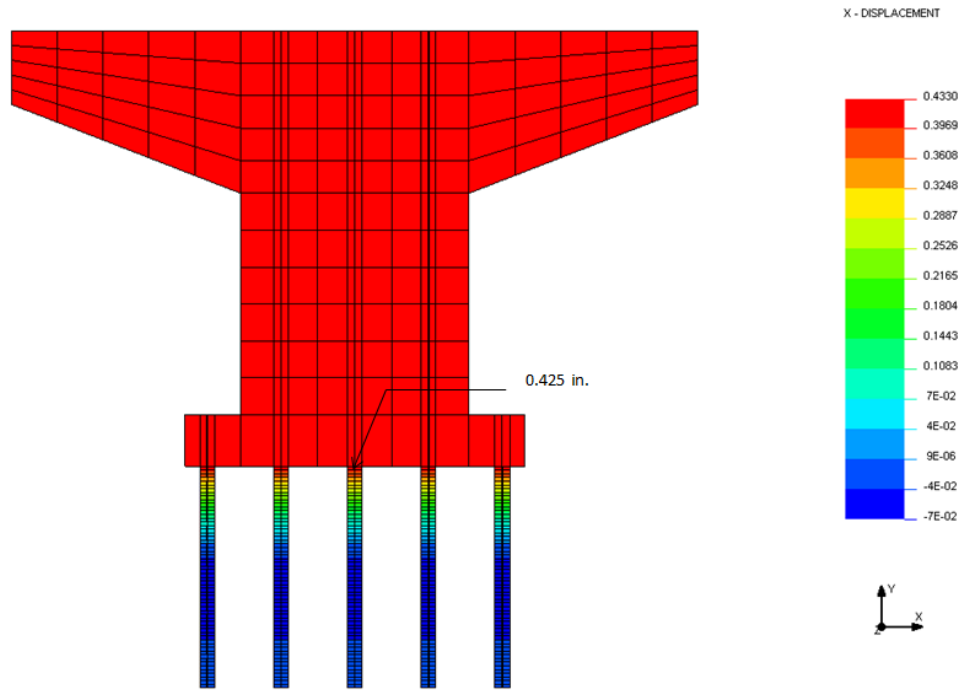
Figure B.23 NISA finite element result for Test Model 7

DISPLACED-SHAPE
MX DEF= 4.36E-01
NODE NO.= 8986
SCALE = 1.0
(MAPPED SCALING)
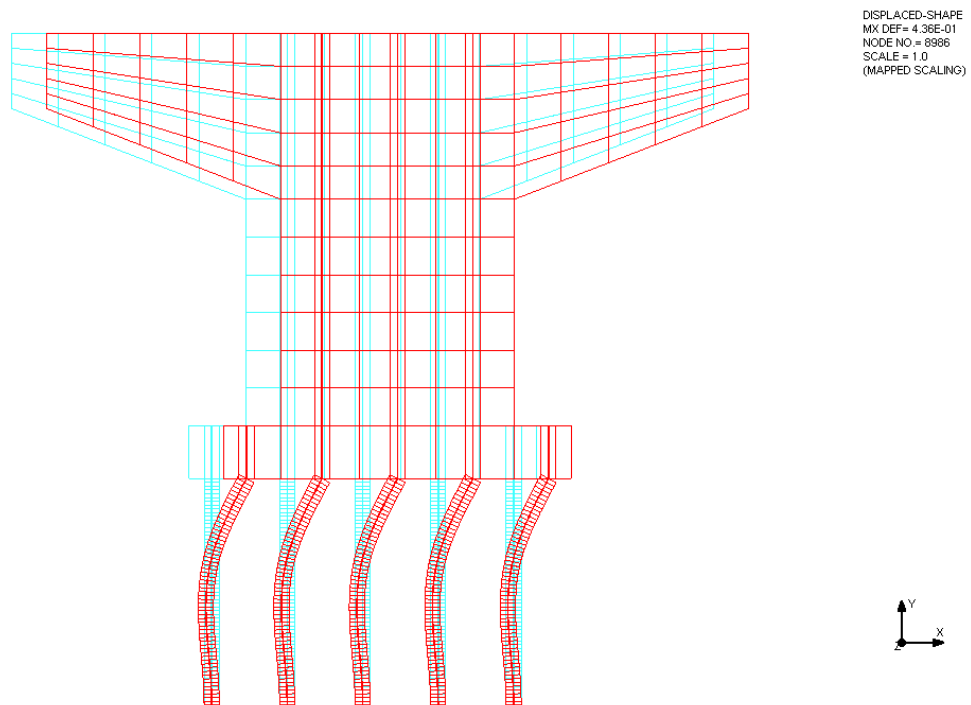
Figure B.24 Lateral deflection for Test Model 7 (in scale of 1)
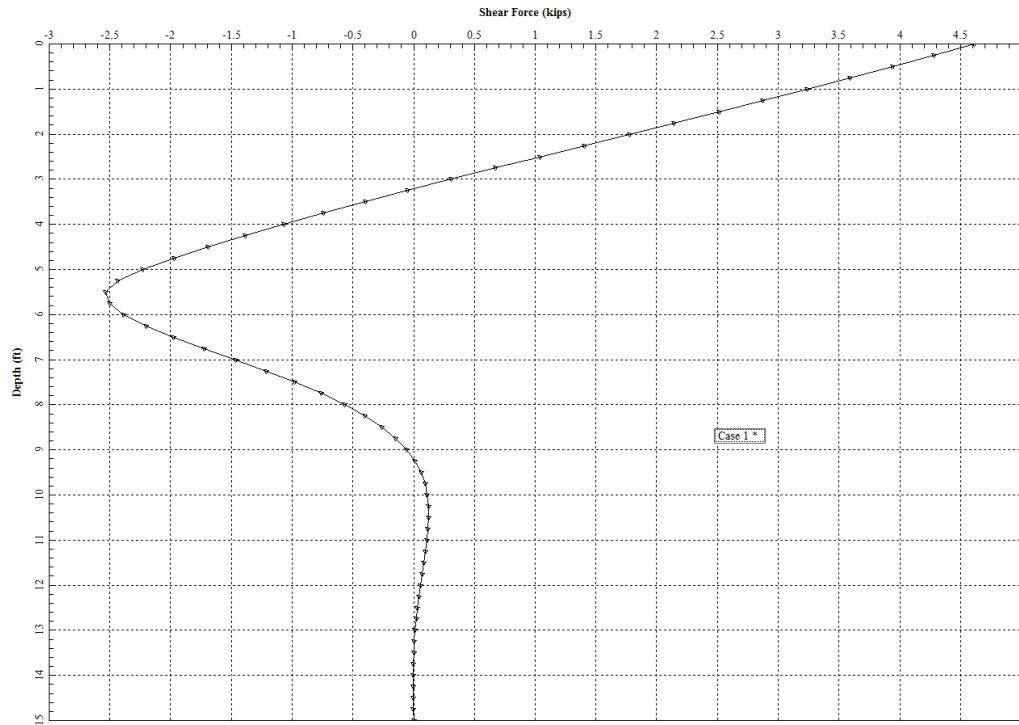
Figure B.25 Model 8 shear force along the pile depth (LPile)
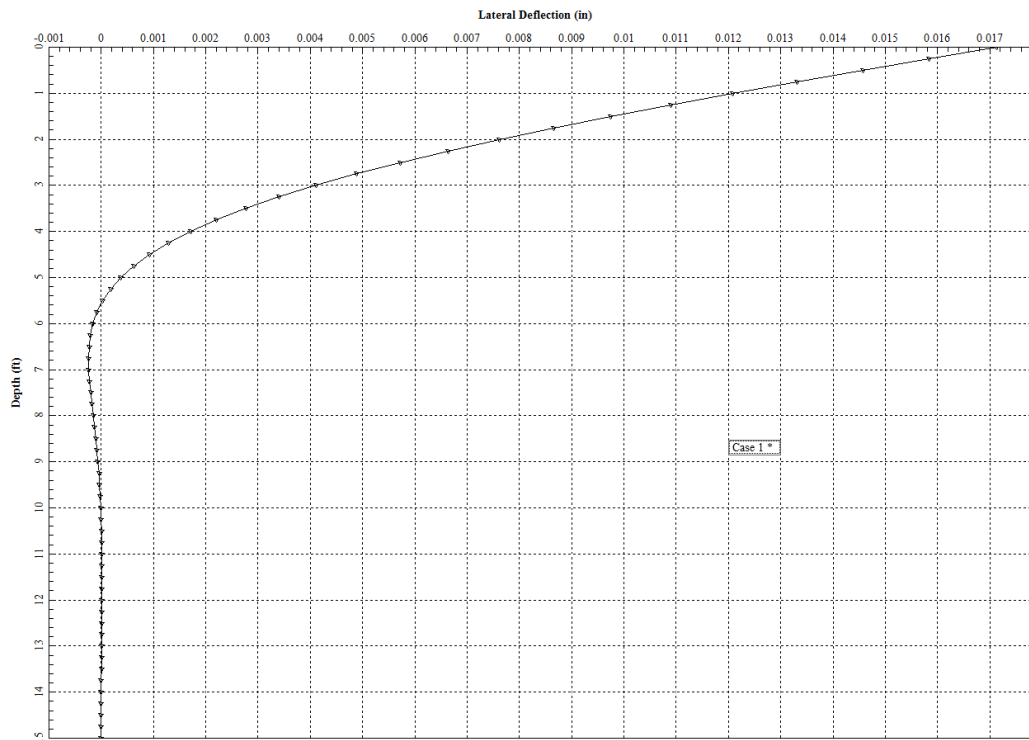
Figure B.26 Model 8 lateral deflection along the pile depth (LPile)
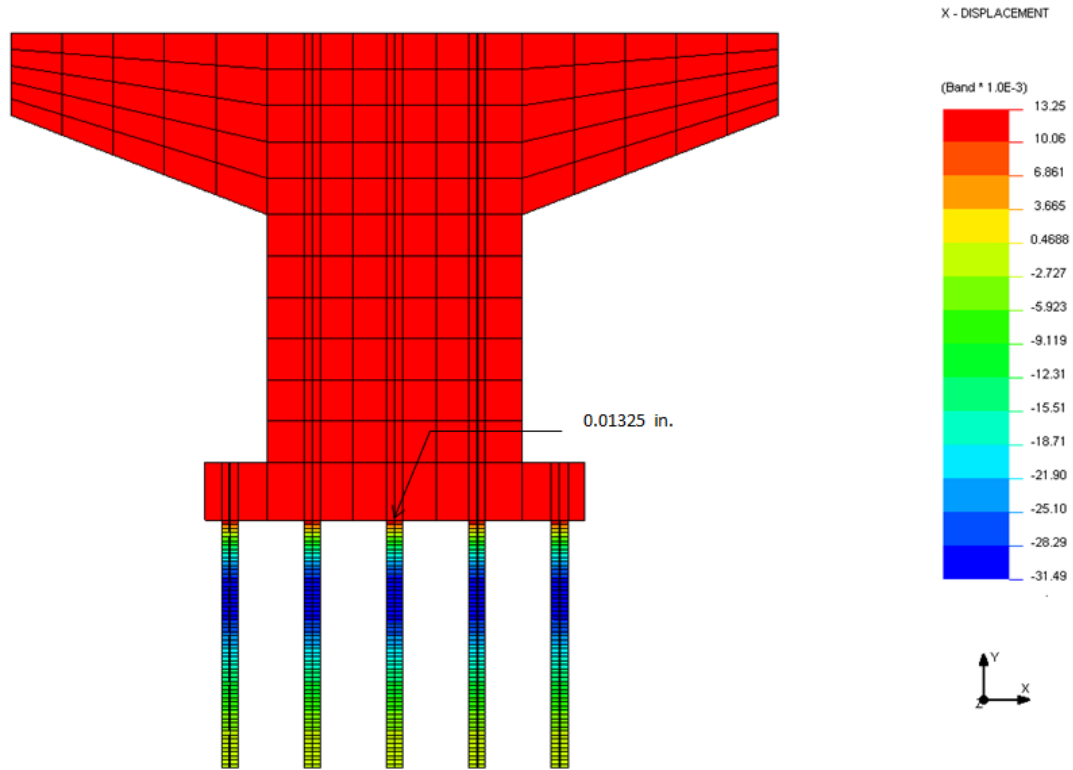
Figure B.27 NISA finite element result for Test Model 8
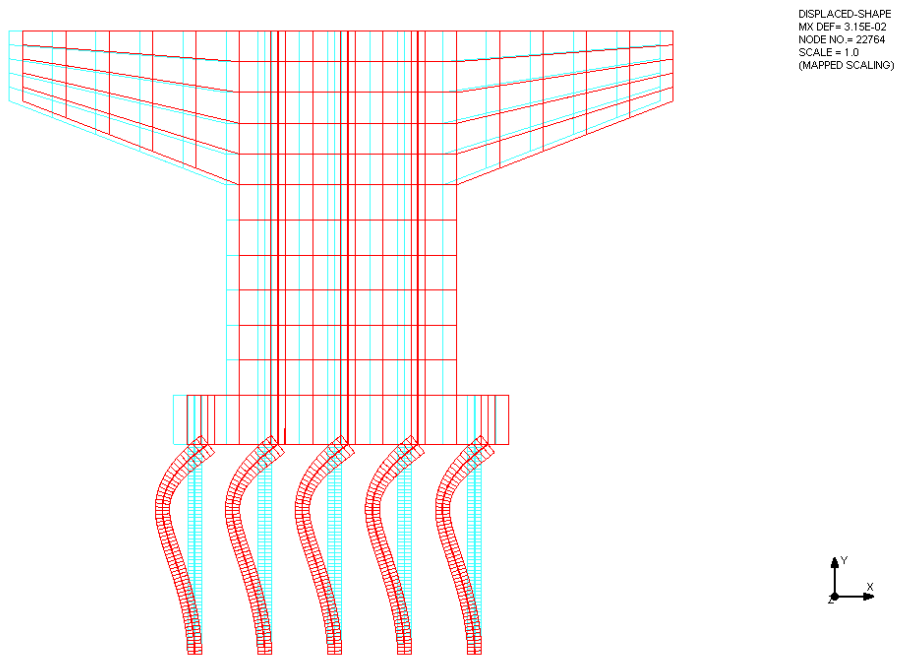
Figure B.28 Lateral deflection for Test Model 8 (in scale of 1)
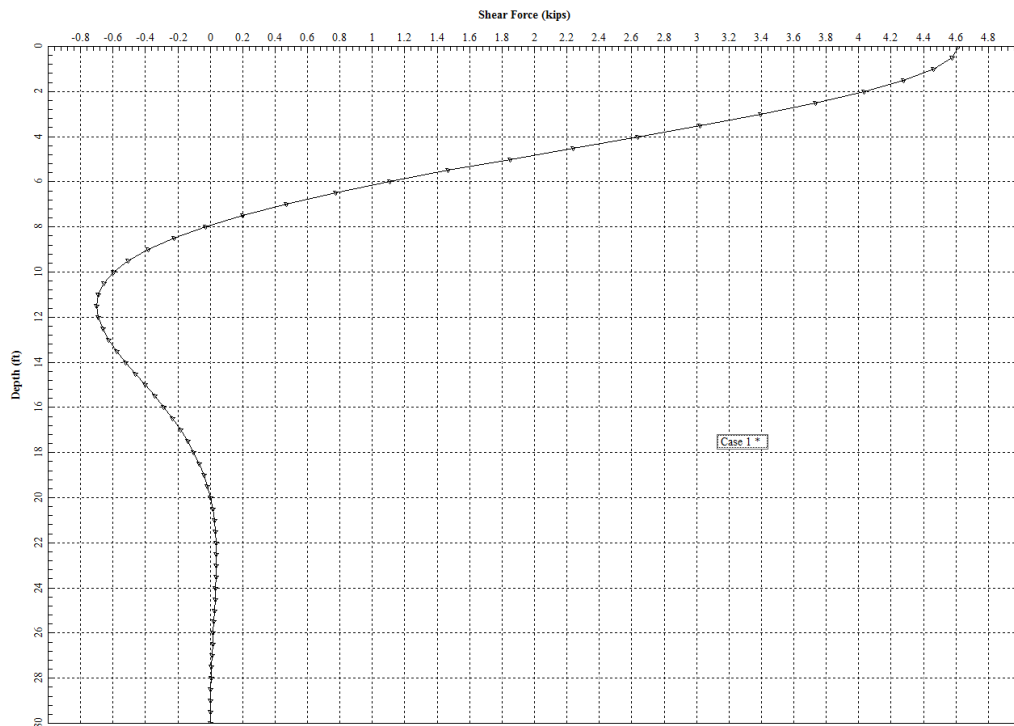
Figure B.29 Model 9 shear force along the pile depth (LPile)
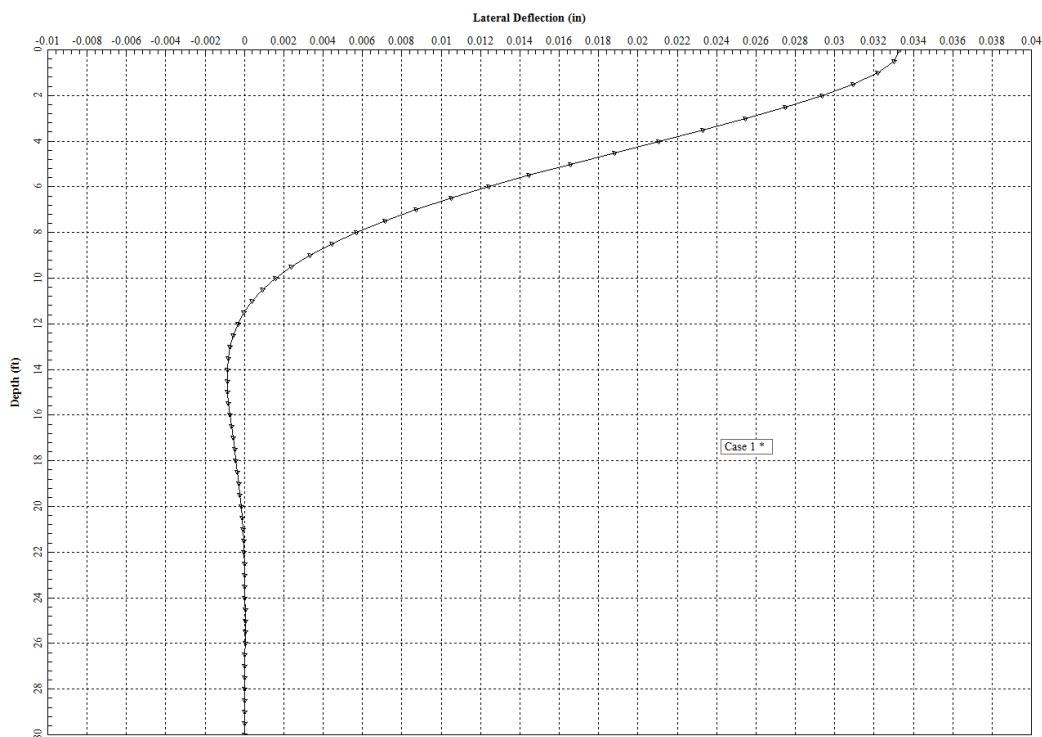
Figure B.30 Model 9 lateral deflection along the pile depth (LPile)
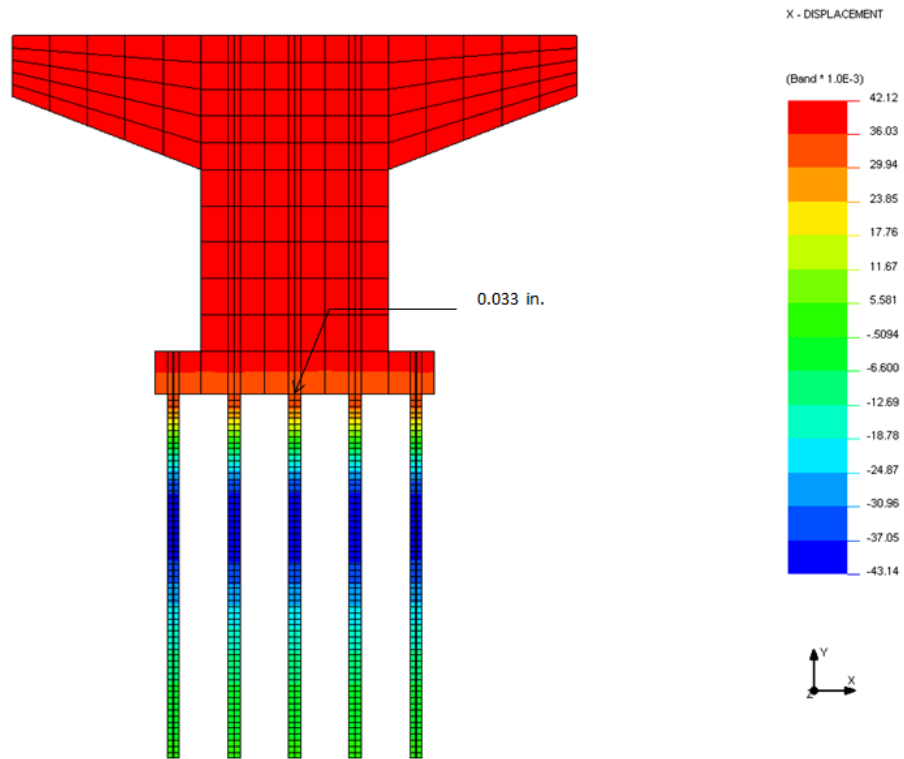
Figure B.31 NISA finite element result for Test Model 9
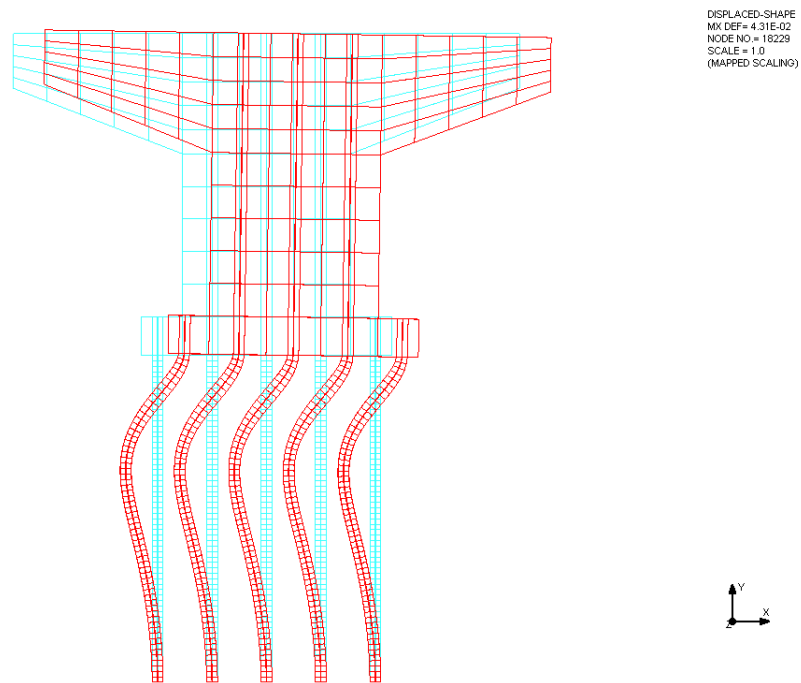
Figure B.32 Lateral deflection for Test Model 9 (in scale of 1)
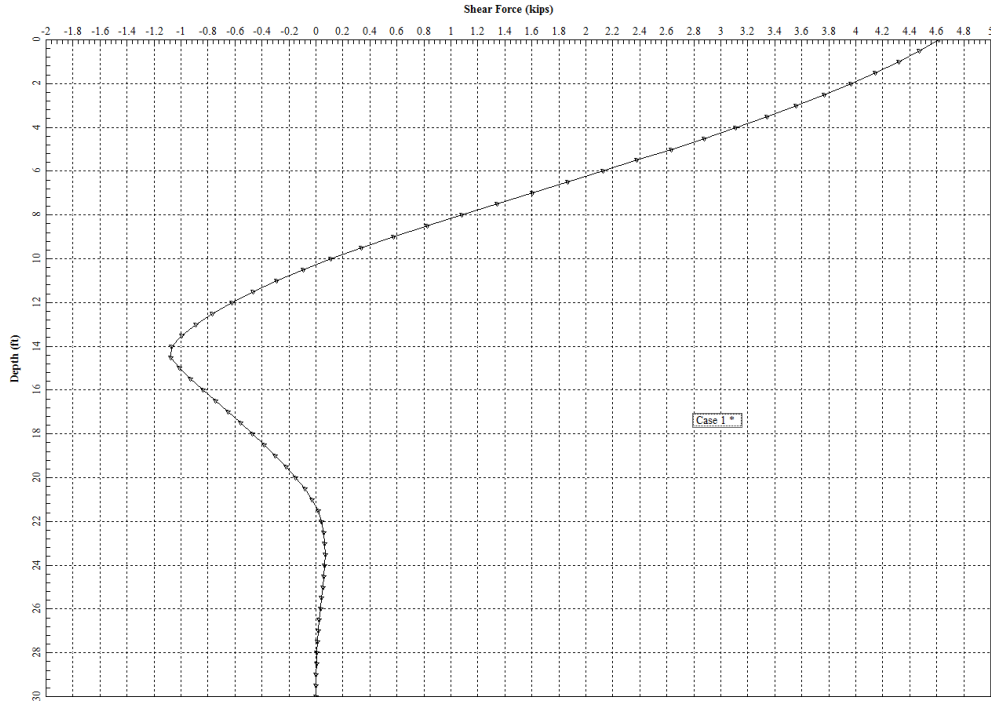
Figure B.33 Model 10 shear force along the pile depth (LPile)
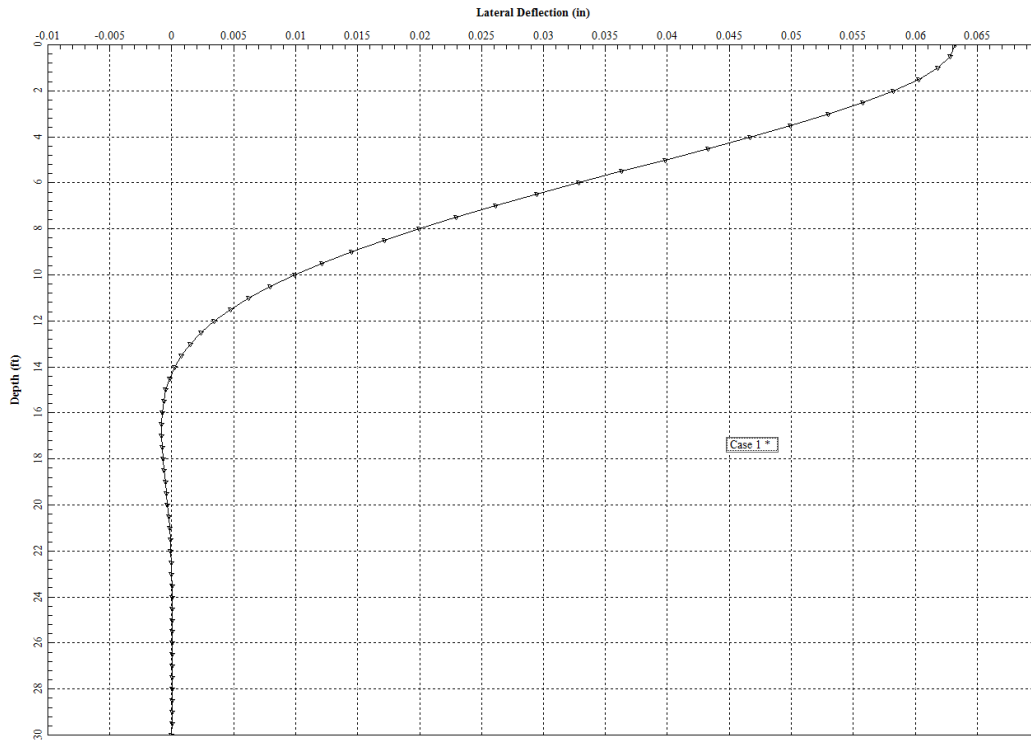
Figure B.34 Model 10 lateral deflection along the pile depth (LPile)
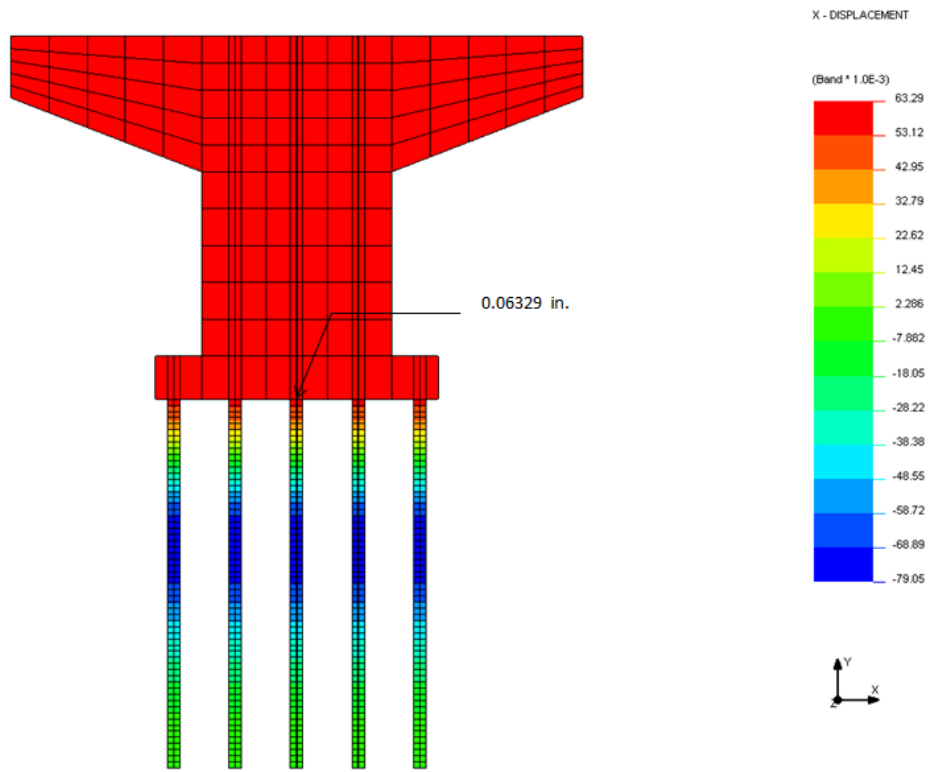
Figure B.35 NISA finite element result for Test Model 10
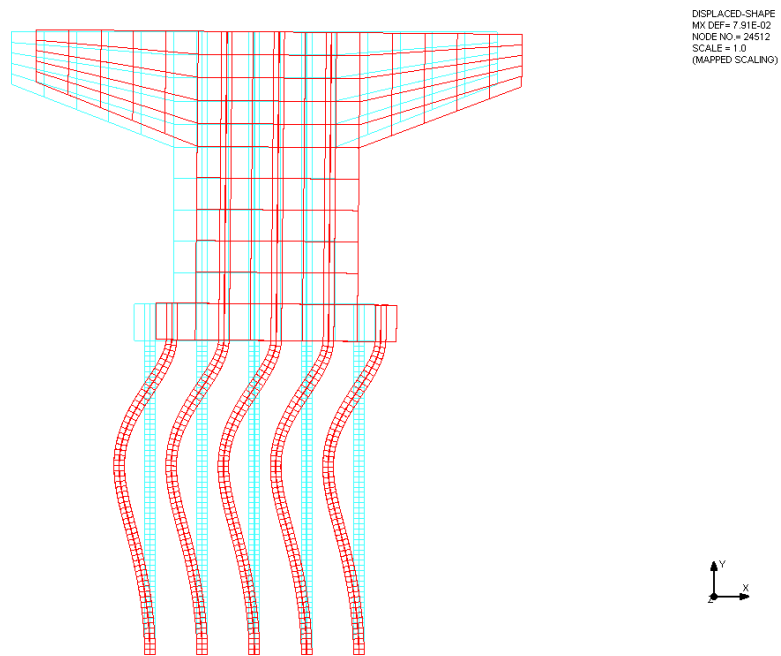
Figure B.36 Lateral deflection for Test Model 10 (in scale of 1)
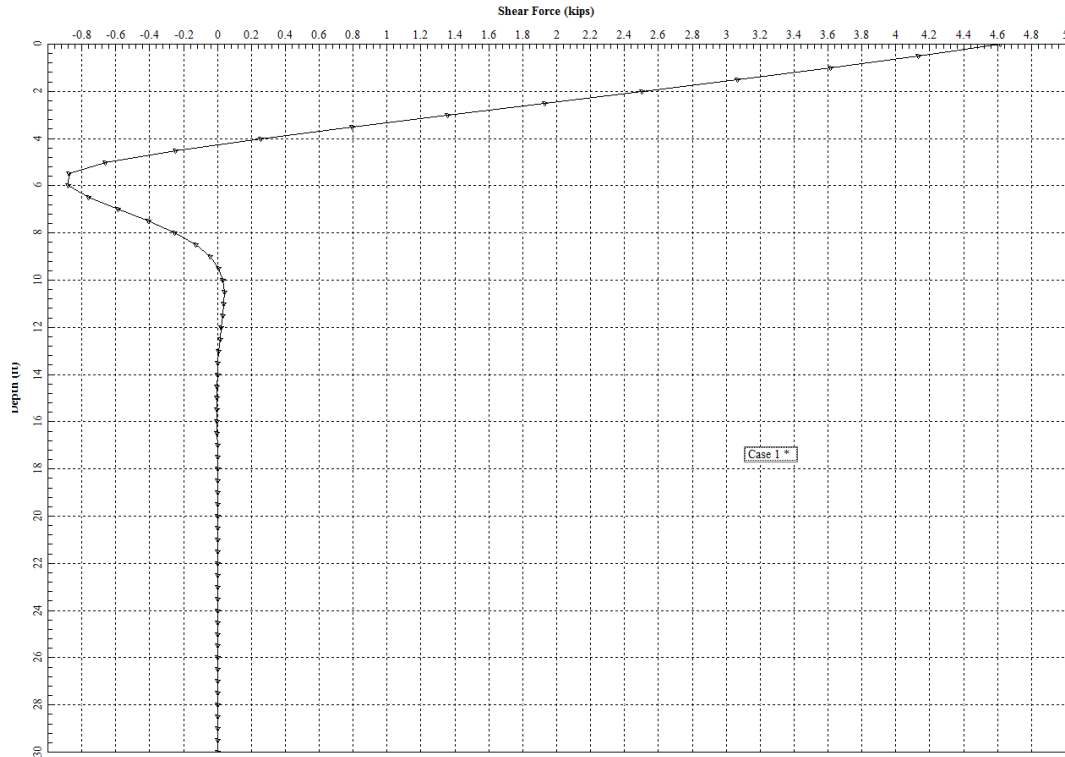
Figure B.37 Model 11 shear force along the pile depth (LPile)
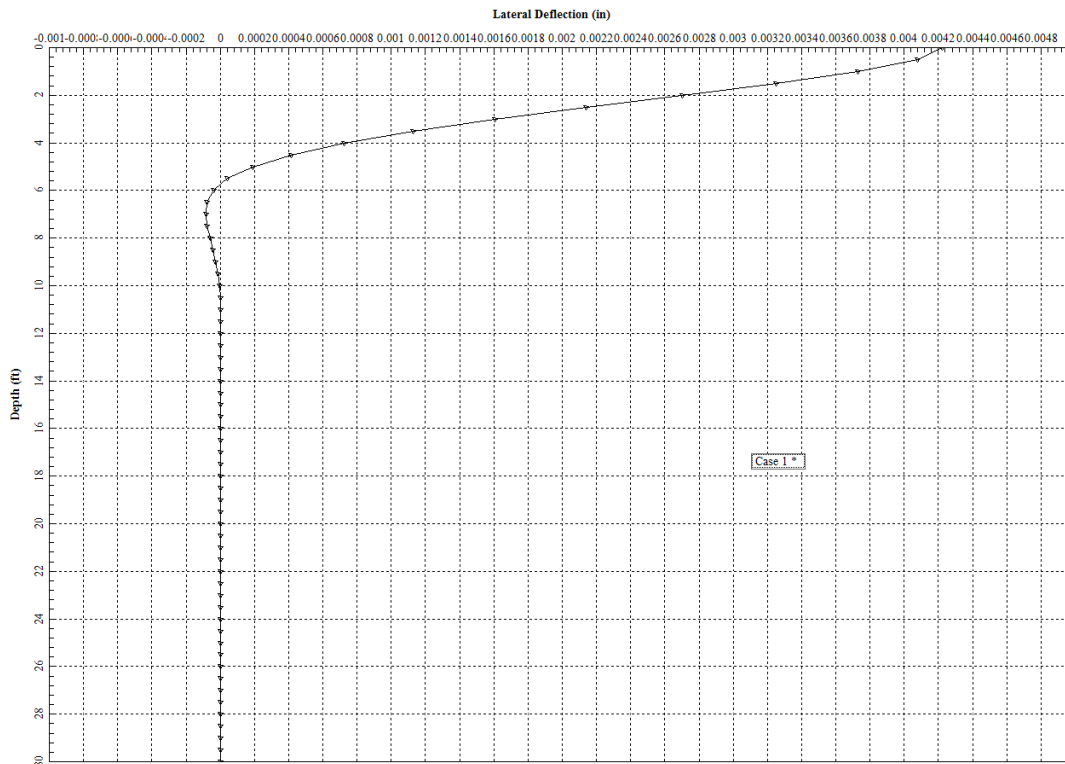
Figure B.38 Model 11 lateral deflection along the pile depth (LPile)
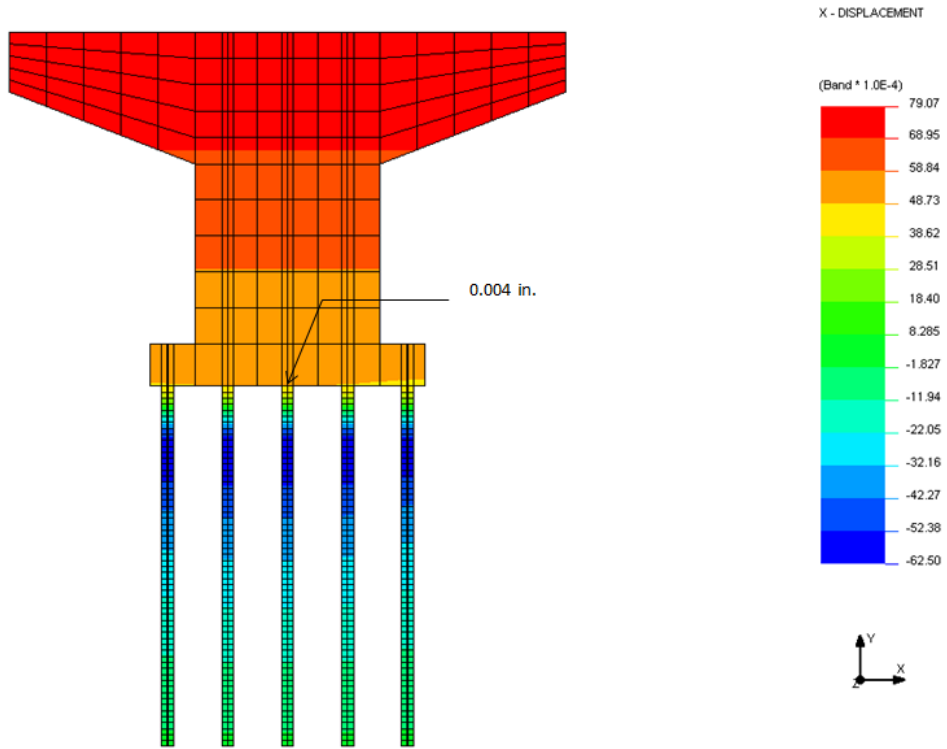
Figure B.39 NISA finite element result for Test Model 11
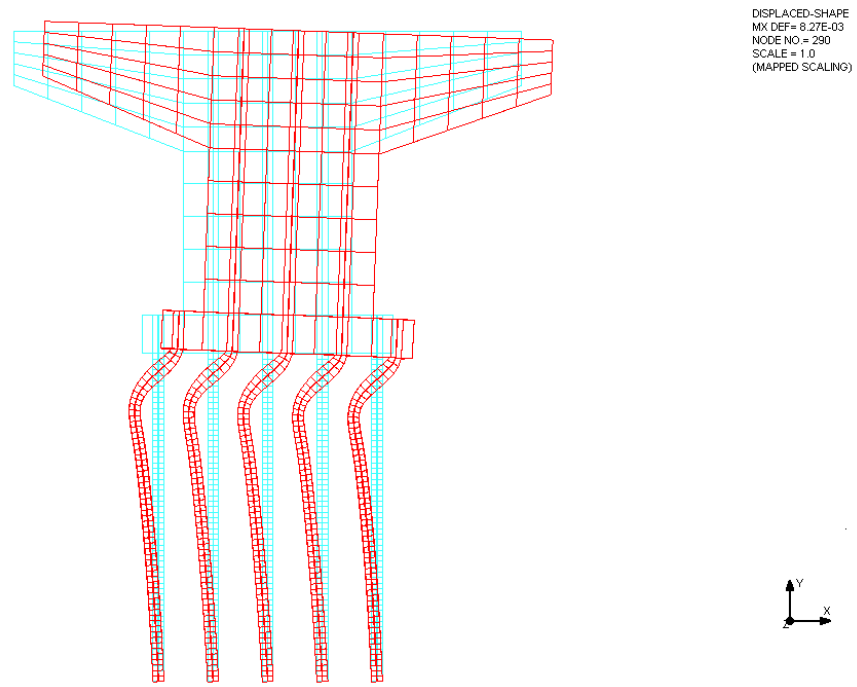
Figure B.40 Lateral deflection for Test Model 11 (in scale of 1)
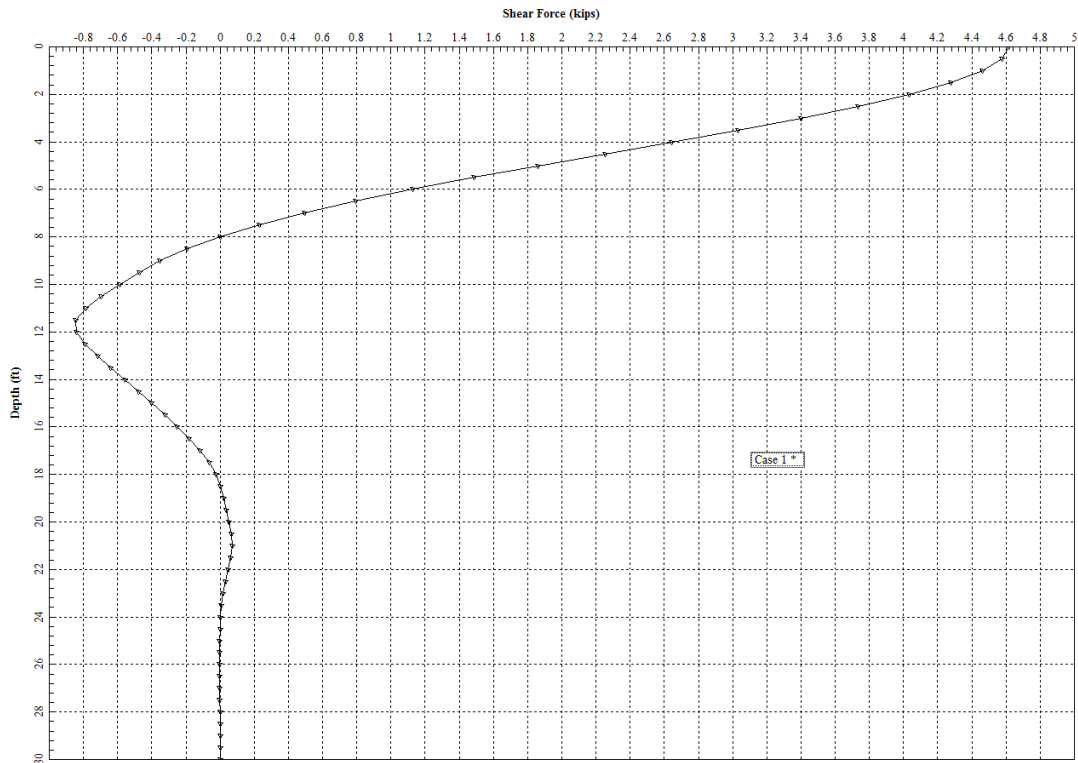
Figure B.41 Model 12 shear force along the pile depth (LPile)
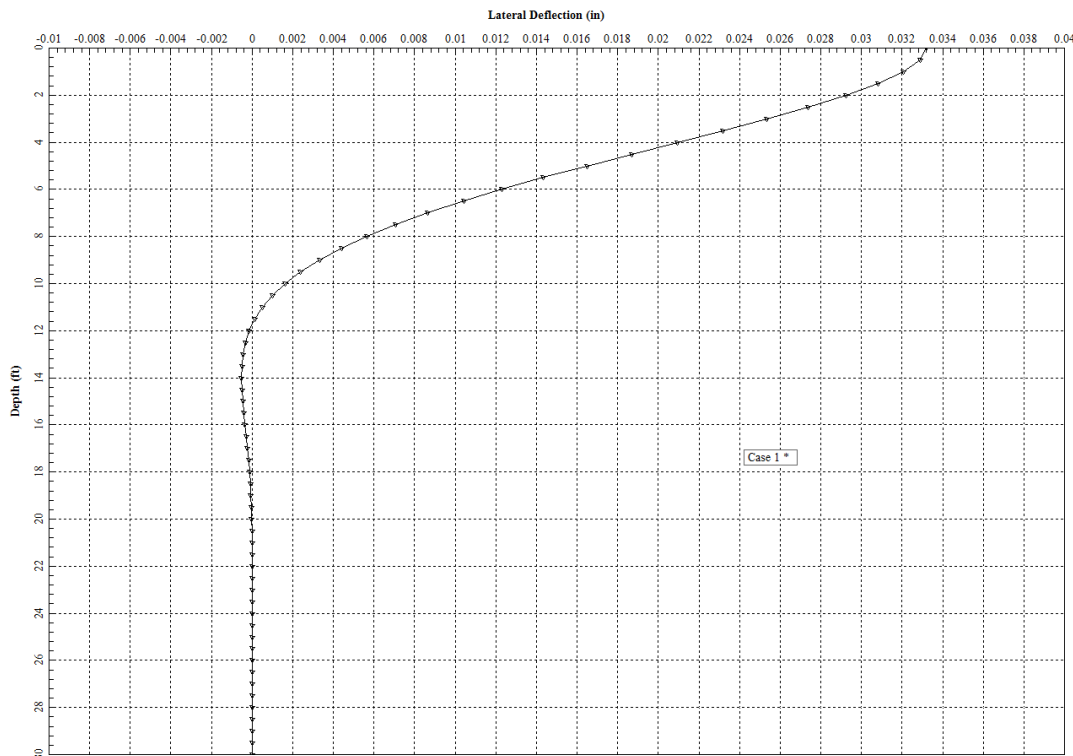
Figure B.42 Model 12 lateral deflection along the pile depth (LPile)
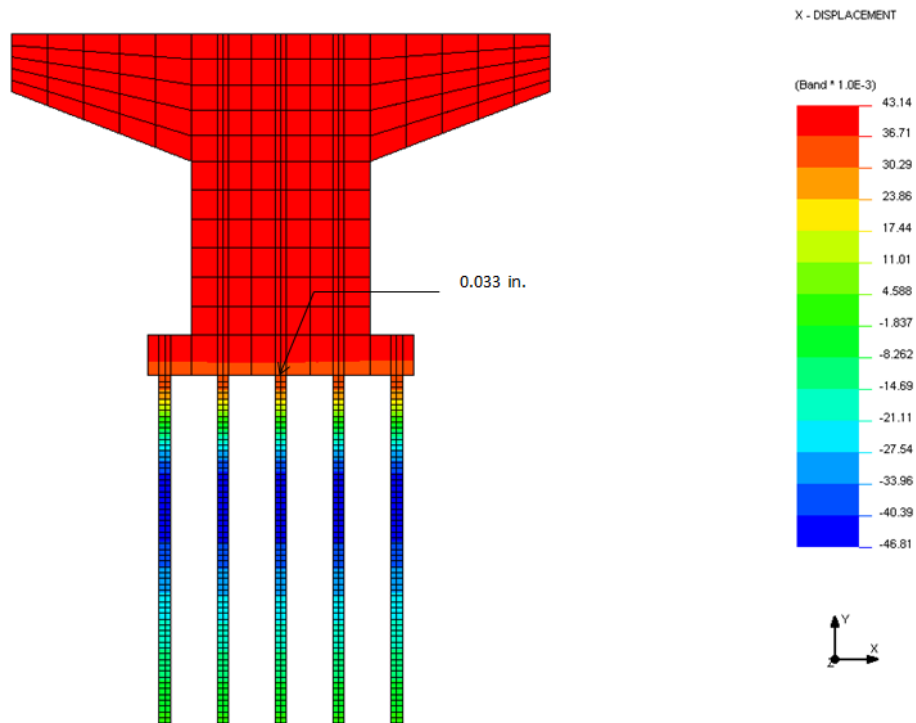
Figure B.43 NISA finite element result for Test Model 12
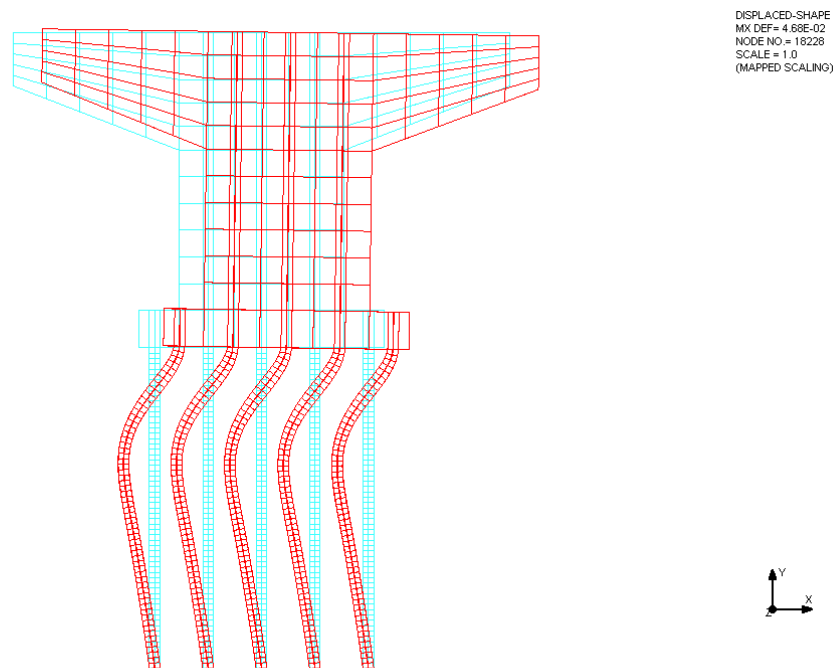
Figure B.44 Lateral deflection for Test Model 12 (in scale of 1)
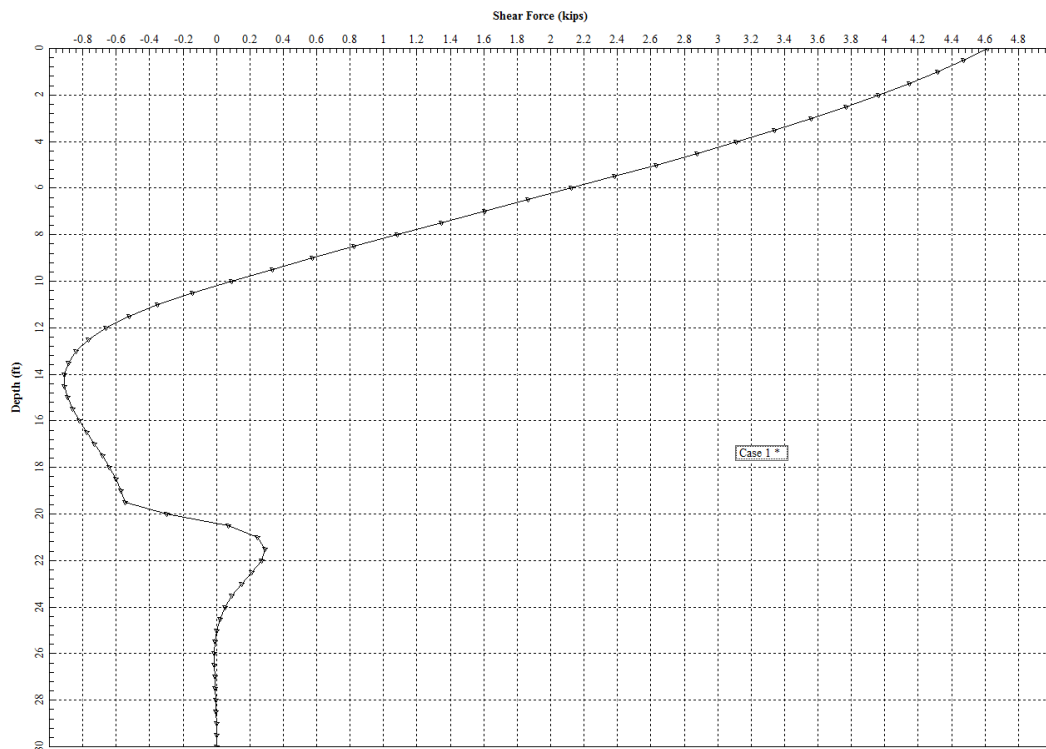
Figure B.45 Model 13 shear force along the pile depth (LPile)
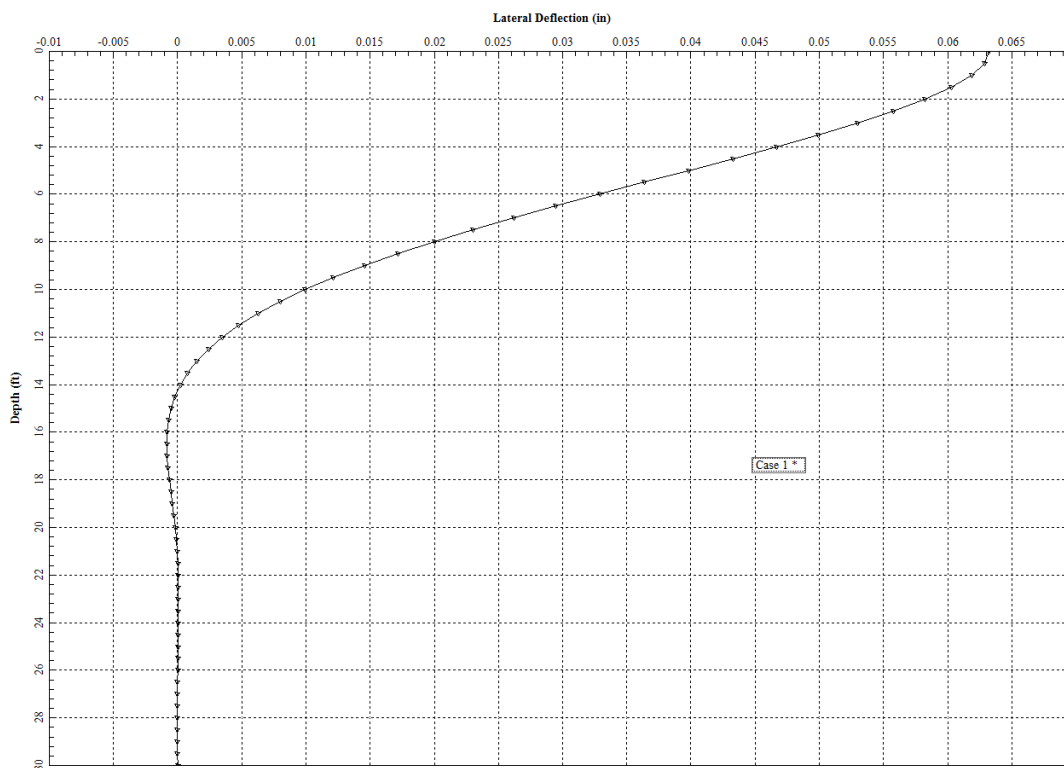
Figure B.46 Model 13 lateral deflection along the pile depth (LPile)
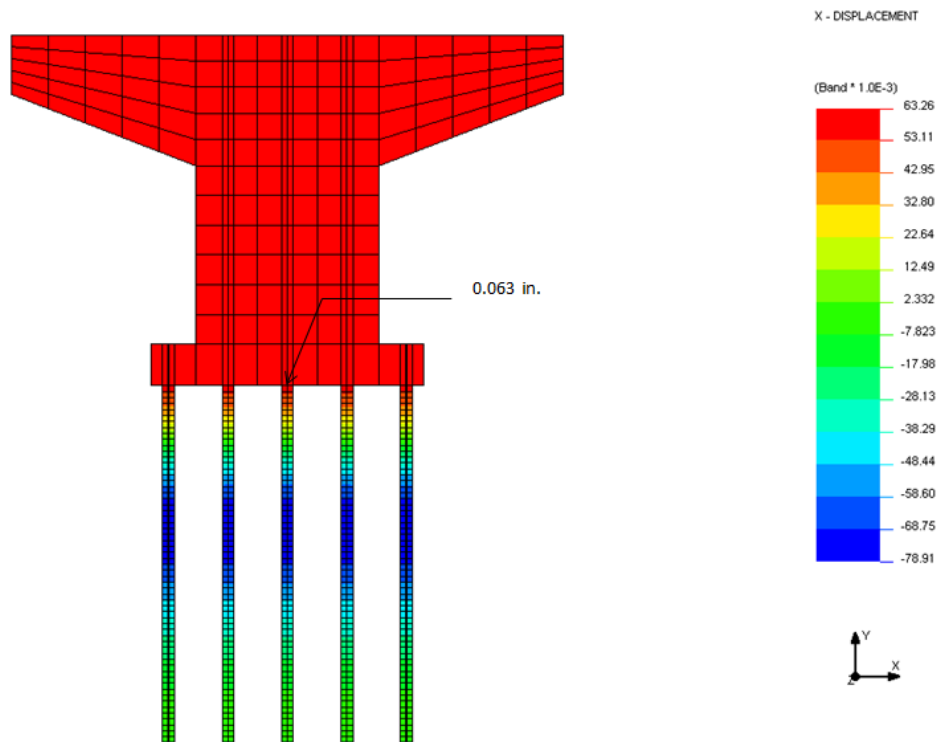
Figure B.47 NISA finite element result for Test Model 13
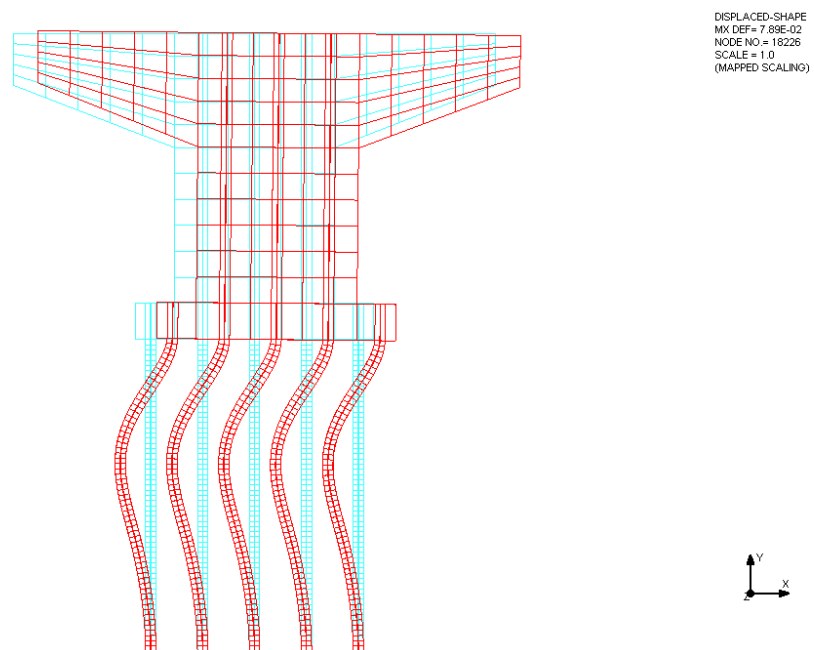
Figure B.48 Lateral deflection for Test Model 13 (in scale of 1)

Figure B.49 Model 14 shear force along the pile depth (LPile)

Figure B.50 Model 14 lateral deflection along the pile depth (LPile)

Figure B.51 NISA finite element result for Test Model 14

Figure B.52 Lateral deflection for Test Model 14 (in scale of 1)

Figure B.53 Model 15 shear force along the pile depth (LPile)

Figure B.54 Model 15 lateral deflection along the pile depth (LPile)

Figure B.55 NISA finite element result for Test Model 15

Figure B.56 Lateral deflection for Test Model 15 (in scale of 1)

Figure B.57 Model 16 shear force along the pile depth (LPile)

Figure B.58 Model 16 lateral deflection along the pile depth (LPile)
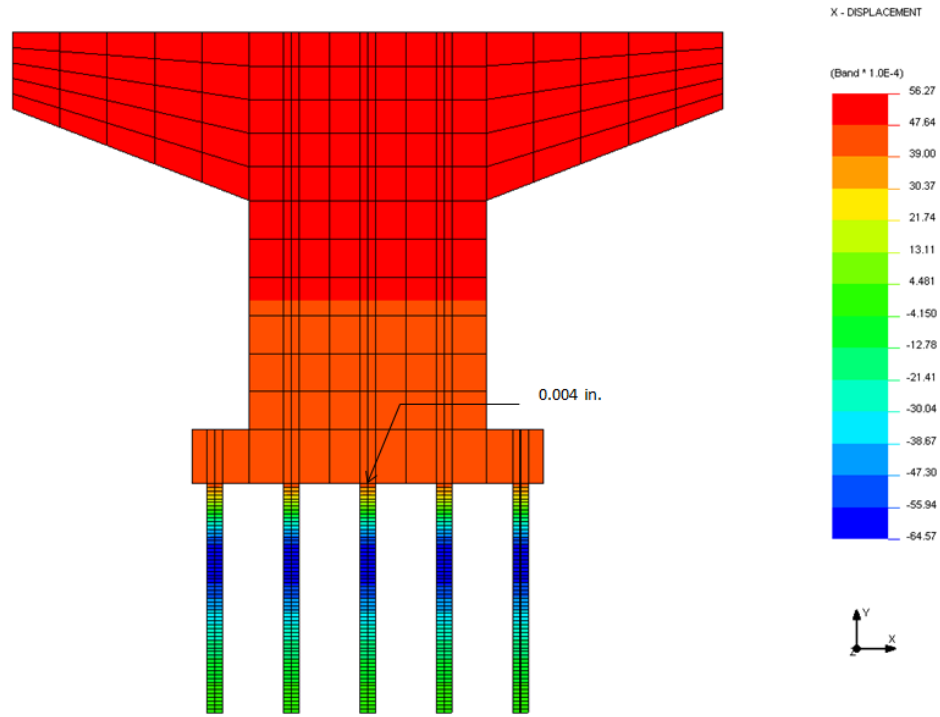
Figure B.59 NISA finite element result for Test Model 16

Figure B.60 Lateral deflection for Test Model 16 (in scale of 1)

APPENDIX C

NIAS FINITE ELEMENT ANALYSIS RESULTS
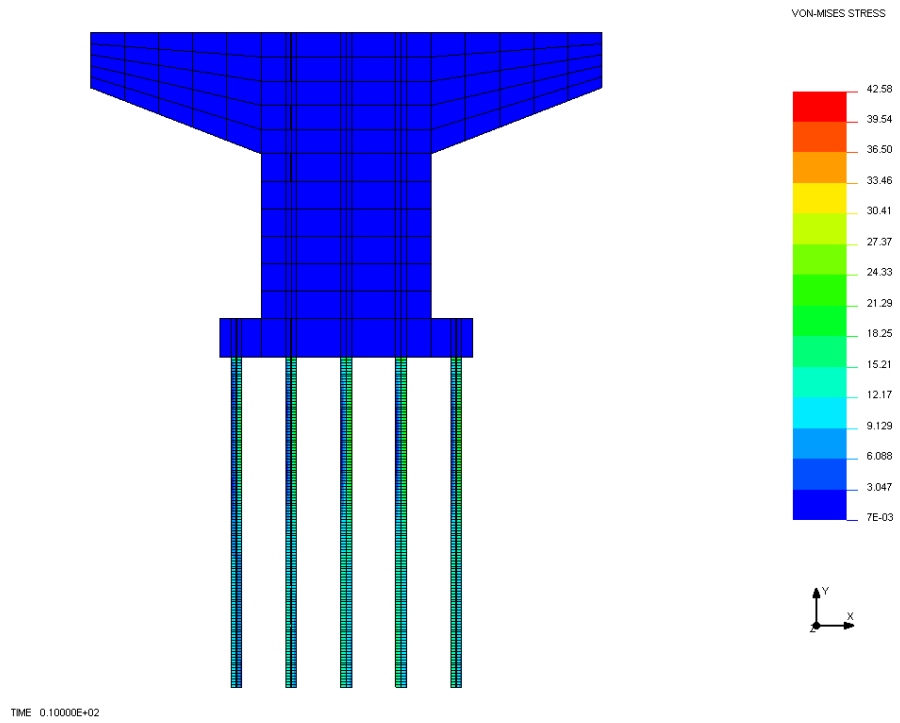
Figure C.1 Von-mises stress of Model 2 under NISA FEM analysis
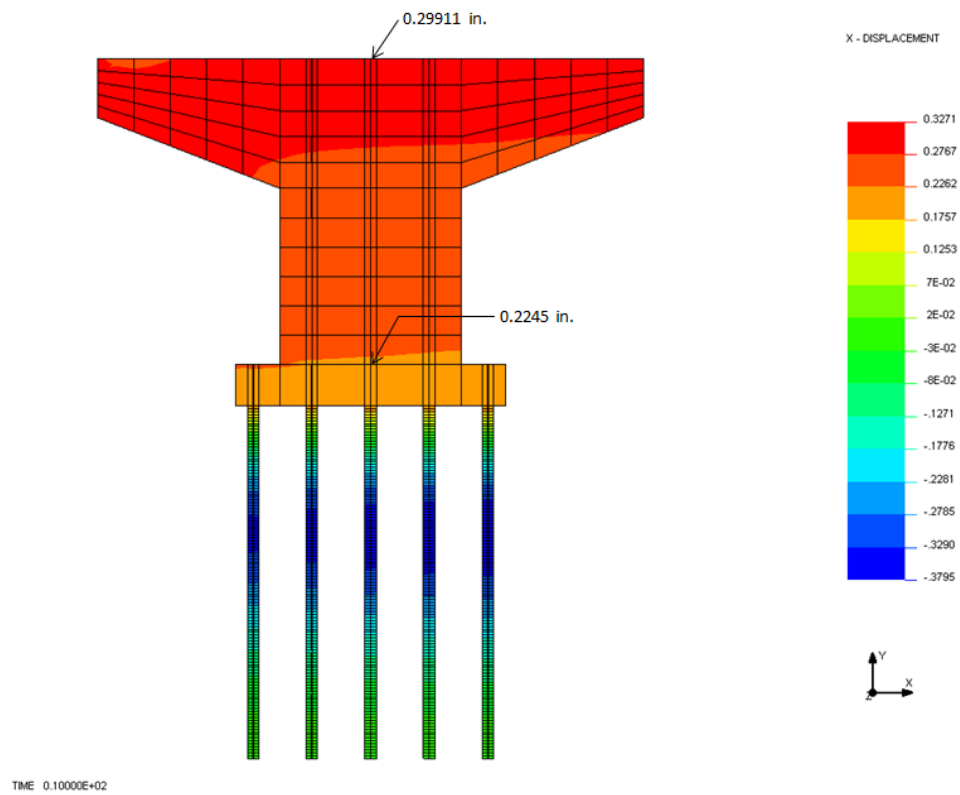
Figure C.2 Lateral displacement of Model 2 under NISA FEM analysis

DISPLACED-SHAPE
MX DEF= 4.66E-01
NODE NO.= 38052
SCALE = 100.0
(ACTUAL SCALING)

TIME 0.10000E+02
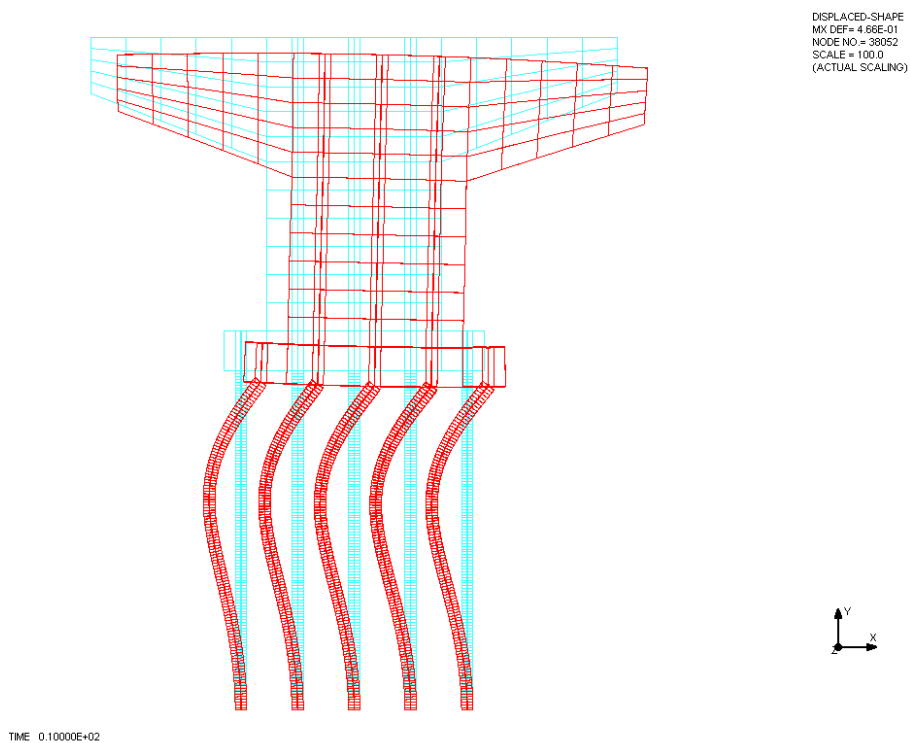
Figure C.3 Lateral defection of Model 2 under NISA FEM analysis
(in scale of 100)

VON-MISES STRESS

42.59
39.55
36.51
33.47
30.42
27.38
24.34
21.30
18.26
15.22
12.17
9.132
6.090
3.048
6E-03

TIME 0.10000E+02
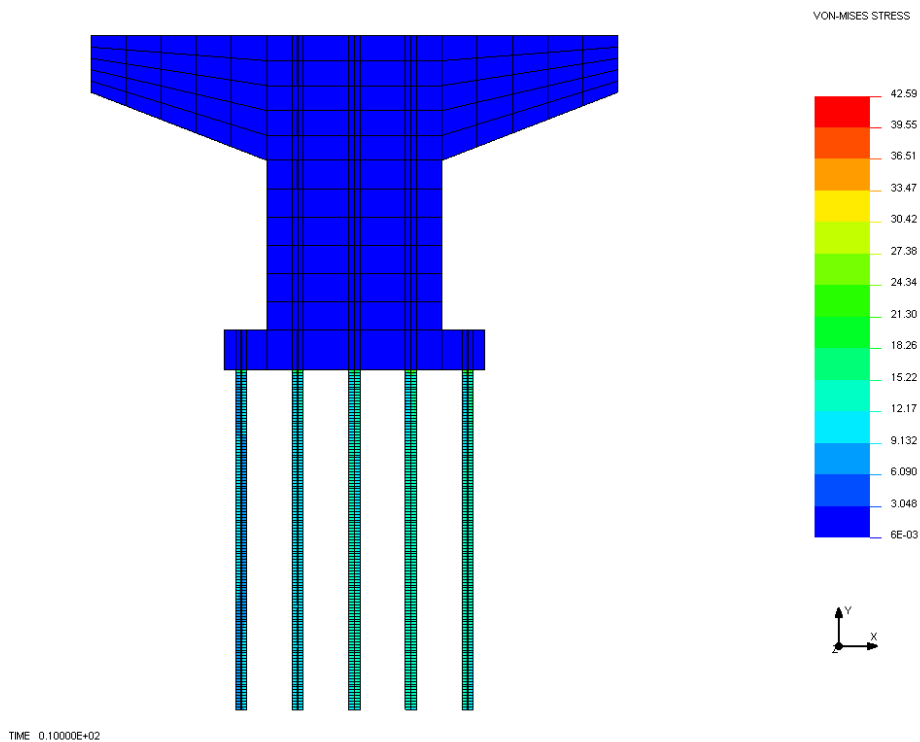
Figure C.4 Von-mises stress of Model 3 under NISA FEM analysis
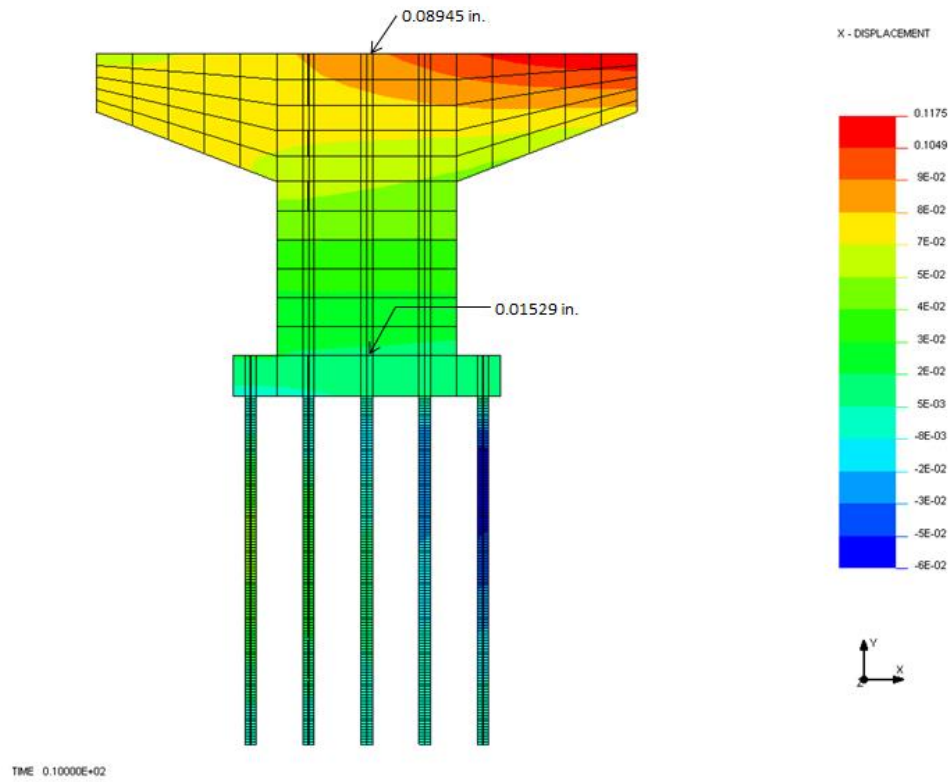
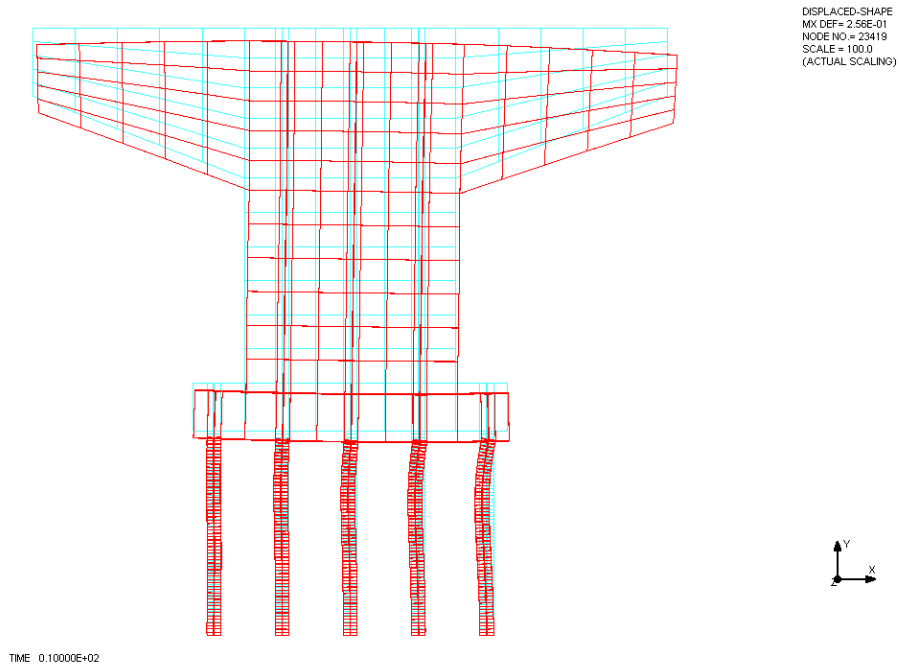*Figure C.5* Lateral displacement of Model 3 under NISA FEM analysis
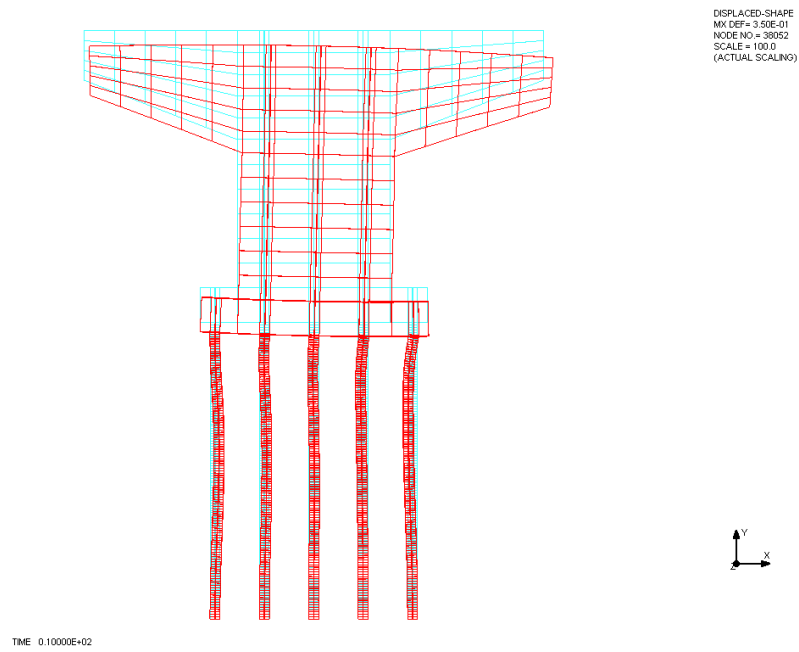
Figure C.6 Lateral defection of Model 3 under NISA FEM analysis
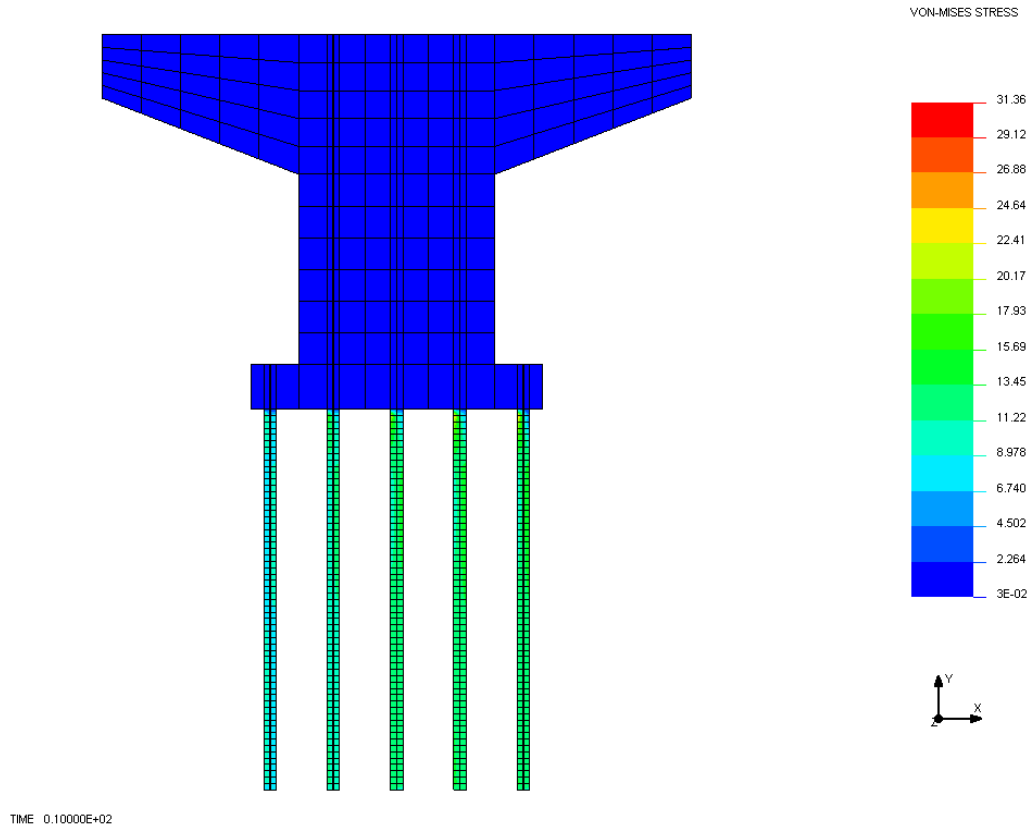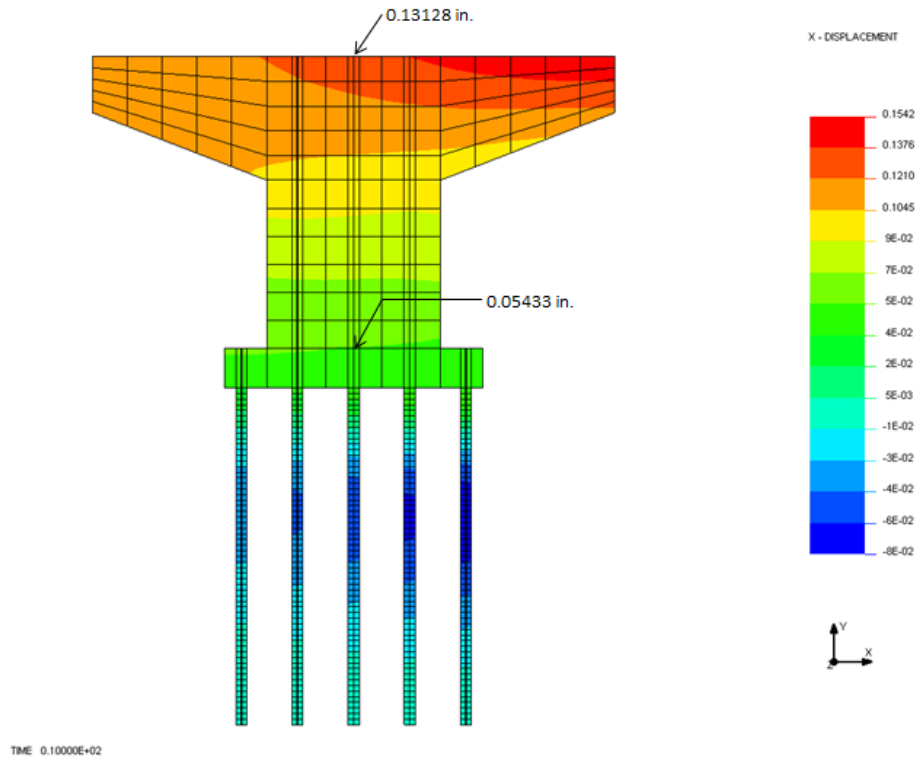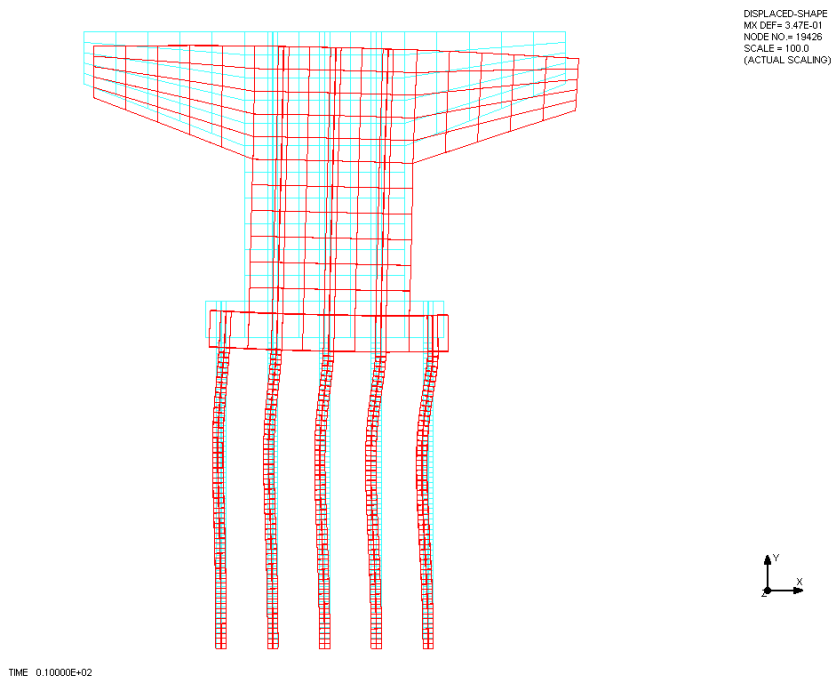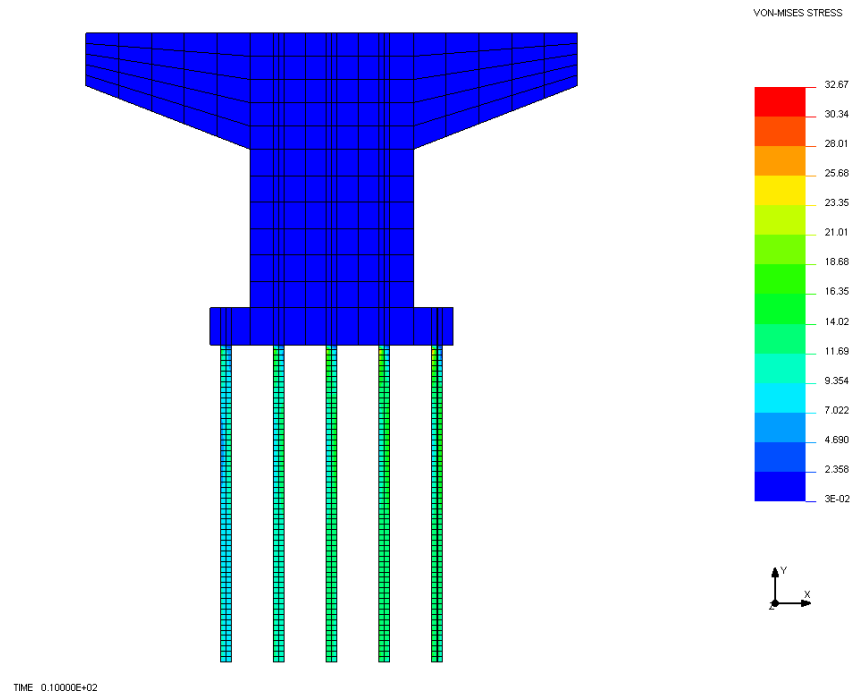(in scale of 100)
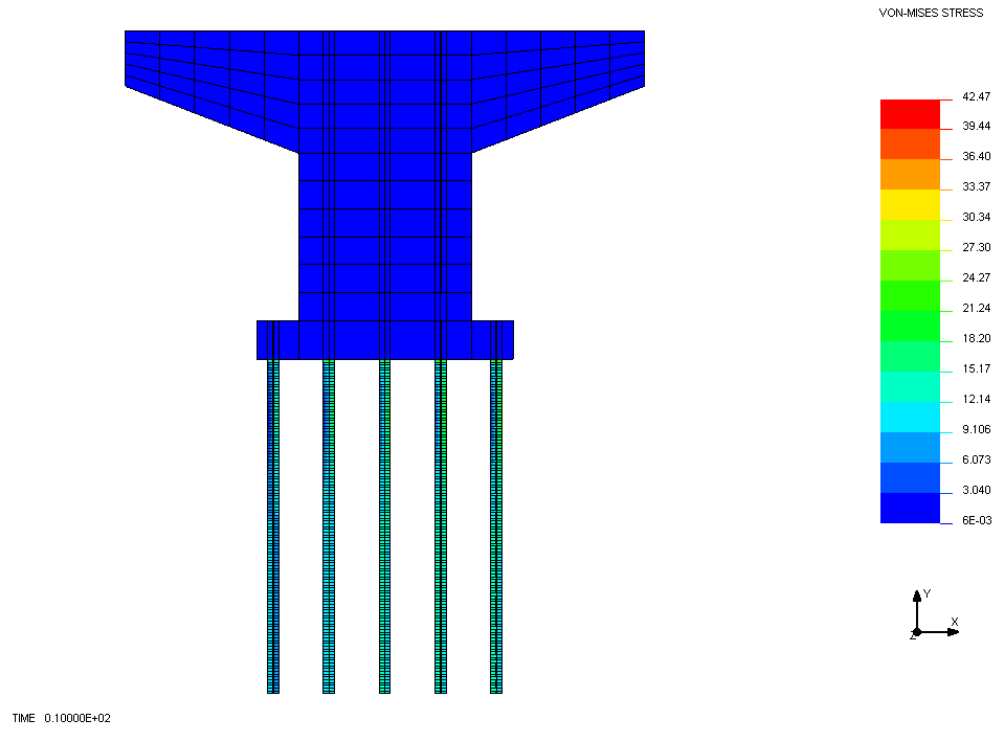
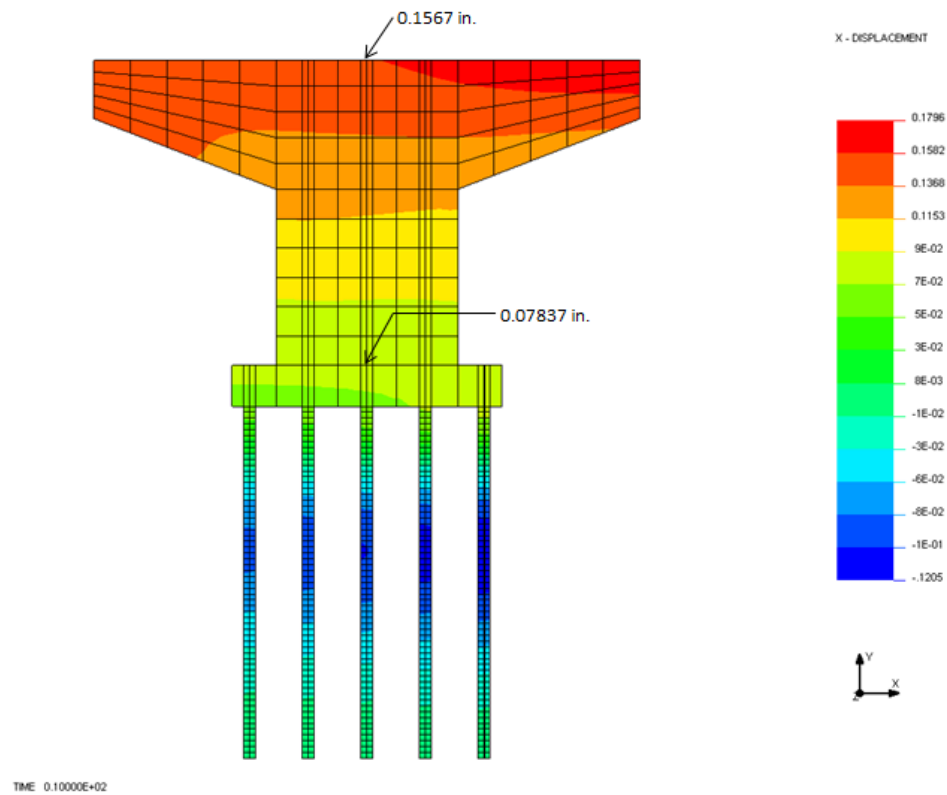*Figure C.7* Von-mises stress of Model 4 under NISA FEM analysis
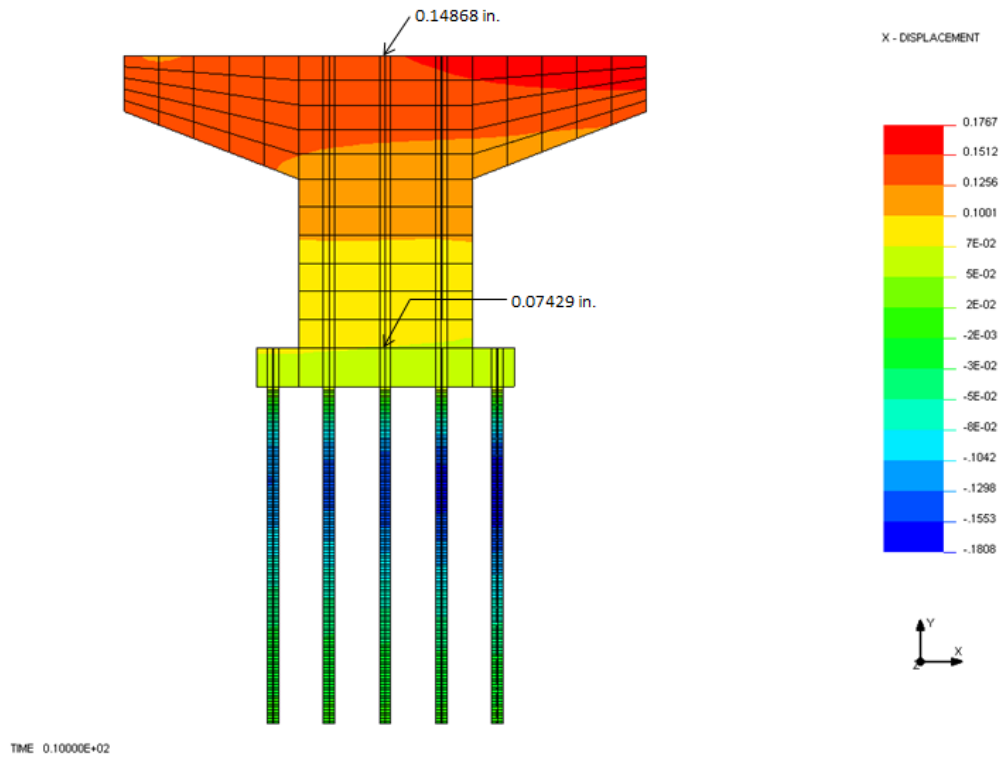
Figure C.8 Lateral displacement of Model 4 under NISA FEM analysis

DISPLACED-SHAPE
MX DEF= 3.75E-01
NODE NO.= 38052
SCALE = 100.0
(ACTUAL SCALING)

TIME 0.10000E+02
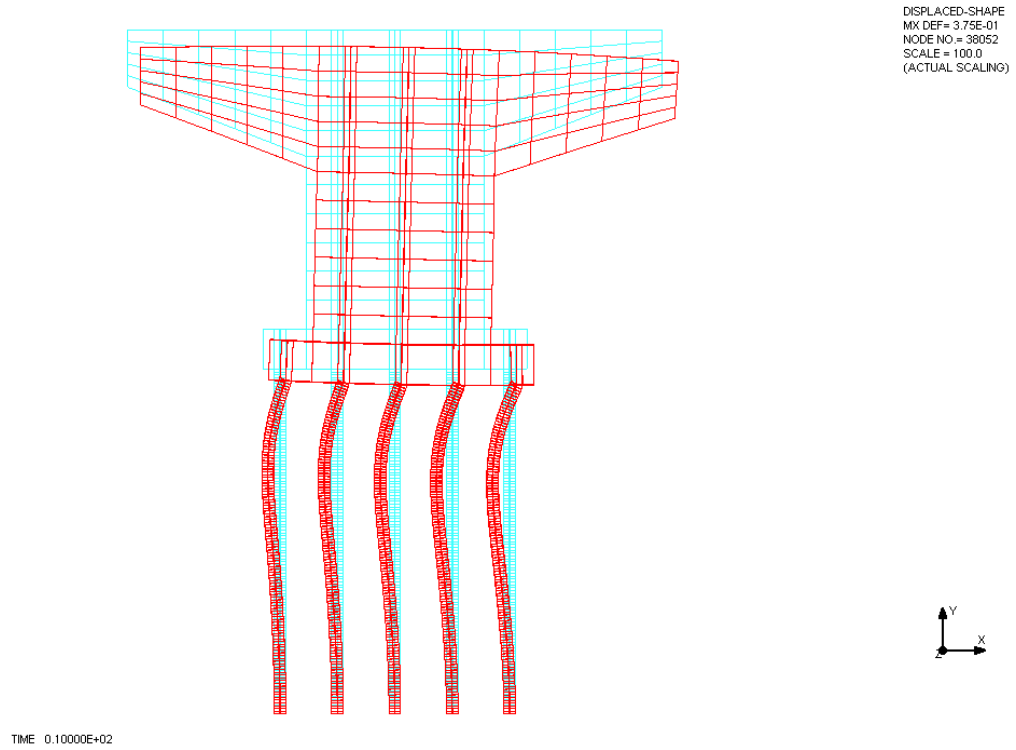
Figure C.9 Lateral defection of Model 4 under NISA FEM analysis
(in scale of 100)

VON-MISES STRESS

| 42.58 |
| 39.54 |
| 36.50 |
| 33.45 |
| 30.41 |
| 27.37 |
| 24.33 |
| 21.29 |
| 18.25 |
| 15.21 |
| 12.17 |
| 9.129 |
| 6.088 |
| 3.047 |
| 7E-03 |

TIME 0.10000E+02
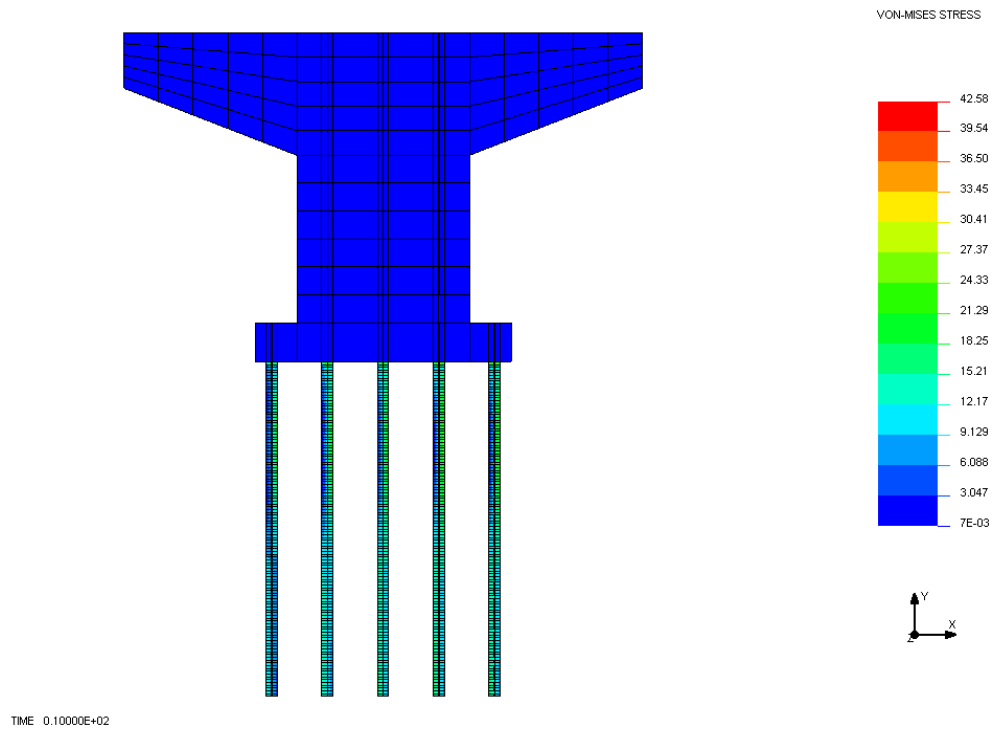
Figure C.10 Von-mises stress of Model 5 under NISA FEM analysis

0.29758 in.

0.22298 in.

X - DISPLACEMENT

0.3256
0.2757
0.2258
0.1759
0.1260
8E-02
3E-02
-2E-02
-7E-02
-.1235
-.1734
-.2233
-.2732
-.3231
-.3730

TIME 0.10000E+02
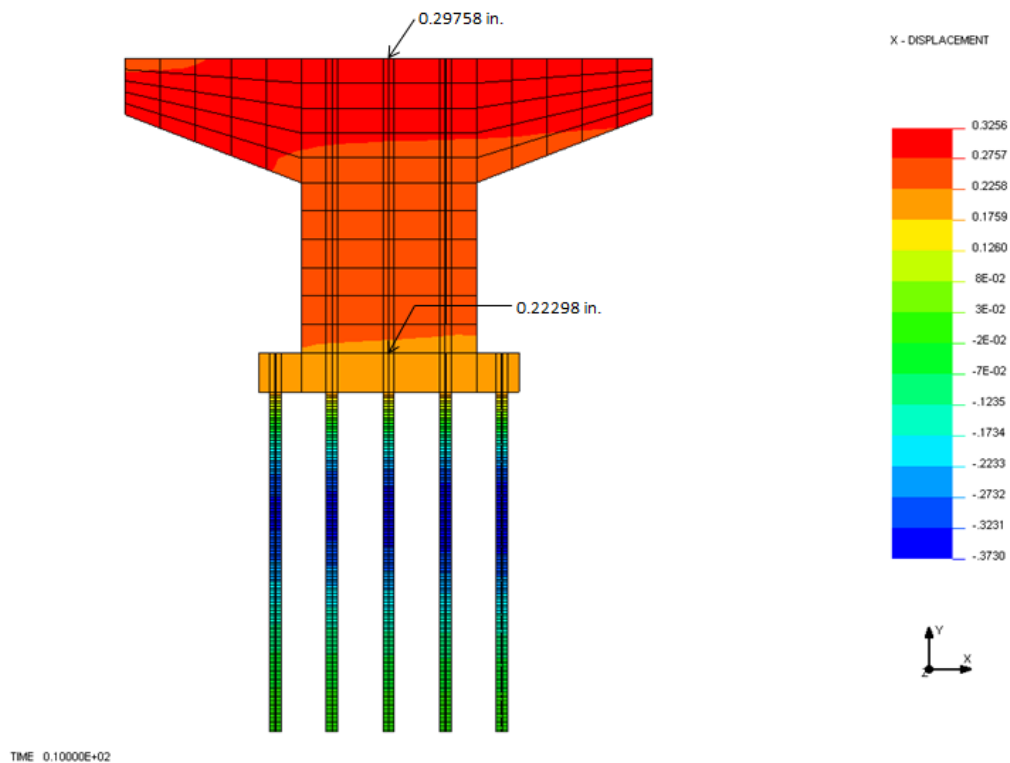
Figure C.11 Lateral displacement of Model 5 under NISA FEM analysis

DISPLACED-SHAPE
MX DEF= 4.65E-01
NODE NO.= 38052
SCALE = 100.0
(ACTUAL SCALING)

TIME 0.10000E+02
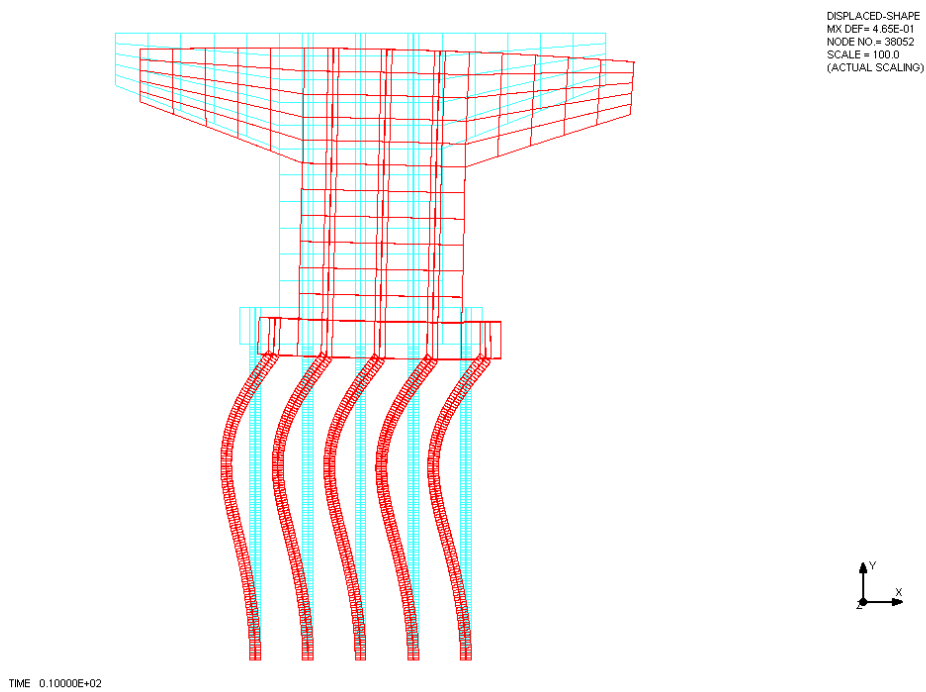
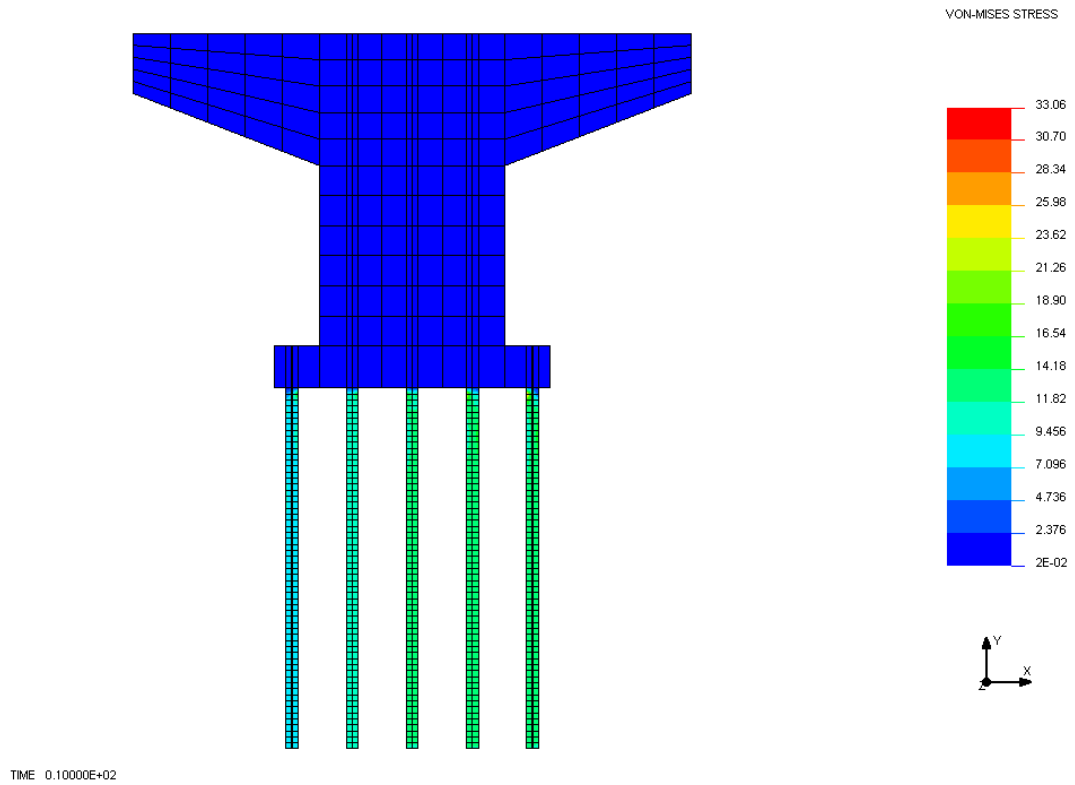*Figure C.12* Lateral defection of Model 5 under NISA FEM analysis
(in scale of 100)
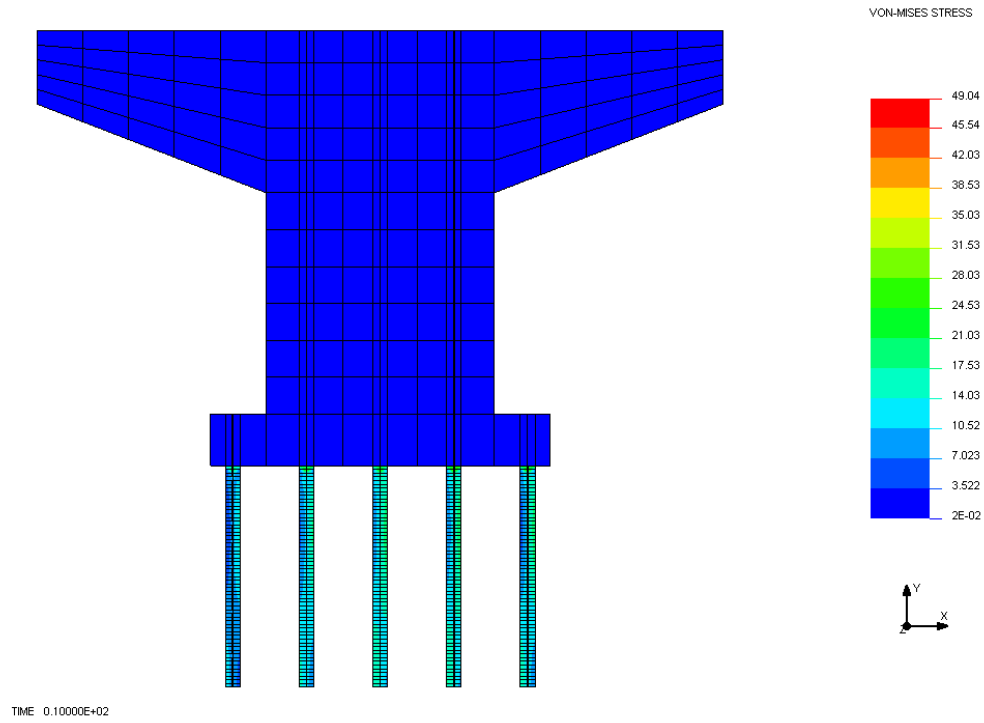
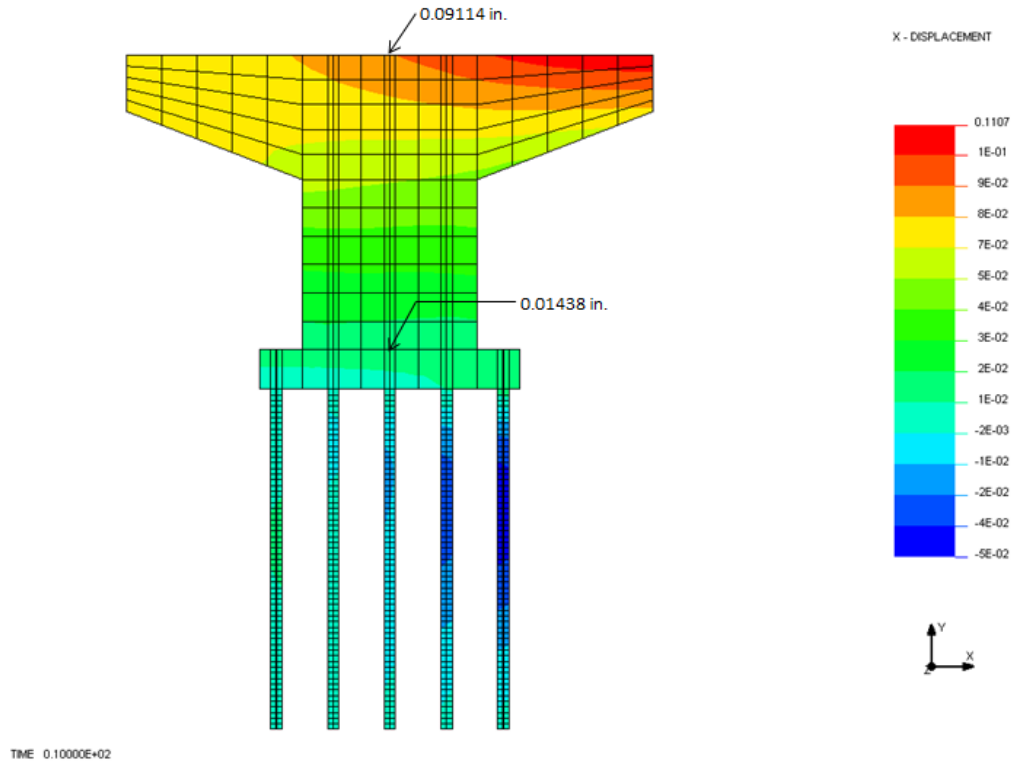*Figure C.13* Von-mises stress of Model 6 under NISA FEM analysis
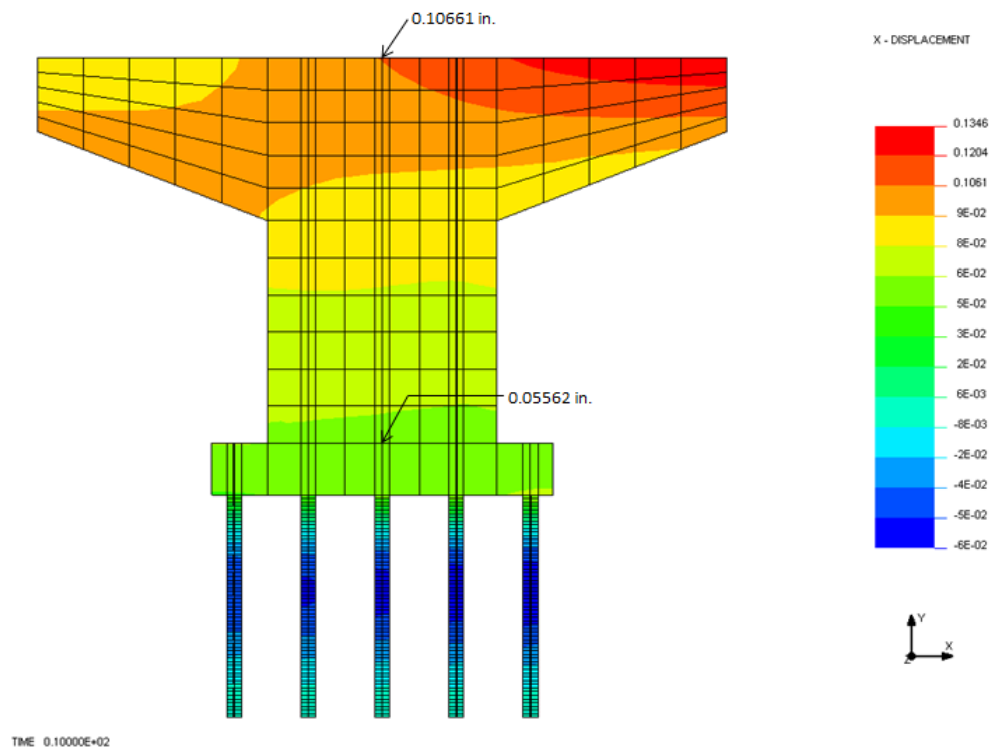
Figure C.14 Lateral displacement of Model 6 under NISA FEM analysis

DISPLACED-SHAPE
MX DEF= 2.76E-01
NODE NO.= 23419
SCALE = 100.0
(ACTUAL SCALING)

TIME 0.10000E+02
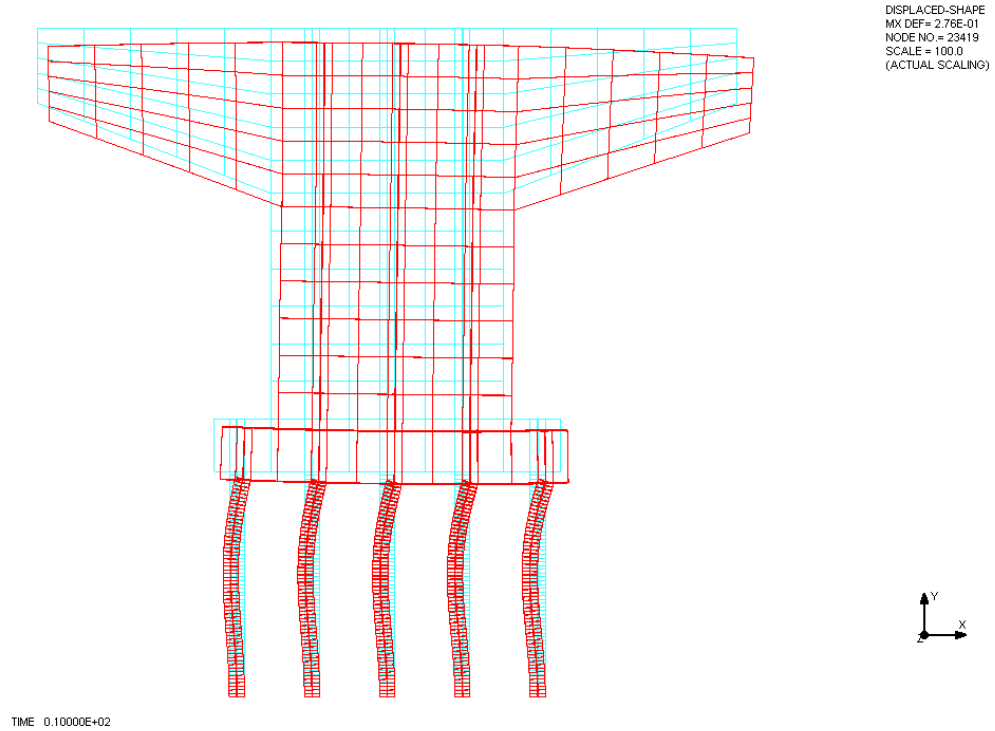
Figure C.15 Lateral defection of Model 6 under NISA FEM analysis
(in scale of 100)

VON-MISES STRESS

49.08
45.58
42.07
38.57
35.07
31.56
28.06
24.55
21.05
17.54
14.04
10.53
7.029
3.525
2E-02

TIME 0.10000E+02
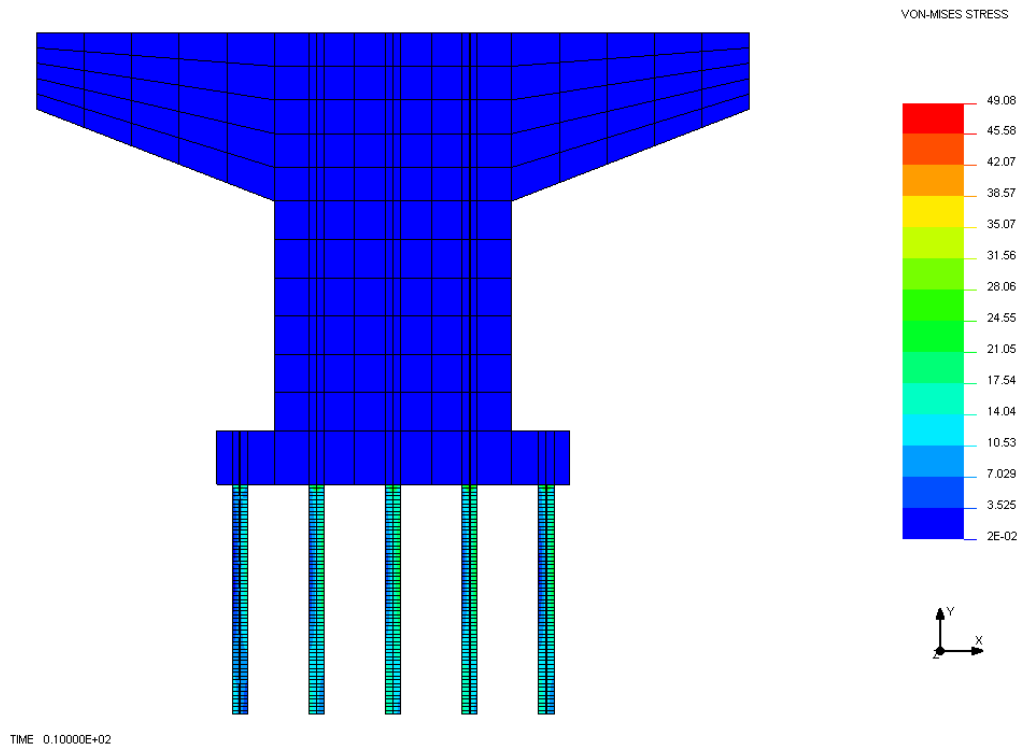
Figure C.16 Von-mises stress of Model 7 under NISA FEM analysis
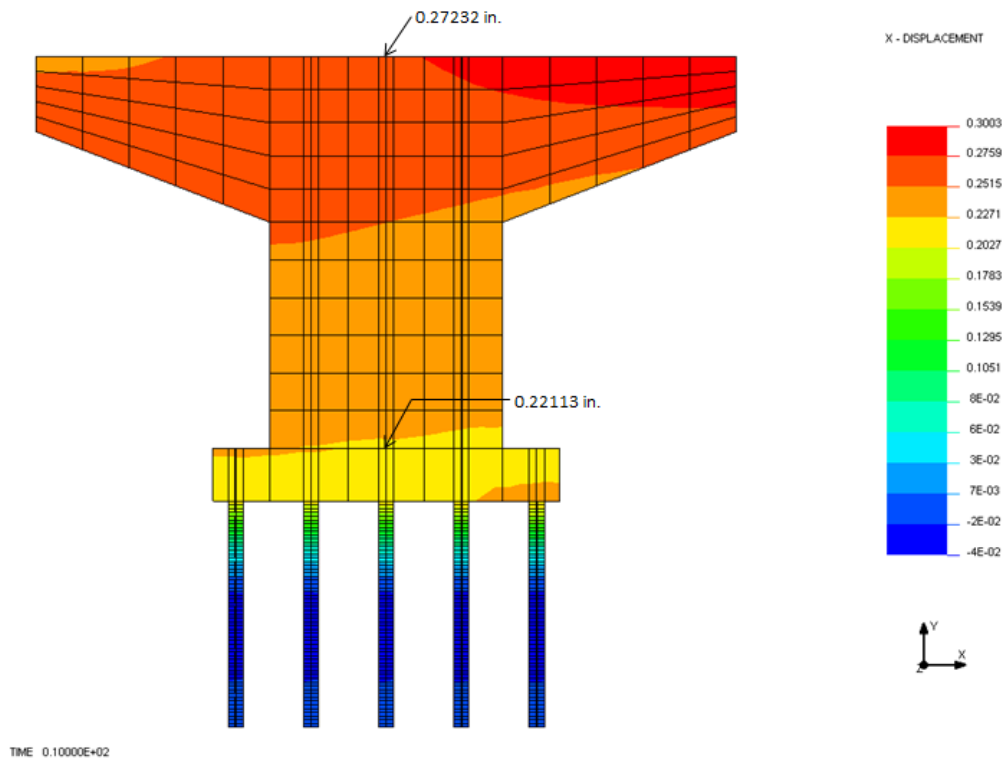
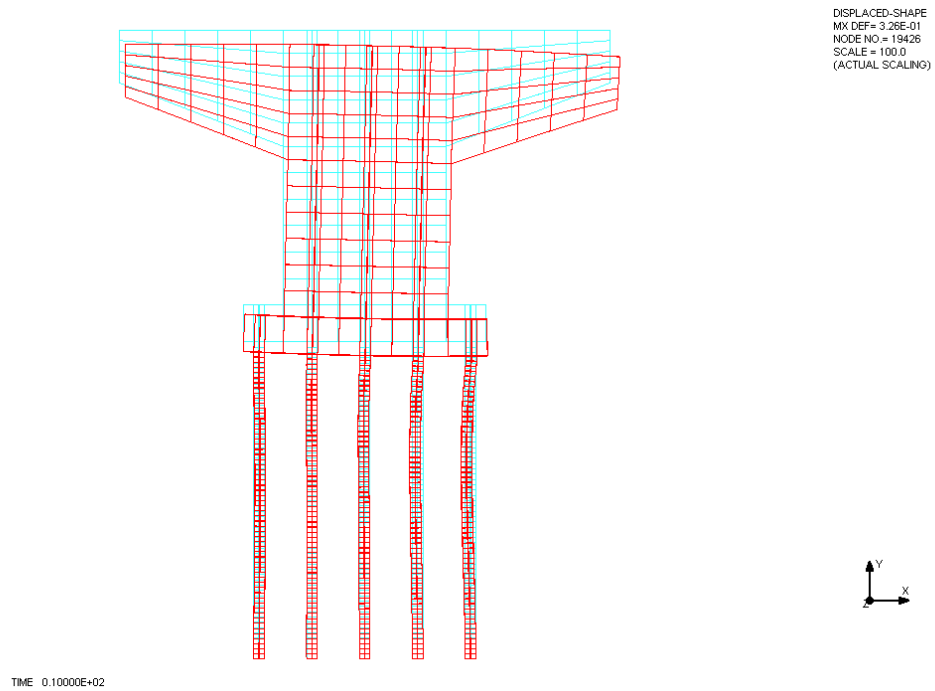*Figure C.17* Lateral displacement of Model 7 under NISA FEM analysis
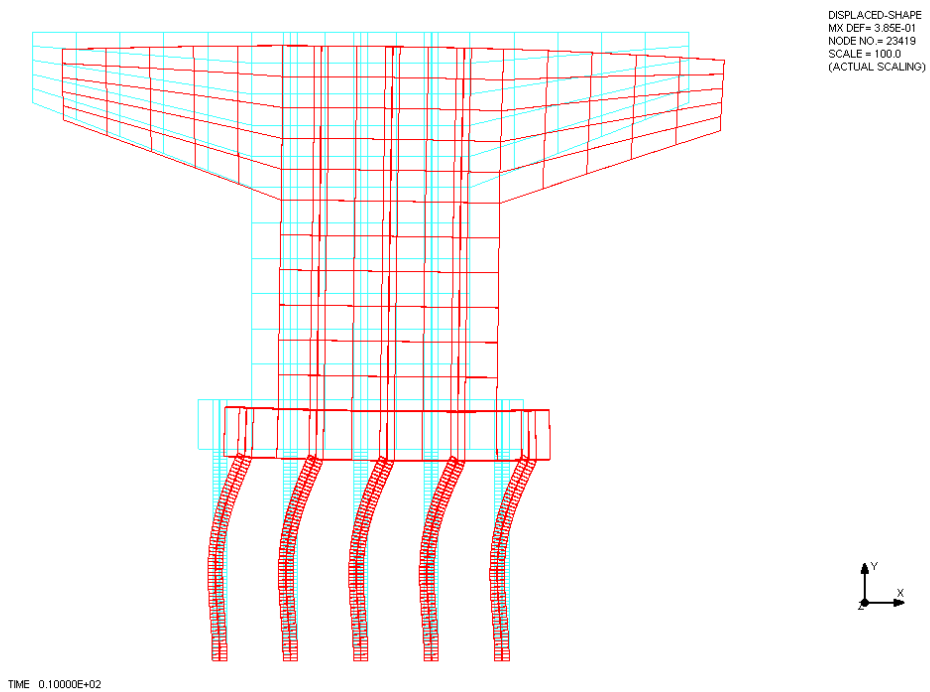
Figure C.18 Lateral defection of Model 7 under NISA FEM analysis
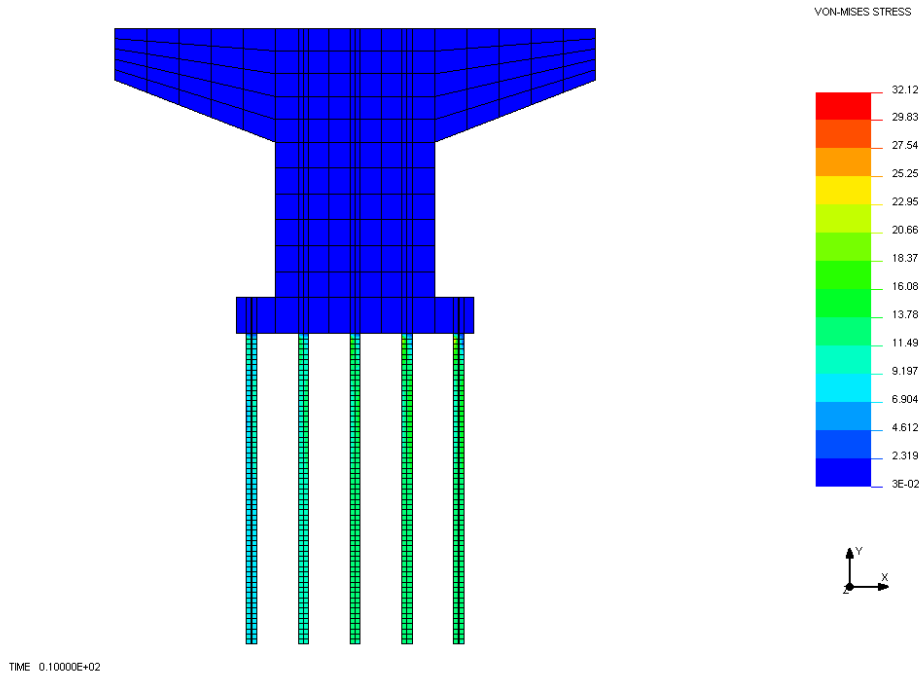(in scale of 100)
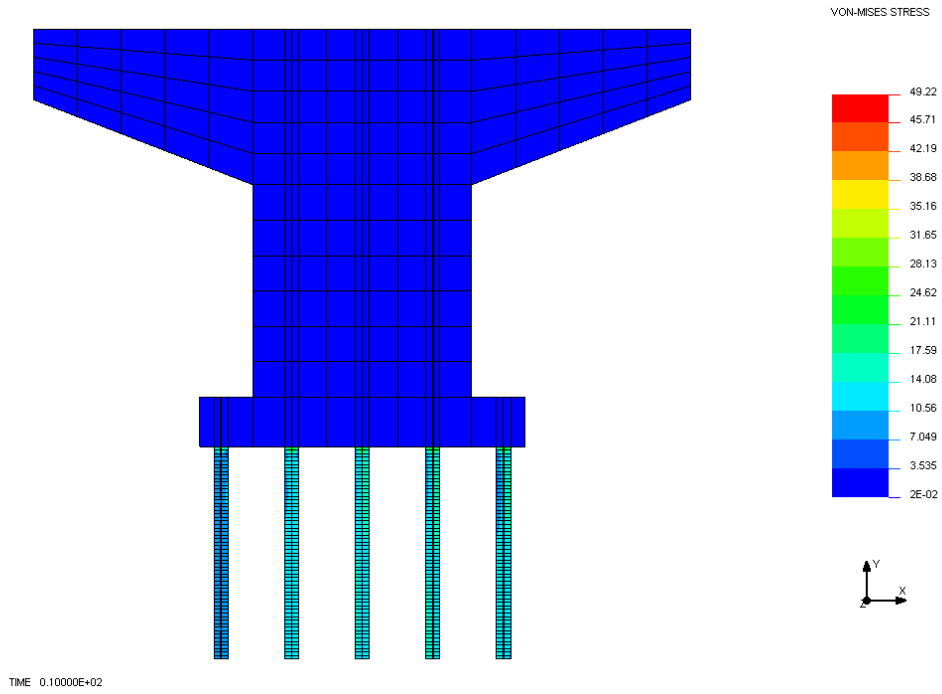
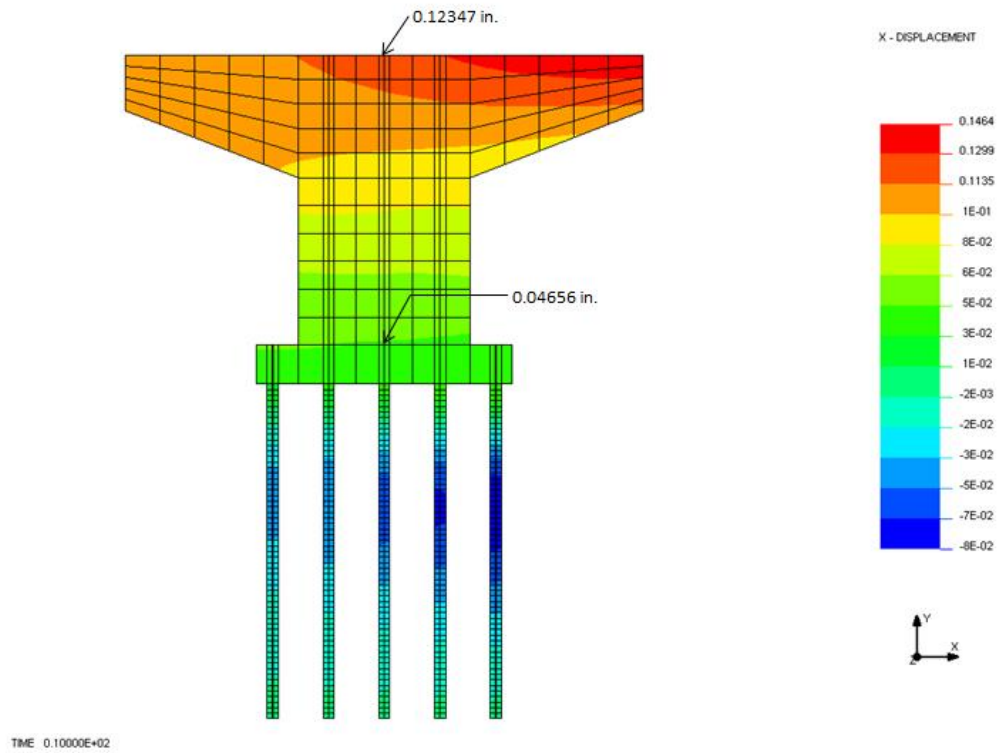*Figure C.19* Von-mises stress of Model 8 under NISA FEM analysis
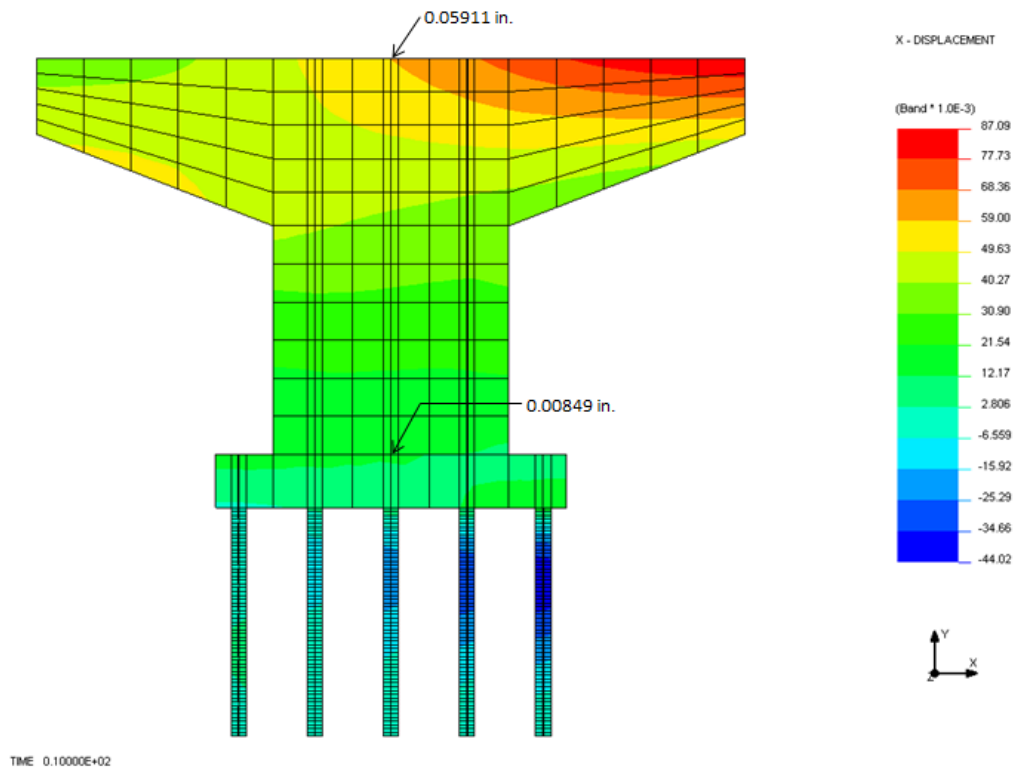
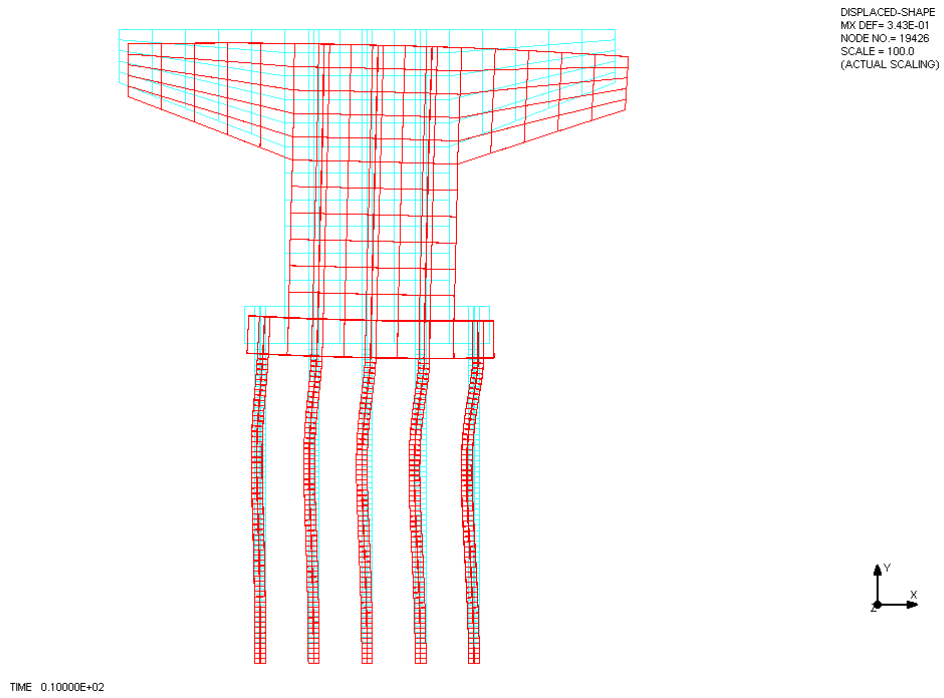*Figure C.20* Lateral displacement of Model 8 under NISA FEM analysis

DISPLACED-SHAPE
MX DEF= 2.56E-01
NODE NO.= 23419
SCALE = 100.0
(ACTUAL SCALING)

TIME 0.10000E+02

Figure C.21 Lateral defection of Model 8 under NISA FEM analysis
(in scale of 100)

VON-MISES STRESS

31.36
29.12
26.88
24.64
22.41
20.17
17.93
15.69
13.45
11.22
8.978
6.740
4.502
2.264
3E-02

TIME 0.10000E+02

Figure C.22 Von-mises stress of Model 9 under NISA FEM analysis

Figure C.23 Lateral displacement of Model 9 under NISA FEM analysis

Figure C.24 Lateral defection of Model 9 under NISA FEM analysis
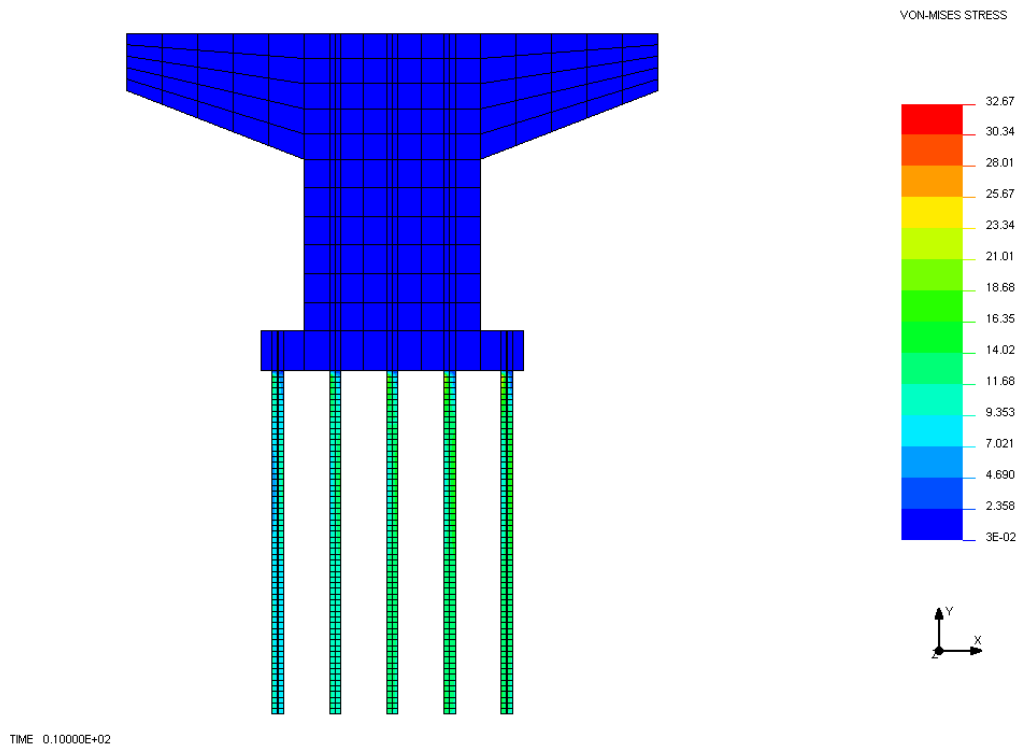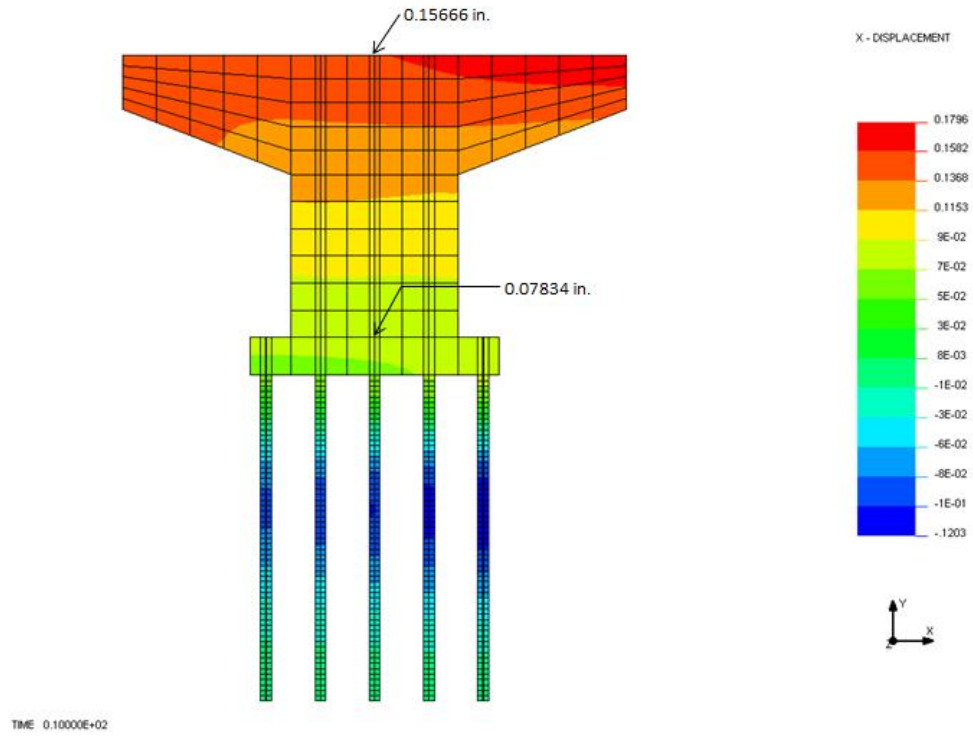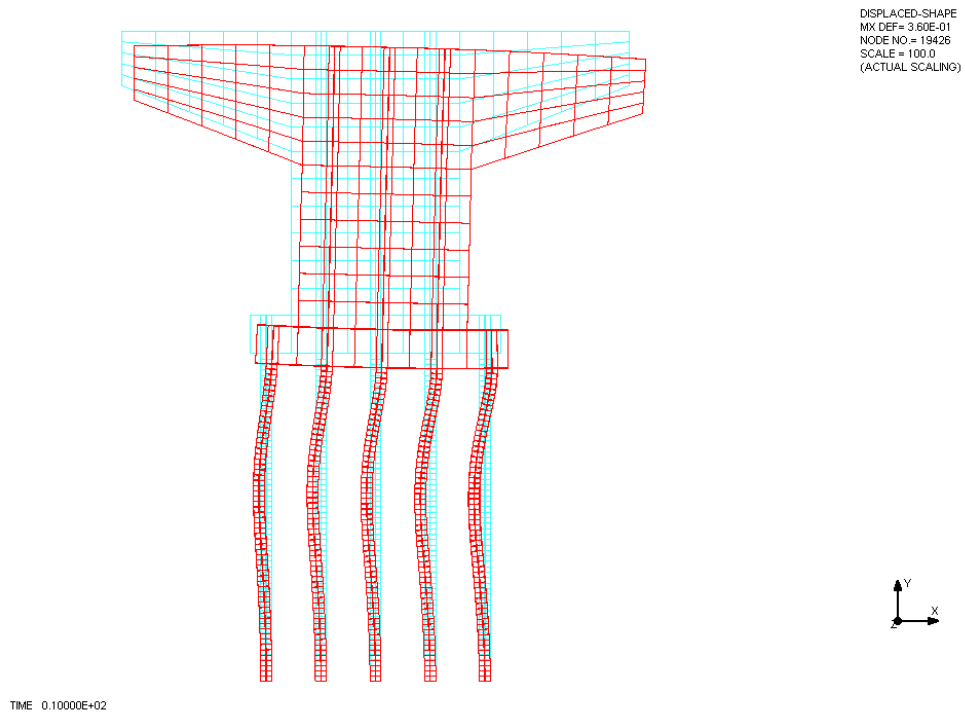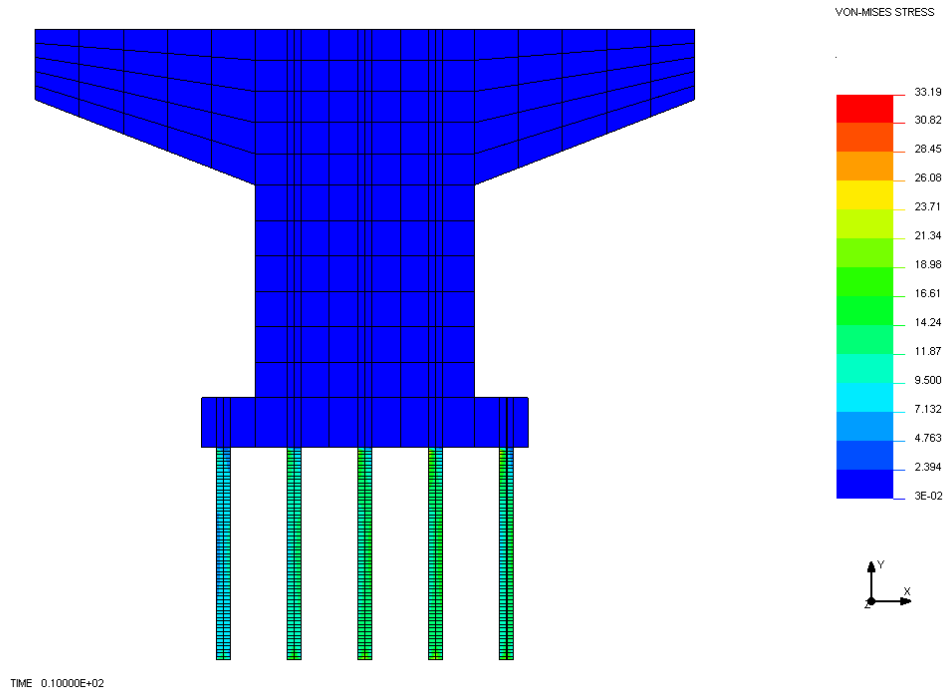(in scale of 100)

Figure C.25 Von-mises stress of Model 10 under NISA FEM analysis

Figure C.26 Lateral displacement of Model 10 under NISA FEM analysis

DISPLACED-SHAPE
MX DEF= 3.60E-01
NODE NO.= 19426
SCALE = 100.0
(ACTUAL SCALING)

TIME 0.10000E+02
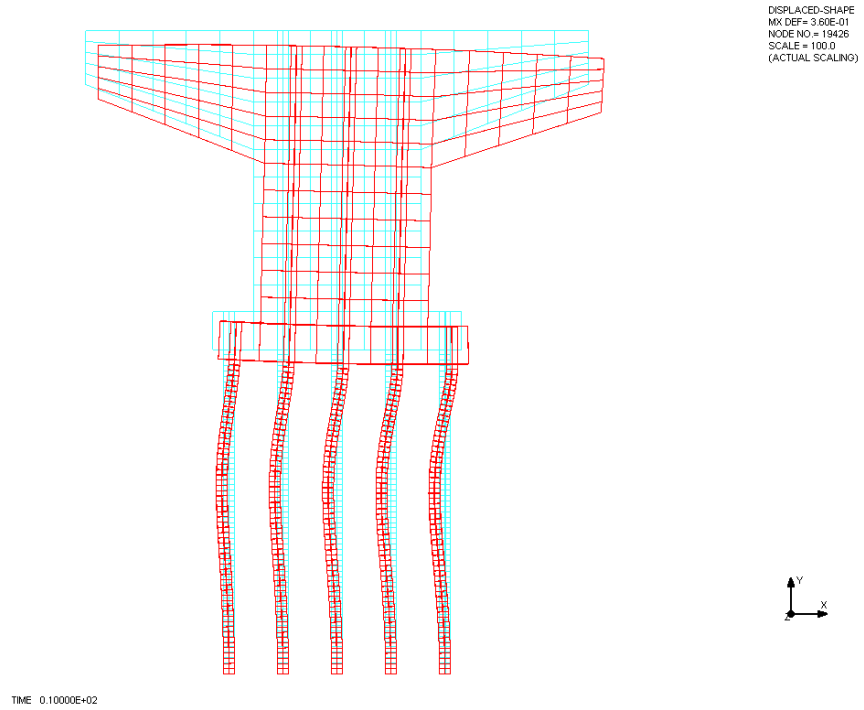
Figure C.27 Lateral defection of Model 10 under NISA FEM analysis
(in scale of 100)

VON-MISES STRESS

| 33.06 |
| 30.70 |
| 28.34 |
| 25.98 |
| 23.62 |
| 21.26 |
| 18.90 |
| 16.54 |
| 14.18 |
| 11.82 |
| 9.456 |
| 7.096 |
| 4.736 |
| 2.376 |
| 2E-02 |

TIME 0.10000E+02

Figure C.28 Von-mises stress of Model 11 under NISA FEM analysis

Figure C.29 Lateral displacement of Model 11 under NISA FEM analysis

Figure C.30 Lateral defection of Model 11 under NISA FEM analysis
(in scale of 100)

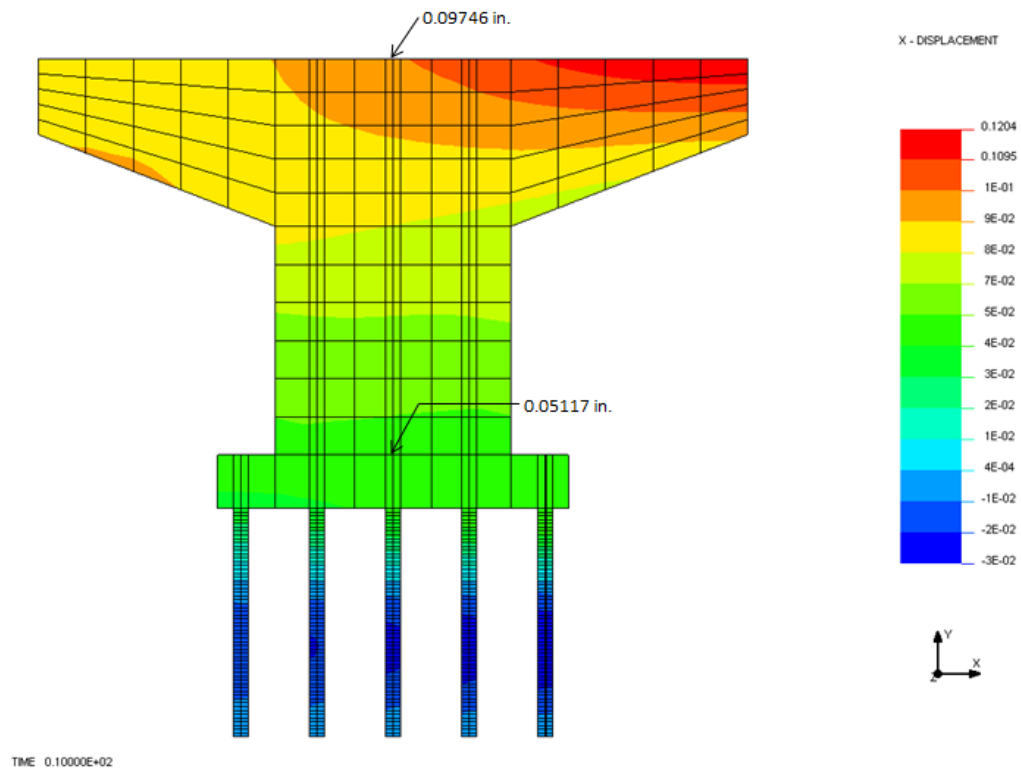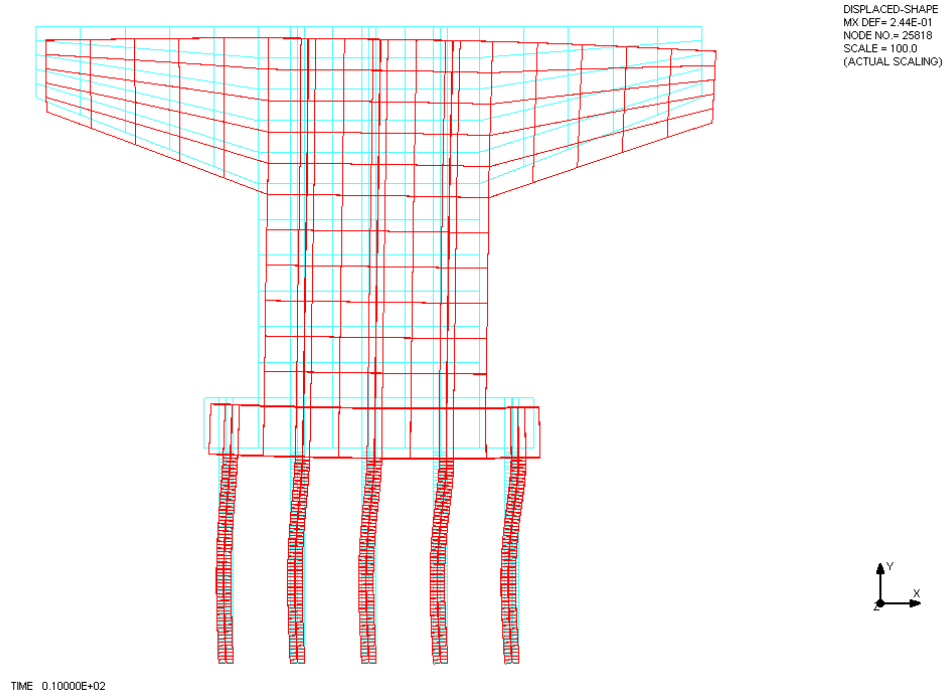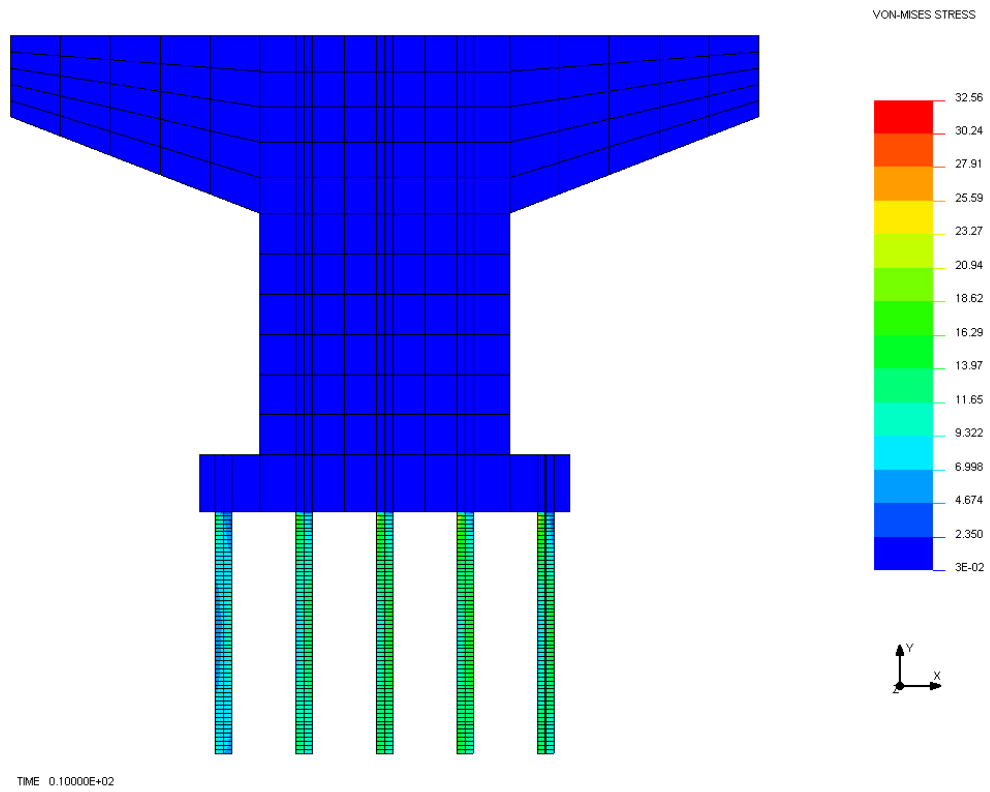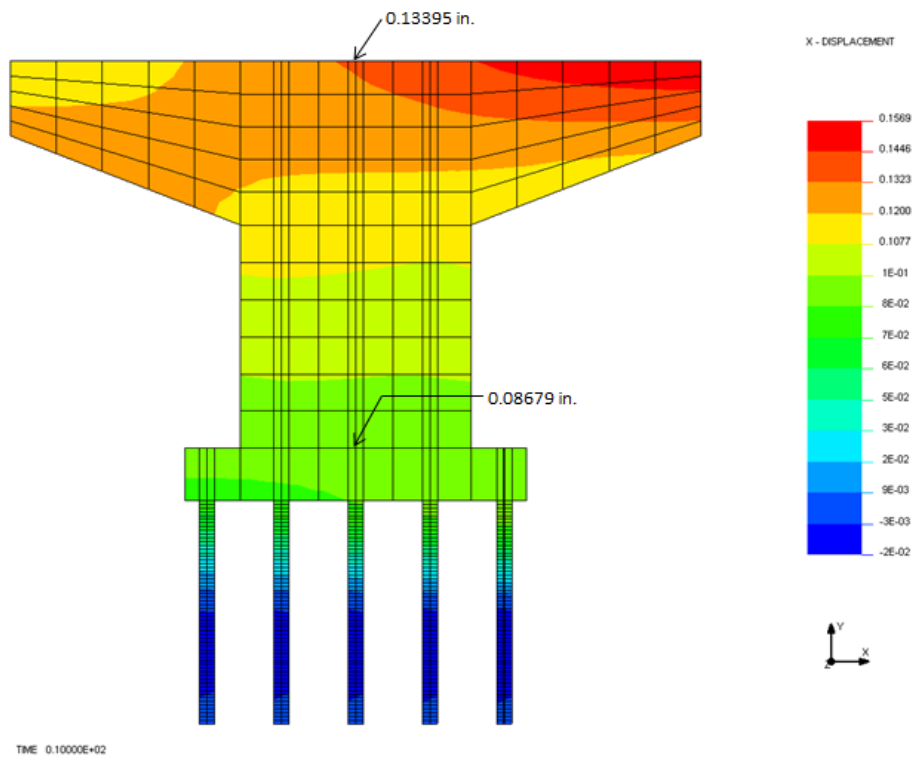*Figure C.31* Von-mises stress of Model 12 under NISA FEM analysis

Figure C.32 Lateral displacement of Model 12 under NISA FEM analysis

TIME 0.10000E+02

Figure C.33 Lateral defection of Model 12 under NISA FEM analysis
(in scale of 100)

TIME 0.10000E+02

Figure C.34 Von-mises stress of Model 13 under NISA FEM analysis

Figure C.35 Lateral displacement of Model 13 under NISA FEM analysis
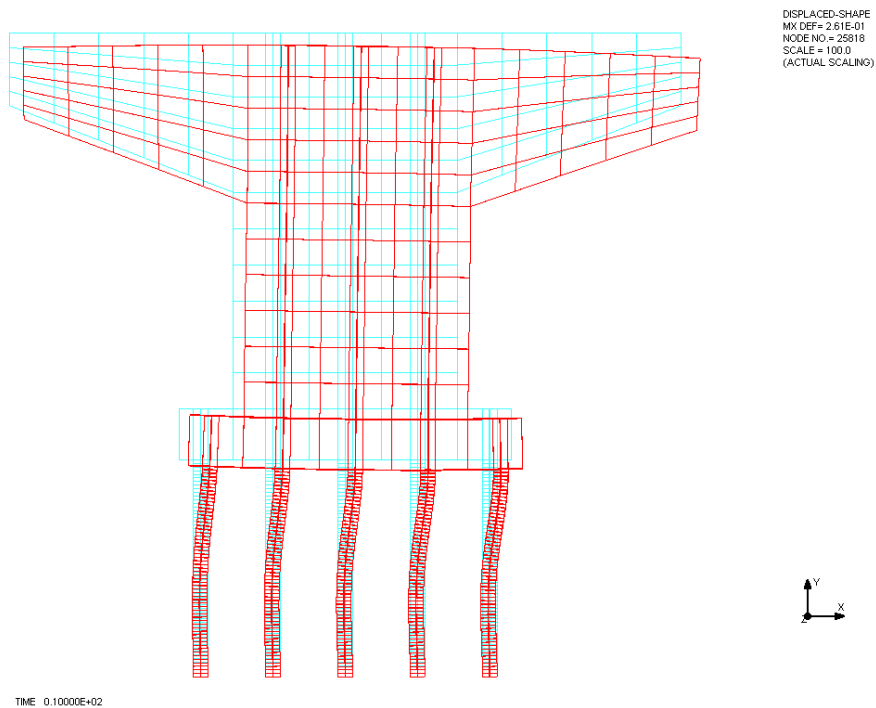

Figure C.36 Lateral defection of Model 13 under NISA FEM analysis
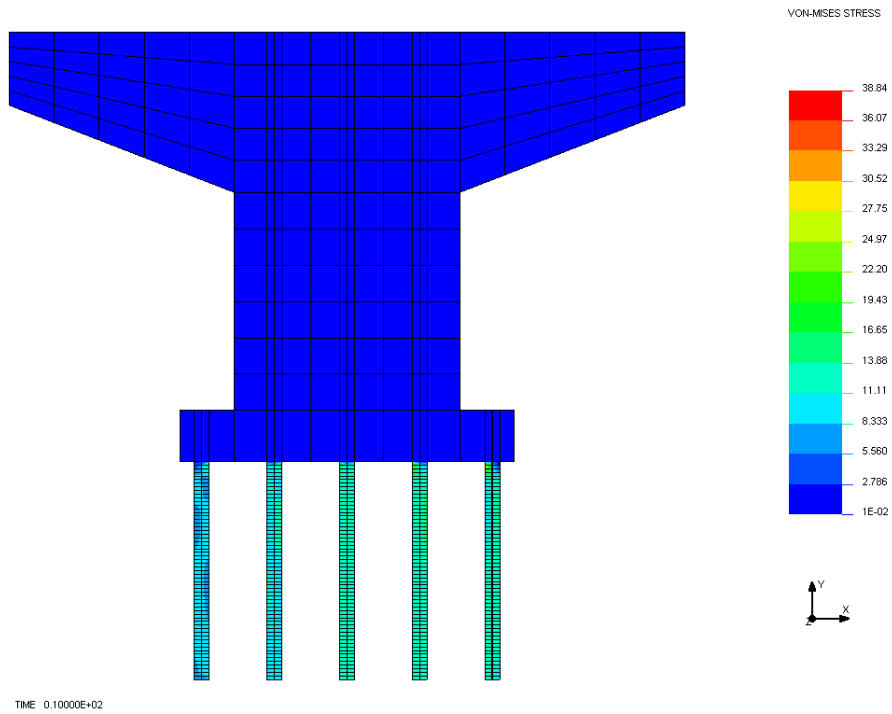(in scale of 100)

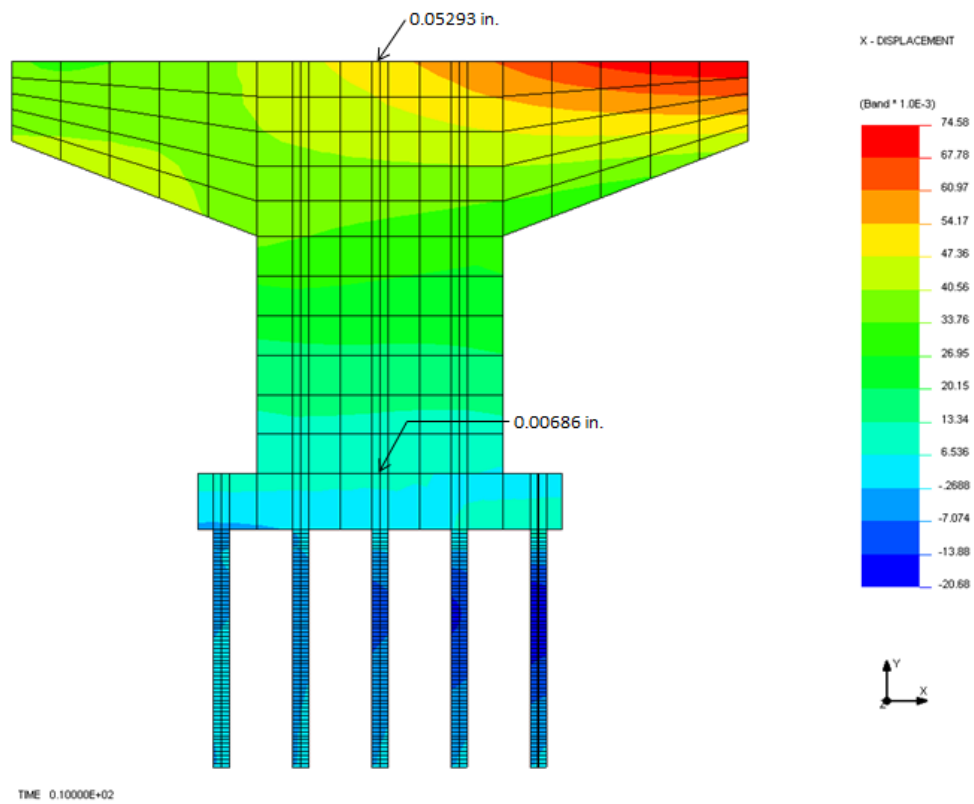*Figure C.37* Von-mises stress of Model 14 under NISA FEM analysis

Figure C.38 Lateral displacement of Model 14 under NISA FEM analysis

DISPLACED-SHAPE
MX DEF= 2.44E-01
NODE NO.= 25818
SCALE = 100.0
(ACTUAL SCALING)

TIME 0.10000E+02

Figure C.39 Lateral defection of Model 14 under NISA FEM analysis
(in scale of 100)

VON-MISES STRESS

32.56
30.24
27.91
25.59
23.27
20.94
18.62
16.29
13.97
11.65
9.322
6.998
4.674
2.350
3E-02

TIME 0.10000E+02

Figure C.40 Von-mises stress of Model 15 under NISA FEM analysis

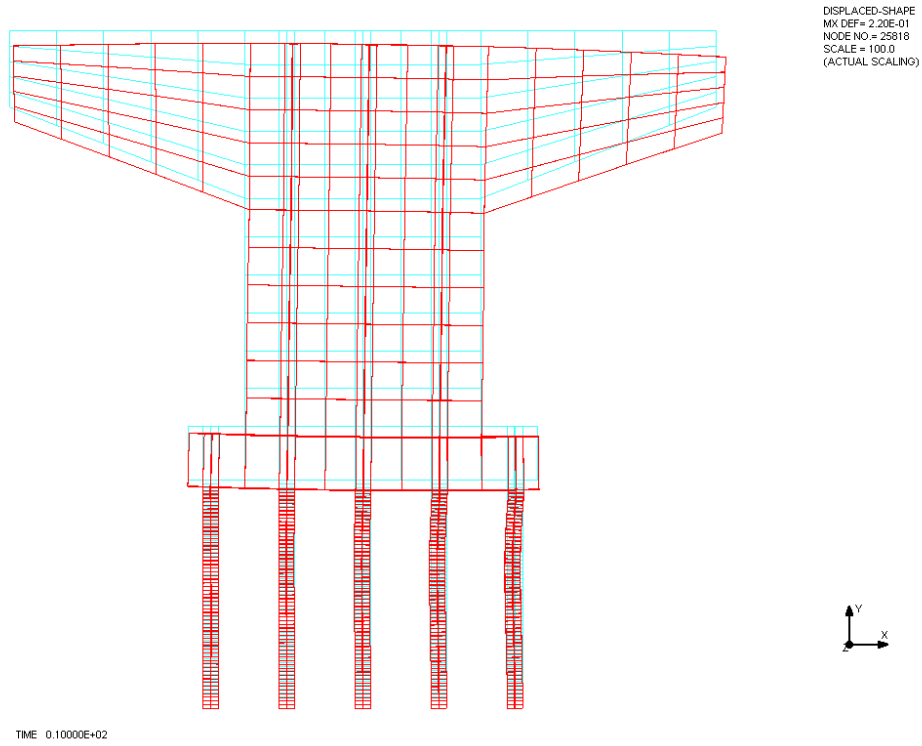*Figure C.41* Lateral displacement of Model 15 under NISA FEM analysis

Figure C.42 Lateral defection of Model 15 under NISA FEM analysis
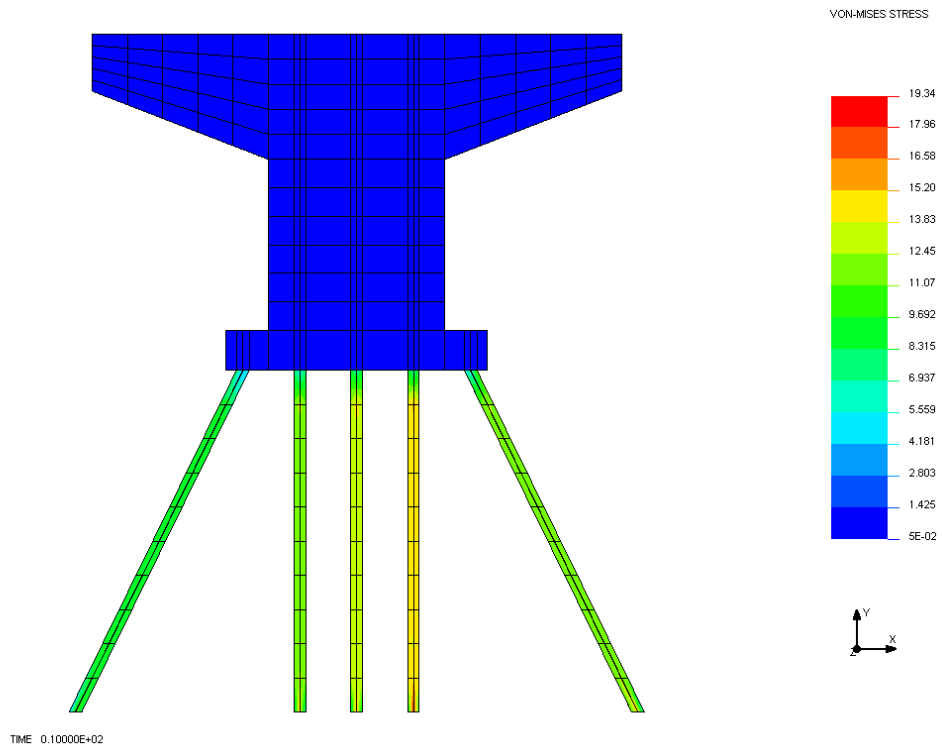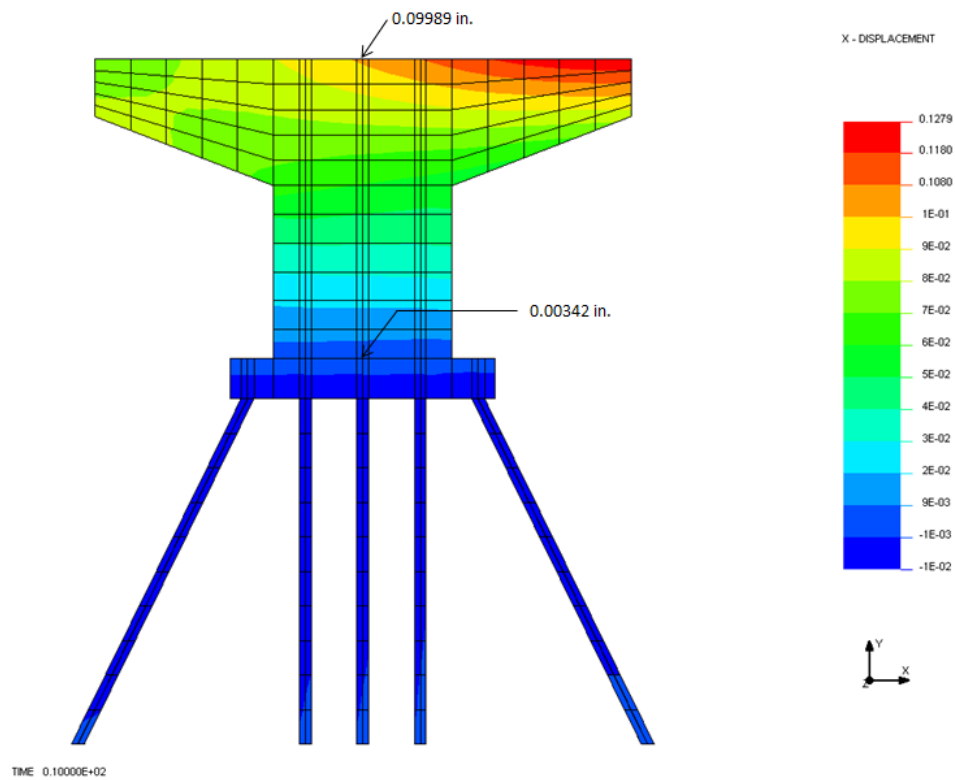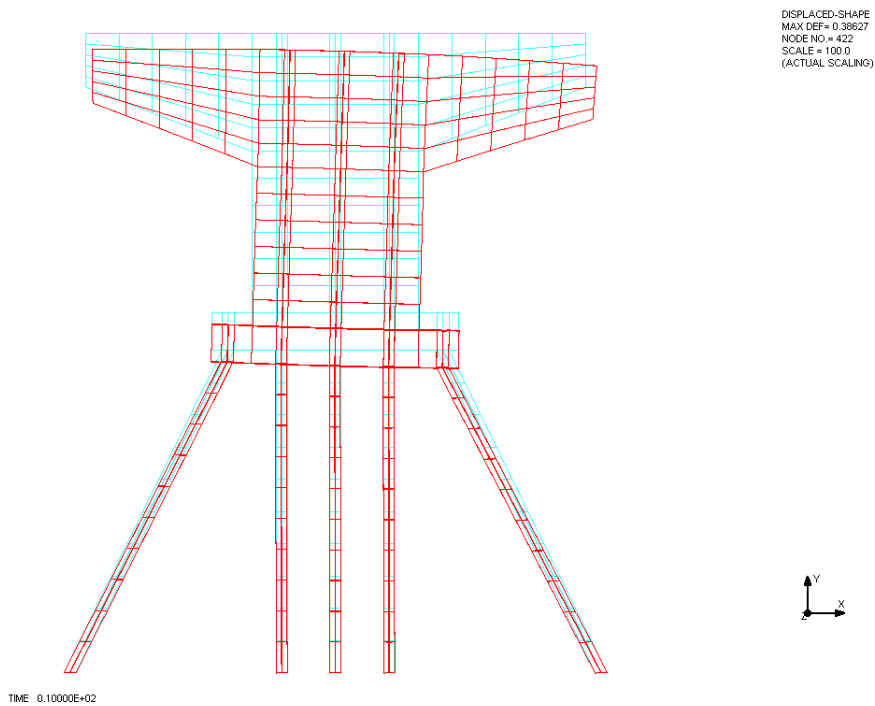(in scale of 100)

Figure C.43 Von-mises stress of Model 16 under NISA FEM analysis

Figure C.44 Lateral displacement of Model 16 under NISA FEM analysis

TIME 0.10000E+02

Figure C.45 Lateral defection of Model 16 under NISA FEM analysis
(in scale of 100)

VON-MISES STRESS

| 19.34 |
| 17.96 |
| 16.58 |
| 15.20 |
| 13.83 |
| 12.45 |
| 11.07 |
| 9.692 |
| 8.315 |
| 6.937 |
| 5.559 |
| 4.181 |
| 2.803 |
| 1.425 |
| 5E-02 |

TIME 0.10000E+02

Figure C.46 Von-mises stress of Model 17 under NISA FEM analysis

Figure C.47 Lateral displacement of Model 17 under NISA FEM analysis

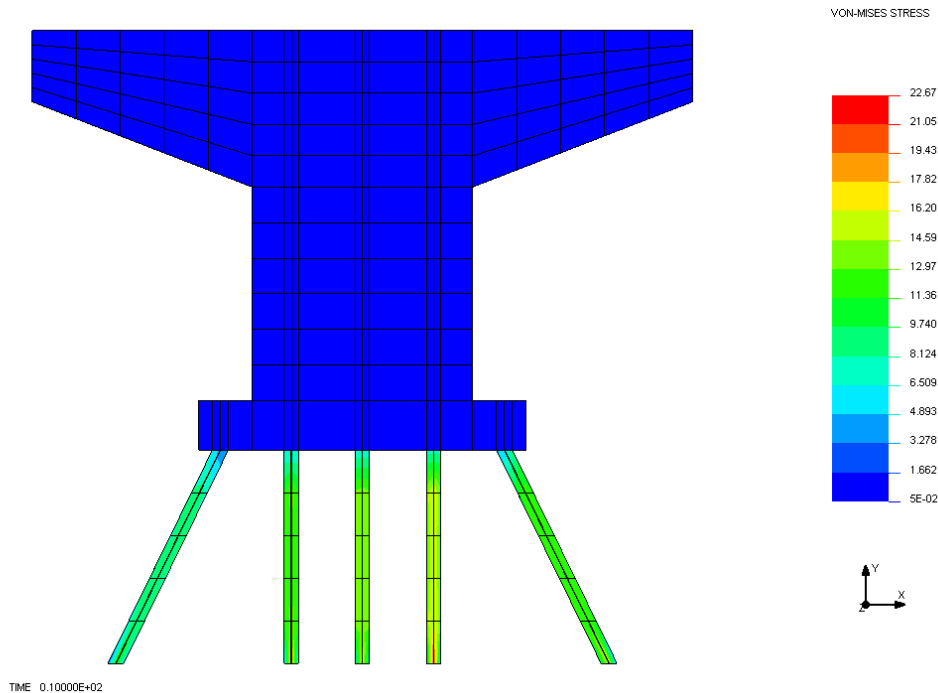*Figure C.48* Lateral defection of Model 17 under NISA FEM analysis
(in scale of 100)

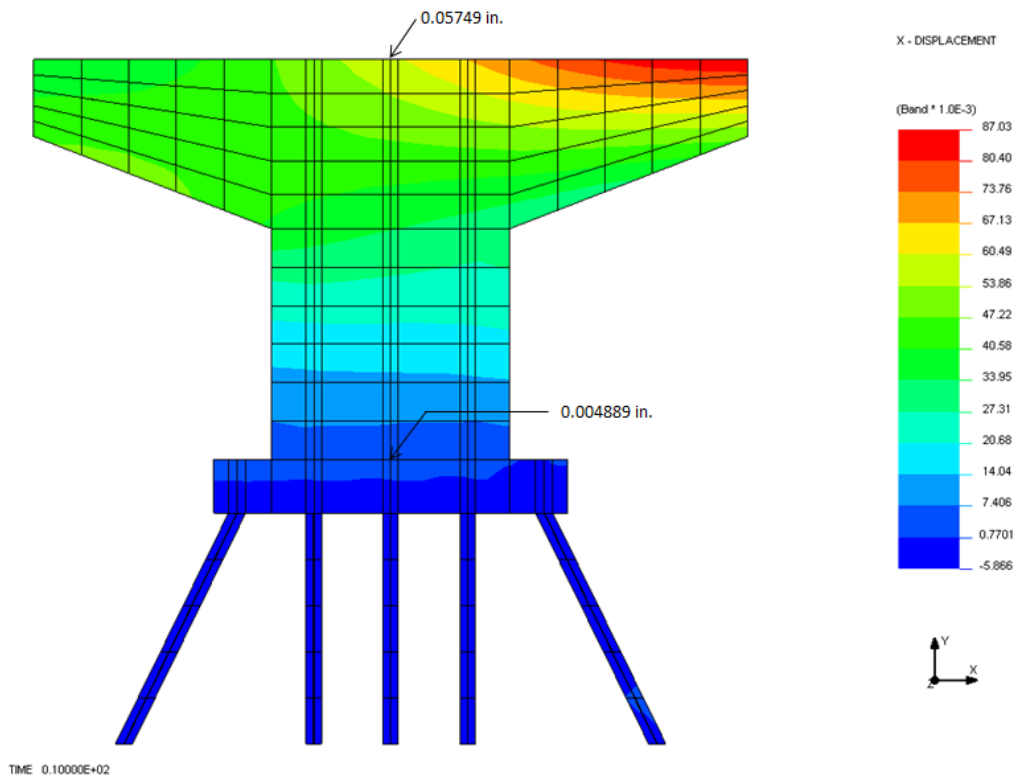*Figure C.49* Von-mises stress of Model 18 under NISA FEM analysis

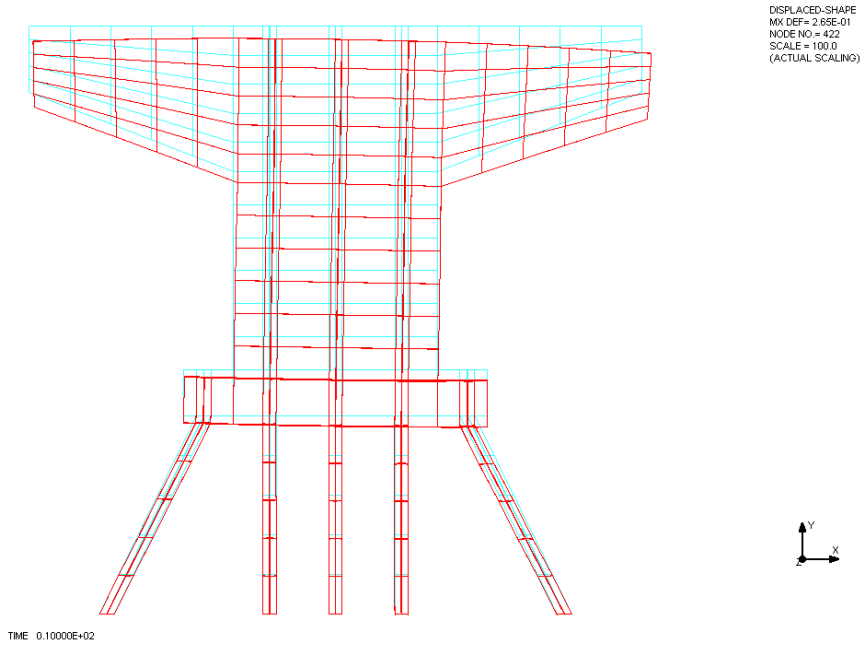*Figure C.50* Lateral displacement of Model 18 under NISA FEM analysis

DISPLACED-SHAPE
MX DEF= 2.65E-01
NODE NO.= 422
SCALE = 100.0
(ACTUAL SCALING)

TIME   0.10000E+02

Figure C.51 Lateral defection of Model 18 under NISA FEM analysis
(in scale of 100)

VON-MISES STRESS

19.55
18.15
16.76
15.36
13.97
12.58
11.18
9.787
8.393
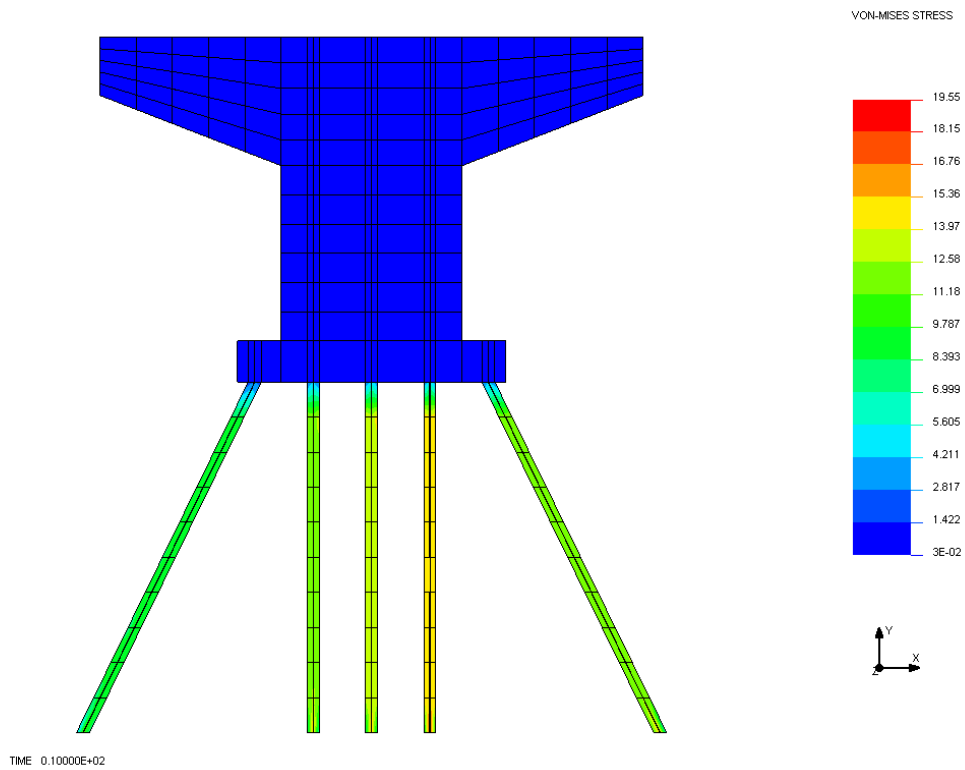6.999
5.605
4.211
2.817
1.422
3E-02

TIME   0.10000E+02

Figure C.52 Von-mises stress of Model 19 under NISA FEM analysis
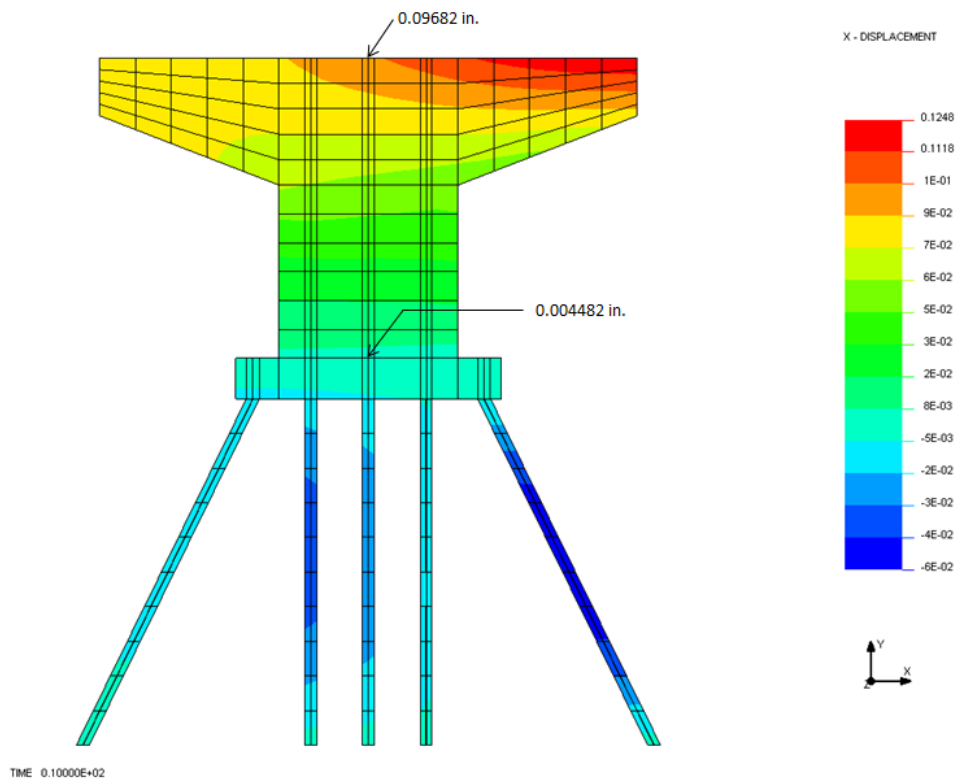
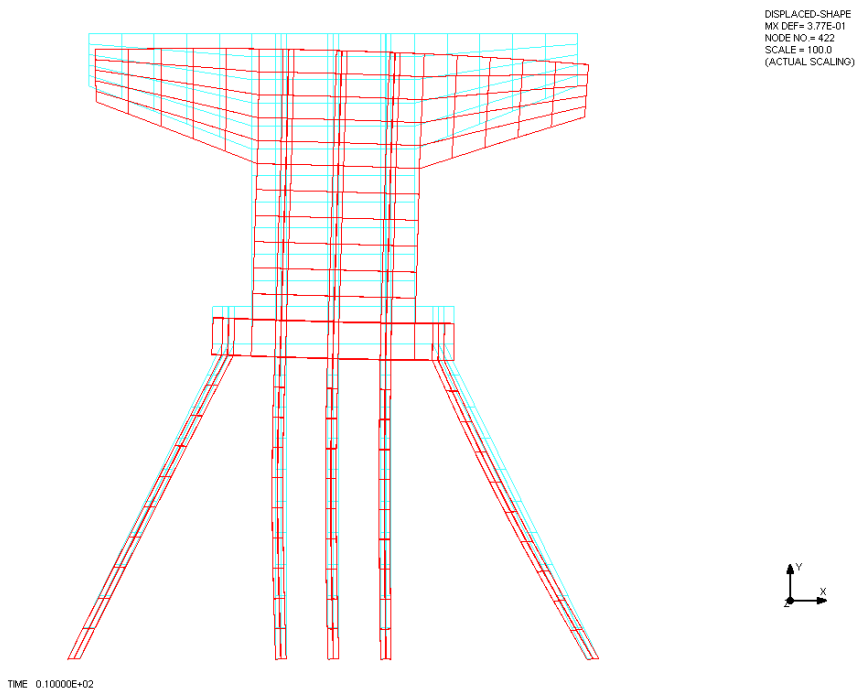*Figure C.53* Lateral displacement of Model 19 under NISA FEM analysis

Figure C.54 Lateral defection of Model 19 under NISA FEM analysis
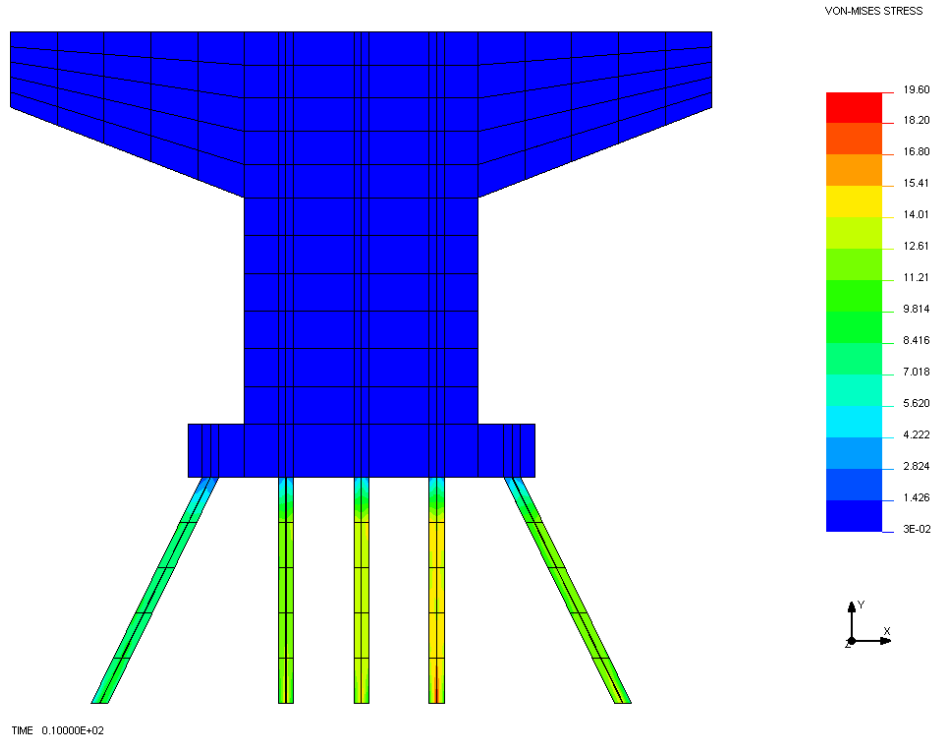(in scale of 100)

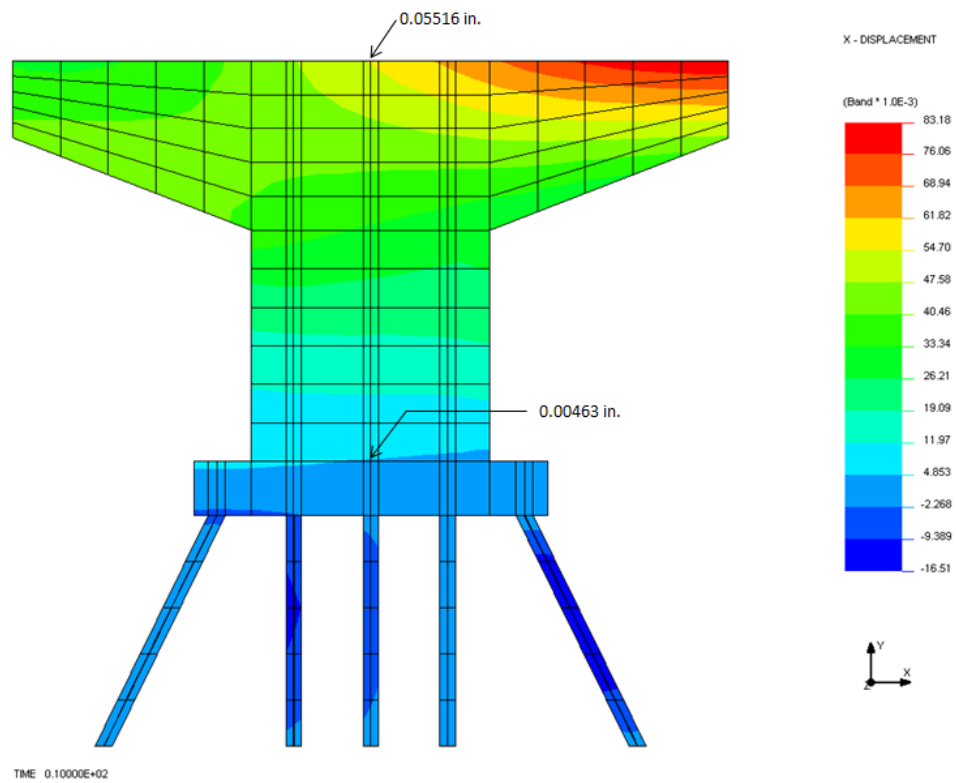*Figure C.55* Von-mises stress of Model 20 under NISA FEM analysis

Figure C.56 Lateral displacement of Model 20 under NISA FEM analysis

DISPLACED-SHAPE
MX DEF= 2.50E-01
NODE NO.= 4307
SCALE = 100.0
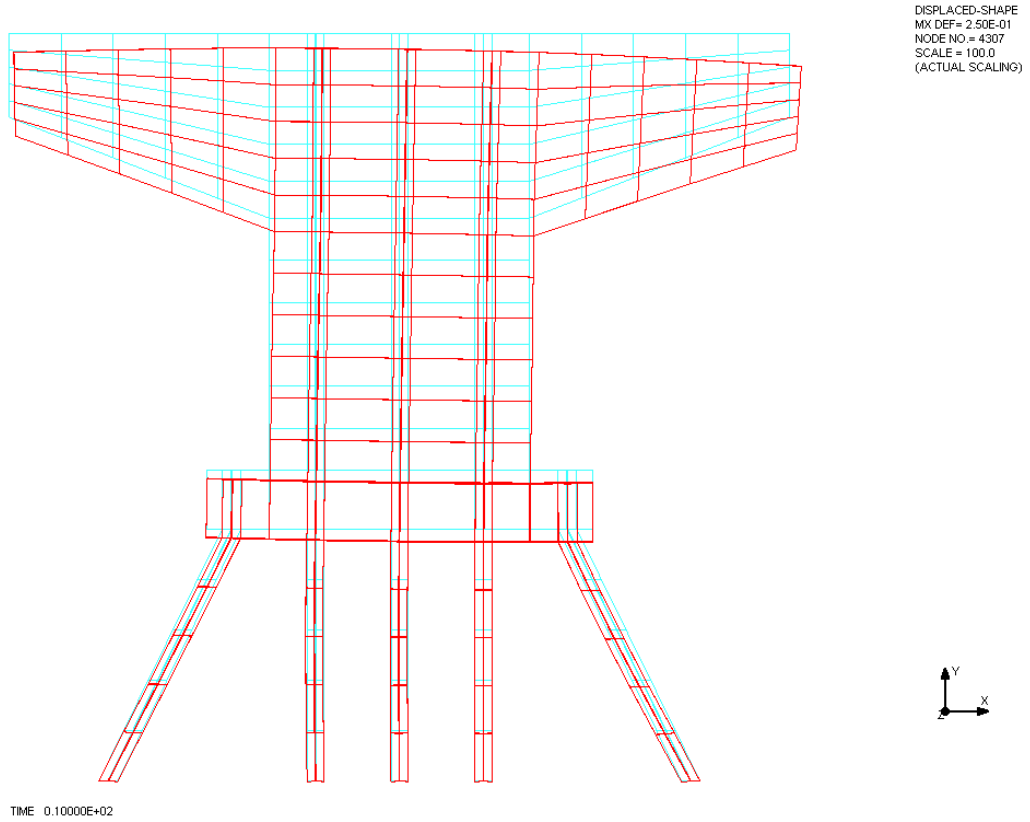(ACTUAL SCALING)

TIME 0.10000E+02

Figure C.57 Lateral defection of Model 20 under NISA FEM analysis
(in scale of 100)

VITA

Graduate School
Southern Illinois University

Yunyi Jiang

alexyunyijiang@gmail.com

Shenzhen University, China
Bachelor of Science in Civil Engineering, Civil and Environmental Engineering, June 2011

Southern Illinois University Carbondale
Master of Science in Structural Engineering, Civil and Environmental Engineering, May 2013

Dissertation Paper Title:
    FOOTING FIXITY OF BRIDGE PIER WITH END-BEARING PILE FOUNDATION

Major Professor: Dr. J. Kent Hsiao

Publications:
- Hsiao, J. K., & Jiang, A. Y. (2016). Post-Tensioned Box Girder Bridge An Analysis Approach Using Equivalent Loads. *International Journal of Bridge Engineering*, *4*(1).
- Hsiao, J. K., & Jiang, A. Y.(2014). FOOTING FIXITY EFFECT ON PIER DEFLECTION. *International Journal of Bridge Engineering (IJBE)*, *2*(2).